The Development and Application of Single Particle Mass Spectrometry Techniques for the Analysis of Pharmaceutical Aerosols

Anthony P. New

PhD Thesis

University of Edinburgh, 2009

The work presented in this thesis is the original work of the author, except where specific reference is made to other sources. It has not been submitted in part, or in whole, for any other degrees.

Anthony New   October 2009

5 July 2010 .

Acknowledgements

Abstract

Single particle mass spectrometry techniques were applied to the analysis of aerosol particles originating from inhaler devices, used to deliver pharmaceuticals for the treatment of lung disease such as asthma.

The inhalation products studied were Seretide® for which the formulated drug product is composed of a blend of fluticasone propionate (FP) which is a corticosteroid and salmeterol xinofoate (SX) which is a long acting β-agonist. It has been suggested previously that the formation of particles that are composed of both FP and SX by co-association can give improved efficacy: however in the past it has been difficult to analyze this type of co-associated particle. Hence, the purpose of the work described in this thesis was to develop single particle mass spectrometry methods that could assess the degree of co-association between FP and SX in fine aerosolized particles emitted from the inhaler devices.

Two types of inhaler device were investigated and these were pressurized metered dose inhalers (pMDIs) and dry powder inhalers (DPIs). The formulated product for pMDIs was a blend of FP and SX held in a suspension of propellant in a pressurized canister. The formulated product for the DPIs is comprised of a blend of FP and SX and an excipient lactose.

Two commercial single particle mass spectrometers were used in this work; an Aerosol Time-of-Flight Mass Spectrometer (TSI, Shoreview, MN, USA) and an Aerodyne Aerosol Mass Spectrometer (Aerodyne, Billerica, MA, USA). Although the general layout of these instruments was similar in that they are both comprised of an

inlet, a particle sizing region and a mass spectrometer, there were some differences in their design. For example, the ionization source of the Aerosol Time-of-Flight Mass Spectrometer used a single step process involving laser ablation and ionization while the Aerodyne Aerosol Mass Spectrometer used a two step process involving thermal desorption from a hot plate followed by electron ionization. These instruments were compared and evaluated in terms of their design and the characteristics of the data acquired on aerosols of pharmaceutical materials.

Data analysis methods for single particle mass spectrometry were developed based on the mass spectrometric fragmentation patterns indicative of either pure or co-associated particles. Data analysis was performed by either using representative ions from the mass spectrum taken from each particle or by using multivariate statistical analysis as a pattern recognition tool applied to the complete mass spectrum for each particle.

High levels (above 50%) of co-association were found in the emitted doses from both pMDI and DPI products. Although the design of each instrument was different, reasonable agreement in the levels of co-association was found as long as the size of particle that was analyzed by the mass spectrometer in each case was taken into account.

Finally a comparison of the applicability of each of the commercial single particle mass spectrometers to the analysis of materials taken from pharmaceutical aerosols was made. Recommendations for future work on instrument development and further applications for inhalation products are given.

Contents

Chapter 1 - Introduction

Chapter 2 - Instrumentation

Chapter 3 – The Application of Single Particle Mass Spectrometry to the Analysis of Inhalation Products

Chapter 4 – Data Analysis for Aerosol Time-of-Flight Mass Spectrometry (AToFMS)

Chapter 5 – Determination of Co-association using Aerosol Time-of-Flight Mass Spectrometry (AToFMS)

Chapter 6 - Data Analysis Methods for Aerodyne Aerosol Mass Spectrometry (AAMS)

Chapter 7- The Determination of Co-association using Aerodyne Aerosol Mass Spectrometry (AAMS)

Chapter 8 - Conclusions

Chapter 9 –Suggested Future Work

Appendices

Abbreviations

Abbreviation	Term
AAMS	Aerodyne Aerosol Mass Spectrometer
ACI	Andersen Cascade Impactor
AToFMS	Aerosol Time-of-Flight Mass Spectrometer
CI	Chemical Ionisation
COPD	Chronic Obstructive Pulmonary Disease
COA	Cellulose Octaacetate
dc	Direct Current
DPI	Dry Powder Inhaler
EI	Electron Ionisation
ESI	Electrospray Ionisation
FDA	Food and Drug Administration
FP	Fluticasone Propionate
FPANDSX	Fluticasone Propionate AND Salmeterol Xinofoate
FPORSX	Fluticasone Propionate OR Salmeterol Xinofoate
FWHM	Full Width to Half Maximum
GSK	GlaxoSmithKline
HPLC	High Pressure Liquid Chromatography
HIV	Human Immunodeficiency Virus
ICS	Inhaled Corticosteroid
IT-MS	Ion Trap Mass spectrometry
LABA	Long Acting β-Agonist
LASER	Light Amplification by Stimulated Emission of Radiation
LC/MS	Liquid Chromatography/Mass spectrometry
LDI	Laser Desorption Ionization
m/z	Mass to Charge Ratio
MS	Mass spectrometer
MHRA	Medicines and Healthcare Products Regulatory Agency
MVA	Multivariate Statistical Analysis
MW	Molecular weight
Nd:YAG	Neodynium:Yttrium Aluminium Garnet
PAT	Process Analytical Technology
PCA	Principle Component Analysis
PI	Photo-Ionization
PMF	Positive Matrix Factorization
pMDI	Pressurized Metered Dose Inhaler

(The table is continued on the next page)

(Abbreviations continued from previous page).

Abbreviation	Term
PMF	Positive Matrix Factorization
rf	Radio Frequency
RSD	Relative Standard Deviation
SDI	Surface Desorption Ionization
SEM	Scanning Electron Microscope
SPMS	Single Particle Mass Spectrometry
SX	Salmeterol Xinofoate
ToF	Time-of-Flight
USA	United States of America
UV	Ultra Violet
WHO	World Health Organisation

Chapter 1

Introduction

1.1 Introduction

Single particle mass spectrometry (SPMS) can give detailed information on aerosol particle size and composition *in-situ*, in near real-time[1]. In the past, SPMS has been predominantly used to investigate environmental aerosols; these studies are important as aerosol particles found in the environment, such as automobile emissions or industrial waste emissions, can potentially have a detrimental effect on human health[2].

The interaction of particles with lung tissue can also have a positive effect on human health[3]. Medicinal products composed of particles of drug material are designed, manufactured and incorporated in inhaler devices used for the treatment of lung disease such as asthma. A significant amount of the chemical analysis of these types of materials involves particle size measurement and composition determination, therefore the application of SPMS to the analysis of medicinal aerosols is an attractive concept.

Information obtained on particle size and composition, *in-situ* in pharmaceutical aerosols, using SPMS equipment may give some real benefit in increasing the understanding of current inhalation products and improving future manufacturing processes and products. Hence the major objectives of this research were (i) to develop SPMS techniques for the analysis of inhalation products, (ii) to use SPMS to investigate co-association in particles taken from inhalation products and (iii) to evaluate the application of two commercially available SPMS instruments to the analysis of inhalation products.

1.2 The Drug Discovery and Development Process

The pharmaceutical industry is a complex, expensive and time consuming business[4]. The process of drug discovery and development has an associated high risk (not least in financial terms), but with potentially high rewards in terms of the discovery of medicines for the treatment of life-threatening diseases.

The classical process of drug discovery involved the synthesis of small molecules followed by biological testing to ascertain pharmacological activity. The active ingredients in GSK's "blockbuster" drug products (those which have made more than one billion dollars per year) such as Paxil® for depression[5, 6], Tagamet® an anti-ulcer treatment[7, 8] and Seretide® for lung disease[9, 10, 11], were developed in this way.

In the 1980s, many compounds were synthesized individually then submitted for biological testing, whereas during the 1990s, the drug discovery divisions of many of the larger pharmaceutical companies automated this process. Using this approach millions of compounds per year are screened in disease areas such as cancer, cardio-vascular disease, central nervous system disorders, infectious disease, HIV, and lung disease[12,13].

At the time of writing, as the market is so competitive, many of the larger and well established Pharmaceutical companies (termed 'Big Pharma') are undergoing a restructuring process. Moreover, it appears likely that the small biopharmaceutical companies of today will become the 'Big Pharma' companies of the future. This is because, in recent years, the approach to drug discovery has changed; for example during the biotechnology boom of the late 1990s, drug discovery platforms based on monoclonal antibodies[14], and on antisense or gene-therapy[15, 16], produced drugs based on larger biological molecules rather than smaller synthetic ones, giving products that are easier to protect *via* intellectual property.

Having identified an active drug compound, the development of an efficacious formulated drug product that can be successfully marketed can be a technically complex process. New drugs must be shown to be safe and to have an efficacy

advantage over currently marketed compounds. Hence, for compounds that show biological activity and reach early development there is still a high attrition rate typically because of safety issues, or because only minimal advantage over existing products can be shown. Moreover, during the course of the drug development process, the pharmaceutical company must fulfil the requirements of the regulatory authorities. Agencies such as the Food and Drug Administration (FDA)[17] in the USA and the Medicines and Healthcare Products Regulatory Agency (MHRA)[18] in Europe have a remit to ensure patient safety and enforce strict guidelines on drug development and marketing.

The patent on a new chemical entity *i.e.* the drug compound *per se*, lasts for 20 years[19]. Therefore the pharmaceutical company has a limited time to develop the compound into a formulated product, test it for safety and efficacy, and then to market it.

The significance of the finite lifetime of the patent is that when the patent has lapsed, generic drug companies may start to produce the given product. The cost of research and development for the generic company is minimal so invariably generic companies can sell similar products at a discount compared with the price charged by the original company. This typically results in a reduction in sales for the company that invested in research and development to produce the original product and reduces (or finishes) their involvement with the given product.

It is a challenging task to understand the biology and chemistry of the drug compound, produce a formulated product and establish the manufacturing process within a finite amount of time. Hence, within the pharmaceutical industry there is a constant search for new technologies that may aid the understanding of the processes and products involved, as well as methods for progressing compounds through development as fast as possible while retaining the quality of the process and product.

Clearly, there would be some advantage in reducing the time taken for drug development in terms of (a) getting the product to the patient and (b) recouping the many millions of dollars that are invested to develop each drug from active compound to marketed product.

Chemical analysis is an important part of many of the stages of the drug development process and many of the chemical analyses performed in the drug discovery and development processes are based on high performance liquid chromatography (HPLC). For example, stability testing and accelerated degradation studies commonly rely on this technique. However, to be able to perform HPLC analysis the sample must be in the appropriate format. For example, to analyze the drug content of a tablet, the sample preparation might involve dissolution, filtration extraction and/or derivatization of the tablet material[20,21]. This is resource-intensive and time-consuming especially as there may be a need to analyze many thousands of tablets every year.

Hence within the pharmaceutical industry there is a constant evaluation of novel analytical technologies that may enable the faster chemical analysis and greater understanding of pharmaceutical related materials. For example, recently it has been shown that a tablet may be analyzed non-invasively and automatically with techniques such as near infra-red[22] or Raman spectroscopy[23]. It may be possible to reduce the time and cost of each analysis in the future using this approach.

1.3   Lung Disease

One of the major disease areas targeted by GlaxoSmithKline (GSK) is that of lung disease of which the two major types are asthma and chronic obstructive pulmonary disease (COPD).

Asthma is a chronic disease characterized by recurrent attacks of breathlessness and wheezing. During an asthma attack the lining of the bronchial tubes swells causing the airways to narrow, reducing the air flow into and out of the lungs. According to World Health Organisation (WHO) estimates, in 2007, 300 million people suffered from asthma and 210 million suffered from COPD[24]. The causes of asthma are not currently completely understood although allergens, tobacco smoke and chemical irritants such as air pollutants have been identified as triggers for the disease. Asthma can be controlled by avoidance of these triggers for example through life-style

changes such as smoking cessation[24] and by treatment using inhalation products such as those described in Section 1.4.

COPD is a more severe lung disease, which is characterised by chronic obstruction of lung airflow that interferes with normal breathing and is not fully reversible. The common terms 'chronic bronchitis' and 'emphysema' are included within the COPD term. The most common symptoms of COPD are breathlessness, excessive sputum production and a chronic cough. The causes of COPD include tobacco smoke (including passive exposure), air pollution and occupational aerosols, dusts and chemicals. COPD is controlled[25] by the avoidance of tobacco smoke (and other irritating dust particles) and by treatment using inhalation products such as those described in the next section.

1.4   Characteristics of Inhalation Products

Medicines for the treatment of lung disease are typically based on drug particles delivered directly to the lung (for increased speed of response to the drug), *via* an aerosol produced by either a dry powder inhaler (DPI) or a pressurized metered dose inhaler (pMDI) and such devices are termed inhalation products. The analysis of material from this type of product is based on the particle size and the drug dose, and it is typically performed using an Anderson Cascade Impactor (ACI)[26] which is discussed in more detail later in this section. Analyses to determine the particle size distribution can be performed on the formulated product using ACI but do not give speciation data, *i.e.* whether particles contain drug, excipient or both and in what ratio. Also, sample preparation and analysis of samples using an ACI can be both time consuming and complex.

Asthma is typically treated with corticosteroids[27], β-agonists[28] or a combination of both[29]. Examples of corticosteroids include fluticasone propionate (FP) and budesonide; examples of β -agonists include salmeterol xinofoate (SX) and formeterol. The active pharmaceutical ingredients in the GSK inhaler devices investigated in the studies described in this thesis were FP and SX and the chemical

structures of these compounds are shown in Table 1.1. Some of the major products in the asthma/COPD market are shown in Table 1.2.
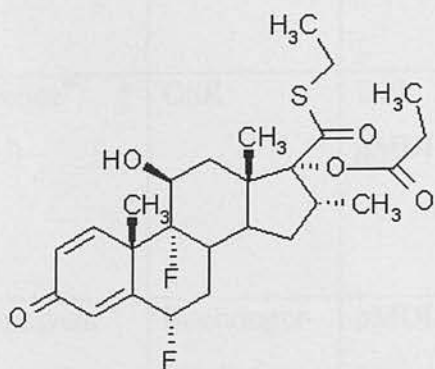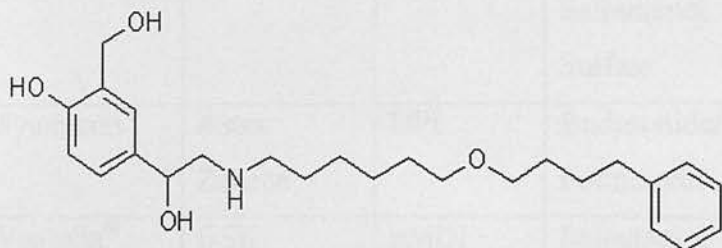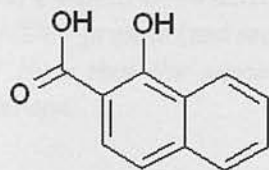
	Fluticasone propionate (FP) $C_{25} H_{31} F_3 O_5 S$ MW 500
	Salmeterol xinofoate (SX) Salmeterol (free base) $C_{25} H_{37} N O_4$ MW 415
	Xinofoate $C_{11} H_8 O_3$ MW 188

Table 1.1. *The chemical structure, chemical formulae and molecular weights for the inhaled corticosteroid (ICS) fluticasone propionate (FP) and the long acting β-agonist (LABA) salmeterol xinofoate (SX), the active drugs in many GSK inhaler products.*

Product	Company	Device*	Active drug	Used for	Reference
Serevent®	GSK	DPI	Salmeterol Xinofoate	COPD, Asthma	30
Flovent®	GSK	DPI	Fluticasone Propionate	COPD, Asthma	31
Seretide® † (EU)	GSK	DPI and pMDI	Fluticasone Propionate/ Salmeterol Xinofoate	COPD, Asthma	11
Combivent®	Boehringer-Ingelheim	pMDI	Ipratropium Bromide/ Salbutamol Sulfate	COPD, Asthma	32
Symbicort®	Astra Zeneca	DPI	Budesonide/ Formeterol	Asthma	33
Ventolin®	GSK	pMDI	Salbutamol	Asthma	34

*Table 1.2. Examples of marketed inhalation products used for the treatment of asthma and chronic obstructive pulmonary disorder (COPD). * DPI =Dry powder inhaler, pMDI= pressurized metered dose inhaler, see text for a more detailed description. † Note that the same product is marketed as Advair® in the US and Seretide® in Europe.*

The formulations in the dry powder inhalers produced by GSK use FP or/and SX as the active drugs. These are available as prescription medicines such as Flovent® a blend of FP and lactose[30] or Serevent® a blend of SX and lactose[31]. DPIs are also available as a combination of both FP and SX blended with lactose and this type of inhaler is discussed in detail in Section 1.5.

Lactose is used as an excipient in many of the GSK DPI products. Excipients are materials added to the formulation that have no therapeutic activity. In this case lactose provides bulk to the formulation and is used as a carrier for the active drug(s).

The Diskus® DPI, consists of a strip of blisters as shown in Figure 1.1(b) held within the Diskus® device shown in Figure 1.1(a). On actuation of the device the blister is ruptured and the contents (a single dose) inhaled by the patient.
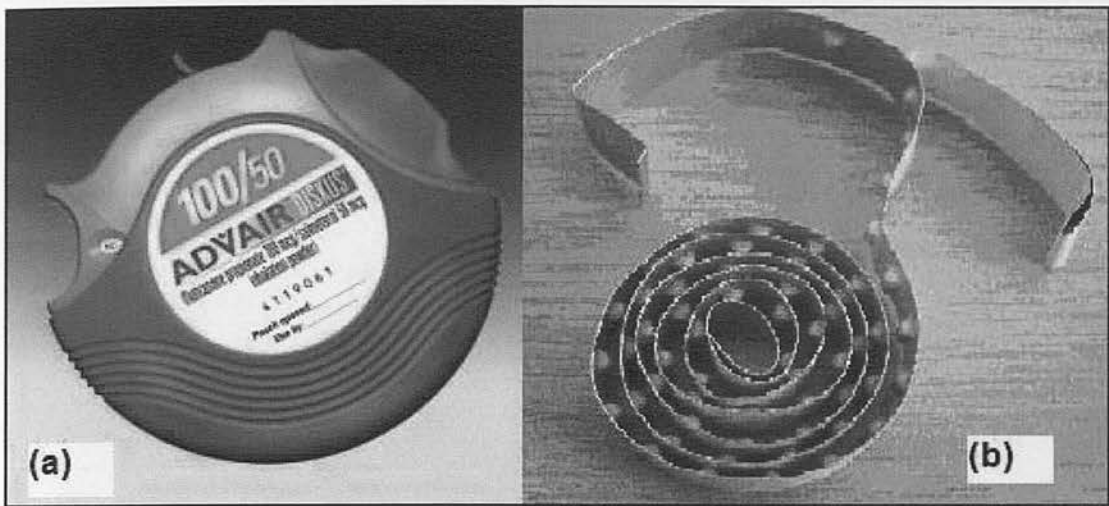
Figure 1.1. A photograph of (a) The Diskus® device and (b) the strip of blisters containing the formulated product. The formulated product is delivered to the patient as the blister is ruptured, by actuation of the device. Note that this product is marketed as Advair® in the US and Seretide® in Europe[35].

Three formulations of Seretide® DPI of varying drug strength were investigated in the studies reported in this thesis; FP 500 µg /SX 50 µg, FP 250 µg /SX 50 µg and FP 125 µg /SX 50 µg. The range of formulations covers adult and paediatric therapies. Throughout this thesis these formulations are referred to by the shortened term "FP/SX 500/50" *etc.*

An alternative DPI device (Gemini®) currently under development, was also investigated during the work reported in this thesis. This device allowed two blisters to be ruptured for each actuation and in this case FP and SX were separately blended with lactose so that the FP and SX were not mixed until the device was actuated.

The pressurized metered dose inhaler (pMDI), is an alternative inhaler device which consists of a canister containing a suspension of the drug, in a propellant, together with a surfactant. A diagram of a pMDI canister is shown in Figure 1.2 together with a photograph of the device. When activated, the pMDI gives a short burst of the drug suspension which is released in the form of a polydisperse aerosol. The amount of material in the aerosol is metered by a valve in the device.

The product range for the GSK pMDI devices is analogous to the DPI range in that the formulations are based on FP, SX or a combination of both. The combination products used in this thesis comprised the formulations FP 250 µg /SX 25 µg, FP 125

µg /SX 25 µg and FP 50 µg /SX 25 µg (as for the DPI devices these will be referred to by the shortened term "FP/SX 50/25" *etc.*).
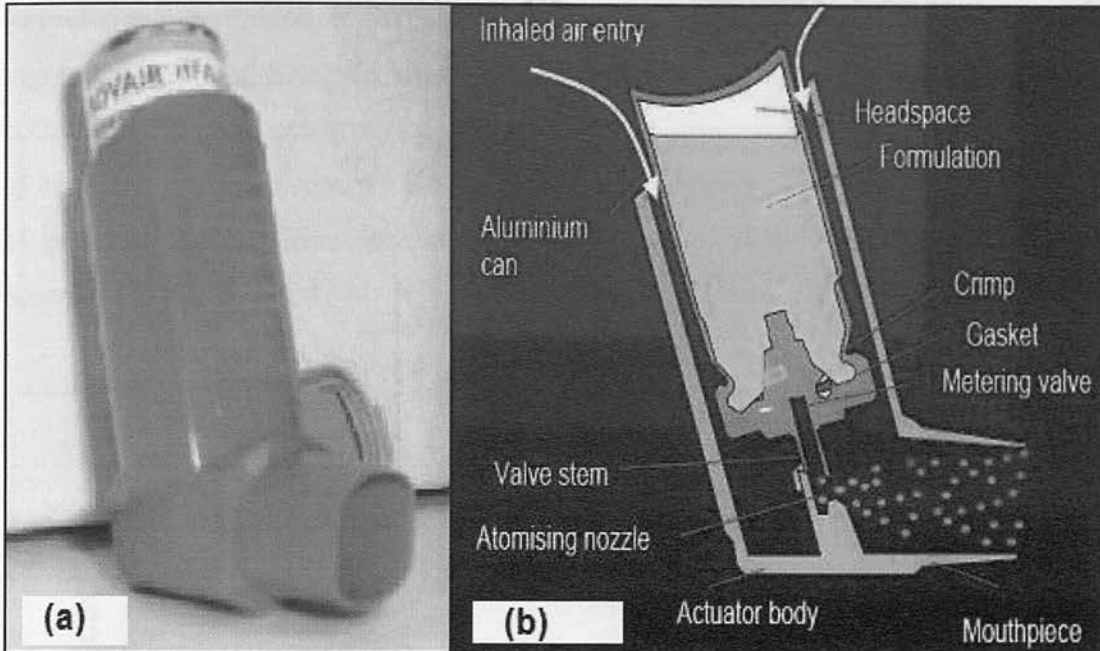
Figure 1.2. (a) Photograph of metered dose inhaler device (b) diagram showing the internal components of the pMDI device[35].

1.5 Synergy Between Drugs in Combination Inhalers

Although corticosteroids and β-agonists can be prescribed separately, in clinical practice it has been found that two drugs in combination give a significantly greater efficacy than the individual drugs, or the anticipated efficacy for the sum of the individual compounds[36].

This study[36] is summarized in the graph given in Figure 1.3, which shows the efficacy after dosing with (i) either FP or SX (shown as traces (d) and (e))(ii) FP and SX concurrently (shown as trace (b)) and (iii) as a blend from the same inhaler (Seretide®) (shown as trace (a)). The graph shows that the efficacy is lowest when the two materials are dosed separately and highest when dosed as a blend. The expected efficacy of the sum of FP and SX is exceeded by the two inhalers administered concurrently; however, a blend of FP and SX gives a much higher efficacy than anticipated.

A synergistic effect may explain the higher than anticipated increase in efficacy for the blend of FP and SX (Seretide®) and it could be derived from both compounds making contact with the same lung tissue cells simultaneously. Also, if the formulations contained individual particles that were comprised of both active ingredients (FP and SX), this would give an increased likelihood of the deposition of both drugs simultaneously on the same lung tissue, compared with the administration of both drugs *via* two separate inhalers[36]. Hence, an investigation of the composition of particles emitted from inhalation products was a major objective of the work described in this thesis.
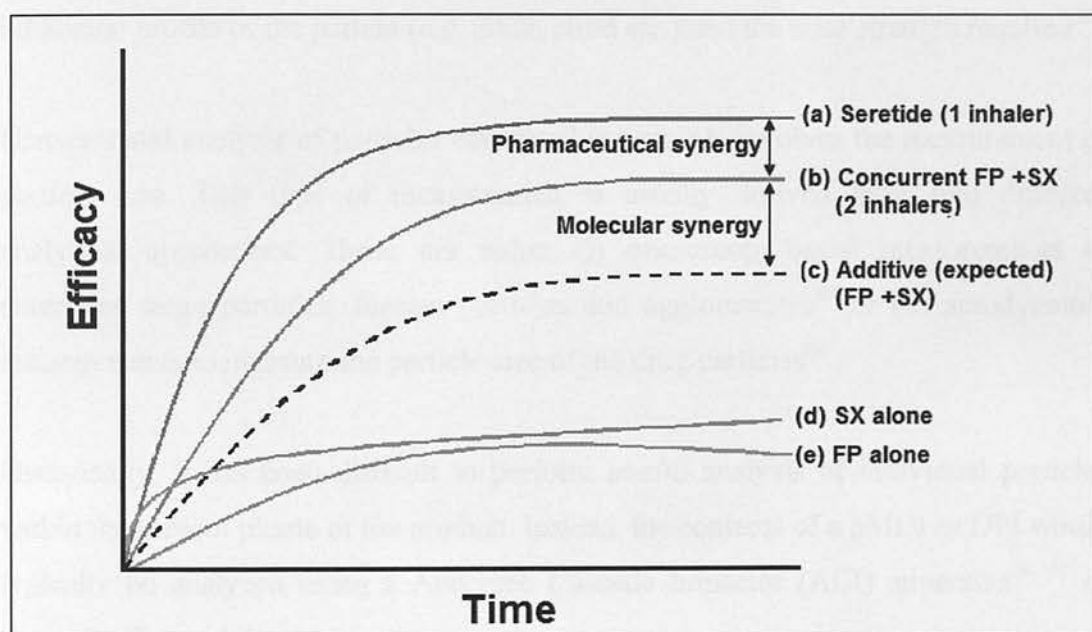
Figure 1.3. *The relative efficacy of FP and SX dosed (a) as a blend in a single Seretide® inhaler (b) concurrently with two separate inhalers, (c) the expected additive effect and, (d) and (e) as SX or FP alone. The top curve (a) shows a much higher than expected efficacy for a blend of FP and SX than for the two drugs administered separately or concurrently suggesting a synergistic effect [36].*

1.6 The Analysis of Inhalation Products

There are several analytical tests that are performed on the pharmaceutical materials that originate from commercially available inhaler devices[37]. Most of the analytical work performed on inhalation products is centred on the determination of particle size and overall composition.

The size of the particles originating from inhalation products is an important aspect of their mode of action. Intuitively, it might be expected that if the particles are too small then they could be prone to the typical tidal effects seen during respiration, *i.e.* the particles might be inhaled but then rapidly exhaled without depositing and therefore have no pharmacological effect. In contrast, if the particles are too large they could be expected to lodge in the upper airways (typically the throat) and then be swallowed without reaching the lung.

In practice when designing inhalation products, a number of factors are considered including the required target region of the lung, the deposition mechanism, the inhalation profile of the patient (*e.g.* adult, child *etc.*) and the dose strength required[38].

Conventional analysis of particles contained in aerosols involves the measurement of particle size. This type of measurement is usually derived from two different analytical approaches. These are either (i) microscopy-based measurements to determine large particles, foreign particles and agglomerates[39] or (ii) aerodynamic measurements to measure the particle size of the drug particles[40].

Historically, it has been difficult to perform *in-situ* analysis of individual particles within the aerosol plume of the product. Instead, the contents of a pMDI or DPI would typically be analyzed using a Andersen Cascade Impactor (ACI) apparatus[26, 41] as shown in Figure 1.4.

The ACI is effectively used as a surrogate *in-vivo* technique to mimic the penetration of particles into the lung. The depth of penetration of particles of different size is shown by the diagram to the right in Figure 1.4. For example, particles of diameters between 2.1 and 3.3 µm will be collected at Stage 4 which equates to particles reaching the secondary bronchi[42].

For the analysis of materials produced by an inhaler, the inhaler device is actuated and the contents swept into the ACI. A flow of air passes through the stack of plates and particles are deposited onto a particular plate depending on aerodynamic size and inertia. Hence if the particle has enough inertia it will be deposited onto the plate, which means that the larger particles are deposited onto the plates in the first stages of

the ACI. As the jets get smaller with each stage, the air velocity becomes faster and the smaller particles collect sufficient inertia to be deposited on the plates of the final stages of the ACI. Each of the series of plates is then washed and the washings assayed off-line using HPLC.
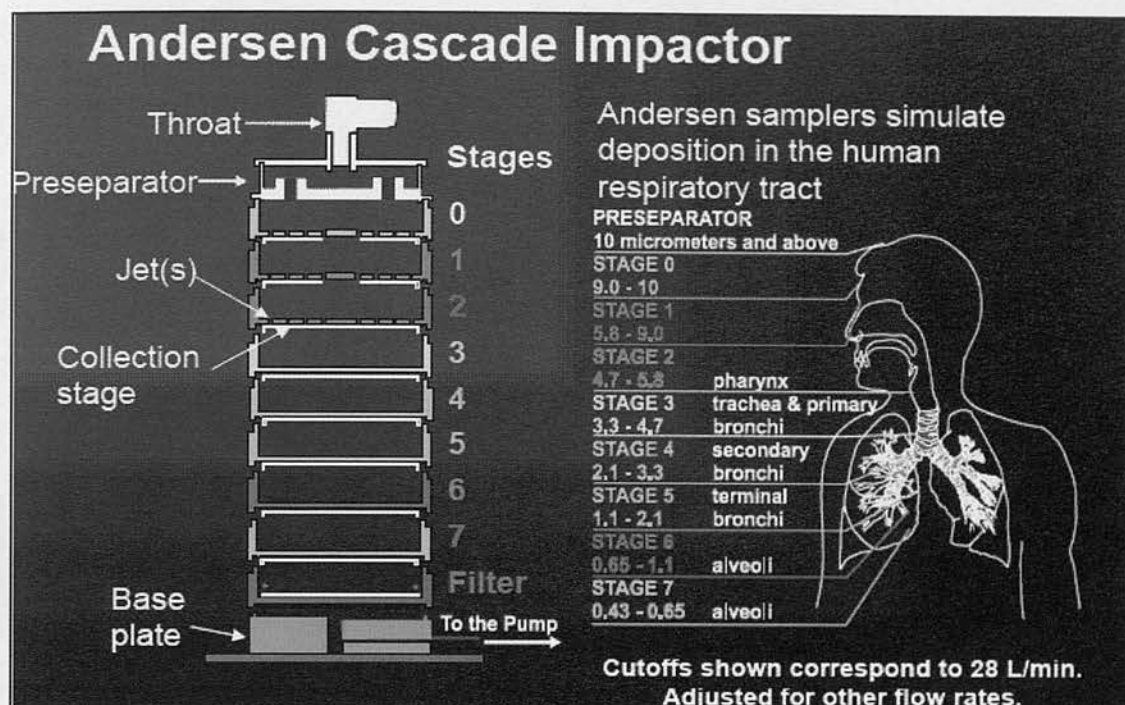
Figure 1.4. The Andersen Cascade Impactor (ACI). The left side of panel shows the 7 plates of the ACI device each of which will catch particles in different size ranges. The right side of the panel shows the significance of these particle size ranges in terms of the depth of penetration into the lungs(particle sizes given in μm) [35].

The ACI effectively gives an averaged measurement of the composition of groups of particles; however, to be able to study co-association, further detail is required to the extent of an assessment of the composition of each of the individual particles within a given sample population.

A previous study of individual particles taken from inhaler devices used Raman imaging of plates taken from the ACI to identify and classify the particles and to assess the co-association between FP and SX in pMDIs[43]. This work reported that co-association could be measured and the degree of co-association estimated based on statistical analysis. However, the Raman imaging technique used was relatively slow (a few hours per sample) and could measure only relatively small numbers of particles per experiment.

The ACI and Raman techniques described above are both off-line techniques *i.e.* the sample is collected and then analyzed at a later time. Limitations for off-line techniques include the possibility of artefact formation due to a change in the physical and/or chemical constitution of the analyte, for example during transportation or storage. Also, off-line analysis can involve a complex and resource-intensive sample preparation step, typically to extract the drug from the matrix of excipients included in the formulation.

Hence it would be of great benefit to develop and apply an analytical technique, applicable to inhalation products, that would allow analysis of particles directly from the aerosol plume and provide insight into the identity of the active pharmaceutical ingredients within each particle.

A technique that could deliver information on particle size and give detailed information on the composition of particles found in pharmaceutical aerosols might help to improve our understanding of this type of product and improve the formulation of future medicines.

1. 7 Single Particle Mass Spectrometry (SPMS)

The single particle mass spectrometer is capable of measuring both particle size and composition in near real-time directly from the aerosol[1]. The development of single particle mass spectrometry (SPMS) started in the early 1970s with a major driver being the analysis of atmospheric aerosols[44, 45].

A diagram to show the regions of a typical single particle mass spectrometer is given in Figure 1.5. The instrument comprises an inlet, a particle sizing region, a vaporization/ionization section and a mass spectrometer. Much of the development of this type of instrumentation has focussed on one or more of these areas.

A more detailed account of the development of SPMS is given in Section 2.2 together with a detailed description of the two commercially available instruments used to acquire the data presented in this thesis.
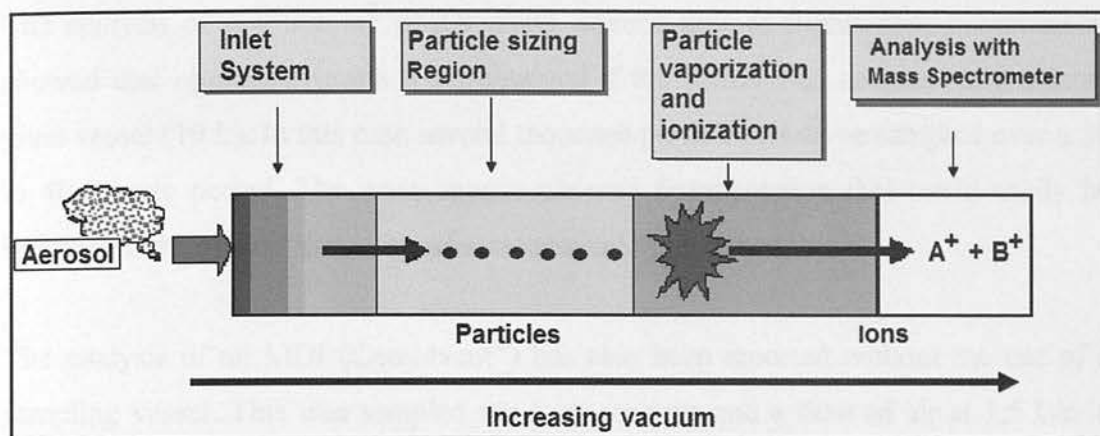
Figure 1.5. *The major components of a single particle mass spectrometer. The inlet system converts a cloud of particles from an aerosol into a particle beam; the size of each particle is then measured before it is vaporized and ionized prior to the analysis of composition using the mass spectrometer.*

In the past, the main application for this type of instrument has been in environmental monitoring. Atmospheric aerosols have been shown to consist of a variety of materials including pollutants[46], cigarette smoke[47], fibres[48], and biological material such as bacterial or fungal spores[49]. Hence, the technique of SPMS has been used to analyze particles found in atmospheric aerosols of the particle types listed above (pollutants[50, 50a,50b], cigarette smoke[51], fibres[52], bio-aerosols[53]) as well as many other types of particle found in the atmosphere. These studies are important as it is well known that particulate matter can interact with lung tissue and result in lung disease[54, 55].

Some of the particles in atmospheric aerosols studied by SPMS are in a similar size range to the drug particles found in inhalation products. Although the application of this technique to pharmaceutical aerosols is an attractive concept, reports of such applications in the literature are rare.

1.8 Application of Single Particle Mass Spectrometry to the Analysis of Pharmaceutical Aerosols

The real time (or near real-time) acquisition of data on particle size and composition has the potential to give unique information on the particles within the aerosols produced by both DPIs and pMDIs. Previous reports of the application of SPMS to pharmaceutical analysis are discussed below.

The analysis of a Ventolin® pMDI using aerosol time-of-flight mass spectrometry showed that optimum results were obtained if the pMDI was actuated into a large glass vessel (19 L). In this case several thousand particles could be sampled over a 30 to 40 minute period. The mass spectra showed fragmentation that could easily be interpreted in terms of the active pharmaceutical ingredients[56].

The analysis of an MDI (Combivent®) has also been reported without the use of a sampling vessel. This was sampled *via* a spacer tube and a flow of air at 1.5 L/min was used to sweep material into the AToFMS instrument. For these experiments indicative ions in the mass spectra were used as markers for specific compounds; for example the ions at *m/z* 79/81 from the Br⁻ ion were shown to be unique for one of the active pharmaceutical ingredients (ipratropium) and *m/z* 97/99 was shown to be unique to the sulphate counter-ion[57, 58].

For some initial work on the study of co-association between active pharmaceutical ingredients in inhalation products, using an AToFMS instrument, a sampling chamber was used to introduce the sample to the instrument. In that study, unequivocal evidence of co-association between the active drugs in the Symbicort® Turbuhaler® (Budesonide/ Formeterol) DPI, was not obtained. In contrast, good evidence for the presence of co-association between the active pharmaceutical ingredients in a Seretide® (SX and FP) DPI was obtained[59].

1.9 Data Analysis for Single Particle Mass Spectrometry.

Inhalation products are well defined in terms of the pharmaceutical ingredients that are used in the formulation. Whereas for environmental aerosols many unknown compounds (perhaps 10s or 100s) need to be detected and identified, there are only a few (typically 3 or 4) components in the formulation of the inhalation products. Moreover samples of standards of the pharmaceutical ingredients and excipients are readily available, which is not always the case for environmental analysis.

For pMDIs the materials in the formulation consist of drug compound(s) and propellant. If the aerosol is expanded into a glass vessel, the propellant evaporates and

typically is not detected by the mass spectrometer. This means that for a pMDI containing two active drug compounds (*e.g.* FP and SX), there are three possible categories of particle composition. These are pure FP particles, pure SX particles and particles that consist of a mixture of FP and SX because of co-association between the two compounds.

For DPIs the materials in the formulation consist of drug compound(s) and a carrier, typically lactose. This means that for a DPI containing two active drug compounds (*e.g.* FP and SX), there are seven possible categories of particle composition. These are pure FP, pure SX or pure lactose (La) and also FP/SX, FP/La, SX/La and FP/SX/La.

In a typical data set obtained from a SPMS experiment, a mass spectrum is associated with an individual particle. The SPMS mass spectrum typically shows many ions across the *m/z* scale and there may commonly be a few hundred particles in every data set. Clearly there is potential for acquiring large amounts of data and a co-ordinated approach to the data analysis is required both in terms of interrogating individual samples and in comparison of different sample sets.

Multivariate Statistical Analysis (MVA)[60] can be extremely useful for the analysis of large complex data sets and has been applied to SPMS data as a pattern recognition tool. This can be useful for both single sample analysis and for comparing data sets.

1.10 References

(1)   Aerosol mass spectrometry: An introductory review. D. Nash, T. Baer and M. Johnson. *Int. J. Mass Spectrom.* 258, 2-12 (2006).

(2)   An association between air pollution and mortality in 6 United States cities. D.W. Dockery, C.A. Pope, X.P. Xu, J.D. Spengler, J.H. Ware, M.E. Fay, B.G. Ferris and F.E. Speizer. *New Eng. J. Med.* 329, 1753-1759 (1993).

(3)   Fluticasone versus placebo for chronic asthma in adults and children. N.P. Adams, J.C. Bell, T.J. Lassrerson, P.W. Jones and C.J. Cates. *Cochrane database of systematic reviews (Wiley). Issue 2, Art. N° CD00315 DOI 10.1002/14651858 CD003135 pub 3.*

(4)   The price of innovation; new estimates of drug development costs. J.A. DiMassi, R.W. Hansen and H.G. Grabowski. *Journal of Health Economics.* *22, 151-185 (2003).*

(5)   United States Pharmacopeia (USP); Monogram on Paroxetine (the active drug in Paxil ®and Seroxat®).
http://www.pharmacopeia.cn/v29240/usp29nf24s0_m61180.html
(Accessed 25 July 2008)

(6)   GlaxoSmithKline Pharmaceuticals Paxil® information website.
http://www.PaxilCR.com (Accessed 25 July 2008)

(7)   United States Pharmacopeia (USP); Monogram on Cimetidine (The active ingredient in Tagamet®).
http://www.pharmacopeia.cn/v29240/usp29nf24s0_m17670.html   (Accessed 25 July 2008)

(8)   GlaxoSmithKline   Pharmaceuticals   Tagamet®   information   website.
http://www.tagamethb.com/ (Accessed 25 July 2008).

(9)   United States Pharmacopeia (USP); Monogram on Fluticasone Propionate
http://www.pharmacopeia.cn/v29240/usp29nf24s0_m34220.html.
(Accessed 25 July 2008)

(10)   British Pharmacopoeia; Monograph for Salmeterol Xinofoate, (2007).
http://www.pharmacopeia.co.uk (Accessed 25 July 2008).

(11)   GlaxoSmithKline   Pharmaceuticals   Advair®   information   website
http://www.Advair.com (Accessed 25 July 2008)

(12)   High throughput screening in drug discovery. Editor J. Huser, (Series Editors R. Mannhold, H. Kubinyi and G. Folkes). Wiley (2007). ISBN 978-3-527-31283-2.

(13)   Drug discovery: The leading edge. T. Chapman. *Nature.* *430, 109 - 115 (2004).*

(14)   Reshaping human antibodies for therapy. L. Riechmann, M. Clark, H. Waldermann and G. Winter. *Nature.* *332, 323-7 (1988).*

(15)   Antisense   Oligodeoxynucleotides   and   Antisense   RNA: Novel Pharmacological and Therapeutic Agents. B. Weiss, (ed.): CRC Press, Boca Raton, FL, (1997). ISBN-10:08493855520.

(16)   Antisense RNA gene therapy for studying and modulating biological processes. B. Weiss, G. Davidkova and L-W. Zhou. *Cell. Mol. Life Sci.* *55,*

17

334-358, (1999).

(17)   United States Food and Drug Administration (FDA) Regulatory guidelines. http://www.fda.gov/cder/regulatory/default.htm. (Accessed 25 July 2008)

(18)   Medicines and Healthcare products Regulatory Authority (MHRA) http://www.mhra.gov.uk/index.htm. (Accessed 25 July 2008)

(19)   *World Patent Information web site.* http://www.wipo.int/sme/en/faq/pat_faqs_q7.html (Accessed 25 July 2008)

(20)   Method development and validation for the HPLC assay (potency and related substances) for 20 mg paroxetine tablets. J. Lambropoulos, G. A. Spanos and N.V. Lazaridis. *J. Pharm. and Biomed. Analysis. 19, 793-802 (1999).*

(21)   HPLC method for the determination of cimetidine in tablets. The United States Pharmacopeia/ The national formulary, USP 24/NA19 Tablet analysis by HPLC United States Pharmacopeia Convention Inc, Rockville, MD, USA p412 -414 (2000).

(22)   Synthetic calibration for efficient method development: Analysis of tablet API concentration by near infra-red spectroscopy. R.P.Codgill, T.Herkert, C.A. Anderson and J.K. Drennen. *J. Pharma. Innov. 2, 93-105 (2007).*

(23)   Non-invasive bulk analysis of pharmaceutical tablets and capsules using the transmission Raman method. P. Matousek and A.W. Parker. *Central Laser Facility Annual Report, (2006 to 2007). http://www.clf.rl.ac.uk* (Accessed 25 July 2008).

(24)   World Health Organisation, (2007) (http://www.who.int/respiratory/en/ Accessed 25 July 2008).

(25)   World Health Organisation fact sheet (COPD) Number 315 August 2006. http://www.who.int/mediacentre/factsheets/fs315/en/. (Accessed 25 July 2008)

(26)   The cascade impactor: An instrument for sampling coarse aerosols. K.R. May. *J. Sci. Instrum. 22, 187-195, (1945).*

(27)   Multi-centre randomized placebo-controlled trial of inhaled fluticasone propionate in patients with chronic obstructive pulmonary disease. P. Paggiaro, R. Dahle, I. Bakran, L. Frith, K. Hollingworth and J. Efthimiou. *Lancet. 351, 773–80, (1998).*

(28)   Salmeterol, a new long acting inhaled β2 adrenoceptor agonist: comparison with salbutamol in adult asthmatic patients. A. Ullman and N. Svedmyr. *Thorax. 43, 674-678, (1988).*

(29)   Comparison of combination inhalers *vs* inhaled corticosteroids alone in moderate persistent asthma. D.K.C. Lee, C.M. Jackson, G.P. Currie, W.J. Cockburn and B.J. Lipworth. *Brit. J. Clin. Pharm. 56(5), 494–500, (2003).*

(30)   Information from the electronic medicines compendium on Serevent® *http://emc.medicines.org.uk/emc/assets/c/html/DisplayDoc.asp? format=original&documentid=3762.* (Accessed 25 July 2008).

(31)   GlaxoSmithKline Pharmaceuticals Flovent® information website *http://www.floventdiskus.com/* (Accessed 4 Sept 2008).

(32)   Boehringer-Ingelheim Pharmaceuticals, Combivent® information website http://www.combivent.com (Accessed 25 July 2008).

(33)   Astra-Zeneca Pharmaceuticals Symbicort® information website *http://www.mysymbicort.com/symbicort/controlling-your-asthma/asthma-control.aspx* (Accessed 25 July 2008).

(34)   GlaxoSmithKline Pharmaceuticals Ventolin® information website *http://www.ventolin.com* (Accessed 25 July 2008).

(35)   Personal Communication. P.Burnnell, GSK Ware.

(36)   Enhanced synergy between fluticasone propionate and salmeterol inhaled from a single inhaler versus separate inhalers. H. Nelson, K. Chapman, S. Pyke, M. Johnson and J. Pritchard. *J. Allergy Clin. Immunol. 112, 29-36, (2003).*

(37)   US Pharmacopoeia Chapter 601. Aerosols, nasal sprays, metered dose inhalers, and dry powder inhalers. *http://www.usp.org* (Accessed 25 July 2008).

(38)   The science of nebulised drug delivery. C. O'Callaghan, P.W. Barry. *Thorax. 52 (Suppl. 2), S31-S44, (1997).*

(39)   Foreign Particles Testing in Orally Inhaled and Nasal Drug Products. J. Blanchard, J. Coleman, C.D. Abreu-Hayling, R. Ghaderi, B. Haeberlin, J. Hart, S. Jensen, R. Malcolmson, S. Mittelman, L.M. Nagao, S. Sekulic, C. Snodgrass-Pilla, M. Sundahl, G. Thompson and R. Wolff. *Pharma. Res. 21, 2137-2147, (2004).*

(40)   Performance of a TSI aerodynamic particle sizer. B. Chen, Y.S. Cheng, and C.H. Yeh. *Aerosol Sci. Technol. 4, 89-97, (1985).*

(41)   Squeezing blood out of a turnip; why the pharmaceutical industry struggles so much with impactor data. S.Stein. *AAPS,ITFG meeting "Applications and Calibration for Cascade Impaction" 30 September 2005.* http://www.aapspharmaceutica.com/inside/Focus_Groups/IT/imagespdfs/ Stein.pdf#search=%22Andersen%20cascade%20Impaction%22 (Accessed 25 July 2008).

(42)   Experimental determination of the regional deposition of aerosol particles in the human respiratory tract. W. Stahlhofen, J. Gebhart and J. Heyder. *American Industrial Hygiene Association Journal. 41, 385-399, (1980).*

(43)   Co-deposition of salmeterol and fluticasone propionate by a combination inhaler. A. Theophillus, A. Moore, D. Prime, S. Rossomanno, B. Whitcher and H. Chrystyn. *Int. J. Pharmaceutics. 313, 14-22, (2006).*

(44)   The characterization of aerosols distributed with respect to size and composition. S.K. Freidlander. *Aerosol Sci. 1, 295-307, (1970).*

(45)   The characterization of aerosols distributed with respect to size and composition part 2. S.K. Freidlander. *Aerosol Sci. 2, 331-340, (1971).*

(46)   Air pollution and health – Good news and bad. C.A. Pope. *New England Journal of Medicine. 351, 1132-1134, (2006).*

(47)   The role of oxidative stress in lung injury induced by cigarette smoke. Z. Kluchova and R. Tkacova. *Biologia. 61, 643-650, (2006).*

(48)   The epidemiology of asbestos-related diseases. J. Niklinski, W. Niklinska, E. Chyczewska, J. Laudanski, W. Naumnik, L. Chyczewski and E. Pluygers. *Lung Cancer. 45 (Suppl. 1), S7 - S15, (2003).*

(49)   Bio-aerosols Handbook. Editors C. S. Cox and C. M. Wathes. CRC Press: Boca Raton, Florida, (1995). ISBN-13:978-0873716154.

(50)   Recent advances in our understanding of atmospheric chemistry made possible by on-line aerosol analysis instrumentation. R.C. Sullivan and K.A. Prather. *Anal.Chem. 77, 3861-3886, (2005).*

(50a)   Particulate Emissions from Commercial Shipping: Chemical, Physical, and Optical Properties. D. Lack, J. Corbett, T. Onasch, B. Lerner, P. Massoli, P. Quinn, T. Bates, D. Covert, D. Coffman, B. Sierau, S. Herndon, J. Allan, T. Baynard, E. Lovejoy, A. Ravishankara. *Journal of Geophysical Research - Atmospheres, 114, D00F04, (2009).*

(50b) Oxygenated Fraction and Mass of Organic Aerosol from Direct Emission and Atmospheric Processing Measured on the R/V Ronald Brown During TEXAQS/GoMACCS 2006. L. Russell, S. Takahama, S. Liu, L. Hawkins, D. Covert, P. Quinn, and T. Bates.. *Journal of Geophysical Research - Atmospheres 114, D00F05, (2009).*

(51) Study of cigarette smoke aerosol using time-of-flight mass spectrometry R. Yadav, K. Saoud, F. Rasouli, M. Hajaligol and R. Fenner. *J. Anal. and App. Pyrolysis. 72, 17-25, (2004).*

(52) A single particle characterization of a mobile versatile aerosol concentration enrichment system for exposure studies. E.J. Freney, M.R. Heal, R.J. Donovan, N.L. Mills, K. Donaldson, D.E. Newby, P.H.B. Fokkens and F.R. Cassee. *Particle and Fibre Technology. 3, 8, (2006).*

(53) Desorption/ionization fluence thresholds and improved mass spectral consistency measured using flattop laser profile in the bio-aerosol mass spectrometry of single bacillus endospores. P.T. Steele, A. Srinvastava, M. Pitesky, D. Fergenson, H. Tobais, E.E. Gard and M. Frank. *Anal. Chem. 77, 7448-7454, (2005).*

(54) Particle-lung interactions. H. Schulz. *Journal of Aerosol Science. 30, (Suppl 1), S585-S588 (1999).*

(55) Reduction in fine particulate air pollution and mortality. F. Laden, J. Schwartz, F.E. Speizer and D.W. Dockery. *Am. J. Resp. Crit. Care Med. 173, 667-672, (2006).*

(56) Single particle characterization of albuterol metered dose inhaler aerosol in near real time. C. Noble and K. Prather. *Aerosol Sci.Technol. 29, 294-306, (1998).*

(57) Identification of APIs by AToFMS in individual particles actuated from Combivent MDI. R. Karisson, M. Gailli, F. Etzler. *Proceedings of 'Drug Delivery to the Lungs XIII' Symposium London, December 2002.*

(58) Species selective and single particle size and compositional analysis for respiratory drug delivery products and powders. T.B. Fields. *Polymeric Materials Science and Engineering, 87, 337, (2002).*

(59) Applications and evaluation of an aerosol time-of-flight mass spectrometer. E. Freney, *PhD Thesis, School of Chemistry, University of Edinburgh, March 2006.*

(60) Chemometrics: Data analysis for the laboratory and chemical plant. R. Brereton. First edition (2003), Wiley-Blackwell. ISBN 0-471-489 786.

Chapter 2

Instrumentation

2.1 Introduction

In the first part of this chapter the historical development of single particle mass spectrometers, from the early 1970s to the present time, is discussed with an emphasis on the instruments and techniques used for the work described in this thesis.

For the single particle mass spectrometry experiments on inhalation products no sample preparation was required. However because material is released from the inhaler device during a short period (less than 1 second) after actuation, it was necessary to condition the sample using the apparatus described in Section 2.4.1.

In the latter part of this chapter (Sections 2.4.2 and 2.4.3) a detailed description is given of the operation of the commercially available Aerosol Time-of-Flight Mass Spectrometer (AToFMS) (TSI, Shoreview, MN, USA) and the Aerodyne Aerosol Mass Spectrometer (AAMS) (Aerodyne, Billerica, MA,USA).

2.2 A Brief History of Single Particle Mass Spectrometry

In the early 1970s a proposal was outlined for an instrument that could identify the chemical composition of aerosols in real-time (or near real-time). It was predicted that the linking the composition and size of each individual particle in a given aerosol would be very useful, but was difficult with the contemporary instrumentation[1]. Among the drivers for developing the single particle mass spectrometry technique, was the importance of measuring particle size and composition in relation to lung function. This aligned the analysis of particles with mass spectrometry and aerosols that could interact with the lungs; for example, cigarette smoke[2].

The main features of single particle mass spectrometers are summarized in Section 1.7. The history of some of the most significant advances of single particle mass spectrometry since the early 1970s is summarized in Table 2.1[3 to 24]. Several reviews of this area are available in the literature[3,4,5] and only a brief overview is given here. Much of the development of this type of instrumentation has been focussed on the inlet system, the particle sizing region and the mass spectrometer, and these are described in more detail in Section 2.3.

2.3 The Components of the Single Particle Mass Spectrometer

2.3.1 Inlets

The inlet device has a role in delivering the particles from the aerosol cloud into the mass spectrometer as a focussed beam[25]. The first SPMS instruments used a needle valve and a pinhole orifice to introduce the sample into the ionization source region[6]. This type of inlet was not very efficient in terms of particle transmission (*e.g.* Davis[6] reported a particle transmission/detection efficiency of 0.2 to 0.3 %) as it was susceptible to errors because of beam divergence[7]. Later a more controlled method for sample introduction was developed where the particles entered the instrument through a capillary-nozzle inlet[8].

A nozzle-skimmer inlet was used on a number of versions of the AToFMS instrument[16]. A diagram of a nozzle-skimmer inlet is shown in Figure 2.1. Using this device a particle beam is formed when the aerosol expands through the converging nozzle into the vacuum. For this inlet, the pressure differential between the atmosphere at ~760 Torr and the inside of the inlet at ~2 Torr (1 Torr = 133 Pa), causes the gas to undergo a supersonic expansion during which small particles are accelerated to higher terminal velocities than the larger particles[26]. The size-dependent velocity distribution is the basis for determining the aerodynamic diameter of particles and is discussed further in Section 2.3.2.

Year	Inlet	Particle sizing method	Ionization technique	Mass spectrometer	Author (Ref)	
1973	Needle/valve	Ion signal intensity	SDI	Magnetic Sector	Davies	(6,7)
1974	Needle/valve	None	SDI	Quadrupole	Lassiter	(8)
1976	Capillary nozzle	Ion signal intensity	SDI	Magnetic Sector	Stoffels	(9)
1981	Capillary, skimmer	Ion signal intensity	SD/EI	Quadrupole	Allen	(10)
1982	Nozzle- skimmer	Aerodynamic sizing	SD/EI	Magnetic Sector	Sinha	(11)
1988	Capillary inlet	Aerodynamic sizing	LDI	Time-of-Flight (ToF)	Marijnssen	(12,13)
1991	Nozzle skimmer	None	LDI	Linear ToF	Johnson	(14)
1993	Nozzle skimmer	Light scattering	LDI	Reflectron ToF	Murphy	(15)
1994	Nozzle skimmer	Aerodynamic sizing	LDI	Reflectron ToF	Prather	(16)
1995	Nozzle skimmer	Aerodynamic sizing	LDI	Reflectron ToF	Johnson	(17)
1996	Aerodynamic lens	Aerodynamic sizing	LDI	Linear ToF	Spengler	(18)
1998	Aerodynamic lens	Light scattering	APCI	Ion trap	Hoffman	(19)
2000	Aerodynamic lens	Aerodynamic sizing	Hotplate/ EI	Quadrupole	Jayne	(20)
2005	Nozzle skimmer	Aerodynamic sizing	CI	Ion trap	Whitten	(21)
2005	Aerodynamic lens	Aerodynamic sizing	Hotplate/ EI	Reflectron ToF	Jayne	(22)
2006	Aerodynamic lens	Aerodynamic sizing	Li + Attachment	Reflectron ToF	Canagaratna	(23)
2006	Aerodynamic lens	Aerodynamic sizing	Photoionization	Reflectron ToF	Northway	(24)

Table 2.1. History of the most significant advances in single particle mass spectrometry: Ionization techniques abbreviated as SDI = Surface Desorption Ionization, EI = Electron Ionization, LDI = Laser Desorption Ionization, CI = Chemical Ionization, APCI = Atmospheric Pressure Chemical Ionization.

24

Figure 2.1 shows that the inlet device consists of a nozzle and a skimmer; the function of the nozzle is as an interface between the atmosphere and the first stage of vacuum i.e. it allows a reduction in pressure (to ~2 Torr (~266 Pa)). The function of the skimmer, located prior to the particle sizing region, is primarily to collimate the particle beam.

A limitation of the nozzle-skimmer interface is that not all of the particles are transmitted with equal efficiency. It has been shown that the larger particles are transmitted with a higher efficiency than smaller particles, and that a correction must be used to relate the transmission efficiency to the aerodynamic diameter of each particle[27]. This correction is effectively a calibration which is used to scale the AToFMS data to yield continuous mass concentrations as a function of particle size over the sampling time and has been applied in a number of environmental studies[27]. However the data presented in this thesis, acquired using the nozzle-skimmer inlet, was used only to determine the presence of co-association independently of the particle size measurement; hence a correction factor was not applied in this case.
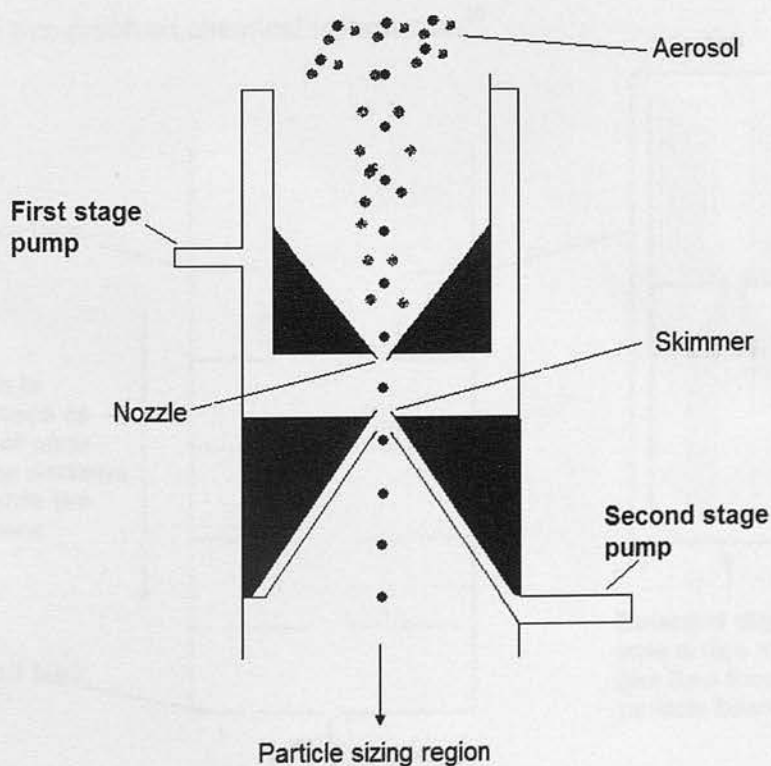
Figure 2.1. Diagram of the nozzle-skimmer inlet used for the AToFMS instrument. As there is a pressure drop across this inlet, particles are accelerated to different velocities depending on size before entry to the particle sizing region.

The aerodynamic lens is an alternative inlet currently employed by the two commercially available instruments[28, 29]. This device consists of a series of six lenses (discs) with orifices ranging from the largest at the entrance lens (typically 5 mm) to the smaller exit aperture (typically 3 mm) as shown in Figure 2.2[30, 31].

As the aerosol passes through the first lens the larger particles are focussed towards the central axis of the aperture. Conversely, smaller particles remain outside the centre line along the path of the expanding gas stream. This is also shown in Figure 2.2.

The second lens focuses more of the smaller particles and refocuses some of the larger particles that may have drifted due to diffusion. So, as the particles pass through each of the orifices of decreasing size, the beam becomes progressively narrower, until at the exit orifice particles emerge as a highly focussed particle beam of low divergence[23].

The main advantage of the aerodynamic lens is that it gives higher particle transmission efficiency (especially for smaller particles) which results in improved temporal and size-resolved chemical information[30].
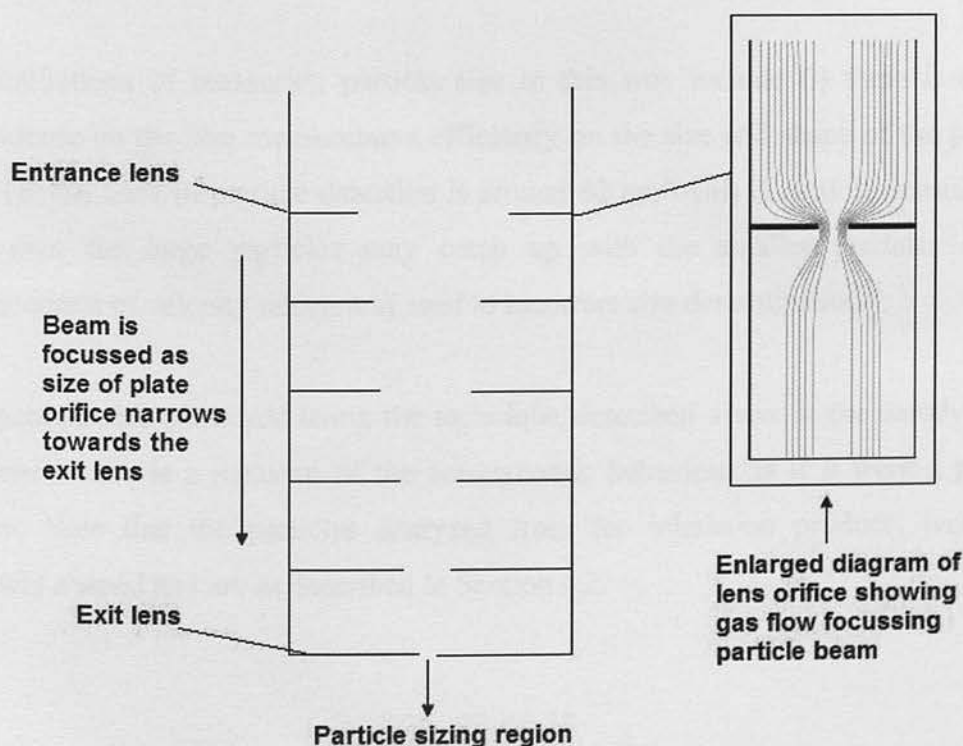
Figure 2.2. Diagram of an aerodynamic lens inlet as used on the AToFMS and AAMS instruments. Particles in the aerosol are focussed into a narrow beam by the narrowing lens orifices, prior to the particle sizing region[30, 31].

2.3.2 Particle Sizing Methods

Early particle sizing methods were based on a comparison of the number of ions detected by the mass spectrometer and the number concentration measured with a condensation nuclei counter (an optical method used for counting particles). Using this method a range of sizes from 4 nm to 1.3 µm could be measured[6, 7].

Later SPMS instruments used optical detection so that the intensity of the light scattered as the particle crossed a laser beam could be correlated to particle size[32, 33]. Further development of optical detection resulted in instruments equipped with two lasers in the particle sizing region, hence the time taken for particles to travel between the two laser beams (the transit time) could be measured[34]. The transit time could then be converted into an aerodynamic particle size scale if the instrument was calibrated with particles of a known size, typically polymer beads[35]. This type of sizing technique relies on particles of different sizes having different terminal velocities as they are accelerated into the particle sizing region by the pressure differential between the inlet and particle sizing region. In this case the smaller particles experience the highest acceleration and gain the highest terminal velocity.

The limitations of measuring particle size in this way include (i) there is a high dependence on the size measurement efficiency on the size and shape of the particle [32, 36], (ii) the limit of particle detection is around 80 nm[32] (iii) if particle densities are high then the large particles may catch up with the smaller particles during measurement of velocity which may lead to incorrect size determination[36].

The particle size measured using the technique described above is the aerodynamic diameter which is a measure of the aerodynamic behaviour as if it were a perfect sphere. Note that the particles analyzed from the inhalation products were not regularly shaped and are as described in Section 4.2.

2.3.3 Ionization Techniques

The commercial instruments used for the work described in this thesis used either laser desorption ionization (as in the case of the AToFMS instrument) or electron ionization (as in the case of the AAMS instrument) and an overview of these techniques is given, together with a brief discussion of other ionization techniques used during the development of SPMS.

2.3.3.1 Surface Desorption Ionization

With the first instruments ionization was achieved when particles hit a heated metal (typically rhenium) filament or ribbon held at high temperature, (in the range 500 to 2000 °C) resulting in formation of neutral and ionic species [6, 7, 8, 9].

2.3.3.2 Electron Ionization

Electron ionization is a technique that is based on the interaction of a beam of electrons with analyte molecules in the gas phase. Hence, prior to electron ionization (EI), it is necessary to vaporize the particle and various methods for doing this in SPMS instruments have been reported. In the early 1980s an SPMS instrument was built that used a heated coiled wire to vaporize the samples which were then ionized using a beam of electrons[10]. The efficiency of the vaporization was later improved by using a V-shaped filament[11] or in the case of the Aerodyne instruments a hotplate as described in Section 2.4.3.

By convention electron ionization mass spectra are acquired at 70 eV because this gives a yield of ions close to the maximum and also a yield that is near constant over a small voltage range[37]. The beam of energetic electrons (shown in Equation 2.1 as e⁻) interact with the analyte molecules (M) in the gas phase by passing close to or through the molecule[38]. This can lead to electronic excitation in the molecule by promoting an electron from a lower to higher orbital or ejection from the molecule to leave a positive ion. In the latter case (as summarized in Equation 2.1), the ion formed is a radical cation or molecular ion which may initially exist in an excited energy state

$(M^+)^*$. Relaxation from this higher energy state can result in fragmentation (as summarized, by Equation 2.2), which is unique to that particular molecule:

$$M + e^- \rightarrow (M^+)^* + 2e^- \qquad\qquad \textbf{Equation 2.1}$$

$$(M^+)^* \rightarrow (M^+) + A^+, B^+, etc. \qquad\qquad \textbf{Equation 2.2}$$
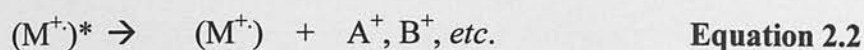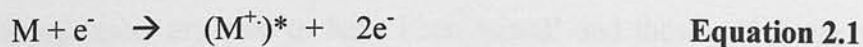
2.3.3.3 Laser Desorption and Ionization

Laser ablation involves a short pulsed, high power laser beam focused onto a surface or, in the case of SPMS instruments, focussed onto a particle. The amount of ablation depends on the wavelength of the laser, pulse duration, fluence and laser beam profile[39].

The ablation process involves the transfer of energy from the laser beam to the atomic lattice causing melting and vaporization. Following ablation of solid surfaces the laser beam can interact with the expanding plasma plume. The absorption of laser energy by the plasma depends strongly on the laser wavelength; typically plasma absorption is greater at longer wavelengths. Short UV wavelengths penetrate the plasma more efficiently and directly initiate bond breaking in the sample[40].

Ionization of organic compounds with a laser will only occur if the compound absorbs radiation at the wavelength of the laser[41]. With most instruments vaporization and ionization of particles is achieved in a single step[12 to 15]. In this case, for organic species extensive fragmentation can result in spectra that are difficult to interpret. However, if two lasers are used the ablation and ionization steps are decoupled and each may be separately adjusted specifically for the compound(s) of interest[42, 42a]. Clearly this results in a much more complex instrument and such systems are not yet commercially available.

The ablation laser can be synchronized with the particle sizing lasers as in the case of the AToFMS instrument (This is described in more detail in Section 2.4.2). In this case, the transit time of the particle between the two sizing laser beams is measured and hence the time at which the ablation laser needs to fire to hit the particle can be

computed. The alternative to synchronizing the sizing and ablation lasers is to continuously fire the ablation laser; however, the probability of hitting a particle with the laser beam then becomes much lower[41]. Note that particles which are detected by both timing lasers are said to have been 'sized' and those which are desorbed and ionized by the third laser to produce mass spectra are said to be 'hit'[27].

2.3.3.4 Soft Ionization Methods

Many of the ionization methods used in SPMS are highly energetic. In some cases so much so that the vaporization / ionization technique can reduce the particle material to the elemental form. For particles that contain organic materials, detail of the structure can be lost if extensive fragmentation occurs[40,43]. Hence, some instruments have been fitted with ionization sources capable of softer ionization, in an attempt to detect intact organic species.

For example an SPMS instrument was equipped with a modified atmospheric pressure chemical ionization (APCI) source. Particles were sampled through a ceramic tube into the centre of the APCI ion source. The aerosol together with a sheath flow of nitrogen was introduced into an interface vaporizer held at temperatures up to 450 °C. Airborne particles were then vaporized at atmospheric pressure without impacting on the vaporizer surface and the resulting gas phase molecules reacted with primary ions generated by a corona discharge in the ion source region[19].

Lithium ion attachment has been demonstrated during SPMS experiments on oleic acid. This type of experiment results in the formation of a Li adduct ion and in the case of oleic acid the ion at m/z 289 due to $(M + Li)^+$ dominates the mass spectrum[23].

Vacuum ultraviolet photoionization has also been recently introduced as an option for soft ionization of materials during a SPMS experiment. This was shown to give mass spectra with minimal fragmentation and hence an improved method for speciation of organic materials[24].The use of tunable UV radiation from a synchrotron with SPMS instruments has also been demonstrated[44, 45]. In this case mass spectra were obtained that showed only the molecular ion (M^+); example applications include stearic acid and oleic acid.

2.3.4 Mass Analyzers

Four types of mass analyzer have been prominent in the development of SPMS; these are the magnetic sector, the quadrupole, the ion-trap mass spectrometer and the time-of-flight (ToF) mass analyzer. As with other mass spectrometry experiments each has advantages depending on the information required from the experiment. The instruments used to produce the data described in this thesis were based on either quadrupole or ToF analyzers, and a detailed description is given for these, together with a brief discussion of the magnetic sector and ion trap analyzers.

2.3.4.1 Magnetic Sector Mass Analyzers

For the single focussing magnetic sector mass spectrometer a magnetic field is used as the mass analyzer. At the exit of the ionization source, small potentials are applied to a pair of electrodes used to focus the ion beam that enters the magnetic field through an ion slit which is used to control the width and shape of the ion beam.

The magnet causes the ion beam to be deflected in a circular path[37] as shown in Figure 2.2a. The magnitude of the deflection depends on the momentum of the ion.
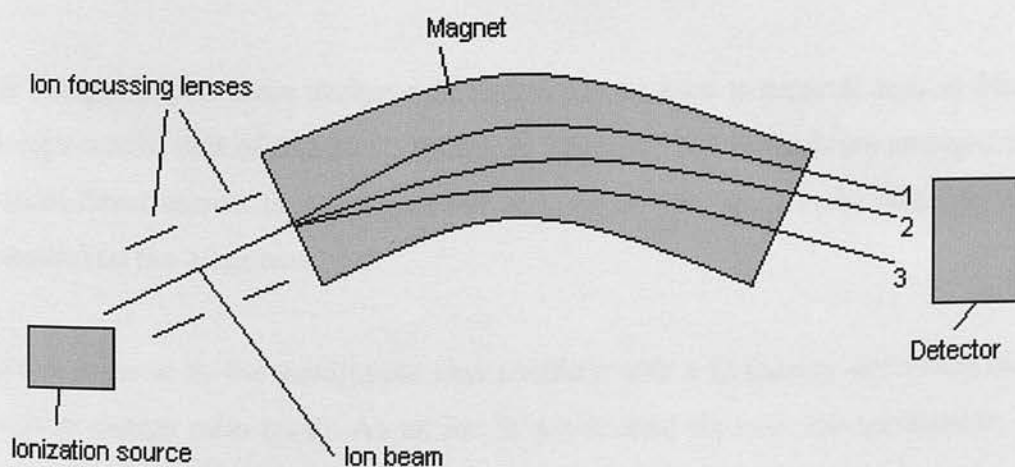
Figure 2.2a. *Diagram of magnetic sector mass spectrometer. Shows ion beam containing ions of different m/z values are separated by the influence of the magnetic field. Ions 1, 2 and 3 are deflected by different amounts depending on m/z value. In this case Ion 3 is the heaviest and is deflected the least. Ion 1 is the lightest and deflected the most* [37,38].

The *m/z* value of the ions which can pass though the exit slit depends on the radius of the ion path (r), the magnetic field, the field strength(B) and the ion accelerating potential (V, volts) as defined by :

$$m/z = \frac{B^2 r^2}{2V}$$

This is derived on the basis that ions of charge e have all been given the same kinetic energy $eV = \frac{1}{2} mv^2$ (but different velocities v) in acceleration, and that the force excerted by the magnet (Bev) must be equal to the centrifugal force mv^2/r. Spectra are obtained on magnetic sector instruments of this type by holding the voltage V constant while varying the field on the magnet B[37].

Most of the mass spectrometers used for single particle mass spectrometry in the early 1970s were based on magnetic sector analyzers. For example the instrument described by Davis[6,7] was a conventional magnetic sector analyzer but with an inlet and ionization source modified to allow single particle analysis. The magnetic sector analyzers had the advantage of good resolution but were disadvantaged by a slow scan rate. These instruments were also heavy and so not portable[6, 7, 9, 11].

2.3.4.2 Quadrupole Mass Analyzers

For the quadrupole mass analyzer electric fields are used to separate ions as they pass along a central axis of four rods. As shown in Figure 2.3, the rods are arranged so that a fixed direct current (dc) is applied to one pair of rods and a radio frequency (rf) ac potential on the other two.

At the entrance to the quadrupole ions oscillate with a frequency depending on their mass to charge ratio (*m/z*). As an ion is accelerated through the quadrupole, if the frequency is compatible, the ion will travel all the way through to the detector. If the strength and frequency of the electric fields are varied then a range of *m/z* values can be filtered to produce a mass spectrum. The passage of an ion through the quadrupole is described by the Mathieu equation[46].
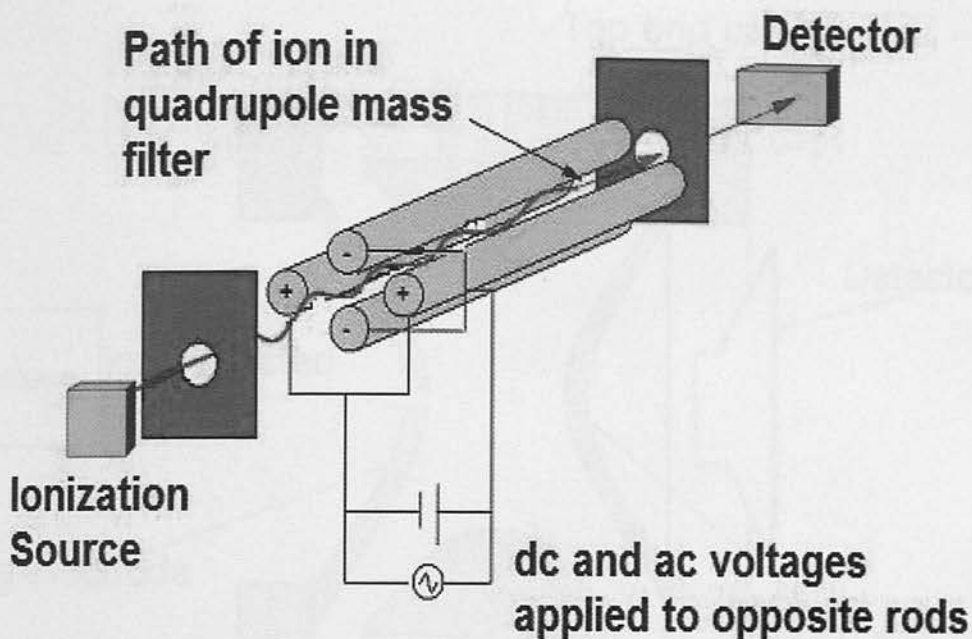
Figure 2.3. *Diagram of a quadrupole mass analyzer. Voltages are applied to the quadrupole rods so as to allow ions of specific m/z to travel though to the detector. Varying the voltage allows scanning of an m/z range*[46].

As the quadrupole is a scanning device and the scanning speed is relatively slow (compared with the data acquisition speed of a ToF), only one ion per particle could be measured when used in SPMS experiments. This meant that representative marker ions were used to confirm the presence of a given compound in each particle rather than the full scan spectra.

Towards the end of the 1970s decade an SPMS instrument was built that used a quadrupole mass filter as the mass analyzer[10]. As this type of instrument was physically smaller and lighter than the magnetic sector instruments used previously, this meant that the instrument could be transported and used in the field.

2.3.4.3 Ion Trap Mass Spectrometry

The quadrupole ion trap is an ion storage and mass analysis device. The trap consists of a ring (doughnut shaped) electrode and two end caps as shown in Figure 2.2b and these form an electric field in which the ions are trapped. Hence instead of the ions passing through a central axis of rods as per the quadrupole (as discussed in Section 2.3.4.2), the ions are trapped in a 3-dimensional volume and detected based on their mass to charge (*m/z*) ratio[47,48].
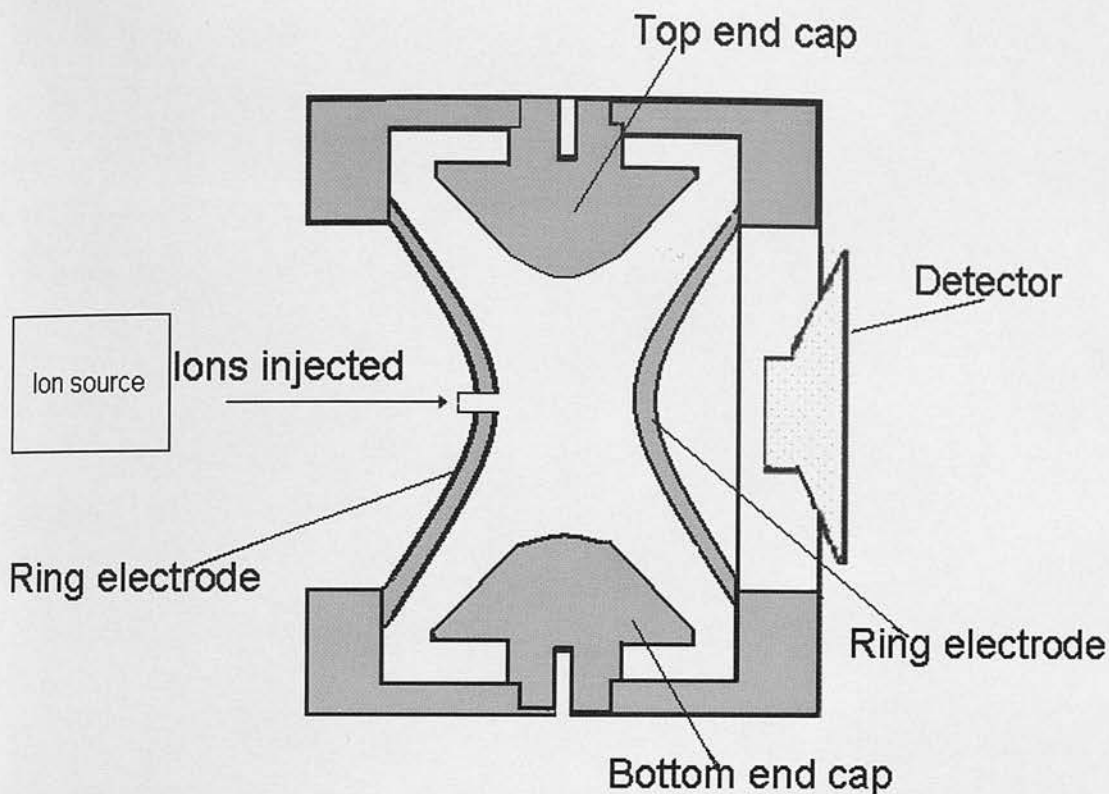
Figure 2.2b. Schematic of ion trap mass analyzer[47].

Ions created in the ionization source (for example by electron ionization (EI), electrospray (ESI), or matrix-assisted laser desorption ionization (MALDI)) are focused into the ion trap using an electrostatic lens system.

If too many ions are stored in the trap, a distortion of the electrical fields may occur leading to an overall reduction in performance and this is known as a space-charge effect. To reduce these effects the ions are allowed into the trap via an electrostatic gate which pulses open and closed to inject ions into the ion trap. The pulses can be adjusted to prevent overloading of the trap. The pulsing of the ion gate differentiates ion traps from "beam" instruments such as quadrupoles where ions continually enter the mass analyzer[48].

The ion trap is typically filled with helium to a pressure of about 1 mtorr (133 mPa). Collisions with helium dampen the kinetic energy of the ions and contracts trajectories toward the centre of the ion trap, enabling trapping of injected ions.

Trapped ions are further focused toward the centre of the trap through the use of an oscillating potential, applied to the ring electrode. An ion will be stably trapped depending upon the values for the mass and charge of the ion, the size of the ion trap ,

the oscillating frequency of the fundamental radio frequency voltage (rf), and the amplitude of the voltage on the ring electrode.

An advantage of the ion trap is that is can be used for MS/MS analysis, which adds to the selectivity of the experiment and increases the amount of structural information available on the analyte of interest.

An SPMS experiment reported in the late 1980s was based on an ion trap mass spectrometer. This type of instrument has the advantage of selectivity through its tandem mass spectrometry capability. Also it was able to scan fast enough to give a full mass spectrum of each particle[19, 21].

2.3.4.4 Time-of-Flight Mass Analyzers

Time-of-flight analyzers offer an advantage over scanning instruments (such as quadrupole mass analyzers) as data acquisition rates are much faster; thus in the SPMS experiment a full mass spectrum (or several full mass spectra) may be collected for each particle[49, 50].

The early ToF based SPMS instruments typically used a linear ToF but these instruments were capable of only low poor mass resolution[14]. The instruments designed and built in the late 1990s were based on reflectron ToF instruments and these were capable of giving mass spectra with improved mass resolution. The commercially available aerosol time-of-flight mass spectrometer described in Section 2.4.2, is comprised of two reflectron ToF analyzers so that positive and negative ions from the same particle may be detected simultaneously[16]. A series of instruments currently commercially available from Aerodyne are based on a reflectron ToF[22] including an instrument that is capable of accurate mass measurement of ions observed in the mass spectra of single particles[51].

A separation of ions within a ToF analyzer is achieved because the velocity and hence flight time is dependent on mass, *i.e.* the heavier ions take a longer time to arrive at the detector than the lighter ions.

Ions created in the ion source are accelerated into the flight-tube by an electrical potential in the source region. As the ions of mass (m) enter the flight-tube they move at a velocity (v) acquired from their initial acceleration in the ionization source. As they leave the ionization source, all ions have the same kinetic energy (KE) as shown by Equation 2.3.

$$KE = \tfrac{1}{2}\, m_1 v_1^{2} = \tfrac{1}{2}\, m_2 v_2^{2} = \tfrac{1}{2}\, m_3 v_3^{2} \; etc. \qquad \textbf{Equation 2.3}$$

So for a range of molecular weights (m_1, m_2 *etc.*) and in this case assuming that the ion is singly charged (*i.e.* $z = 1$), the velocity (v) of each ion is given by Equation 2.4 in which the KE is constant.

$$v = \sqrt{\frac{2 \times KE}{m}} \qquad\qquad \textbf{Equation 2.4}$$

When the ions are produced in the source there is a small spread of kinetic energies which originates partly because ions are formed in different regions of the source; as a result they are accelerated to slightly different final kinetic energies[49]. In a linear ToF this small spread of kinetic energies can result in poor resolution. If a reflectron, as shown in Figure 2.4, is used to correct the energy spread an improved resolution is obtained.

The reflectron consists of a number of parallel concentric electrodes to which a potential ramp is applied. As ions enter the reflectron they slow down, stop and are then accelerated in the opposite direction. Ions with a higher energy penetrate the reflectron deeper than ions with lower energy. Hence, faster ions travel deeper into the reflectron than slower ions of the same mass to charge ratio. This causes slower and faster ions to reach the detector at the same time hence a good resolution is achievable.
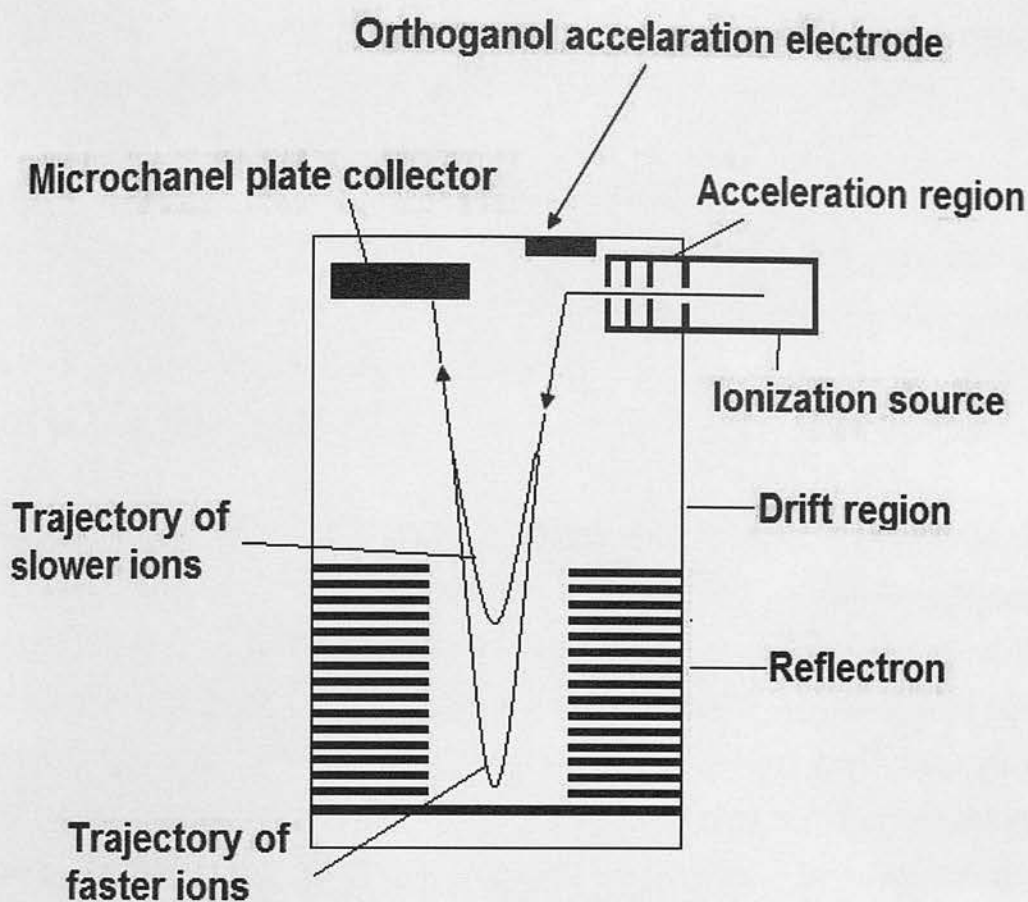
Figure 2.4. *Diagram of a reflectron time-of-flight (ToF) mass analyzer. The ion beam path through the reflectron is such that the ion energies are focussed hence enhancing the resolution (compared with a linear ToF instrument)[49].*

2.4 Instrumentation for the Study of Inhalation Products

The instrumentation used for the work described in this thesis is discussed below. For the single particle mass spectrometry experiments on inhalation products, no sample preparation was required although the sample was conditioned prior to analysis *via* a sampling apparatus which is described in Section 2.4.1.

The latter part of this chapter (Sections 2.4.2 & 2.4.3) describes the commercially available instruments that were evaluated during the course of this work.

2.4.1 Sample Conditioning Apparatus

For a SPMS experiment to monitor an environmental aerosol, the local atmosphere can be sampled and analyzed over a period of hours or days. For inhalation Product

analysis, the SPMS experiment needs some modification as material is released from the inhaler device during a short period (less than 1 second) after actuation.

Hence, experiments on aerosols derived from inhalation products were performed by actuation of the device into a settling chamber. The SPMS instrument was used to sample and analyze the particles held in Brownian motion typically over a period of 10 to 15 minutes. The technique described and used in this work was similar to a technique previously reported[52] but with some modification[53] as described below.

Figure 2.5 shows the sample introduction apparatus used to condition materials from a dry powder inhaler (DPI). Also a photograph of this apparatus is shown in Figure 2.6. The DPI device was actuated, placed in an airtight plastic chamber and then a flow of air at approximately 60 L min^{-1} generated with a 3 litre syringe was used to carry the particles from the inhaler through a twin impinger[54] to the 5 L glass settling chamber. The impinger stage was included so as to remove the larger particles (> 6 µm) present (many of which were captured in the water trap in the lower stage of the twin impinger); thus avoiding blockage of the MS inlet. Scanning electron microscope images of the larger particles are described in Section 4.2.

The sample conditioning apparatus was cleaned between runs by either back flushing with air or by washing with solvent.
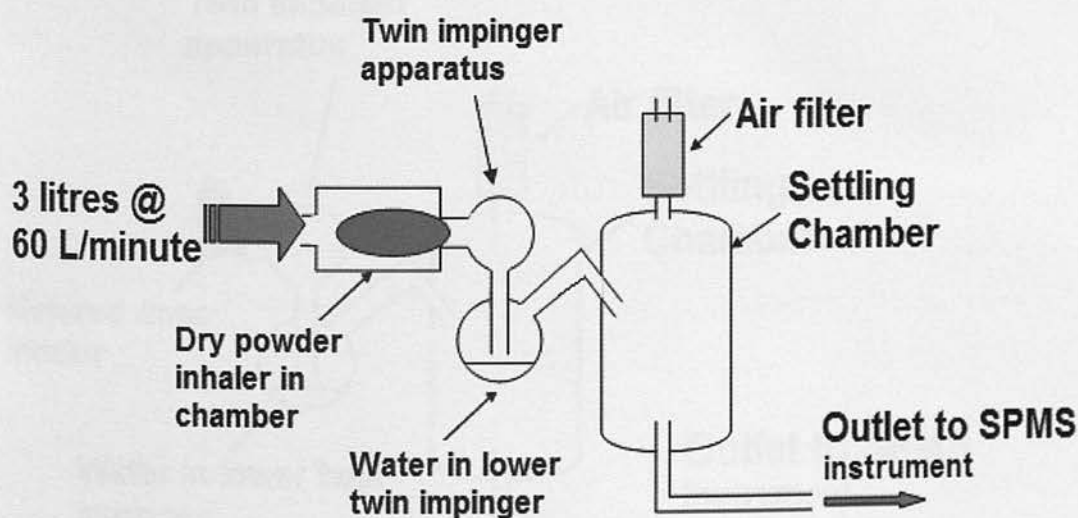
Figure 2.5. Diagram of sample introduction apparatus for DPIs in SPMS experiments. The DPI was actuated, placed in the airtight chamber and a flow of air carried the powder into the twin impinger.
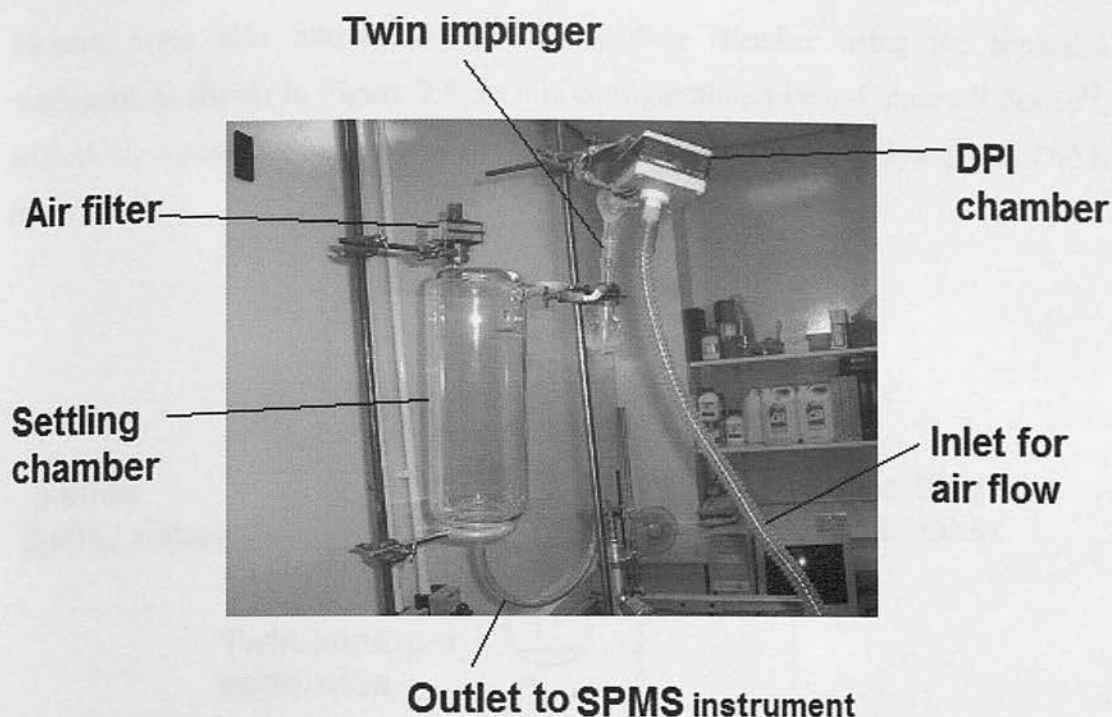
Figure 2.6. *Photograph of sample introduction apparatus for DPIs in single particle mass spectrometry experiments (photograph show the apparatus connected to the aerodynamic lens inlet of the AToFMS instrument).*

The contents of pressurized metered dose inhalers (pMDIs) were also sampled from the settling chamber using a similar apparatus to that described above, except that as the pMDI device contains a propellant, an additional flow of air was not required to transfer the particles into the settling chamber. Hence, the device was actuated directly into the twin impinger, as shown in Figure 2.7.
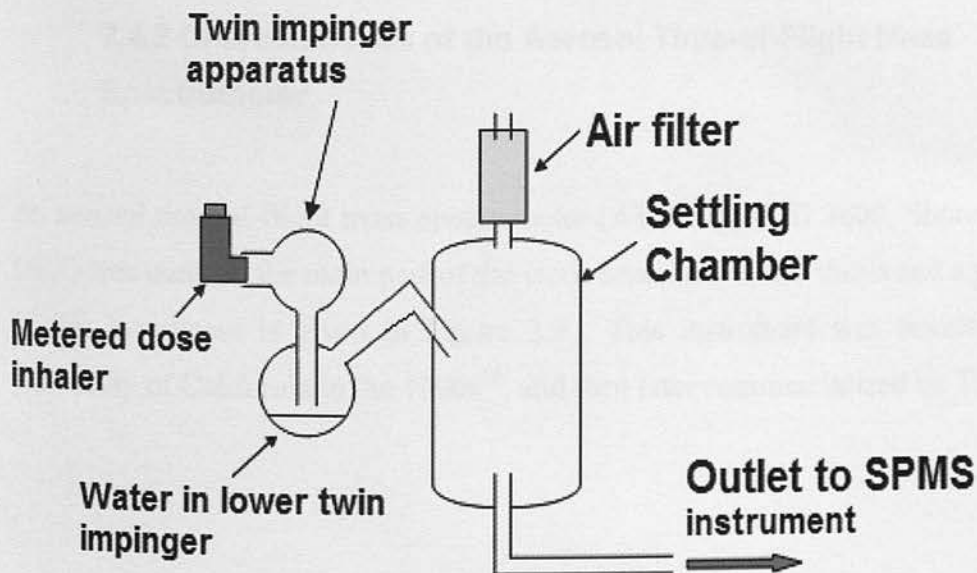
Figure 2.7. *Diagram of sample introduction apparatus for pMDI in single particle mass spectrometry experiments. The pMDI was actuated directly into the twin impinger; Material flowed through the impinger then into the settling chamber.*

Powders were also introduced into the settling chamber using the apparatus configured as shown in Figure 2.8. In this configuration a Penn-Century™ device[55], (effectively a powder syringe) was used to inject the powder into a flow of air of 60 L min^{-1}.
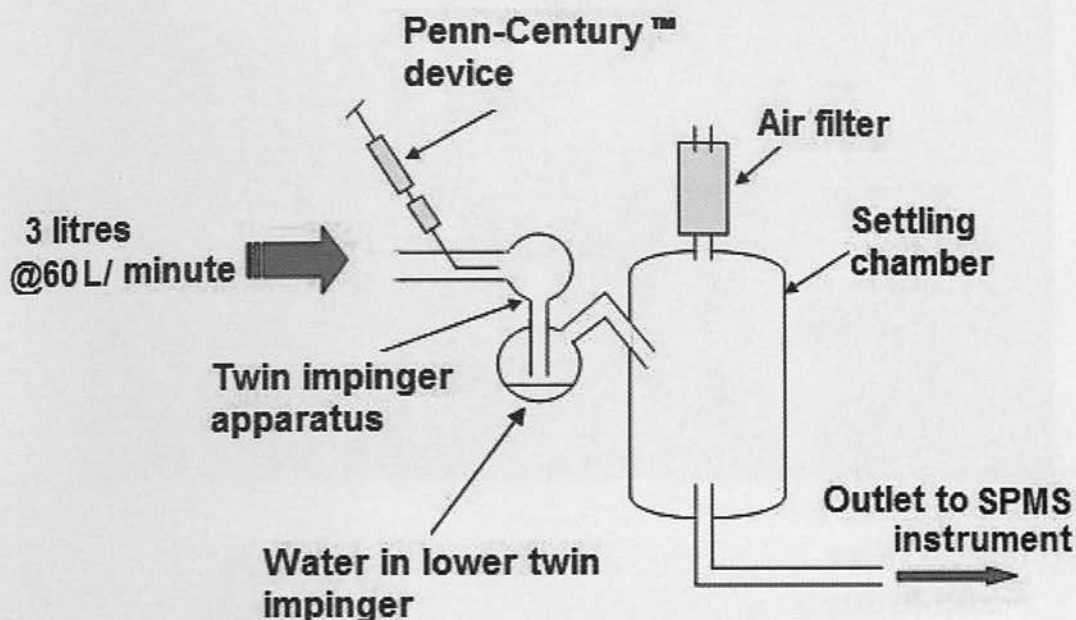
Figure 2.8. *Diagram of sample introduction apparatus for powders in single particle mass spectrometry experiments. The powder is loaded into the Penn-Century™ device (effectively a powder syringe) then injected into a flow of air which carries the sample particles through the twin impinger, then into the settling chamber.*

2.4.2 Characteristics of the Aerosol Time-of-Flight Mass Spectrometer

An aerosol time-of-flight mass spectrometer (AToFMS) (TSI 3800, Shoreview, MN, USA) was used for the main part of the work described in this thesis and a photograph of this instrument is given in Figure 2.9. This instrument was developed at the University of California in the 1990s[56], and then later commercialized by TSI[57].
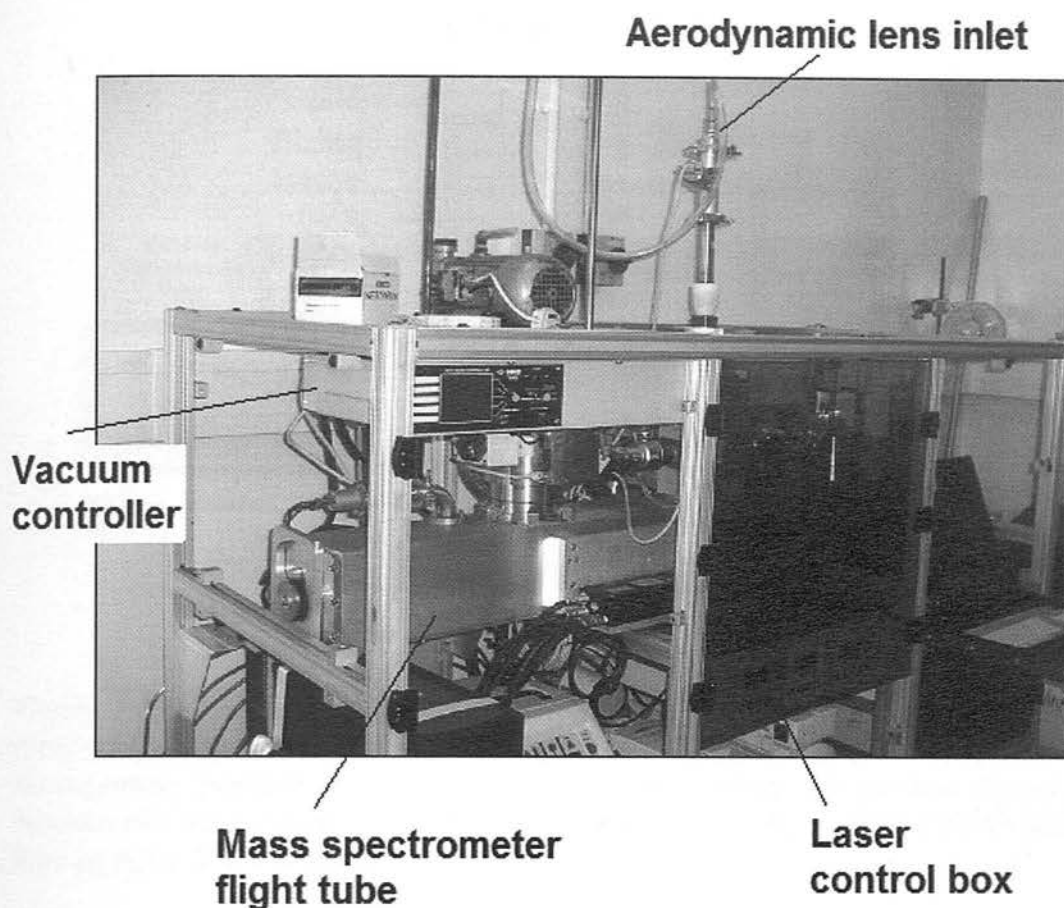
Figure 2.9. *Photograph showing some features of the TSI 3800 AToFMS instrument.*

The instrument is attached to a mobile metal frame and was powered by a 240 V mains supply or generator. The frame is approximately 170 (width) x 75 (depth) x 130 (height) cm and the complete system weighs approximately 200 kg and it is thus easily transportable which is important for *in-situ* environmental monitoring.

Figure 2.10 shows a cross section of the AToFMS instrument; the inlet, the particle size region and mass spectrometer are described below. The vacuum system allows the area between the nozzle and first skimmer to be maintained at a pressure of 2 Torr, the particle sizing region at approximately 5 x 10^{-5} Torr and the mass spectrometer region at approximately 2.0 x 10^{-7} Torr (1 Torr = 133 Pa).
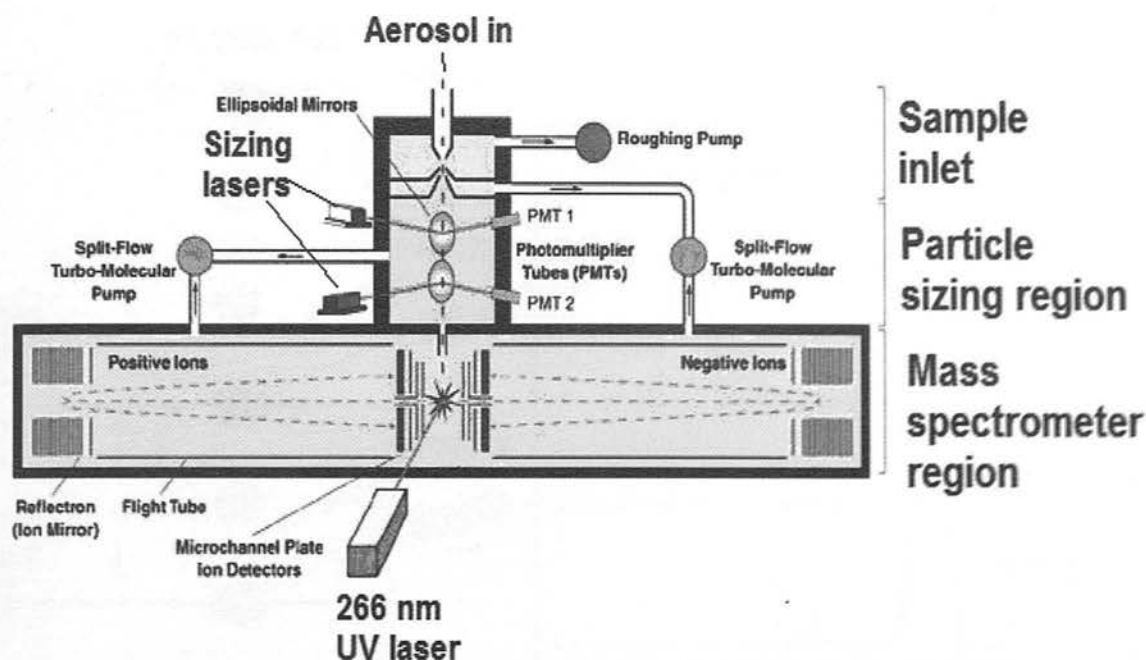
Figure 2.10. *A schematic of the TSI AToFMS instrument. The instrument shown was fitted with a nozzle-skimmer inlet which was later upgraded to an aerodynamic lens. Aerodynamic particle size is determined by measuring the particle transit time between two laser beams. The mass spectrometer region consists of a dual reflectron time-of-flight (ToF) analyzer* [56, 57].

The measurement of aerodynamic particle size was developed based on the transit time of each particle between two laser beams. The transit times was calibrated using standards of known size (polymer beads) and then converted from transit times into particle diameters[11, 12, 13].

Figure 2.11 shows a schematic of the particle sizing region of the instrument which consists of two laser beams which form a timing circuit. A particle passes through the first laser beam and the scattered light initiates the timer and when it passes through the second laser beam the scattered light stops the timer and the transit time for the particle is noted. This circuit is calibrated using particles of known size and hence the aerodynamic particle size of the analyte can then be calculated[32].
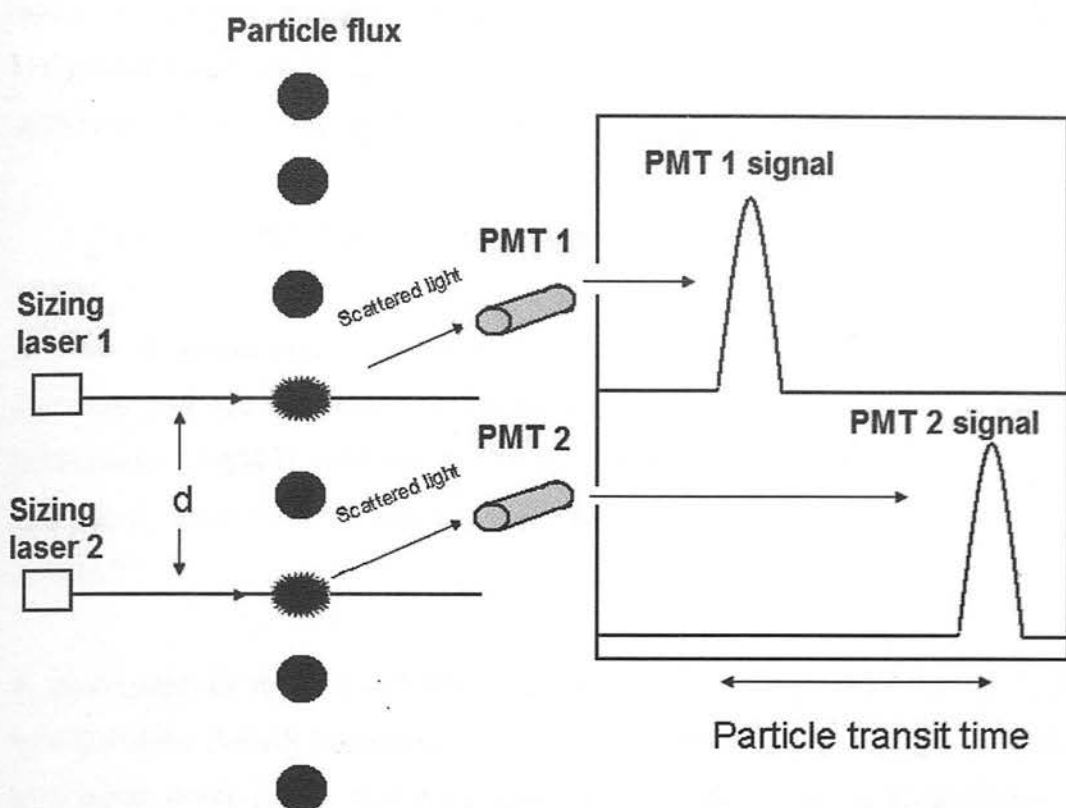
Figure 2.11. *The particle sizing region of the AToFMS instrument* [58]. *The velocity of each particle can be calculated from the time taken for particles to travel the known distance (d). Particle velocities are converted to a measure of aerodynamic size by calibration using particles of known size (typically polymer beads).*

After sizing, the particles pass into the mass spectrometer where they are ablated and ionized using a Nd: YAG laser. For the Nd:YAG laser the fundamental wavelength is in the near infra-red (near-IR) at 1064 nm and for the AToFMS instrument the optical frequency is quadrupled to give a wavelength of 266 nm[33]. The Nd: YAG laser incorporated into the AToFMS instrument, has a 5 ns pulse width, generates pulses of up to 1.0 mJ and is synchronized with the particle sizing lasers. The laser ablation technique is discussed in Section 2.3.3.3. For the AToFMS instrument the laser energy is set to the required value and the actual value produced for each pulse is measured.

The AToFMS instrument utilises two reflectron time-of-flight mass analyzers, of opposite polarity, which allows the simultaneous detection of both positive and negative ions from the same particle. The ability of the instrument to analyze both positive and negative ions simultaneously maximizes the amount of information obtained on a single particle. This is especially important for environmental samples

where the samples can only be analyzed once. For the analysis of inhalation products it is useful to acquire positive and negative ion spectra on the same particle especially in the case of drug compounds which are salts – for example, salmeterol xinofoate.

2.4.3 Characteristics of the Aerodyne Aerosol Mass Spectrometer

A series of aerosol mass spectrometry (AMS) instruments have been described in the literature and are commercially available from Aerodyne[59]. The Aerodyne AMS instruments (AAMS) used for the work described in this thesis were based on a quadrupole mass analyzer (Q-AAMS)[20], or a reflectron ToF mass analyzer (TOF-AAMS)[22].

A photograph of the ToF-AAMS is shown in Figure 2.12. As with the AToFMS instrument the AAMS instrument is powered by a mains power supply and is attached to a metal frame and is easily transportable. The frame size is approximately 104 (width) x 61 (depth) x 124 (height) cm.
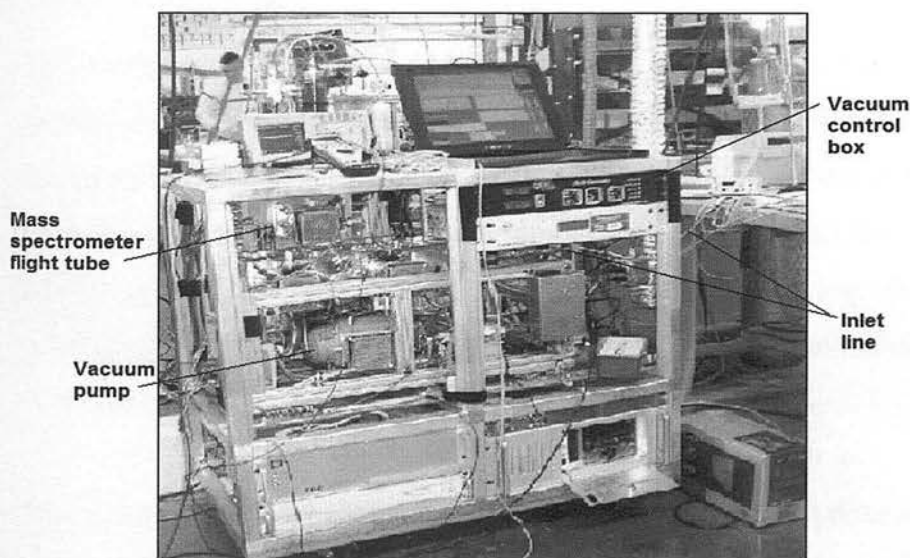
Figure 2.12. Photograph showing some key features of the Aerodyne Aerosol Mass Spectrometer.

A diagram of a cross section of the ToF-AAMS instrument is shown in Figure 2.13. Similarly to the AToFMS instrument, the AAMS instrument is comprised of three regions *i.e.* a sample inlet, a particle sizing region and a mass spectrometer. Three turbo-molecular pumps are used to reduce the background pressure across these regions from 2 Torr at the inlet, to 10^{-3} Torr in the particle size region and then to 10^{-5}

Torr in the mass spectrometer (1 Torr = 133 Pa),. A description of each region of the instrument is given below.
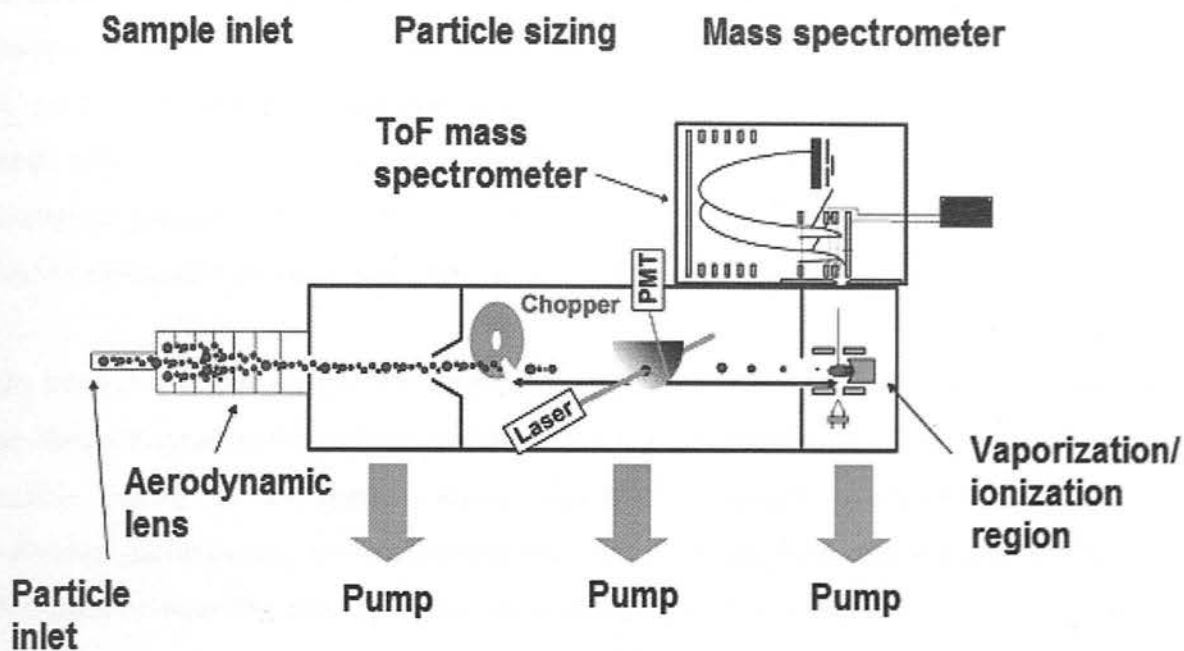
Figure 2.13. Diagram of the ToF-AMS instrument (Aerodyne) to show sample inlet, particle sizing and mass spectrometer regions of the instrument[58].

The sample inlet for the AAMS instrument includes an aerodynamic lens and a general description of this type of device was given in Section 2.3.1. The Aerodyne aerodynamic lens is approximately 30 cm long and the discs are of 13 mm diameter[30]. Particles in Brownian motion in the sampled atmosphere enter the lens where the gas flow is approximately 8 m sec $^{-1}$. The particles are accelerated through the lens by gas-particle collisions[28] and when they exit, they typically have a velocity of between 50 to 200 m sec $^{-1}$.

The focussed particle beam exits the aerodynamic lens and is directed into the particle sizing chamber where a measurement of the aerodynamic particle size is made. Time-resolved detection of the particles, coupled with the known flight distance, gives the velocity from which the particle aerodynamic diameter is obtained[23].

The start time for the particle sizing measurement is determined from the point at which the particle passes through a chopper wheel. The chopper wheel also modulates the particle beam so that the particle size region is not swamped and individual particles may be detected and analyzed. The chopper wheel is 5 cm in diameter with

two radial slits giving a sample duty cycle of typically 1.0 % when operated at 150 Hz [20, 22].

Generally the AAMS instrument can be used in three modes[23], the first is where the chopper is completely blocked and therefore no particles can pass through. This can be used for collecting a background signal in the mass spectrometer. The second mode (mass spectrum mode) is when the chopper is open and all particles pass through to give an ensemble mass spectrum. This is useful with the quadrupole-based AAMS instrument so that representative (or marker ions) ions can be chosen.

The third chopper mode, particle time-of-flight (P-ToF), is a chopped mode in which the chopper spins and therefore modulates the beam transmission. This controls the particle density in the particle sizing region and prevents overloading so that individual particles may be detected and analyzed. The AAMS instrument is typically alternated between the mass spectrum mode and the P-ToF mode.

For the AAMS instrument based on the quadrupole analyzer (Q-AAMS), in the particle time-of-flight (P-ToF) sizing mode, the average size distribution at pre-selected *m/z* values for the particle population (ensemble) is measured. The P-ToF mode generates mass spectra each measured at a specific particle flight time in a chopper cycle. This gives a two-dimensional matrix with a complete mass spectrum for each chopper cycle in columns and the P-ToF distributions for individual *m/z* values in rows[20, 22].

Particle arrival is indicated by the burst of ion signal at the selected *m/z* after a particle size dependent delay from the opening of the chopper. The particle velocities determined using P-ToF measurements can be converted into aerodynamic diameters by calibration using polymer beads of known size[23].

In the ionization source of the AAMS instruments a hotplate is used to vaporize the sample which is then ionized in the gas phase by electron ionization. Electron ionization is described in detail in Section 2.3.3.2. Under optimised conditions, the electron ionization (EI) spectra obtained using the AAMS instruments are comparable with those found in the National Institute of Standards (NIST) library[23].

The speed of the mass spectral data acquisition is important in the AAMS experiment. The Q-AAMS instrument is limited to detecting one *m/z* value (one ion) per particle, because on the time scale of particle vaporization (approx 100 to 200 μsec) it can only scan a small mass range. This is compared with the data acquisition rate for the ToF-AAMS which is fast enough to give full mass spectra on each single particle and maximizes the amount of data available from each experiment[22].

For older versions of the AAMS instrument, mass spectra were continuously acquired and this gave large data files containing only a few meaningful mass spectra. On more recent AAMS instruments (including the ToF-AAMS used for the work presented in this thesis) the acquisition of mass spectra for each single particle, is triggered by the scattered light when the particle crosses a photodiode beam and in this case the data files are more compact and easier to process[61, 62].

2.5 References

(1)   The characterization of aerosols distributed with respect to size and composition. S.K. Freidlander. *Aerosol Sci. 1, 295-307 (1970).*

(2)   The characterization of aerosols distributed with respect to size and composition part 2. S.K. Freidlander. *Aerosol Sci. 2, 331-340 (1971).*

(3)   Real-time single particle mass spectrometry: a historical review of a quarter of a century of chemical analysis of aerosols. C.A. Noble and K.A. Prather. *Mass Spectrom. Rev. 19, 248-274, (2000).*

(4)   Mass spectrometry of aerosols. D.T. Suess and K.A. Prather. *Chem. Rev. 99, 3007-3035, (1999).*

(5)   Aerosol mass spectrometry: An introductory review. D. Nash, T. Baer and M.V. Johnson. *Int. J. Mass Spectrom. 258, 2-12 (2006).*

(6)   Surface ionization mass spectrometry of airborne particulates. W.D. Davis. *J. Vac. Sci. Technol. 10, 278, (1973).*

(7)   Continuous mass spectrometric analysis of particulates by surface ionization. W.D. Davis. *Environ. Sci. Technol. 11, 587-592, (1977).*

(8)   *In-situ* mass analysis of particles by surface ionization mass spectrometry. W.S. Lassiter and A.L. Moen. *NASA Tech. Memo, NASA, TM X-3211, (1974).*

(9)   A direct inlet for surface ionization mass spectrometry of airborne particles. J. Stoffels. *Int. J. of Mass Spectrom. Ion Phys. 40, 223-234, (1981).*

(10)   Mass spectrometric analyzer for individual aerosol particles. J. Allen and B. Gould. *Rev. Sci. Instruments. 52, 804-809, (1981).*

(11)   Real-time measurement of sodium chloride in individual aerosol particles by mass spectrometry. M. Sinha and S. Freidlander. *Anal. Chem. 57, 1880-1883, (1985).*

(12)   Proposed on-line aerosol analysis combing size determination laser induced fragmentation and time-of-flight mass spectrometry. J.B. Marijnissen, B. Scarlett and P. Verheijen. *J. Aerosol Sci. 19, 1307-1310, (1988).*

(13)   On-line ToF mass spectrometry of aerosols: system characterization. M. Weiss, P. Verheijen, J.B. Marijnissen and B. Scarlett. *J. Aerosol Sci. 26, Suppl. 1, S101-102, (1995).*

(14)   On-line single particle analysis by mass spectrometry. P.J. McKeown, M.V. Johnson and D. Murphy. *Anal. Chem. 63, 2069-2073, (1991).*

(15)   Laser-induced formation thresholds of aerosol particles in a vacuum. D.S. Thomson and D.M. Murphy. *Appl. Opt. 32, 6818-6826, (1993).*

(16)   Aerosol characterization using mass spectrometry. C. Noble, T. Nordemeyer, K. Salt, B. Morrical and K. Prather. *Trends Anal. Chem. 13, 218-222 (1994).*

(17)   On-line chemical analysis of aerosols by rapid single particle mass spectrometry. P. Carson, K. Neubauer, M. Johnson and A. Wexler. *J. Aerosol Sci. 26, 535-545, (1995).*

(18)   Airborne particle analysis. B. Spengler. *Science. 274, 1993-1997, (1996).*

(19)   Molecular composition of organic aerosols formed in the α-pinene/O3 reaction: Implications for new particle formation processes. T. Hoffman, R. Bandur, U. Maggraf and M. Linscheid. *J.Geophys. Res. 103, 25569-25578, (1998).*

(20)   Development of an aerosol mass spectrometer for size and composition analysis of submicron particles. J.T. Jayne, D.C. Leard, X. Zhang, P. Davidovitis, K. Smith, C.E. Kolb and D. Worsnop. *Aerosol Sci. and Technol. 33, 49-70, (2000).*

(21)   Transportable real-time single particle ion trap mass spectrometer. W. Harris, P.T. Reilly, W. Whitten and J. Ramsey. *Rev. Sci. Instruments. 76, 064102, (2005).*

(22)   A new time-of-flight aerosol mass spectrometer (TOF-AMS) – Instrument description and first field deployment. F. Drenick, S. Hings, P. DeCarlo, J.T. Jayne, M. Gonion, K. Fuhrer, S. Weimer, J. Jiminez, K. Demerjian, S. Borrmann and D. Worsnop. *Aerosol Sci. and Technol. 39, 637-658, (2005).*

(23)   Chemical and microphysical characterization of ambient aerosols with the Aerodyne aerosol mass spectrometer. M.R. Canagaratna, J.T. Jayne, J-L. Jimenez, M.R. Afarra, Q. Zhang, F. Drenwick, H. Coe, A. Middlebrook, A. Delia, L.R. Williams, A.M. Trimbourne, M.J. Northway, P.F. DeCarlo, C.E. Kolb, P. Davidovits and D.R. Worsnop. *Mass Spectrom. Rev. 26, 185-222, (2007).*

(24)   Demonstration of a VUV lamp photo-ionization source for improved organic speciation in an aerosol mass spectrometer. M.J. Northway, J.T. Jayne, D.W. Toohey, M.R. Canagaratna, A. Trimbourn, K.-I. Akiyyama, A. Shimono, J-L. Jimenez, P.F. DeCarlo, K.R. Wilson and D.R. Worsnop. *Aerosol Sci. and Technol. 41, 828-839, (2007).*

(25)   Sampling and analysis of individual particles by mass spectrometry. M.V. Johnston. *J. Mass Spectrom. 35, 585-595, (2000).*

(26)   Single particle detection efficiencies of aerosol time-of-flight mass spectrometry during the North Atlantic Marine Boundary layer experiment. M. Dall'Osto, R. Harrison, D. Bedows, E. Freney, M. Heal and R. Donovan. *Environ. Sci. Technol. 40, 5029-5035, (2006).*

(27)   Particle detection efficiencies of aerosol time-of-flight mass spectrometers under ambient conditions. J.O. Allen, D.P. Fergenson, E.E. Gard. L.S. Hughes, B.D. Morrical, M.J. Kleeman, D.S. Gross, M. Galli, K.A. Prather and G.R. Cass. *Environ Sci. Technol. 34, 211-217 (2000).*

(28)   Generating particle beams of controlled dimensions and divergence: I. Theory of particle motion in aerodynamic lenses and nozzle expansions. P. Liu, P. Ziemann, D. Kittleson and P. McMurry. *Aerosol Sci. and Technol. 22, 293-313, (1995).*

(29)   Generating particle beams of controlled dimensions and divergence: II. Experimental evaluation of particle motion in aerodynamic lenses and nozzle expansions. P. Liu, P. Ziemann, D. Kittleson and P. McMurry. *Aerosol Sci. and Technol. 22, 314-324, (1995).*

(30)   Development and characterization of an aerosol time-of-flight instrument with increased detection efficiency. Y. Su, M.F. Sipin, H. Furutani and K.A. Prather. *Anal. Chem. 76, 712-719, (2004).*

(31)   Transmission efficiency of an aerodynamic focussing lens system: comparison of model calculations and laboratory measurement for the aerodyne aerosol mass spectrometer. P.S. Liu, R. Deng, K.A. Smith, L.R. Williams, J.T. Jayne, M. Canagaratna, K. Moore, T.B. Onasch, D.R. Worsnop and T. Deshler. *Aerosol Sci. and Tech. 41, 721-733 (2007).*

(32)   The design of single particle laser mass spectrometers. D.M. Murphy. *Mass Spectrom. Rev. 26, 150-165, (2007).*

(33)   Laser-induced mass analysis of single particles in the airborne state. K-P. Hinz, R. Kaufmann and B. Spengler. *Anal. Chem. 66, 2071-2076 (1994).*

(34)   TSI AToFMS manual p/n 1930036 revision A. June 2004.

(35)   Aerodynamic particle size measurement by laser doppler velocimetry. C.J. Wilson and B.Y.H. Liu. *J. Aerosol Sci. 11, 139-150 (1980).*

(36)   Instrumentation, data evaluation and quantification in on-line aerosol mass spectrometry. K-P. Hinz and B. Spengler. *J. Mass Spectrom. 42, 843-860 (2007).*

(37)   Interpretation of mass spectra. F.W. McLafferty and F. Turecek. Fourth Edition (1993). University Science Books. ISBN 0-935702-25-3.

(38)   Mass Spectrometry for Chemists and Biochemists. M.E. Rose and R.A.W. Johnstone. First edition (1982). Cambridge University Press. ISBN 0521281849.

(39)   Laser ablation in analytical chemistry – a review. R.E. Russo, X. Mao, H. Liu, J. Gonzalez and S.S. Mao. *Talanta. 57, 425-451, (2002).*

(40)   Molecular dynamics simulation of ultrafast laser ablation of fused silica. C. Cheng, A.Q. Wu and X. Xu. *Journal of Physics: Conference series: 59,100-104 (2007).*

(41)   Interpretation of mass spectra from organic compounds in aerosol time-of-flight mass spectrometry. P. Silva and K.A. Prather. *Anal. Chem. 72, 3553-3562, (2000).*

(42)   Coupling two-step laser desorption/ionization with aerosol time-of-flight mass spectrometry for the analysis of individual organic particles. B.D. Morrical, D.P. Fergenson and K.A. Prather. *J Am. Soc. Mass Spectrom. 9, 1068-1073, (1998).*

(42(a)) Comparison between mass spectra of individual organic particles generated by UV laser ablation and in the IR/UV two step mode. A.Zelenyuk, J.Yang

and D.Imre. *International Journal of Mass Spectrometry. 282, 6-12 (2009).*

(43)   Improvements in ion signal reproducibility obtained using a homogeneous laser beam for on-line laser desorption/ionization of single particles. R. Wenzel and K. Prather. *Rapid Commun. Mass Spectrom. 18, 1525-1533, (2004).*

(44)   Synchrotron radiation based time-of-flight mass spectrometer for organic constituents. E.R. Mysak, K.R. Wilson, M. Jimmenez-Cruz, M. Ahmed and T. Baer. *Anal. Chem. 77, 5953-5960, (2005).*

(45)   Coupling a versatile aerosol apparatus to a synchrotron: Vacuum ultraviolet light scattering, photoelectric imaging and fragment free mass spectrometry. J. Shu, K.R. Wilson, M. Ahmed and S.R. Leone. *Rev. Sci. Instruments. 77, 043106, (2006).*

(46)   Quadrupole mass spectrometry and its application. P. Dawson. First edition (1995) Am. Inst. Phys. ISBN-10:1563964554.

(47)   Quadrupole Ion Trap Mass Spectrometry. R. Marsh and J. Todd Second edition (1995). Wiley Interscience. ISBN – 0471488887.

(48)   Mass Spectrometry Principles and Applications. E. DeHoffmann, J. Charette and V. Stroobant. (1996) ISBN-0-471-96697-5.

(49)   Time-of-flight mass spectrometry instrumentation and applications in biological research. R.J. Cotter. First edition (1994). American Chemical Society. ISBN -10 0841234744.

(50)   A global view of LC/MS. R. Willoughby, E. Sheenan and S. Mitrovich. First edition (1998). Global View Publishing. ISBN 0-966081307 (p527-530).

(51)   A field-deployable high-resolution time-of-flight aerosol mass spectrometer. P.F. DeCarlo, J.R. Kimmel, A. Trimbourn, M. Northway, J.T. Jayne, A.C. Aiken, M. Gonin, K. Fuhrer, T. Hovarth, K.S. Docherty, D.R. Worsnop and J-L. Jimenez. *Anal. Chem. 78, 8281-8289, (2006).*

(52)   Single particle characterization of albuterol metered dose inhaler aerosol in near real time. C. Noble and K. Prather. *Aerosol Sci. and Tech. 29, 294-306, (1998).*

(53)   Sample introduction apparatus. D. Prime (GSK). Unpublished work.

(54)   The twin impinger: a simple device for assessing the delivery of drugs from metered dose pressurized aerosol inhalers. G.W. Hallworth and D.G. Westmoreland, *J. Pharm. Pharmacol. 39, 966-972 (1987).*

(55)   Penn-Century, Philadelphia, PA, USA. http://www.penncentury.com/ (Accessed 27 May 2008).

(56)   Real-time analysis of individual atmospheric aerosol particles: design and performance of a portable aerosol time-of-flight mass spectrometer (AToFMS). E.E. Gard, J.E. Mayer, B.D. Morrical, T. Dienes, D.P. Fergenson and K.A. Prather. *Anal. Chem., 69, 4083-4091, (1997).*

(57)   TSI Shoreview, MN, USA. (http://www.tsi.com/). (Accessed 27 May 2008)

(58)   Laser Chemistry, Spectroscopy, Dynamics and Applications. H. Telle, A. Gonzalez-Urena and R.J. Donovan, First Edition (2007), Wiley. ISBN-978-0-471-48571-1.

(59)   Aerodyne Corporation, Billerica, MA, USA http://www.aerodyne.com/ (Accessed 27 May 2008).

(60)   Private Communication from Aerodyne Corporation.

(61)   Laboratory and ambient particle density determinations using light scattering in conjunction with aerosol mass spectrometry. E.S. Cross, J.G. Slowik, P. Davidovits, J.D. Allan, D.R. Worsnop, J.T. Jayne, D.K. Lewis, M.R. Canagaratna and T.B. Onasch. *Aerosol Sci. and Tech. 41, 343-359, (2007).*

(62)   Single Particle Characterization Using a Light Scattering Module Coupled to a Time-of-flight Aerosol Mass Spectrometer E.S Cross, T. Onasch, M. Canagaratna, J.T. Jayne, J. Kimmel, X.-Y. Yu, M.L. Alexander, D.R. Worsnop, and P. Davidovits. *Atmospheric Chemistry and Physics, 9, 7769-7793, (2009).*

Chapter 3

The Application of Single Particle Mass Spectrometry to the Analysis of Inhalation Products

3.1 Introduction

In this chapter, the factors that can influence the appearance of a mass spectrum taken from a single particle mass spectrometry (SPMS) experiment are discussed. Later in this chapter, examples of SPMS mass spectra are presented; the interpretation of these data is important because the identification and classification of each particle in terms of composition is based on the presence of specific ions (or groups of ions), *i.e.* the fragmentation patterns give an insight into the origin of the ions on which the identification and classification of particles is based.

3.2 Factors That Influence Aerosol Time-of-Flight Mass Spectrometry Data

Individual particles can be identified and classified in terms of their chemical composition. The identification of each particle using SPMS spectra is typically based on the unique fingerprint given by each compound. The presence of a given compound in a particle may be determined from the mass spectrum based on the appearance of a few representative (marker) ions or by multivariate statistical analysis of the full mass spectrum. Data analysis methods based on this type of approach for AToFMS data are discussed in more detail in Chapter 4.

The most significant variation for the mass spectra acquired from an AToFMS experiment originates from the laser ablation/ionization process. Other influences on this

type of data include the effects of particle size and shape as well as the ability of the analyte to absorb radiation at the ablation laser wavelength (266 nm).

3.2.1 Ionization and Laser Wavelength

The successful ionization of material ablated from particles depends on the extent to which analyte absorbs the radiation from the AToFMS laser at 266 nm. Figure 3.1 shows the ultra-violet (UV) spectra for FP and SX (taken from HPLC experiments the details for which are given in Appendix A3.2). These data can be used to predict the ease with which FP and SX are likely to be ablated and ionized in the AToFMS instrument.

In the UV spectra shown in Figure 3.1, much of the response at the lower wavelengths is likely to be due to the solvent from the mobile phase used in the HPLC experiment. However, at a wavelength of 266 nm the molar absorptivity of SX was estimated to be approximately double that of FP (calculation shown in Appendix A3). Hence, the AToFMS instrument would be expected to be more sensitive to SX than to FP.
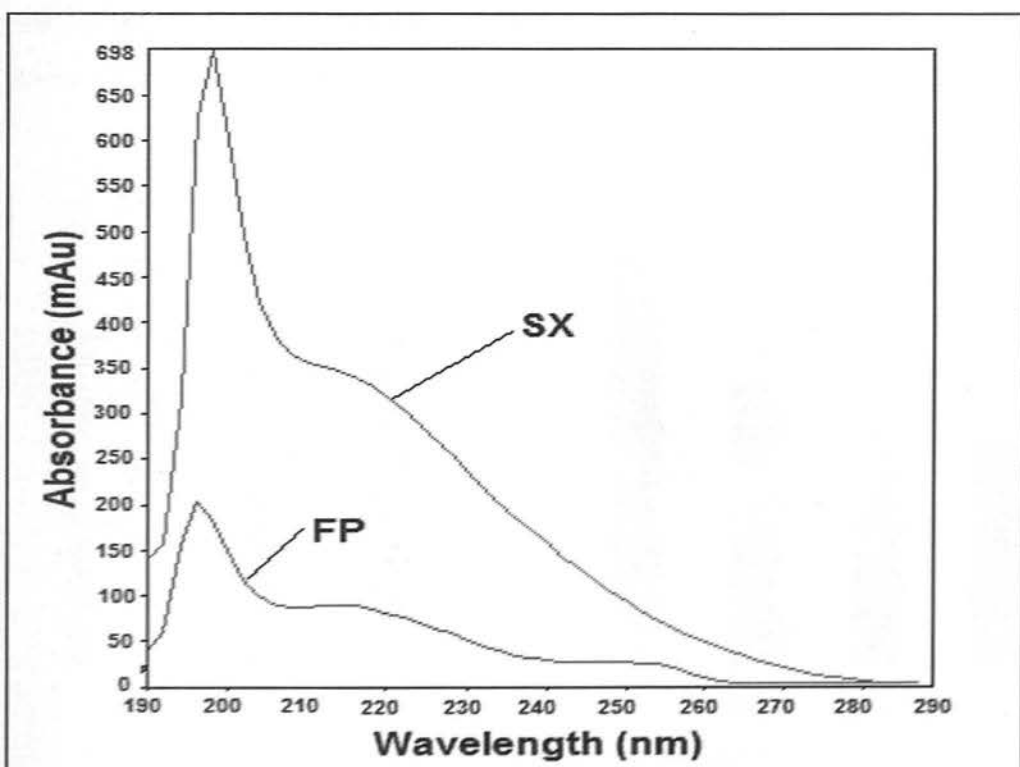
Figure 3.1. Ultra-Violet (UV) spectra of FP (10 mgL^{-1}) (blue trace) and SX (10 mgL^{-1}) (red trace). (Experimental details are given in Appendix A3.2).

3.2.2 The Effect of Laser Energy

Most of the particles that pass through the ionization source are not completely ablated (especially larger particles, > 4 µm) but it is assumed that a representative sample is produced during the ablation process[1,2].

Shot-to-shot variations in the laser beam are most likely to be due to the Gaussian intensity distribution of the laser beam; *i.e.* some particles pass through the high intensity (peak) region while others pass through the lower intensity region (wings)[3]. It has been shown that if the profile of the laser beam is changed from a Gaussian profile to a flat top (top-hat) profile, this results in better shot-to-shot reproducibility; *i.e.* either the particle would (a) not interact with the beam or (b) it would be ionized with reproducible laser fluence[4].

The variation in response is exemplified, by the bar-graph of the peak area for the fluoride ion from FP for a group of particles of similar size shown in Figure 3.2. The laser energy was similar for each particle but a variation was found in the response, in terms of the fluoride ion peak area.
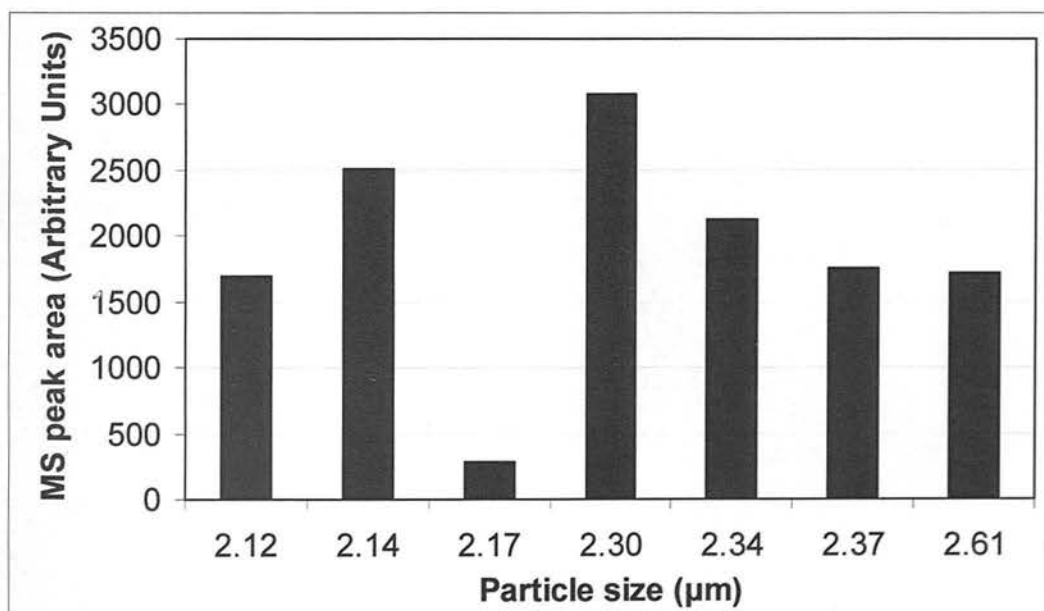
Figure 3.2. *Bar-graph to show the variation in the AToFMS spectra (MS) peak area for the fluoride ion, for a number of particles of similar size. All data shown here were acquired at similar laser energies (0.88 to 0.90 mJ).*

Some examples of positive ion mass spectra taken from AToFMS experiments at high and low energies on single particles ($\sim$ 2 µm) are shown in Figure 3.3. Neither a protonated molecule ($(M+H)^+$ theoretically at m/z 501) nor an intact molecular ion ($M^{+\cdot}$ theoretically at m/z 500) was observed for FP, even at low laser energy.

At high laser energy (> 0.8 mJ) many ions appear in the mass spectra (Figure 3.3 (a) and (c)) at lower m/z values. In this case, the ions with lower m/z values are difficult to interpret in terms of the FP structure, probably because they are due to secondary, tertiary or further fragmentation. At low laser energy (< 0.2 mJ; Figures 3.3 (b) and (d)) the mass spectra show relatively few ions, some of which can be interpreted in terms of the FP structure and this is discussed in Section 3.3.

Table 3.1 lists some of the major ions observed in Figure 3.3 for FP and SX at high and low laser energy. A suggested explanation for these ions is given in Table 3.1.
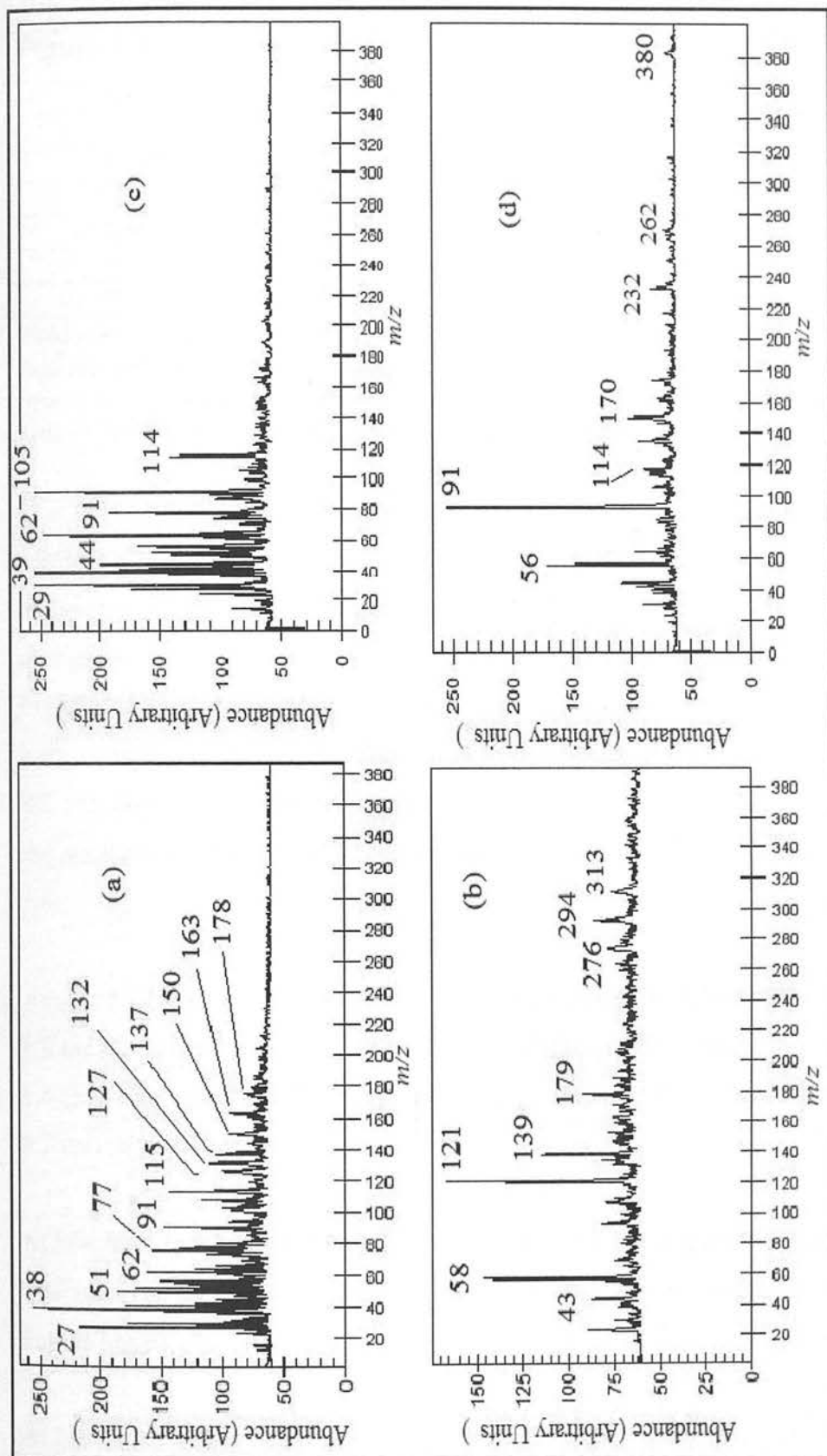
Figure 3.3. *Positive ion AToFMS spectra of (a) a particle of FP aerodynamic size 2.09 μm at high laser energy (0.92 mJ), (b) a particle of FP aerodynamic size 2.03 μm at low laser energy (0.11 mJ), (c) a particle of SX aerodynamic size 1.80 μm at high laser energy (0.87 mJ), (d) a particle of SX aerodynamic size 0.73 μm at low laser energy (0.11 mJ). (Using the nozzle-skimmer inlet).*

High laser energy			Low laser energy	
(Common ions below *m/z* 100)			(Unique higher *m/z* ions)	
Figure 3.3 (a)	Figure 3.3 (c)		Figure 3.3 (b)	Figure 3.3 (d)
FP	SX		FP	SX
27	27		313	398
38	38		294	380
50	50		276	266
62	62		179	114
77	77		139	92
91	91		121	55

Table 3.1. The major ions observed in mass spectra acquired during AToFMS experiments on FP and SX, at high and low laser energy. The table shows the ions below m/z 100 that are common to the mass spectra of both FP and SX and the unique ions at m/z values above 100. Data taken from Figure 3.3.

The effect of altering the laser energy was demonstrated using principal component analysis (PCA), a multivariate statistics based pattern recognition technique[5]. (The technique of principal component analysis is explained in Appendix 3.3. The application of principal component analysis is discussed further in Chapters 4 and 5). Figure 3.4 shows a number of PCA charts where data for pure FP and SX samples were overlaid on each chart. Each point in the cluster of data points shown in red for SX and blue for FP represents a mass spectrum of a single particle. Further detail of the application of principal component analysis to AToFMS data is given in Section 4.4.

Figure 3.4 (a) shows a set of data points for a range of laser energies between 0.2 and 1.0 mJ *i.e.* it combines the data from charts (b) to (f). The remaining figures (Figures 3.4 (b) to 3.4 (f)) show the PCA charts at a range of laser energies from the lowest (< 0.2 mJ) to highest (1.0 mJ).

At low laser energy (< 0.2 mJ) the PCA clusters for the two pure drug compounds are well resolved and this is because the mass spectrum for each component shows unique ions at higher *m/z* values.

At higher laser energies (> 0.8 mJ) the mass spectra (Figure 3.3) show ions at low *m/z* (typically < 100) which are common to both drug compounds. This is reflected in the PCA charts by the convergence of the FP and SX clusters towards similar PCA co-

ordinates as the laser energy is increased. Hence the mass spectral patterns for FP and SX are more easily recognized with PCA at lower laser energies. Further explanation of the fragmentation for FP and SX is given in Section 3.3.
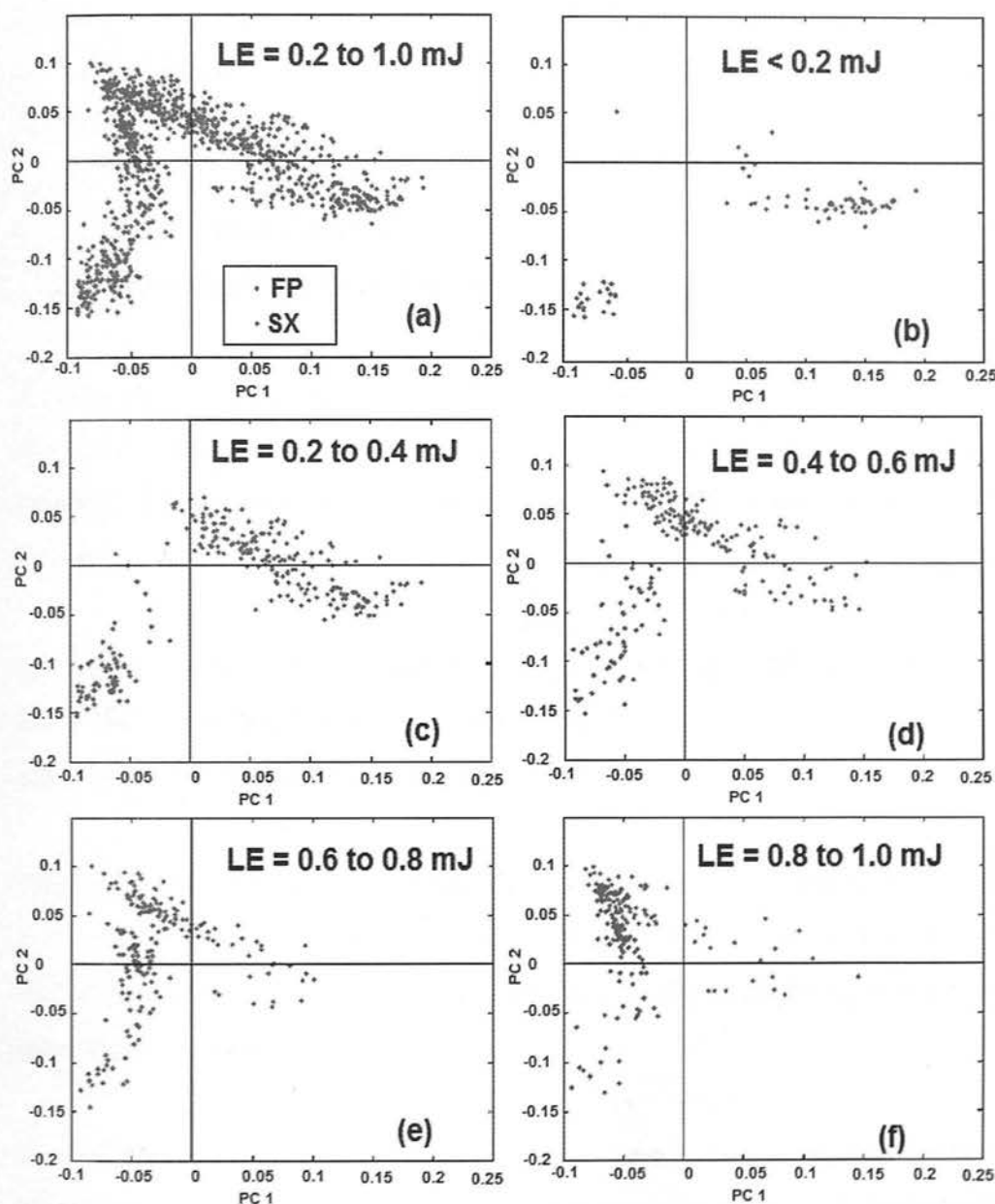
Figure 3.4. *PCA charts to show the effect of varying the laser energy (LE) on PCA clusters of FP and SX. Chart (a) combines the data from charts (b) to (f). Charts (b)to (f) show that as the laser energy increases the clusters converge. This illustrates the points that (a) as the laser energy is increased, more fragments are formed that are common to both compounds and (b) the most unique spectral patterns are observed at low laser energy.*

3.3 Interpretation of AToFMS Spectra

The laser ablation/ionization process results in the formation of both positive and negative ions which are detected simultaneously by the dual (bipolar) mass analyzer. An interpretation of the positive and negative ion mass spectra for FP and SX is given below.

3.3.1 Interpretation of the Aerosol Time-of-Flight (AToFMS) Spectra of Fluticasone Propionate

A suggested fragmentation pattern for FP based on the positive ion mass spectra (Figure 3.3 (a) and (b)) is shown in Figure 3.5. This is typical of the fragmentation obtained for the pure drug acquired at high (> 0.8 mJ) and low (< 0.2 mJ) laser energy.

At low laser energy the FP molecule fragments to give the ion at m/z 333 by the concerted loss of the 17 α and 17β side chains from the D ring of the steroid. The ions at m/z 58 and 43 probably also originate from the 17β side chain.

The ion at m/z 333 loses HF, F and then water to give the ions at m/z 313, 294 and 276, respectively. It is likely that these losses involve trans-elimination of water or hydrogen fluoride from the 6 and 11 positions on the steroid ring, respectively (from the B and C rings of the steroid).

At high laser energies organic molecules have been shown to fragment to give a series of elemental carbon ions C_n^+ or a series of hydrocarbon ions with the formulae C_nH^+, $C_nH_n^+$ etc.[6,7] and similar series of ions are observed for FP.

Further evidence for the assignment of the ions in the mass spectra of the pure compounds was obtained with accurate mass measurements from electrospray LC/MS experiments, the details for which are given in Appendix A3.

$[M+H]^+$ *m/z* 501 (not observed)

m/z	Suggested Ion
27	$C_2H_3^+$
51	$C_4H_3^+$
77	$C_6H_5^+$
91	$C_7H_7^+$
115	$C_9H_7^+$
127	$C_{10}H_7^+$
137	$C_{11}H_5^+$
150	$C_{12}H_6^+$
163	$C_{13}H_7^+$

Low laser energy

High laser energy

m/z 333

-HF

m/z 313

-F

m/z 294

-H_2O

m/z 276

m/z 139

m/z 179

m/z 121

Figure 3.5. *Suggested fragmentation pattern for FP based on the positive ion AToFMS spectra of single particles shown for example in Figure 3.3 (a) & (b). At low laser energy ions that can be interpreted in terms of the FP molecule are observed. At high laser energy the mass spectrum is dominated by hydrocarbon cations.*

61

3.3.2 Interpretation of the AToFMS Spectra of Salmeterol Xinofoate (SX)

A suggested fragmentation pattern for SX based on the positive ion mass spectrum (Figure 3.3 (c) and (d)) is shown in Figure 3.6.

At low laser energy, the SX molecule fragments at the ester oxygen to give the ion at m/z 266, and the alkyl chain breaks to give the tropylium like ion[8] at m/z 91. Ions are observed at m/z 398 and at m/z 380 for the ions produced by the loss of one and two water molecules respectively. This is comparable with the electrospray LC/MS spectrum for SX shown in Appendix A3.

The mass spectrum acquired with higher laser energy shows many ions at the lower m/z values (below m/z 100). At higher laser energy, fragment ions at m/z 171 and 114 from the xinofoate salt can also be observed.
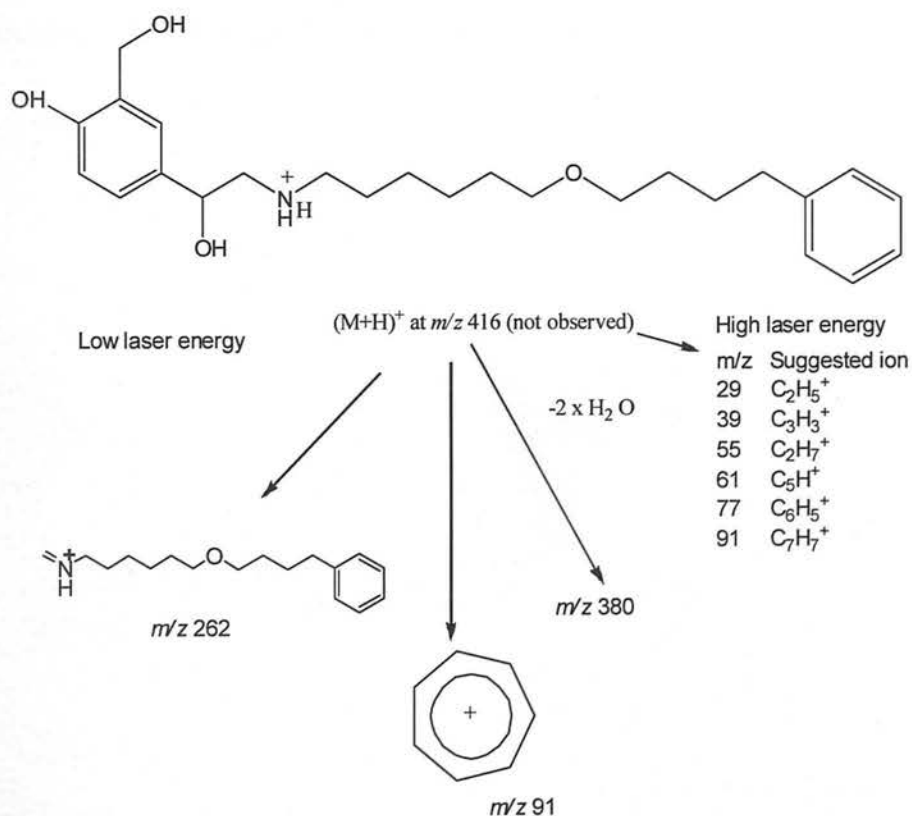
Figure 3.6. Suggested fragmentation pattern of salmeterol based on the AToFMS spectra shown in Figure 3.3 (c) &(d) taken from single particles. At low laser energy ions that can be interpreted in terms of the salmeterol molecule are observed. At high laser energy the hydrocarbon cation series is more prominent.

3.3.3 Interpretation of Negative Ion AToFMS Spectra

The negative ion spectrum for SX is dominated by an ion at m/z 188 due to the xinofoate ion at both high and low laser energy. This ion was found to be a good marker ion for SX and is discussed further in Chapter 4.

The negative ion mass spectra for FP were found to vary with laser energy. The average negative mass spectra for groups of FP particles (rather than for single particles) acquired at various laser energies are shown in Figure 3.7 and these data are summarized in Table 3.2.

The negative ion mass spectra for FP show a series of carbon ions. For example m/z 24, 36, 48, 60, 72 and 96 are consistent with the ions for C_2^-, C_3^-, C_4^- C_5^-, C_6^-, and C_8^-, respectively. There are also series of ions for C_nH^- where n = 2, 4, 6 and 8 at m/z 25, 49, 73 and 97 respectively; for $C_nH_2^-$ where n = 4, 6 and 8 at m/z 50, 74 and 98 respectively; for $C_nH_5^-$ where n = 3, 5 and 7 at m/z 41, 65 and 89, respectively, and for $C_nH_6^-$ where n = 2, 3, 5, 6 and 7 at m/z 32, 42, 66, 78, and 90 respectively.
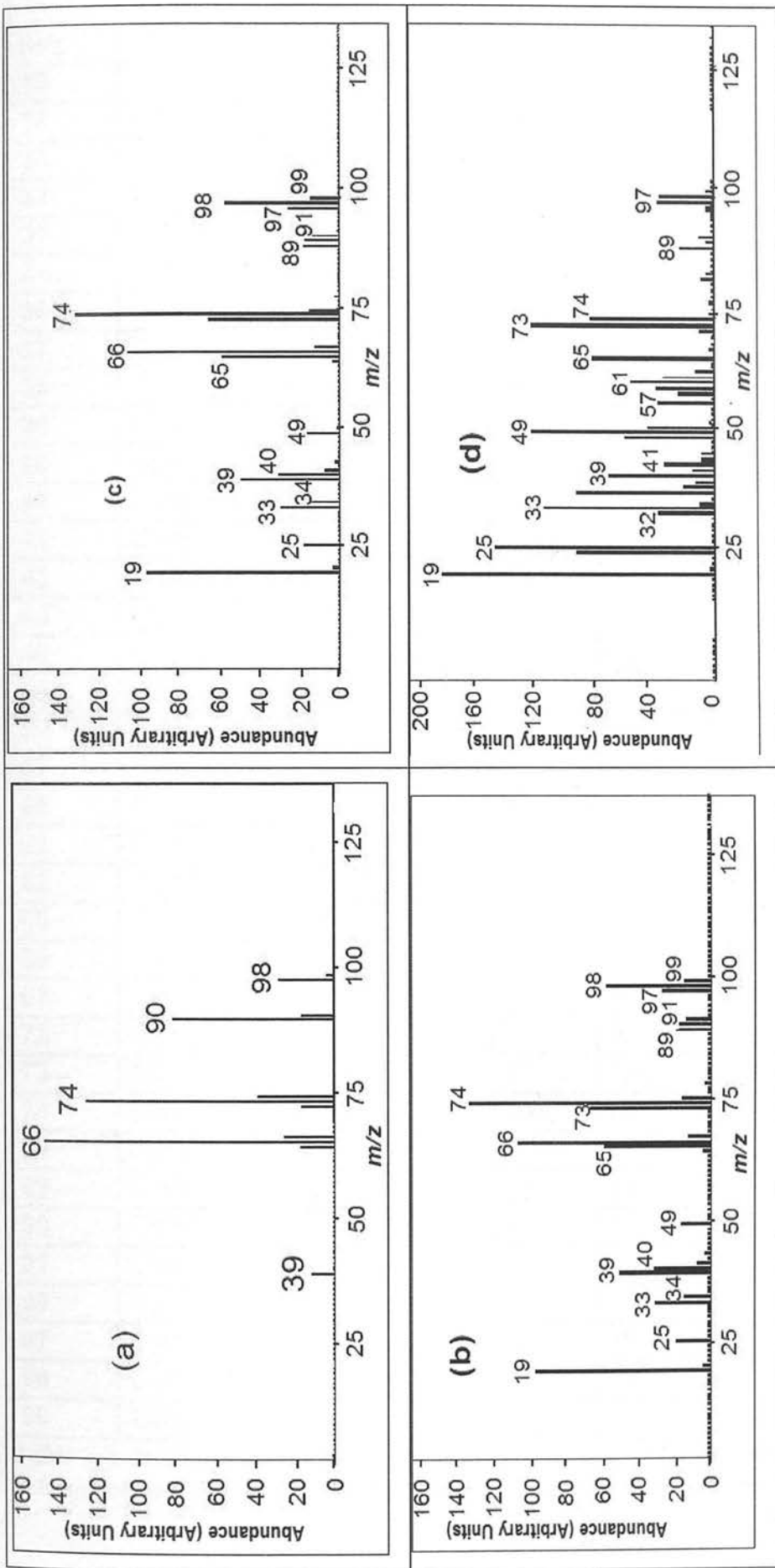
Figure 3.7. *Average negative ion AToFMS spectrum for FP using a nozzle-skimmer inlet and (a) laser energy 0.1 to 0.2 mJ, 37 particles, (b) laser energy 0.4 to 0.5 mJ, 60 particles (c) laser energy 0.6 to 0.7 mJ, 50 particles and (d) laser energy 0.8 to 0.9 mJ, 52 particles.*

64

m/z	Assignment	Laser energy (mJ)			
		0.1	0.45	0.75	0.85
19	F^-	0	105	146	186
24	C_2^-	0	0	34	91
25	C_2H^-	0	25	109	144
32	$C_2H_8^-$	0	0	32	37
33	CH_2F^-	0	40	100	113
34	$H_2S?$	0	15	10	9
36	C_3^-	0	0	35	92
37	C_3H^-	0	0	17	21
38	$C_3H_2^-$	0	0	12	12
39	$C_3H_3^-$	0	52	77	70
40	$C_3H_4^-$	12	32	31	13
41	$C_3H_5^-$	0	8	33	32
42	$C_3H_6^-$	0	0	12	7
43	$C_3H_7^-$	0	0	13	7
44	$C_3H_8^-$	0	0	5	0
48	C_4^-	0	0	27	60
49	C_4H^-	0	17	73	121
50	$C_4H_2^-$	0	0	33	44
57	$CH_3CH_2CO^-$	0	0	19	38
60	C_5^-	0	0	13	40
61	C_5H^-	0	0	15	55
62	$C_5H_2^-$	0	0	11	33
65	$C_5H_5^-$	18	61	69	81
66	$C_5H_6^-$	152	110	61	36
67	$C_5H_7^-$	27	13	7	3
72	C_6^-	0	0	7	9
73	C_6H^-	17	69	97	120
74	$C_6H_2^-$	131	138	106	84
75	$C_6H_3^-$	40	16	0	3
89	$C_7H_3^-$	0	19	18	23
90	$C_7H_6^-$	85	18	4	5
91	$C_7H_7^-$	17	14	0	9
96	C_8^-	0	0	0	5
97	C_8H^-	0	27	32	39
98	$C_8H_2^-$	30	60	35	35
99	$C_8H_3^-$	0	15	0	5

Table 3.2. *Summary and assignment of the negative ions observed using the AToFMS instrument for FP, showing the average intensities of ions at different laser energies.*

Figure 3.8 shows that ions in the series C_n^- (where n= 2 to 6), are not present in spectra acquired at low laser energies, but become abundant as the laser energy is increased. Moreover, it can be seen from Table 3.2 that the signal intensity for many of the ions present varies with the laser energy.

Figure 3.8. *The variation in relative abundance of C_n^- ions as a function of laser energy in the average negative ion AToFMS spectra from FP. The traces shown are m/z 24, 36, 48, 60, and 72 which are consistent with the ions for C_2^-, C_3^-, C_4^- C_5^-, C_6 respectively.*

Alternative assignments for some of the ions shown in Table 3.2 are possible. For example, the ion at *m/z* 33 assigned as $CH_2 F^-$ could also be due to SH^-. The ion at *m/z* 65 given as SCH_2F^-, derived from the terminal of the 17-thiomethyl fluoride side chain, could also be due to $C_5H_6^-$. Also the ion at *m/z* 73 is attributed to the $CO_2CH_2CH_3^-$ ion derived from the 17-ethylcarboxy side chain but could also be due to C_6H^-.

Figure 3.9 shows a comparison of the abundance of C_5^- ions with that of $C_5H_6^-$ ions at varying laser energy, in the average negative ion AToFMS spectra of FP. At low laser energy (0.1 mJ) C_5^- ions are not detected. As the laser energy is increased (approaching 1.0 mJ) the C_5^- ions become more abundant, while the abundance of $C_5H_6^-$ ions decreases.
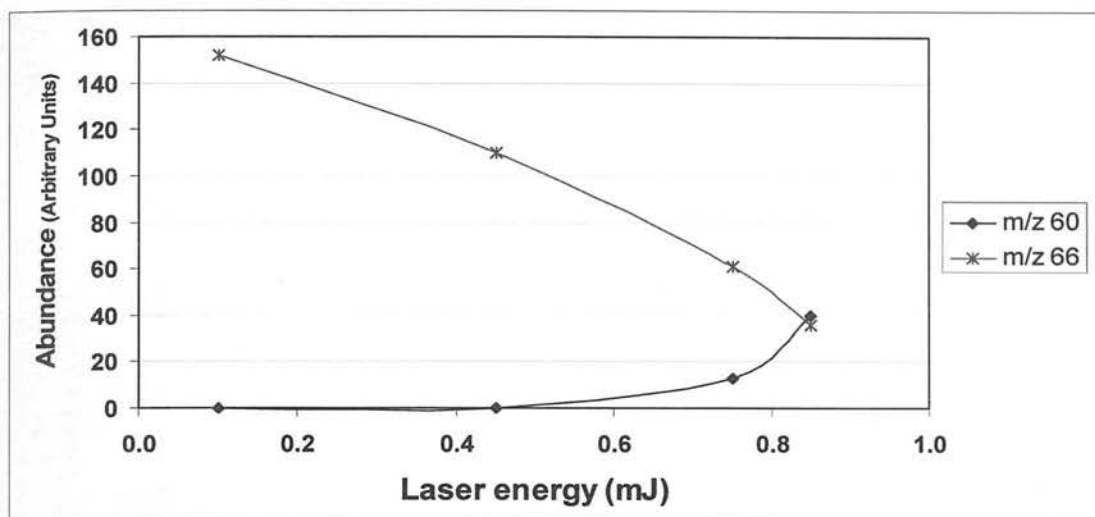
Figure 3.9. *The variation in the relative abundance for m/z 60 due to C_5 and m/z 66 due to $C_5H_6^-$ ions as a function of laser energy in the average negative ion AToFMS spectra of FP.*

Figure 3.10 shows the relative abundance of $C_3H_n^-$ ions as a function of varying laser energies in the average negative ion AToFMS spectra of FP. At low laser energy (0.1 mJ) the ions for $C_3H_5^-$ and $C_3H_4^-$ are prominent; whilst at higher laser energies (approaching 1.0 mJ) the ions with lower number of hydrogen atoms (for example $C_3H_3^-$ and $C_3H_2^-$) are evident. At the maximum laser energy (0.85 mJ), the C_3^- ion (*i.e.* n=0) is the most intense ion in the $C_3H_n^-$ series.
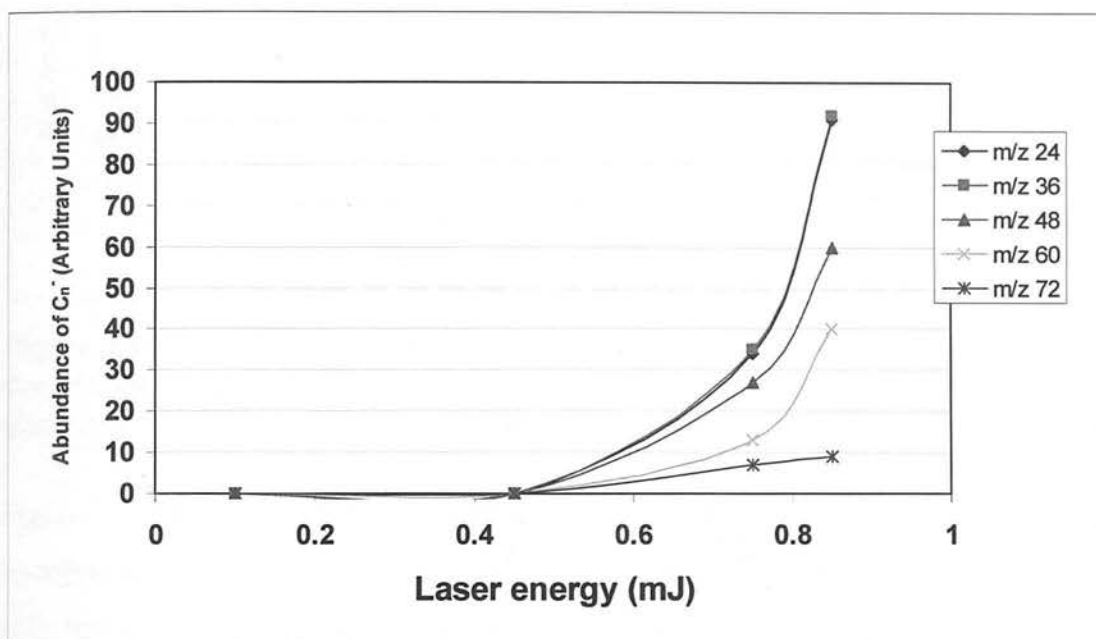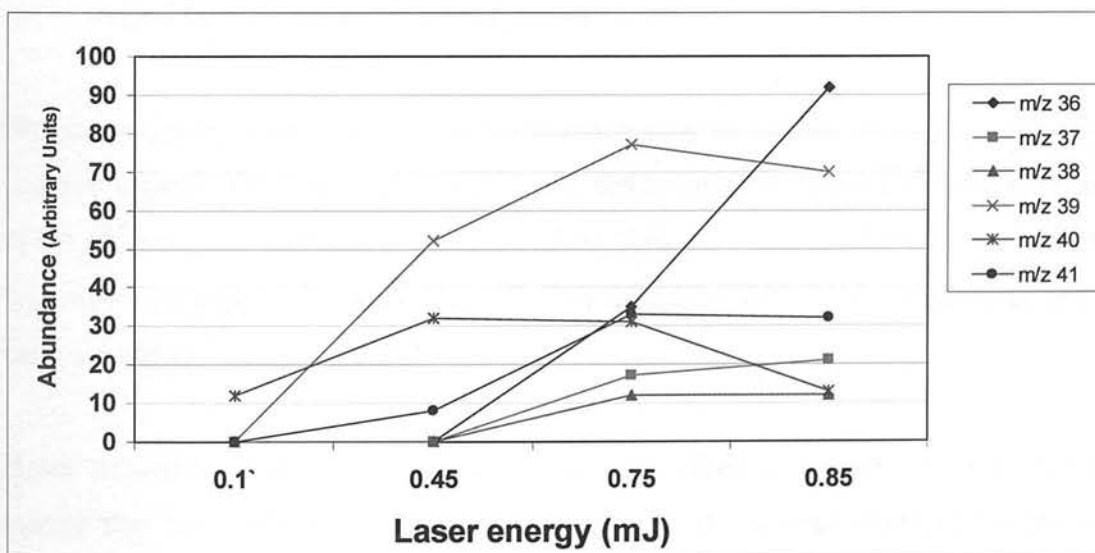

Figure 3.10. *The relative abundance of $(C_3H_n)^-$ ions as a function of laser energy in the average negative ion AToFMS spectra of FP. The traces shown are m/z 36, 37, 38, 39, 40 and 41 which are consistent with the ions for C_3^-, C_3H^-, $C_3H_2^-$, $C_3H_3^-$, $C_3H_4^-$, $C_3H_5^-$ and $C_3H_6^-$ respectively.*

In the negative ion mass spectrum of FP at higher laser energy, the ion observed at m/z -19 is attributed to the fluoride ion (F⁻). The relative abundance of fluoride ions with varying laser energies is shown in Figure 3.11. This demonstrates that fluoride ions are readily formed by using laser energies of greater than 0.4 mJ.
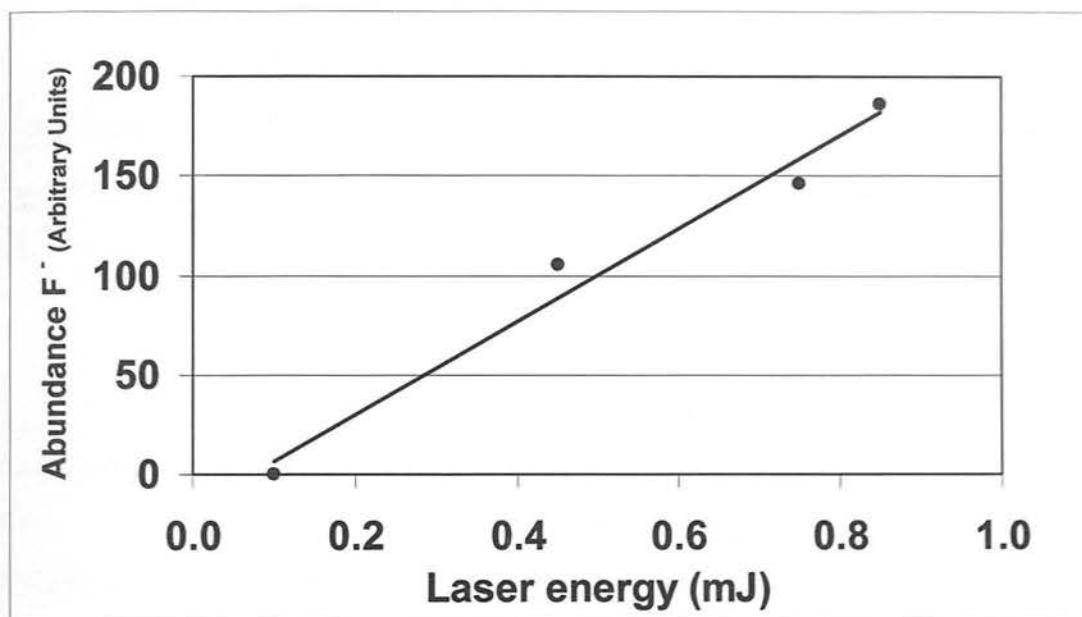
Figure 3.11. *Graph to show the variation in the abundance of the fluoride (F⁻) ion over a laser energy range of 0.1 to 1.0 mJ in the average negative ion AToFMS spectra of FP.*

3.3.4 The Formation of Negative Ions

The processes by which negative ion formation may occur can be categorised as (a) electron capture, (b) dissociative attachment or (c) ion pair formation[9]. As the energy of the electrons increases, or if the ionization source pressure is relatively high, then it becomes increasingly likely that negative ion formation will involve more than one of these processes[10].

If the negative ion is to be stabilized, following electron capture, then the kinetic energy that the electron possesses prior to capture and at least some of the binding energy, needs to be dissipated. This can occur either by (a) radiation, for which the probability is small, or by (b) transferring the energy to a third body (typically an atom or a molecule) *via* a collision[9].

The simplest way in which a negative ion can be formed is by the direct capture of a free electron by a neutral atom or molecule. This electron capture process occurs at low electron energies (less than 1 eV) and is summarized by Equation 3.1, where M is a third body.

$$XY + e^- \leftrightarrow (XY^-)^* + M \rightarrow XY^- + M^+ \qquad \textbf{Equation 3.1}$$
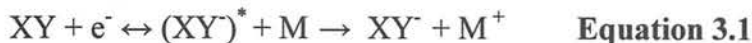
If the electron energy is greater than that required to break a bond and form a negative ion, then direct dissociation, (dissociative attachment) as summarized in Equation 3.2, may occur.

$$XY + e^- \leftrightarrow (XY^-)^* \rightarrow X + Y^- \qquad \textbf{Equation 3.2}$$

At higher electron energies (~10 eV), the molecule can be excited to an unstable state from which it dissociates into a positive and a negative ion, as summarized in Equation 3.3. This differs from the process summarized by Equation 3.2 as the electron is not captured, but provides the source of energy to produce the electronic transition in the molecule.

$$XY + e^- \rightarrow X^+ + Y^- + e^- \qquad \textbf{Equation 3.3}$$
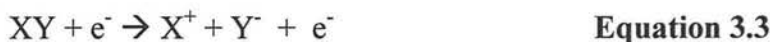
3.3.5 The Influence of Particle Size on Negative Ion Formation

Differences in positive and negative signal intensities and their dependence on particle size suggest that the formation of negative ions may involve more than one mechanism. Laser ablation using UV radiation is known to produce free electrons and the interaction of these electrons with molecules can result in the formation of negative ions typically by dissociative attachment[11, 12]. Furthermore, it has been shown that smaller particles tend to give much higher negative ion yields relative to the total mass of the particle[12].

3.4 Factors that Influence Aerodyne Aerosol Mass Spectrometry (AAMS) Data

Although the Aerodyne Aerosol Mass Spectrometer (AAMS) is of different design to the AToFMS instrument (see Sections 2.4.2 and 2.4.3), many of the factors that influence the data are common to both instruments. For example, particle shape has a major influence on the particle sizing data[13, 14] and as with the AToFMS instrument, vaporization and ionization efficiency are key factors that determine the appearance of the AAMS data[15].

For the AAMS instrument, only ions of one polarity can be analyzed at one time. Although it is possible to detect negative ions with the AAMS, all spectra shown in this section were acquired using positive ion detection as better sensitivity was obtained using this mode.

3.4.1 Operational Modes of the Aerodyne Aerosol Mass Spectrometer (AAMS)

Figure 3.12 compares particle sizing data acquired on the AAMS-ToF instrument in the chopper open mode with the chopper spinning mode. In the chopper open mode average mass spectra for groups of particles can be acquired and in the chopper spinning mode mass spectra can be acquired for single particles as described in Section 2.4.3. From Figure 3.12 it can be seen that the particle size distribution for the chopper spinning mode only involves the smaller particles. Also very few particles were detected in this mode, compared with the many particles observed in the chopper open mode, due to the reduced duty cycle.

For the chopper open mode, the sloping tail for the particles between 10^3 and 10^4 nm is probably due to slow vaporization of large particles[16]. Also, if the particles are of an irregular shape, there may be some divergence of the particle beam so that not all of the particles detected by light scattering hit the hot plate[17].

70
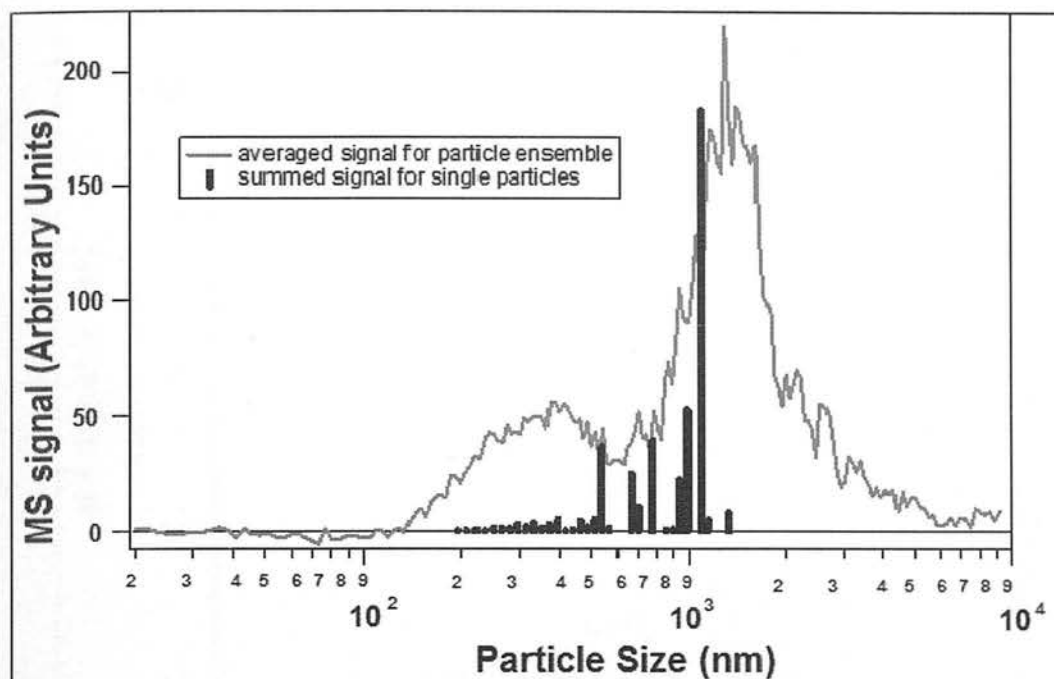
Figure 3.12. *A comparison of particle sizing data in chopper open (green trace) and chopper spinning (black trace) modes, (data shown for sample MDI_4, FP/SX 50/25).*

3.4.2 Vaporization Efficiency

For the AAMS experiments described in this thesis, the hotplate temperature was set at 500 °C and it was assumed that most organic material would flash vaporize at this temperature. Figure 3.13 shows a graph of mass spectral signal versus particle size for particles taken from a pMDI. Larger particles theoretically should give a larger signal; assuming the particles are spherical, the signal size should increase as the cube of the particle radius (as the volume of a sphere is $4/3\pi r^3$).

The data points shown in blue, in Figure 3.13, are within 20% of the third order polynomial line and are nominally assumed to be fully vaporized. The points shown in red are outside this limit and are assumed to be incompletely vaporized. The data acquired for pMDIs using the AAMS instrument, showed that the vaporization efficiency varied between 40 and 70 %.

The incomplete particle vaporization originates predominantly from particle bounce; thus rather than being fully vaporized the particle bounces from the hotplate and remains intact rather than being fully vaporized[17].

71
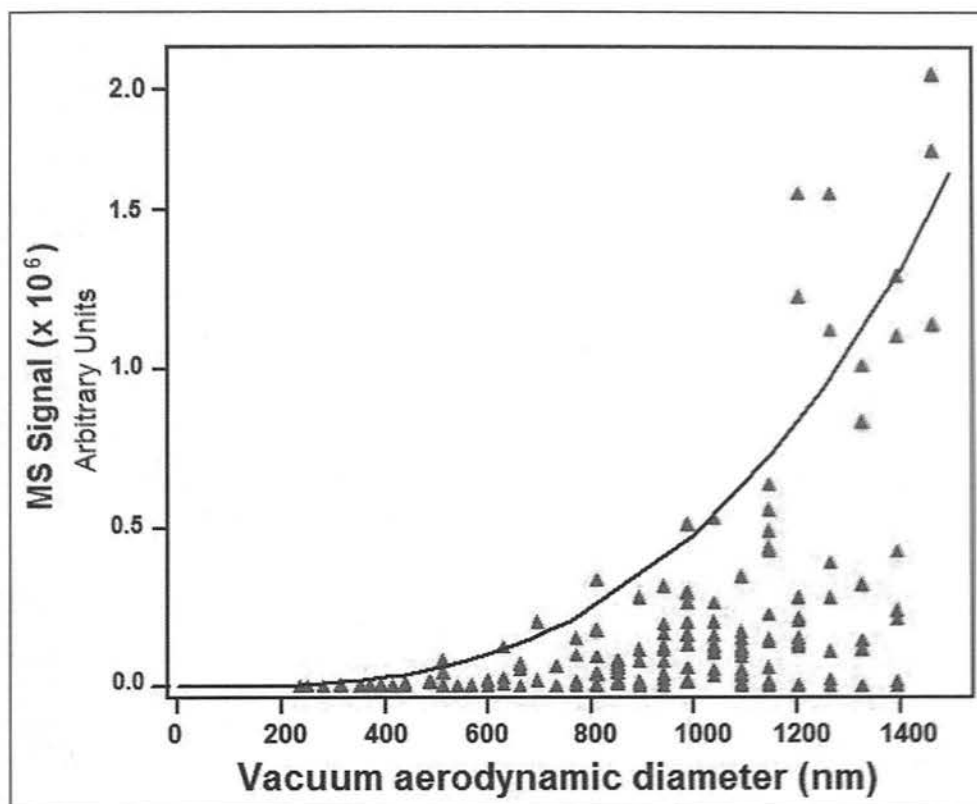
Figure 3.13. *Demonstration of partial vaporization in an AAMS experiment. Blue points - taken as fully vaporized; red points - vaporization is incomplete. Sample MDI_9 FP/SX 250/25.*

3.4.3 The Influence of Particle Size

In some samples, particle composition may vary with particle size. A comparison of the average mass spectra over the particle size range from 200 to 270 nm and from 500 to 1300 nm, from a pMDI sample, is shown in Figure 3.14. These mass spectra are clearly different *i.e.* 3.14 (b) shows ions at *m/z* 91, 114, 121 and 170 which are indicative of SX. For this sample, the smaller particles consist predominantly of FP and the larger particles are a mixture of FP and SX. Further discussion of this data is given in Chapter 6.
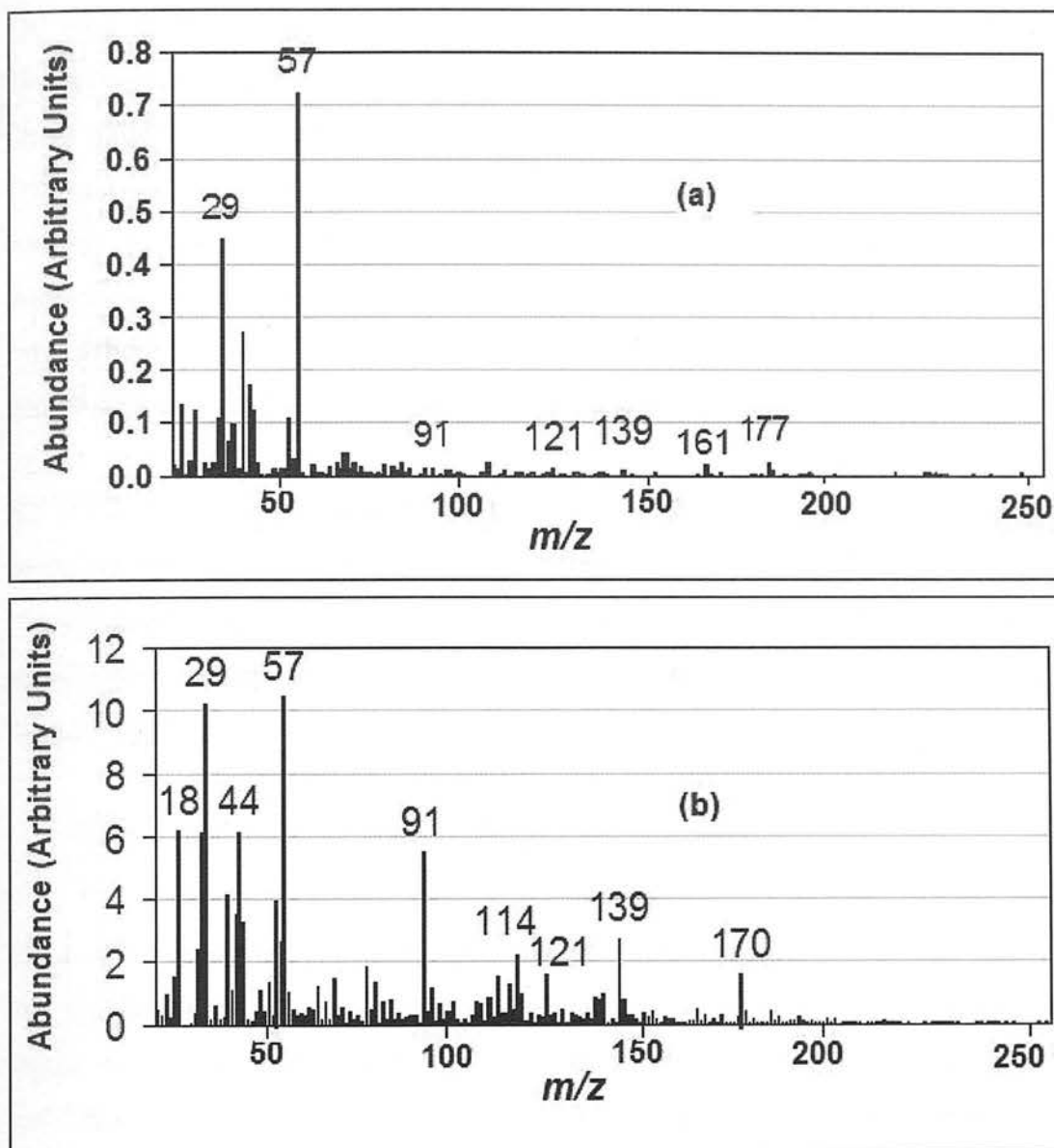
Figure 3.14. *Comparison of mass spectra, for different particle size ranges, from a sample MDI_4 FP/SX 50/25, (a) average mass spectrum for particles in the 200 to 270 nm size range and (b) average mass spectrum for particles in the 500 to 1350 nm size range.*

3.5 Interpretation of Aerodyne Aerosol Mass Spectrometry (AAMS) Data

By analysing the mass spectra from particles of pure compounds, indicative ions for each component were determined (see Chapter 6). The data sets for samples, containing blends of components, taken from dry powder inhalers (DPIs) and pressurized metered dose inhalers (pMDIs), were analyzed and classified using the indicative ions from the pure compounds.

The data shown in the following sections are average spectra that were acquired for the individual components and also for some blends of formulated DPI product using the Q-AAMS instrument. The data from the pure drugs (FP and SX) are shown first, followed by the results for lactose (acquired using a ToF-AAMS instrument) a common excipient. Excipients[18] are materials added to the formulation that have no therapeutic activity; for example lactose is used as a carrier for the active drug in DPI formulations. Finally the Q-AAMS spectra obtained for a blend of active drug compounds and excipients in an inhalation product are presented and discussed.

All of the data shown in Sections 3.5.1 and 3.5.2 were obtained using the quadrupole based AAMS instrument (Q-AAMS) apart from the mass spectrum for lactose which was acquired using the ToF based instrument (ToF-AAMS). Additionally, a similar set of experiments performed using the ToF-AAMS instrument on single particles are discussed in Section 3.5.4.

3.5.1 Q-AAMS Spectra of Drug Compounds

Figure 3.15 shows the Q-AAMS spectrum for FP: it shows that ions with relatively low m/z values (below m/z 200) were observed and some of these were found to be unique to the structure of FP. For example the ion at m/z 57 is assigned to the $H_3CCH_2CO^+$ fragment and the ion at m/z 139 is due to cleavage across steroid ring B as shown in Figure 3.16. This spectrum is comparable with the electrospray LC/MS spectrum for FP shown in Appendix A3.
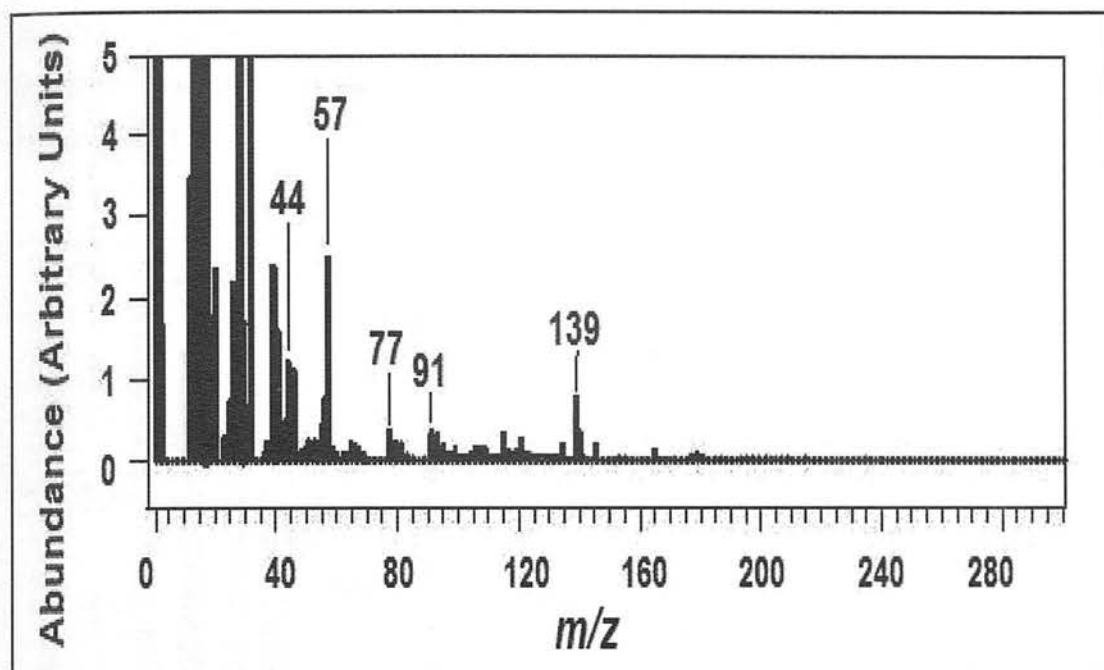
Figure 3.15. *The average mass spectrum of FP acquired using the Q-AAMS instrument, showing marker ions for FP.*
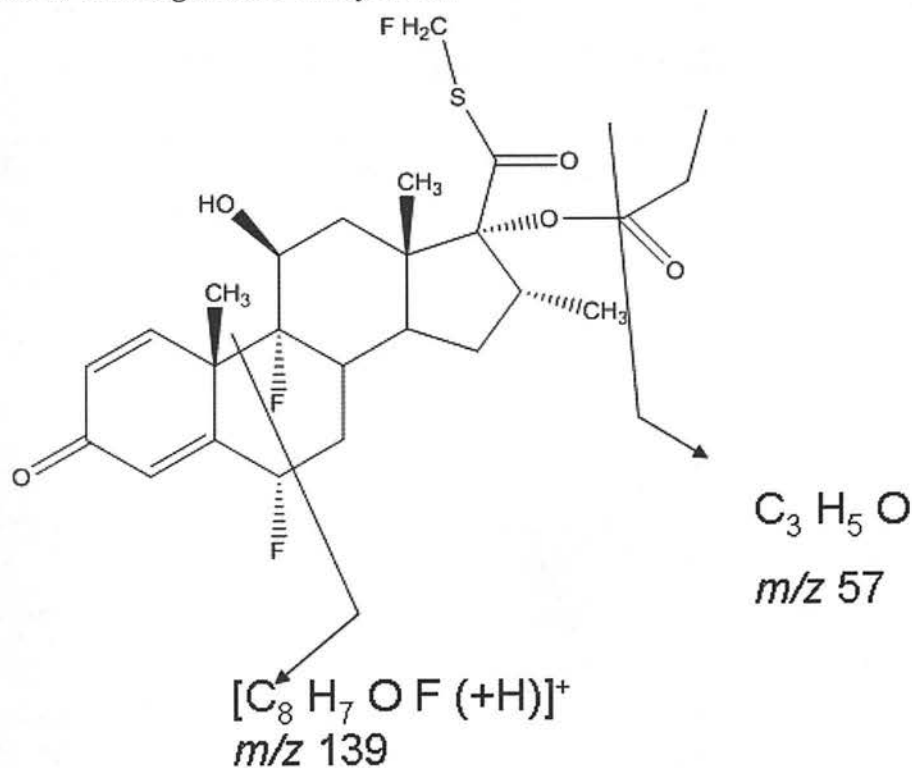
Figure 3.16. *Suggested fragmentation pattern showing origin of the representative marker ions for fluticasone propionate (FP), based on the EI mass spectrum shown in Figure 3.15, acquired using the Q-AAMS instrument.*

The average Q-AAMS EI mass spectrum for salmeterol xinofoate is shown in Figure 3.17. A highly abundant ion appears in the spectrum of SX at m/z 91 due to the tropylium ion and at m/z 170 due to the loss of water from the xinofoate salt and a

75

suggested fragmentation pathway for the major products is shown in Figure 3.18. This spectrum is comparable with the electrospray LC/MS spectrum for SX shown in Appendix A3.
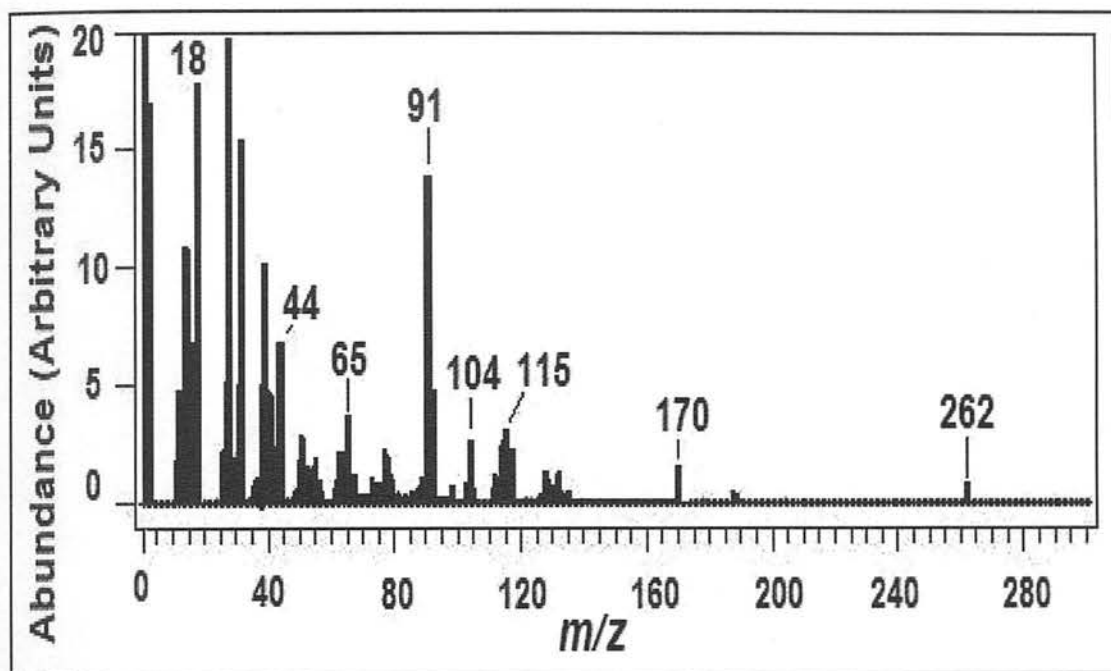
Figure 3.17. *Average mass spectrum of SX, acquired using the Q-AAMS instrument showing marker ions for SX.*

M$^{+\cdot}$ at m/z 415 (not observed)

m/z 262

m/z 91

Xinofoate (Molecular weight 188)

-H$_2$O

m/z 188

-CO$_2$

m/z 170

m/z 144

-COH

m/z 115
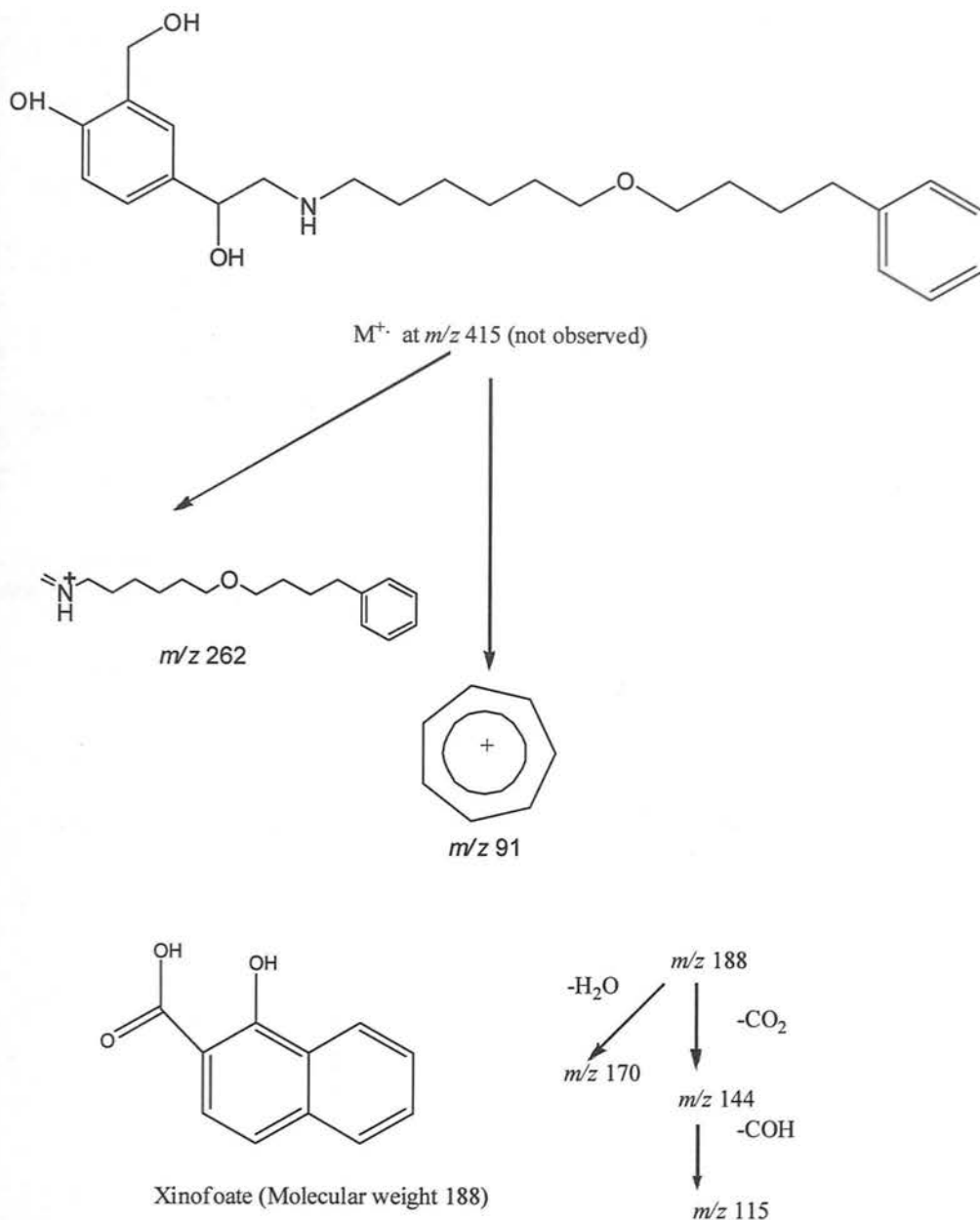
Figure 3.18. *Suggested fragmentation pattern showing origin of the representative marker ions for salmeterol (shown at the top of this figure) and the xinofoate ion, (shown at the bottom of this figure) based on the EI mass spectrum shown in Figure 3.17, acquired using the Q-AAMS instrument.*

3.5.2 AAMS Spectra for Excipients

An advantage of the AAMS (compared with the AToFMS) is that mass spectra of excipients may be acquired. For example the average ToF-AAMS EI mass spectrum for lactose is shown in Figure 3.19 (examples some other mass spectra of excipients acquired using AAMS are given in Appendix A3). Although no intact molecular ion is observed, possibly because of thermal decomposition, a number of unique ions are observed. These are shown in the fragmentation pathway suggested in Figure 3.20.
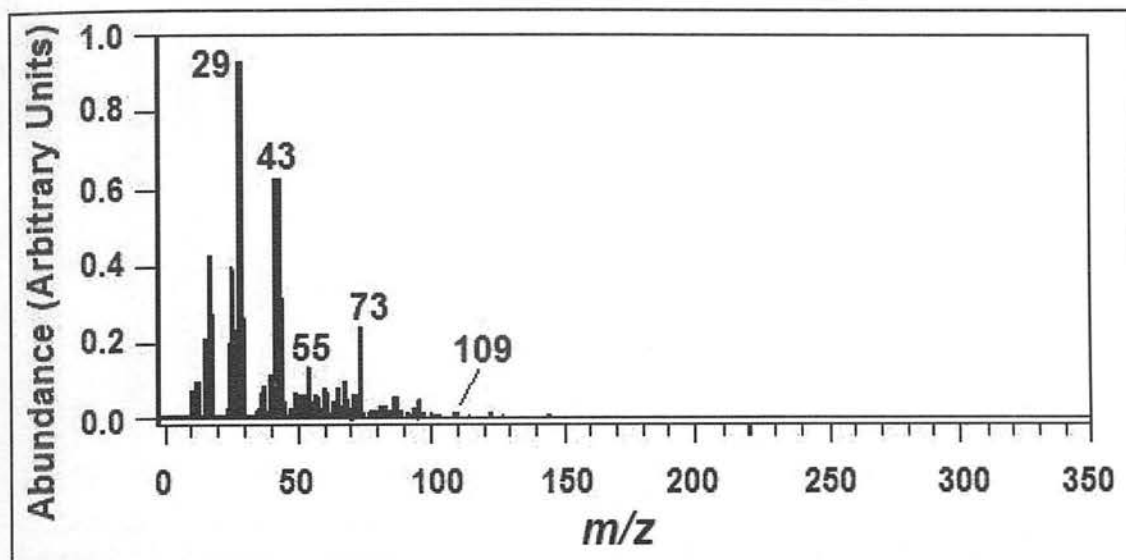
Figure 3.19. *Average ToF-AAMS spectrum of lactose, showing potential marker ions.*

$C_{12}H_{22}O_{11}$

Molecular weight 342

$C_3 H_5 O_2$

m/z 73

m/z 109
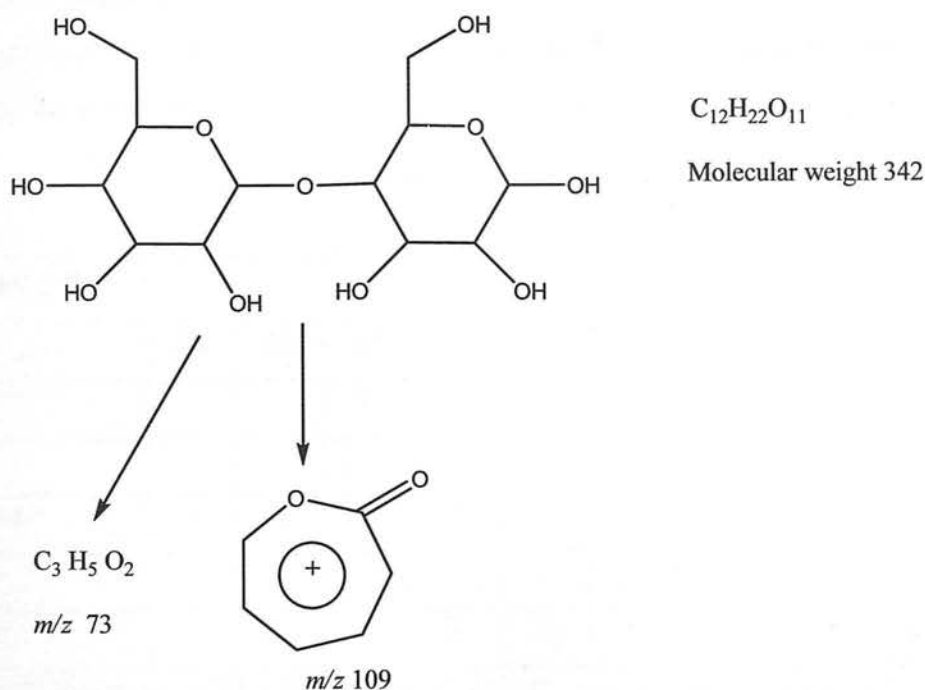
Figure 3.20. *Suggested fragmentation to give representative ions for lactose based on the ToF-AAMS EI mass spectrum shown in Figure 3.19.*

3.5.3 An Example Q-AAMS Spectrum for an Inhalation Product

Figure 3.21 shows the mass spectrum for the FP/SX 50/50 blend with lactose and cellobiose octaacetate (COA) as excipients.

78
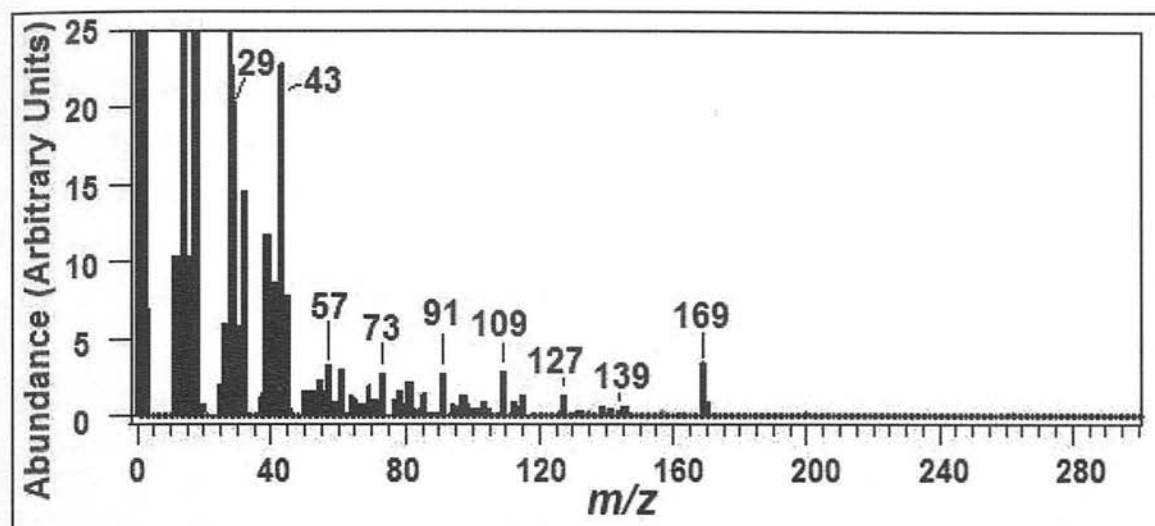
Figure 3.21. *Average Q-AAMS spectrum of 50/50 blend DPI with COA and lactose.*

The unique fragment ions for the individual compounds are shown in Table 3.3. All of these fragments are present in the blend indicating that the blend matrix has minimal effect on the mass spectra of the individual components.

Compound	m/z									
	29	43	57	73	81	91	109	139	169	170
FP			X					X		
SX						X				X
Lactose*	X	X		X			X			
COA†		X			X		X		X	
Blend	X	X	X	X	X	X	X	X	X	X

Table 3.3. *Summary of Q-AAMS spectral data (* Ions for lactose data based on ToF-AAMS spectrum, † Mass spectrum for COA shown in Appendix A3.). An X indicates the ion is present in the given mass spectrum; the data shows that all marker ions are present in the spectrum of the blend.*

3.5.4 ToF-AAMS Spectra for Single Particles

Figure 3.22(a) shows the ToF-AAMS spectrum taken from a single representative FP particle. The ions at *m/z* 57 and *m/z* 139 that were previously shown to be representative of FP from the average Q-AAMS spectrum are clearly visible.

Similarly Figure 3.22 (b) shows the ToF-AAMS spectrum of a SX particle. The ions at *m/z* 91 and 170 that were previously shown to be representative of SX from the average Q-AAMS spectrum are clearly visible.
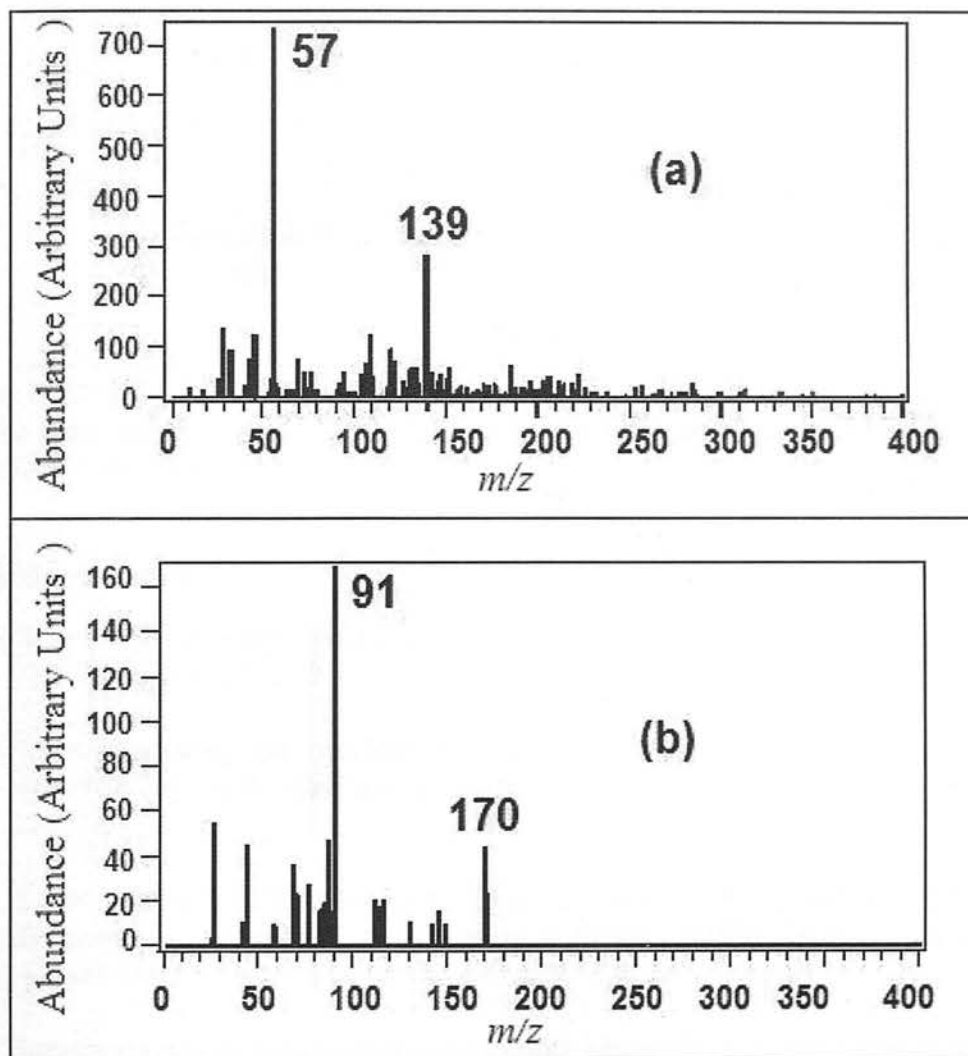
Figure 3.22. *ToF-AAMS spectrum of (a) single particle of FP and (b) single particle of SX. The spectra are labelled with representative ions for each compound.*

Figure 3.23 shows the ToF-AAMS spectrum of a mixed particle. The ions at *m/z* 91 and 170 from SX and *m/z* 57 and 139 from FP are all clearly visible.
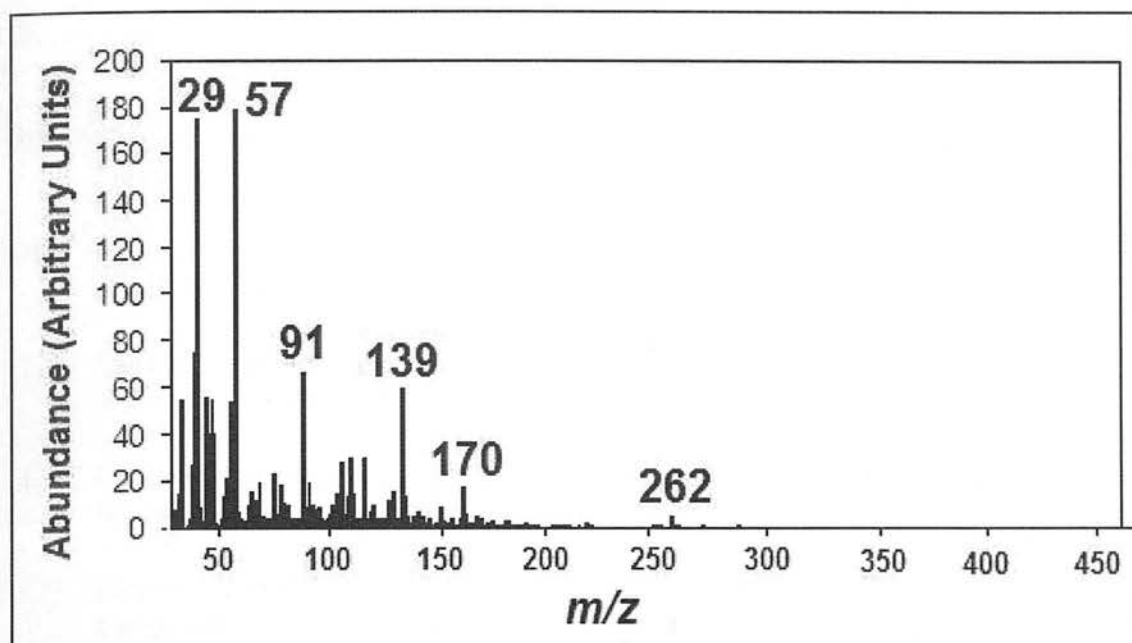
Figure 3.23. *ToF-AAMS spectrum of a single particle containing a mixture of FP and SX. The presence of FP is indicated by ions at m/z 57 and 139 and the presence of SX indicated by the ions at m/z 91, 170 and 262.*

3.6 References

(1)   The design of single particle laser mass spectrometers. D.M. Murphy. *Mass Spectrom. Rev.* 26, 150-165, (2007).

(2)   Instrumentation, data evaluation and quantification in on-line aerosol mass spectrometry. K-P. Hinz and B. Spengler. *J.Mass Spectrom.* 42, (7), 843-860 (2007).

(3)   Laser Chemistry, Spectroscopy, Dynamics and Applications. H. Telle, A. Gonzalez-Urena and R.J. Donovan. First Edition (2007), Wiley. ISBN-978-0-471-48571-1.

(4)   Improvements in ion signal reproducibility obtained using a homogeneous laser beam for on-line laser desorption/ionization of single particles. R. Wenzel and K. Prather. *Rapid Commun. Mass Spectrom.* 18, 1525-1533, (2004).

(5)   Principal component analysis. S. Wold, K. Esbensen and P. Geladi, *Chemometrics and Intelligent Laboratory Systems.* 2, 37-57 (1987).

(6)   Interpretation of mass spectra from organic compounds in aerosol time-of-flight mass spectrometry. P.J. Silva and K.A. Prather. *Anal. Chem.* 72, 3553-3562, (2000).

(7)   Simultaneous detection of positive and negative ions from single airborne particles by real-time laser mass spectrometry. K-P. Hinz, R. Kaufmann and B. Spengler. *Aerosol Sci. and Tech.* 24:4, 233-242, (1996).

(8)   Organic Spectroscopy. W. Kemp. Third edition (1991). MacMillan Publishers Ltd. ISBN 0333181530.

(9)   Negative ions. H.S.W. Massey. Third edition, (1976), Cambridge University Press. ISBN 0 521 207754.

(10)   Negative ion spectra of polyatomic molecules. K. MacNeil and J. Thyne. *Trans. Faraday Soc. 64, 2112, (1968).*

(11)   Laser desorption/ionization of ultrafine aerosol particles. P.Carson, M.Johnson and A.Wexler. *Rapid Commun. Mass Spectrom. 11, 993-996 (1997).*

(12)   Detection of negative ions from individual ultrafine particles. D. Kane, J. Wang, K. Frost and M. Johnston. *Anal. Chem. 74, 2092-2096 (2002).*

(13)   Particle morphology and density characterization by combined mobility and aerodynamic measurements. Part 1: Theory. P. DeCarlo, J. Slowick, D.R. Worsnop, P. Davidovits and J-L. Jimenez. *Aerosol Sci. and Tech. 38, 1185-1205, (2004).*

(14)   Particle morphology and density characterization by combined mobility and aerodynamic measurements. Part 2: Application to combustion-generated soot aerosol as a function of fuel equivalence ratio. J. Slowick, K. Stainken, P. Davidovits, L.R. Williams, J.T. Jayne, C.E. Kolb, D.R. Worsnop, Y. Rudich, P. DeCarlo and J-L. Jimenez. *Aerosol Sci. and Tech. 38, 1206-1222, (2004).*

(15)   Chemical and microphysical characterization of ambient aerosols with the Aerodyne aerosol mass spectrometer. M.R. Canagaratna, J.T.Jayne, J.L. Jiminez, M.R. Afarra, Q. Zhang, F. Drenwick, H. Coe, A. Middlebrook, A. Delia, L.R. Williams, A.M. Trimborn, M.J. Northway, P.F. DeCarlo, C.E. Kolb, P. Davidovits and D.R. Worsnop. *Mass Spectrom. Rev. 26, 185-222, (2007).*

(16)   Private Communication- Aerodyne Research Inc, Billerica, Massachusetts, USA (15 Oct 2007).

(17)   Chemical and Physical Characterization of Aerosols with the Aerodyne Aerosol Mass Spectrometer: Laboratory and Field Applications. D.R. Worsnop, J.T. Jayne, M. Canagaratna, T. Onasch, L.R. Williams, M. Northway A. Trimborn, J. Slowik, P. Davidovits, P. DeCarlo J-L. Jimenez and Q. Zhang. *Lecture at 54th ASMS conference Seattle, US June 2006.*

(18)   Handbook of pharmaceutical excipients. R. Rowe, P. Sheskey and S. Owen. Fifth Edition, (2006), Pharmaceutical Press. ISBN 10 1582120587.

Chapter 4

Data Analysis Methods for Aerosol Time-of-Flight Mass Spectrometry (AToFMS)

4.1 Introduction

This chapter describes how the data processing methods were developed for the analysis of Aerosol Time-of-Flight Mass Spectrometry (AToFMS) data. These methods were then applied to the data taken from AToFMS experiments designed to investigate the degree of co-association in a wide range of samples of inhalation product material; the results from which are presented in Chapter 5.

The AToFMS, datasets are divided into data relating to particle size and mass spectra which are collated and linked through the tables of a Microsoft Access™ database[1]. The MS-Analyze™ software[2] (supplied with the AToFMS instrument) uniquely labels data for each particle with an identifier as it is acquired by the data system. This identifier is used to reference and link data on particle size to the corresponding mass spectra. Data arranged in this way is easily retrieved and interrogated either directly through the database, *via* MS-Analyze™, or *via* third party software such as Matlab™[3]

The identification of particles by the appearance of the mass spectrum was achieved based on (i) the identification of representative marker ions and (ii) on mass spectral fragmentation pattern recognition. Marker ions are fragmentation ions that are representative of a given drug compound. The formulated inhalation product is a well defined blend of two or three compounds (*i.e.* drugs and excipients) hence, it was possible to ensure that the marker ions chosen were representative and unique to each compound. The marker ion analysis shown in this and the next chapter are based on one marker ion per compound. Data analysis methods based multiple marker ions were explored but found to be unreliable hence this approach was not pursued. For

example the use of four marker ions resulted in large numbers of particles (up to 40 %) remaining unclassified. The identification and classification of particles based on composition determined by marker ions is discussed in Section 4.3.

Additionally, the identification of particles based on their mass spectral pattern was performed by using a multivariate statistical analysis based on principal components. In this approach, rather than selecting individual pieces of data it is the variation in the whole of the dataset that is considered. This gives a more complete analysis of the dataset[4] and is generally a more sophisticated approach compared with the use of marker ions. The identification and classification of particles based on composition determined by principal component analysis (PCA) is discussed in Section 4.3. A general description of (PCA) is given in Appendix (A3.3).

The details of the samples of inhalation products used for the data analysis development described in this Chapter are given in Appendix A4.1. A complete list of samples is given in Appendix A5.1.

For the AToFMS experiments described in this and the next chapter, initial data were acquired using the nozzle-skimmer as the sample inlet and a range of laser energy from 0.1 to 1.0 mJ. Further experiments to investigate co-association were performed using low laser energy (0.2 mJ) on the upgraded instrument incorporating an aerodynamic lens inlet. Examples of the data acquired using the nozzle-skimmer and aerodynamic lens inlets (which are described in Section 2.3) are given later in this chapter.

4.2 Particle Size Analysis

Some discussion of the particle sizing data is given in this section although the emphasis of this work was to determine the degree of co-association present. Figure 4.1(a) shows the particle size distribution for particles of pure FP in terms of the number of particles that were detected by light scattering in the particle sizing region of the AToFMS instrument (in this case 5794), compared with the number of particles that were ablated in the mass spectrometer ionization source. In this example 3.5% of

the particles detected in the light scattering region were ablated. The particle size range shown is from 0.3 to 10 μm. Note that particles which are detected by both timing lasers are said to have been 'sized' and those which are desorbed and ionized by the third laser to produce mass spectra are said to be 'hit' (See Section 2.3.3.3).

An enlarged view of the particle size distribution for the FP particles that were ablated is shown in Figure 4.1(b). Most of the particles were found to be in the size range of between 0.75 and 3.5 μm and the average particle size was found to be approximately 2 μm which was expected as the pure FP was micronized[5] before use to an average particle size of 2 μm.
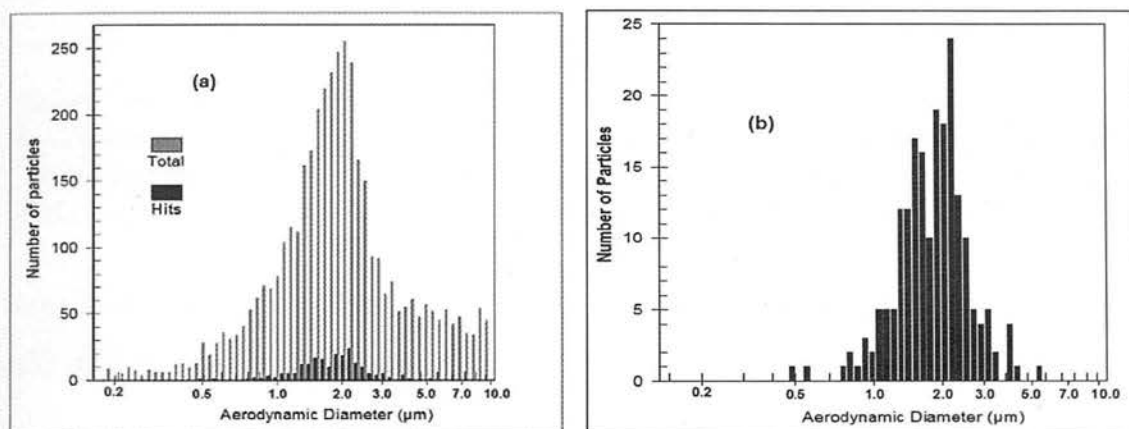
Figure 4.1. *Particle size distribution for pure FP particles introduced via a nozzle-skimmer inlet. (a) shows particles detected by light scattering (Total) and ablated particles (Hits) using the mass spectrometer, (b) shows an expanded normalised view of the ablated particles (Hits). These data were collected at laser energies from 0.1 to 1.0 mJ.*

The nozzle-skimmer inlet does not transmit particles of all sizes equally and the particle size distribution can be corrected[6] (See Section 2.3.1) However, as the primary objective of this thesis was to study co-association a correction for the particle size transmission efficiency was not applied.

Further work was performed using the aerodynamic lens for the experiments described in Chapter 5 to estimate the amount of co-association and to estimate the reproducibility of the measurement.

An example of the particle size distribution for pure FP particles determined under these conditions is given in Figure 4.2(a). This shows a much narrower particle size distribution compared with the nozzle-skimmer inlet (Figure 4.1) and indicates that

the largest particles detected have an aerodynamic diameter of approximately 3 μm. Figure 4.2(b) shows that the ablated particles were smaller than those detected in the particle sizing region with light scattering.
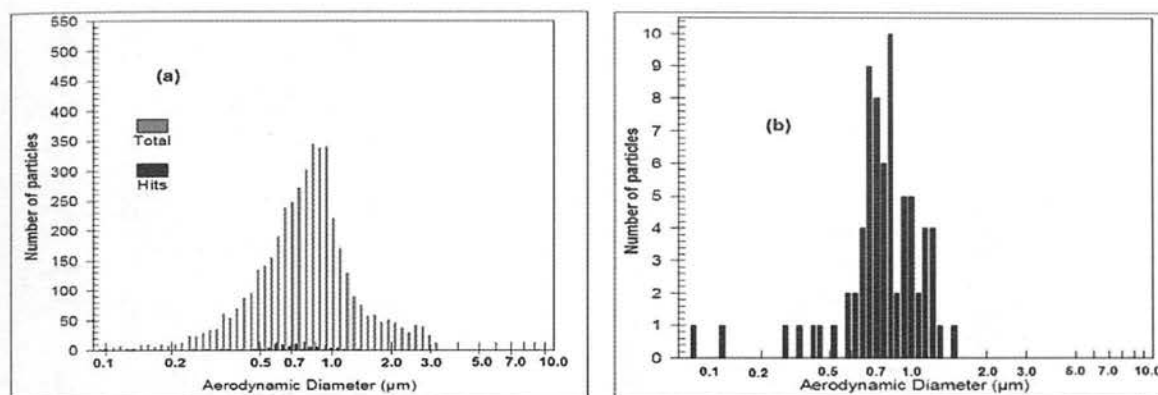
Figure 4.2. *Particle size distribution for pure FP particles introduced via a aerodynamic lens inlet. (a) shows particles as detected by light scattering (Total) and as ablated particles (Hits) using the mass spectrometer (b) shows a normalised view of the ablated particles (Hits). These data were collected at a laser energy of 0.2 mJ.*

Only a few of the particles that are detected in the particle sizing region are ablated and ionized. The hit efficiency for the AToFMS (E_{AToFMS}) is given by Equation 4.1.

$$E_{AToFMS} = P_{MS} / P_{Total} \; X \; 100\% \qquad\qquad \textbf{Equation 4.1}$$

Where: P_{MS} = Number of particles hit by the ablation laser

P_{Total} = Total number of particles detected by light scattering

Table 4.1 summarises the hit efficiency for the data acquired using the AToFMS instrument and shows the average particle size for each dataset. The hit efficiency for particles of SX was shown to be over twice the value for FP due to the fact that SX absorbs energy from the ablation laser (at 266 nm) more efficiently (as shown in Section 3.2). The average size for the particles that were hit (shown in Table 4.1) was 0.4 μm for SX and 0.8 μm for FP.

Table 4.1 also shows the average particle size for each sample; in this case the particle size shown is for the particles that were hit by the ablation laser (as opposed to the total particle population that was detected using light scattering).

	Sample	File	Total Particles (P_{Total})	Particles hit (P_{MS})	Hit efficiency (E_{AToFMS}) %	Av PS* μm
Standards	SX powder	SX4	4129	160	3.9	0.4
	FP powder	FP2	5051	74	1.5	0.8
	Serevent®	SERE_1	6311	121	1.9	1.2
	Flovent®	FLO_1	8336	101	1.2	1.3
pMDI	FP/SX, 250/25	MDI_1	4081	101	2.5	0.9
	FP/SX, 250/25	MDI_2	5006	104	2.1	1.0
	FP/SX, 250/25	MDI_3	3590	102	2.8	0.9
	FP/SX, 250/25	MDI_4	4768	102	2.1	1.0
	FP/SX, 250/25	MDI_5	3836	101	2.6	0.9
pMDI	FP/SX, 125/25	MDI_6	5474	104	1.9	0.9
	FP/SX, 125/25	MDI_7	2899	100	3.4	1.0
	FP/SX, 125/25	MDI_8	3793	101	2.7	0.9
	FP/SX, 125/25	MDI_9	4183	102	2.4	0.9
	FP/SX, 125/25	MDI_10	3960	101	2.6	0.9
pMDI	FP/SX, 50/25	MDI_11	3786	101	2.7	0.8
	FP/SX, 50/25	MDI_12	3406	109	3.2	0.9
	FP/SX, 50/25	MDI_13	3724	101	2.7	0.7
	FP/SX, 50/25	MDI_14	3337	106	3.2	0.8
	FP/SX, 50/25	MDI_15	3813	103	2.7	0.8
DPI	FP/SX, 250/50	DPI_1	5078	68	1.3	1.2
	FP/SX, 250/50	DPI_2	6218	57	0.9	1.3
	FP/SX, 250/50	DPI_3	6621	68	1.0	1.3
	FP/SX, 250/50	DPI_4	7379	79	1.1	1.3
	FP/SX, 250/50	DPI_5	8985	130	1.4	1.3
DPI	FP/SX, 500/50	DPI_7	13484	102	0.8	1.2
	FP/SX, 500/50	DPI_8	11998	109	0.9	1.3
	FP/SX, 500/50	DPI_9	13376	100	0.7	1.2
	FP/SX, 500/50	DPI_10	11428	103	0.9	1.3
	FP/SX, 500/50	DPI_11	12202	102	0.8	1.2

*Table 4.1. AToFMS hit efficiency and particle size data for (i) pure FP and SX (ii) DPIs containing a blend of one active drug and lactose (Flovent® and Serevent®) and (iii) combination pMDI and DPI devices containing both FP and SX. *Av PS = average particle size. An explanation of each sample is given in Appendix A5.1.*

The aerodynamic size of the particle reflects the shape of the particle as well as the size. Hence particles of the same diameter but different shape, will give different transit times that translate into different particle sizes[7].

To investigate the shape of particles found in the materials used, scanning electron microscope (SEM) images were acquired. These images were taken using a Hitachi S-4700, field emission SEM (Hitachi High Technologies America, Pleasanton, CA,

USA). The images of the particles found in the pure powders[8] and in a pMDI are shown in Figure 4.3.

The SEM images give an impression of the two dimensional shape of the particles, and it can be seen that they appear irregularly shaped; for example the FP particles in Figure 4.3 (a) are approximately disc shaped. The images also show some particles that are much larger than those detected using the AToFMS (or the AAMS) instrument. For these experiments, the larger particles were not detected mainly because they were prevented from entering the instrument by the sample conditioning apparatus (See Section 2.4.1).

The shape of the particles taken from the inhaler appears to be different from that of the two active drug compounds. It is speculated that the shape was affected by the co-association between the drug materials, *i.e.* if the greasy FP material were spread onto the surface of the irregular SX particles it may have resulted in the formation of particles with a much smoother surface. However further investigation would be required to prove this to be the case unequivocally.
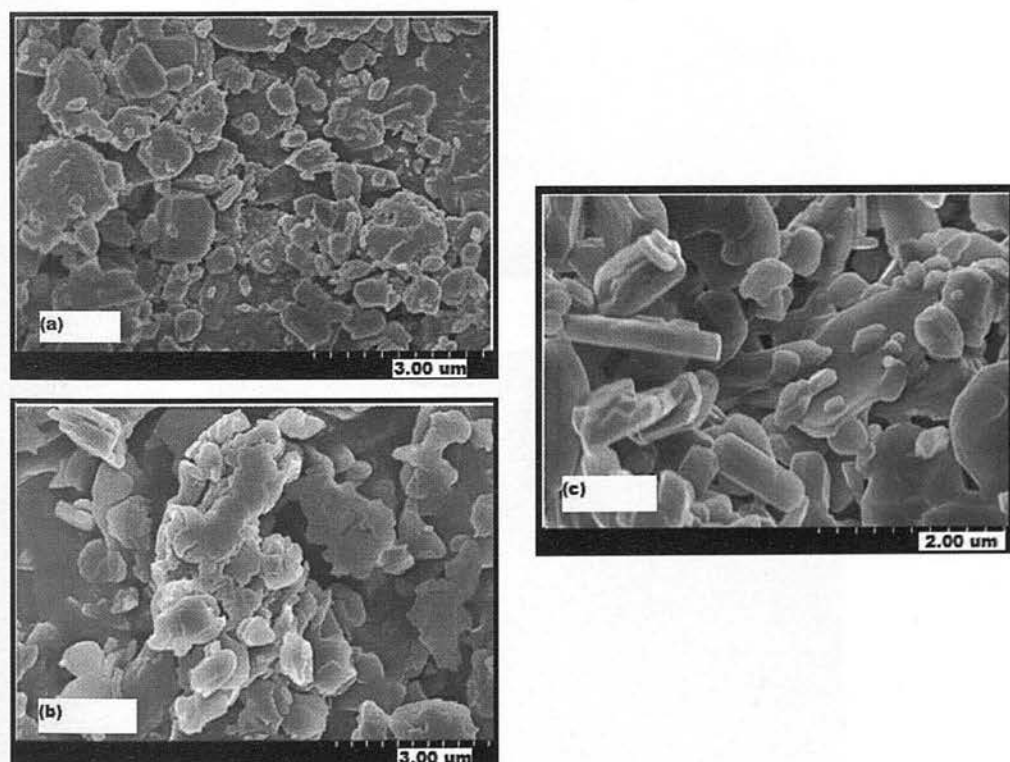
Figure 4.3. *Scanning electron microscope images of particles from (a) FP powder (b) SX powder (c) pMDI inhaler.*

Figure 4.4 compares the SEM images taken from lactose and from material used in a DPI device. Figure 4.4 (a) shows the much larger lactose particles typical of the material used in DPI devices as an excipient. The image shown in Figure 4.4(b) was taken from DPI inhaler particles and shows the larger lactose particles and smaller particles from the drug materials present. Lactose cannot be detected using the AToFMS instrument as it does not absorb light at 266 nm. However, it was found that lactose can be detected using the AAMS instrument, as described in Section 3.5.2. There may be some advantage in the AAMS in this respect as it is able to detect excipients in single particles comprised of mixtures of components. For example the difference between a particle containing FP and a mixture of FP and lactose would be apparent using the AAMS but not with the AToFMS. It may be useful to be able to detect excipients such as lactose in the SPMS experiment however further work would be required to explore the application of this observation.
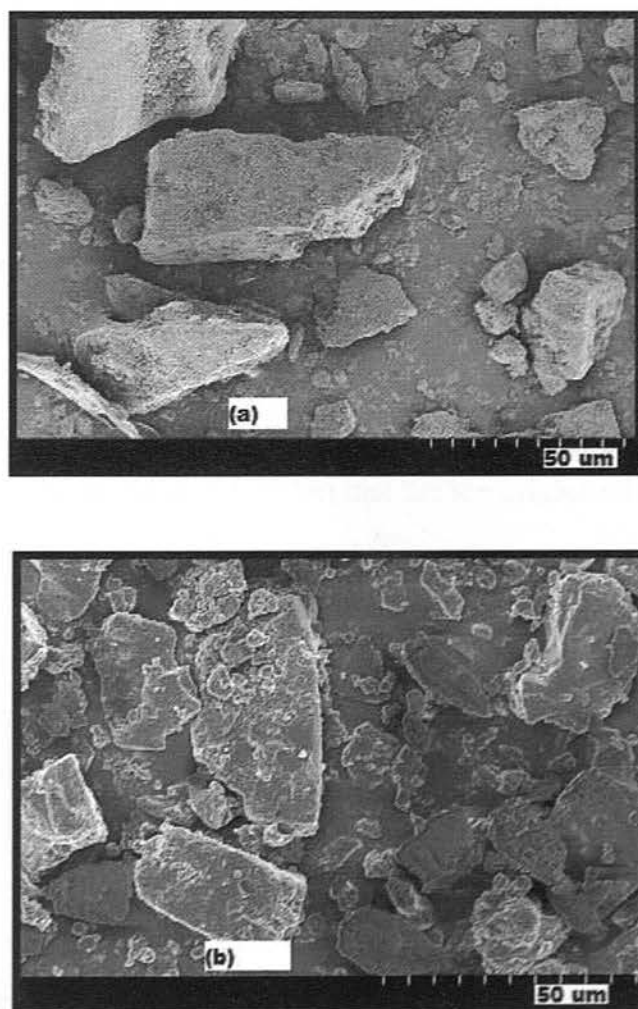
Figure 4.4. *Scanning electron microscope images of particles from (a) lactose powder (b) DPI inhaler.*

4.3 The Identification and Classification of Particles Based on Composition Determined by Marker ions

4.3.1 Identification of Marker Ions for Pure Drug Compounds

The aim of data analysis based on marker ions, is to be able to identify and classify the particles from inhalation products in terms of their composition. In this section the choice of characteristic, marker, fragment ions used to identify particle composition is discussed. An example of the identification of particles from inhalation products is presented later in this chapter (see Section 4.3.2) and the use of classification of particles from AToFMS data sets to determine co-association is described in detail in Chapter 5.

The choice of marker ions from the mass spectra of particles of pure drug material was based on the fragment ions observed in the average AToFMS spectra. The MS-Analyze™ software enables the number of particles that give a mass spectrum showing a particular ion to be counted. Note that the AToFMS is able to detect both positive and negative ions simultaneously (see Section 2.4.2) However the data analysis performed using the MS-Analyze™ software separates the positive and negative ion spectra and labels the ions as such. For example in the data analysis shown in this thesis, a positive ion would be shown as m/z 100 and a negative ion would be shown as m/z -100. For the negative ions m/z -100 does not infer a negative value for the m/z, (clearly impossible!!) but that the ion originated from a negative ion spectrum.

For example Figure 4.5 shows the analysis of a dataset of FP particles in terms of the ions found in the average AToFMS spectrum of FP (see Appendix A4.2). In this figure the x-axis gives the m/z value for each fragment ion and the y-axis shows the number of particles that yield mass spectra that contain the given ion. The most prominent fragment ions for FP shown in Figure 4.5 are at m/z -39, -66, -74, 97 and 58 which means that the majority of the single particles from pure FP gave mass spectra that showed these ions.
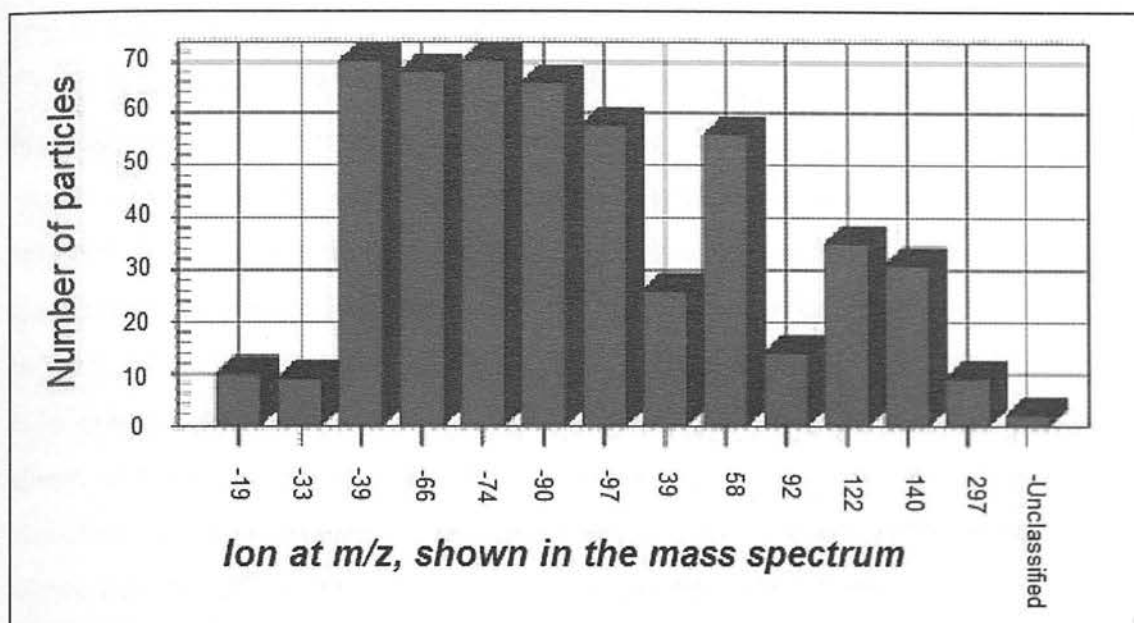
Figure 4.5. *Analysis of the AToFMS dataset of pure FP particles showing potential marker ions for FP. Negative m/z values indicate negative ions, positive m/z values indicate positive ions.*

Analysis of a SX data set is shown in Figure 4.6. The ions from the xinofoate counter-ion at m/z -188, -152 and -144 dominate the negative ion AToFMS mass spectrum and are present in the mass spectra of the majority of the particles. The most prominent positive ions are shown at m/z 115 and 92 however these are present in fewer of the particles analyzed, hence are less indicative of SX compared with than the negative ions mentioned above.
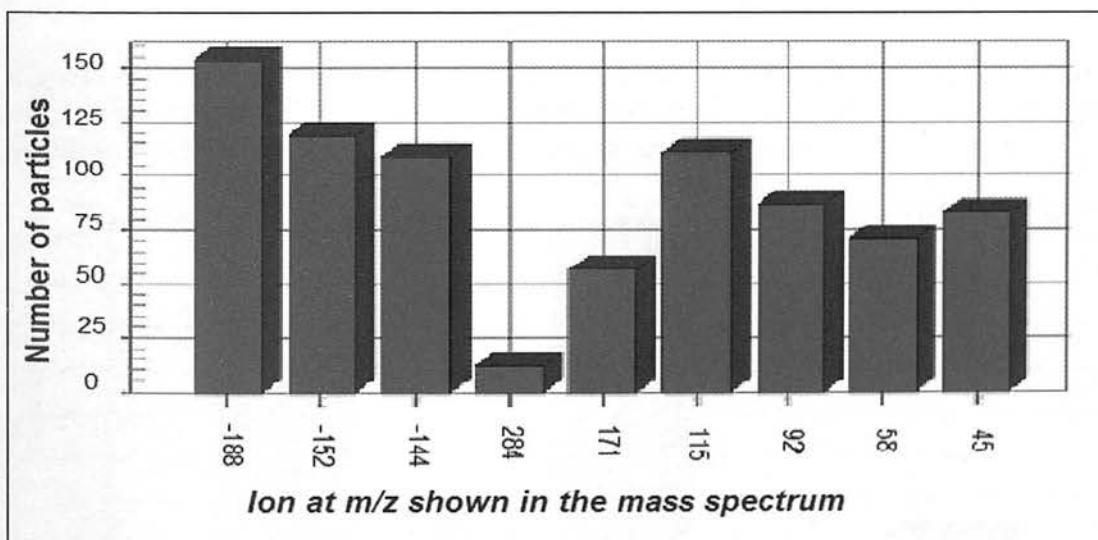
Figure 4.6. *Analysis the AToFMS dataset for pure SX particles showing potential marker ions for SX. Negative m/z values indicate negative ions, positive m/z values indicate positive ions.*

The most prominent ions in Figures 4.5 and 4.6 (*i.e. m/z* -188 for SX and *m/z* -74 for FP where the negative *m/z* values indicate negative ions) were used as marker ions for the data analysis described in Chapter 5. These ions are abundant in the average mass spectra of each of the pure drug compounds, appear in the mass spectra for the majority of the particles of each pure drug compound and are unique to the mass spectrum of each pure drug compound. The use of the marker ions *m/z* -188 for SX and *m/z* -74 for FP was tested on the datasets of the pure drug compounds. Figure 4.7 is an example dataset from pure SX particles and based on the marker ions mentioned above and shows that 96.3 % of the particles from the pure SX material were identified as SX. Similarly, Figure 4.8 shows a dataset from pure FP particles and shows that 94.6 % of the particles from the pure FP material were identified as FP. The Boolean OR operation was used to give the FPORSX category and is discussed in the next section. In this case it is used to show the total number of particles containing FP or SX.
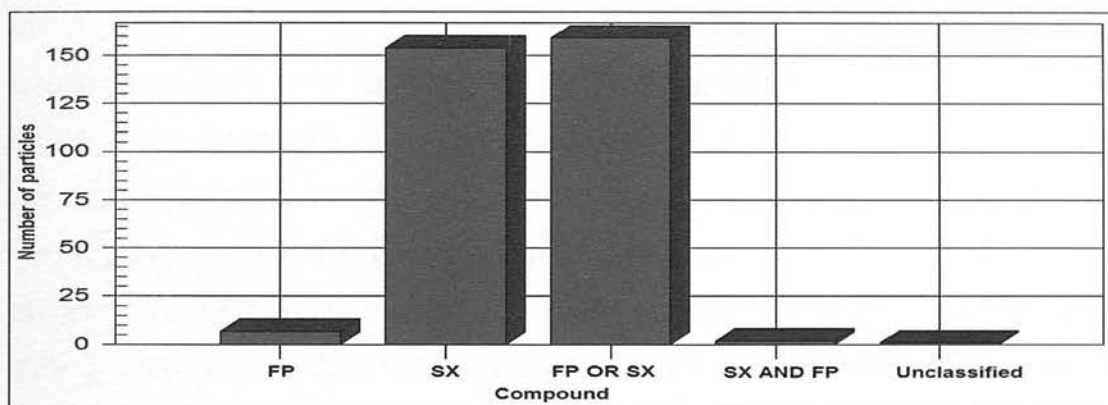
Figure 4.7. Classification of the AToFMS dataset for pure SX particles in terms of one marker ion for FP (m/z -74) and one marker ion for SX (m/z -188); see text above for further details. Negative m/z values indicate negative ions
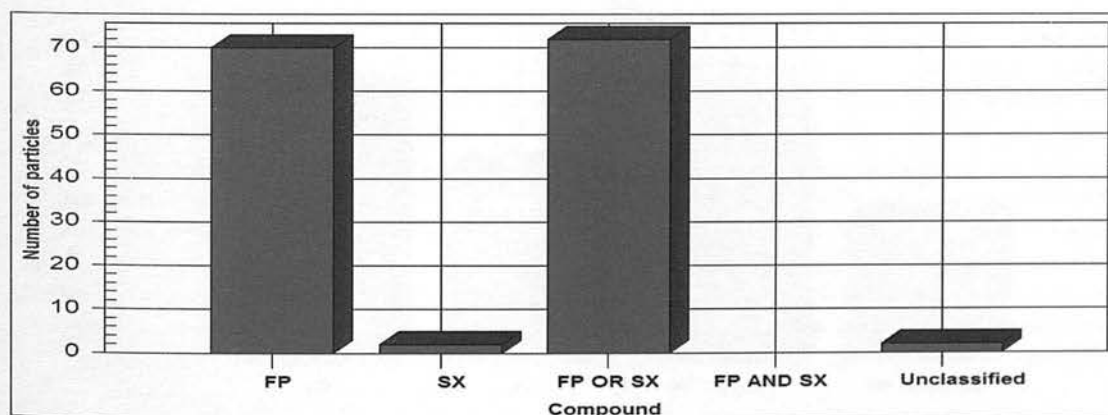
Figure 4.8. Classification of the AToFMS dataset for pure FP particles in terms of one marker ion for FP (m/z -74) and one marker ion for SX (m/z -188); see text above for further details. Negative m/z values indicate negative ions

4.3.2 Classification of Particles from Inhalation Products

The data analysis method based on marker ions was developed further using the MS-Analyze™ software, with the application of 'AND' and 'OR' Boolean operations which were used in the identification of co-associated particles. The formulated product of the pressurized metered dose inhalers (pMDIs) only contains the active drugs FP and SX. This gives the possibility of identifying three types of particle *i.e.* (a) containing FP, (b) containing SX or (c) containing a mixture of both FP and SX (*i.e.* co-associated). The required result from this data analysis is the number of co-associated particles given by 'FPANDSX' which gives a measure of the amount of co-association present. The total number of particles, *i.e.* those identified as containing FP or containing SX is given by 'FPORSX'.

It is noted that in using this method, the category for FP recognizes the presence of FP but does not exclude the presence of SX. Hence when samples containing co-associated particles were analyzed, the FP category showed particles that contained FP *i.e.* from either pure or co-associated particles and similarly the SX category showed particles that contained SX, *i.e.* from either pure or co-associated particles The number of pure FP particles can be calculated by subtracting the number categorised as FP from the number of particles shown as 'FPORSX', however for this work it is the particles composed of a mixture of FP and SX that are of most interest as these are used to measure the degree of co-association present. An example of the classification of the particles taken from a pMDI is shown in Figure 4.9 (FP/SX 250/25; MDI_1).
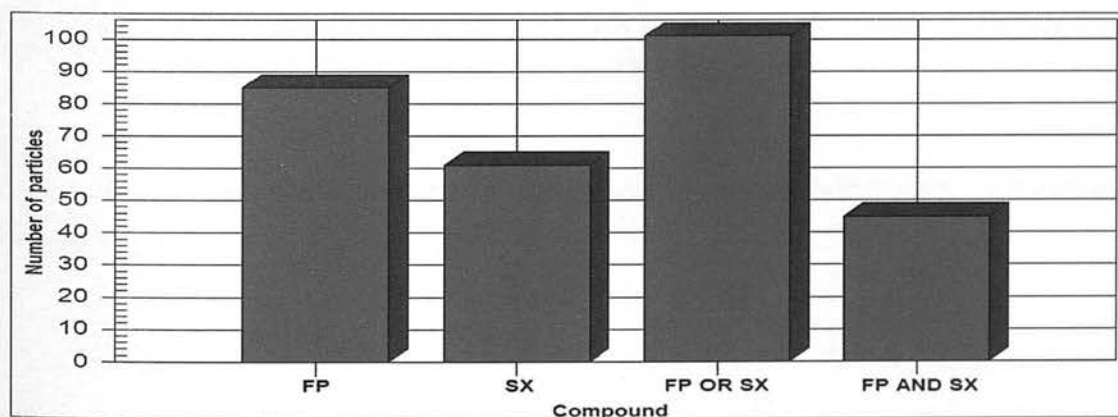
Figure 4.9. An example of the classification of particles from a pMDI based marker ions (m/z -188 for FP and m/z – 74 for SX). The example shown is from MDI_1 (FP/SX 250/25). Negative m/z values indicate negative ions

The formulation for the dry powder inhaler (DPI) samples contained the excipient lactose as well as the active drugs FP and SX. This gives the possibility of forming seven categories of particle *i.e.* pure FP, pure SX, a mixture of FP and SX as well as FP + lactose, SX + lactose and FP + SX + lactose. However, lactose was not detected by the AToFMS instrument which meant that the particle would be identified and classified based only on the drug content; *i.e.* particles containing a mixture of FP + SX + lactose would be classified as FP + SX, particles containing a mixture of FP + lactose would be classified as FP and particles containing a mixture of SX + lactose would be classified as SX.

An example dataset for the particles taken from a DPI (formulation FP/SX 250/50) is shown in Figure 4.10. Further discussion of the data analysis for pMDIs and DPIs based on marker ions is given in Chapter 5.
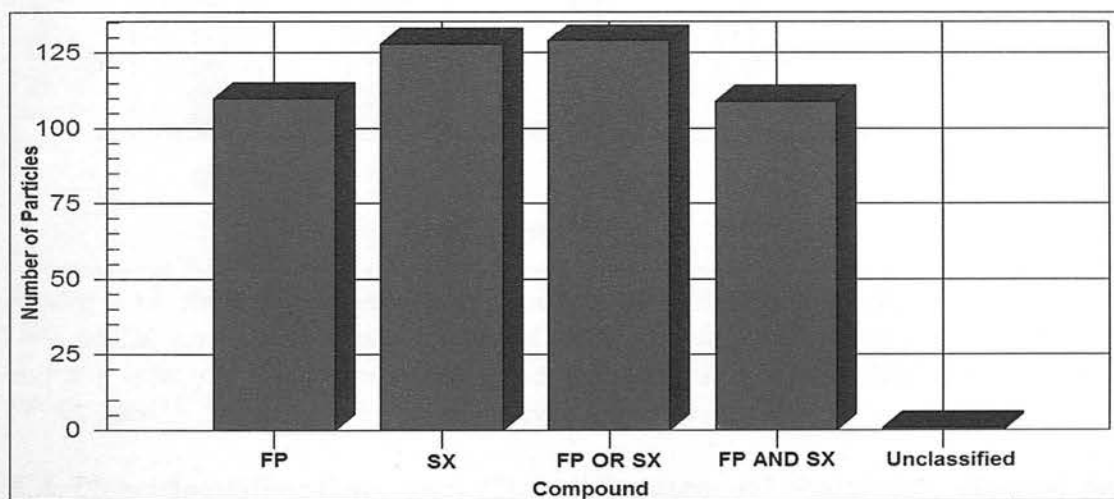
Figure 4.10. *An example of the classification of particles from a DPI based marker ions (m/z -188 for FP and m/z − 74 for SX). The example shown is from DPI_3 (FP/SX 250/50). Negative m/z values indicate negative ions*

4.3.3 Summary of the use of Marker Ions for Identifying and Classifying Particles

To use an ion as a marker for a given compound, the ion must be abundant in the average mass spectrum for the given compound, be unique to the mass spectrum of the given compound and appear in the mass spectrum of the majority of the particles of in the dataset for the given compound.

The identification and classification of particles based on marker ions described in the previous sections is summarized in Figure 4.11 and this includes example data analysis for pMDI, a DPI and the pure drug materials (FP and SX). For the pure drug materials, over 90 % of the particles were identified as FP OR SX with only a small number of particles (typically fewer than 3%) remaining unclassified. This figure also shows that more than 80% of the particles from DPI are co-associated and also that over 40 % of the pMDI particles are co-associated. This result is explored in more detail in Chapter 5.
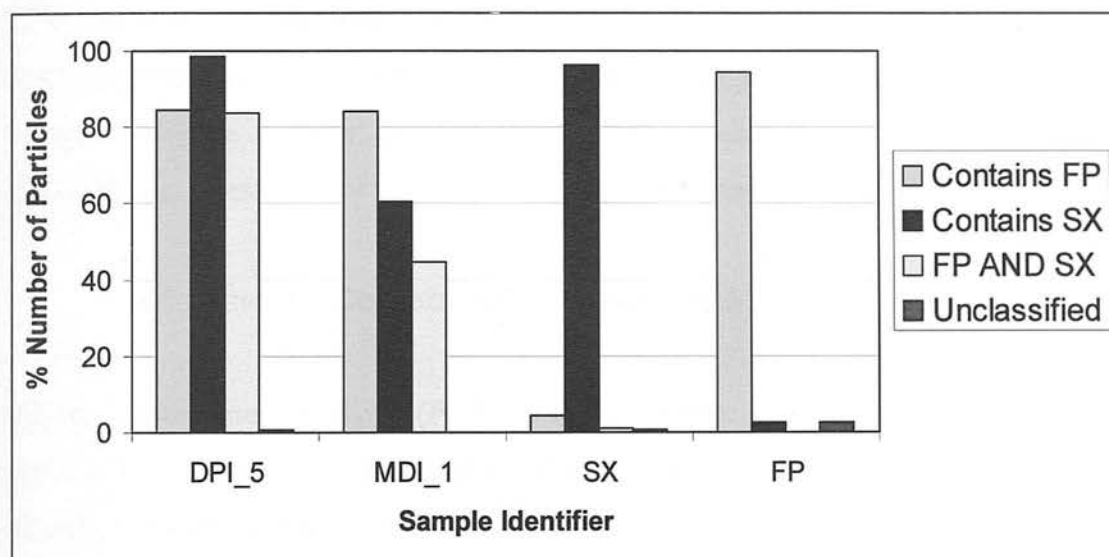
Figure 4.11. An example results set from the classification of particles in samples of DPI, pMDI, and pure FP and SX based on marker ions. These were m/z -74 for FP and m/z -188, for SX. Formulation of samples : DPI_5; FP/SX 250/50 and MDI_1; FP/SX 250/25. Negative m/z values indicate negative ions.

4.4 The Identification and Classification of Particles Based on Composition Determined by Multivariate Statistical Analysis

A pattern recognition technique based on multivariate statistical analysis[4, 9] was applied to the AToFMS data to identify and classify the particles from inhalation products in terms of their composition.

There are major differences in a multivariate analysis approach compared with the use of the marker ion technique described earlier, notably as much of the data acquired is discarded in the marker ion analysis. Also, multivariate analysis offers a much more sophisticated, rigorous and complete analysis of the whole dataset. Moreover, where

the choice of marker ion was based on the average mass spectrum from a group of particles, multivariate analysis is used to investigate variation across the data set in terms of each individual data point (*i.e.* all of the ions from the positive and negative ion mass spectra of each individual particle were included in the multivariate analysis).

A general explanation of how principal component analysis charts are drawn is given in Appendix A3.3. Section 4.4.1 describes the application of the principal component analysis technique to the data initially acquired using an AToFMS instrument equipped with a nozzle-skimmer inlet and by using a range of laser energies. Section 4.4.2 describes how the method was developed further for application to experiments designed to give a more detailed study of co-association in inhalation products including an assessment of the reproducibility of this measurement.

4.4.1 Principal Component Analysis (PCA)

Principal component analysis (PCA) is a multivariate analysis method that can be used to detect trends in large complex datasets, by mathematically generating a series of new variables called principal components. The principal components can be considered as information-rich super variables because they represent the principal source of variability in the dataset. This is a method of identifying patterns in data and highlighting similarities and differences between datasets. Once the patterns have been found, the datasets can be compressed to the principal components with minimal loss of information.

The data matrix from the AToFMS experiment that was analyzed with the PCA software package corresponds to the normalized mass spectra of FP and SX stacked in rows. From PCA, two sets of vectors were extracted, (the scores and the loadings), and these were then projected into charts that show the major trends responsible for most of the variation in the data matrix.

A typical PCA scores plot is given in Figure 4.12 and this shows the clusters of data points taken from separate samples of pure FP and SX that were then overlaid onto the same PCA chart. In this case, the scores within the same cluster indicate the

groups of particles which have similar mass spectra. These data were acquired using the AToFMS equipped with the nozzle-skimmer inlet and using a range of laser energies. The PCA chart shows that there is good resolution between the clusters of data co-ordinates indicating significant differences between the mass spectra of the two compounds.
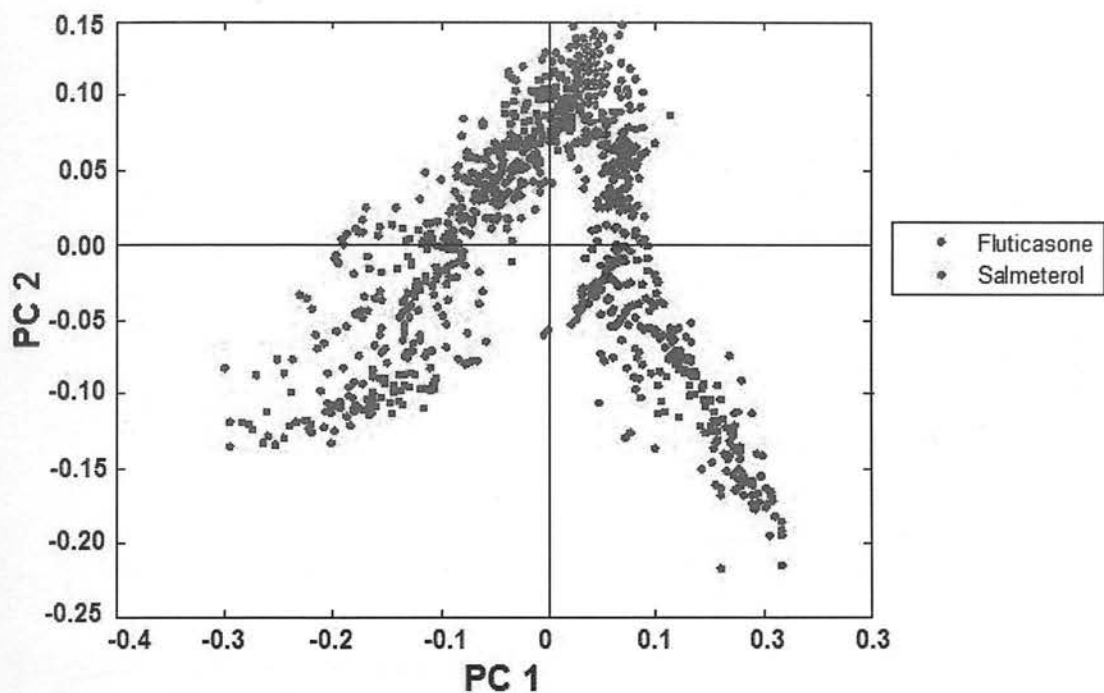
Figure 4.12. *PCA scores plot for separate samples of pure FP and pure SX particles, overlaid on the same PCA chart. Data taken over a range of laser energies from 0.1 to 1.0 mJ, samples (pure FP and SX) were introduced using a nozzle-skimmer inlet.*

An example of a loadings plot for the AToFMS spectra taken from pure FP and pure SX particles is shown in Figure 4.13. The loadings represent the weights ascribed to the original variables (*m/z* values) in projecting the mass spectra in the scores plot. The most influential ions appear in the cluster furthest away from the origin of the loadings plot. Additionally, potential ion markers for a specific group emerging in the scores plot are shown as clusters in analogous regions in the loadings plot.

The loadings plot shown in Figure 4.13 gives an indication of the strongest marker ions which in this example are *m/z* values 139, 57, 121 and 23 for FP; and *m/z* values 91, 55, 44 and 92 for SX . The upper region identifies particularly intense *m/z* values that may occur in both compounds, *i.e. m/z* values 39, 63, 51, and 27. It is noted that the data analysis is based on different marker ions compared with the marker ion

technique described earlier in this chapter. This is mainly because PCA is based on the variation in the dataset compared with the marker ion technique where the markers are chosen from the average mass spectrum.
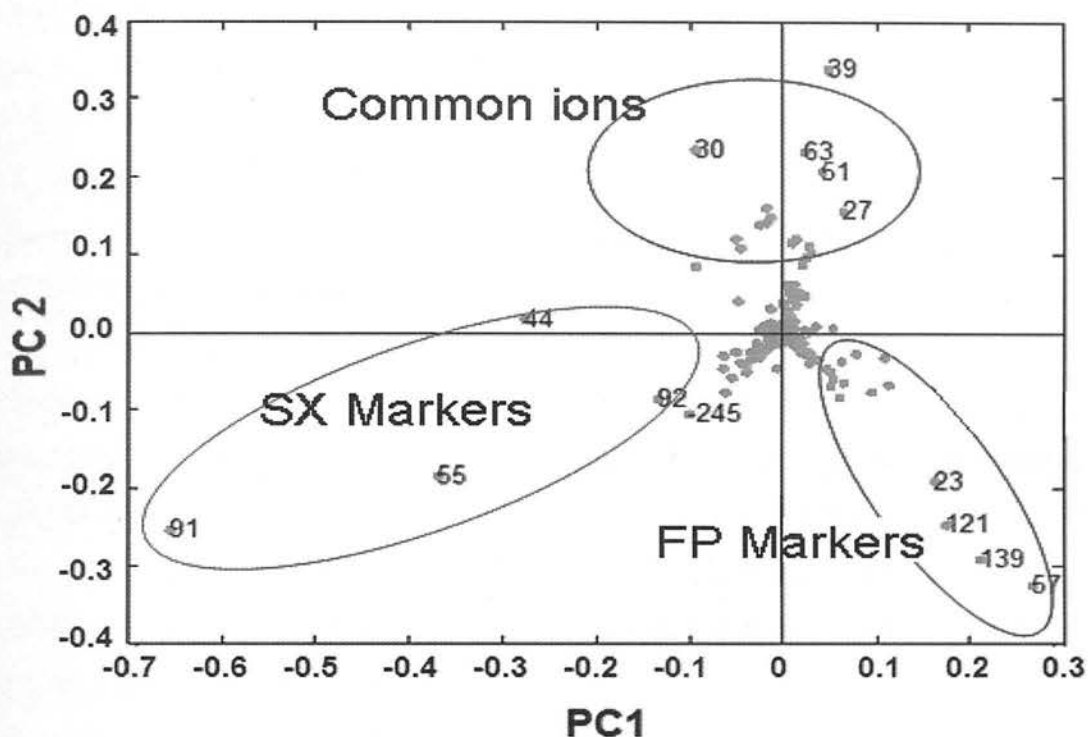
Figure 4.13. *Loadings plot indicating marker ions for each group from the same data as shown in Figure 4.12.*

4.4.2 Assessment of Co-association in Inhalation Products using Principal Component Analysis (PCA)

Initially two types of inhaler device were used to demonstrate the application of PCA to the measurement of co-association, these were: (a) The Seretide® Diskus® inhaler in which the inhalation product consists of a blend of FP, SX and lactose, held in a number of blisters on a tape strip. In this case, the blister is ruptured on use of the inhaler by the patient and the active drugs are administered as a blend (b) The Gemini® Diskus® inhaler, in which the two drugs FP and SX are held in separate blisters which are also ruptured on use by the patient but where the active drugs are administered concurrently as separate powders.

The PCA charts shown in Figure 4.14 indicate that that the degree of co-association is dependent on the method and point at which the particle are mixed. Figure 4.14 shows

co-ordinates from (a) the Seretide® and (b) the Gemini® inhalers overlaid on the co-ordinates from samples of pure FP and SX. The PCA chart in Figure 4.14 (a) shows that the data points from particles from the Seretide® Diskus® formulation sample overlap only minimally with those from the particles of pure FP and SX. This is consistent with the Seretide® Diskus® formulation which is an intimate blend of FP and SX, homogeneously mixed, so there is a high likelihood of co-association. The points on the PCA chart for the Seretide® Diskus® formulation show that the particles are different from the samples of pure FP and SX. Hence, the Seretide® Diskus® formulation was shown to contain particles composed of a mixture of FP and SX, derived from co-association of these compounds.

For the Gemini® Diskus® formulation, the PCA chart shown in Figure 4.14 (b) gives the opposite result to that for the Seretide® Diskus®, in that there is a high degree of overlay with the co-ordinates derived from pure FP and SX; In this case there are only a few co-ordinates in the gap between the FP and SX clusters. This shows that the particles in this inhaler are similar to the individual particles of pure FP and SX. As the materials are mixed together only when the device is actuated by the patient, there is little scope for interaction between FP and SX and hence co-association is unlikely. Hence the PCA chart reflects the fact that the particles found in this type of formulation resemble particles of pure drug compounds.
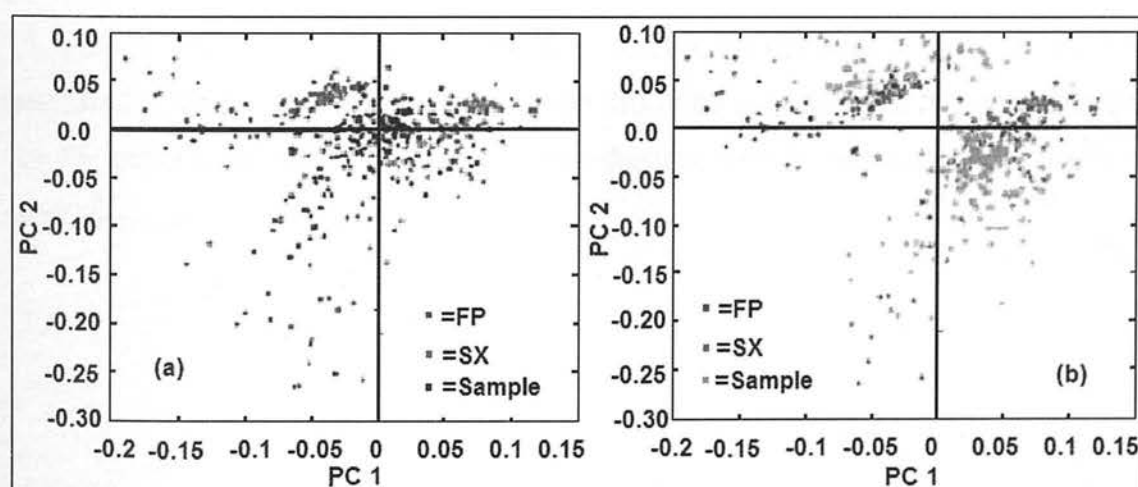
Figure 4.14. *PCA analyses of AToFMS data from inhalers (a) Seretide® Diskus® DPI FP/SX 100/50, (b) Gemini® Diskus® FP/SX 100/50. Both charts were produced by superimposing data from samples onto that from the pure drug compounds. Sample introduction for these data was by nozzle-skimmer inlet. A range of laser energy between 0.6 and 1.0 mJ was used for the acquisition of these data.*

The PCA charts shown in Figure 4.14 were a significant finding during the development of SPMS techniques for the investigation and detection of co-association This results goes some way to validating the approach of the application of PCA to AToFMS data in terms of the identification and classification of the different types of particle present. There may be some advantage in terms of improved efficacy if the particles in an inhaled product are composed of a mixture of the active drugs (FP and SX) due to the synergistic effect discussed in Chapter 1 (see Section 1.5).

4.4.3 Identification and Classification of Particles from Inhalation Products using Principal Component Analysis.

In this section the development of the principal component analysis (PCA) technique for the data analysis from experiments performed to estimate the amount of co-association present in inhaler samples is discussed. A low laser energy was used in this case to maximize the distinction between the spectra for FP and SX particles and the particles were introduced into the instrument *via* the aerodynamic lens. The effect of laser energy on AToFMS data as depicted by the principal component analysis charts and the dependence of the appearance of the mass spectrum on laser energy is discussed in is Section 3.2. The results of the PCA to investigate co-association are presented in Chapter 5.

Figure 4.15 shows the PCA clusters from separate AToFMS runs of pure FP and SX particles overlaid onto the PCA chart. From this chart it is clear that the co-ordinates for FP and SX are distributed into separate clusters, hence gives a good method for identifying and classifying particles.
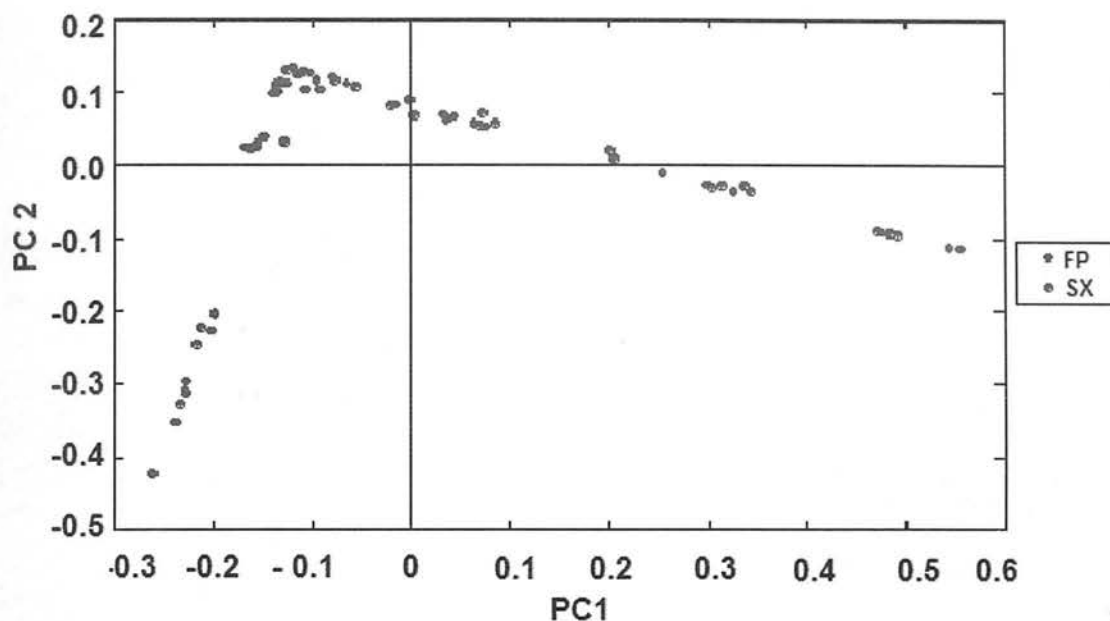
Figure 4.15. *PCA chart showing clusters of data, for pure samples of FP and SX. The sample was introduced via an aerodynamic lens and collected at low laser energy (0.2 mJ).*

Figure 4.16 shows the co-ordinates from a DPI superimposed on the co-ordinates for pure FP and SX particles (as used in Figure 4.15). Many of the co-ordinates appear outside of the clusters for the pure drug materials. For these co-ordinates the DPI particles give a different mass spectral pattern compared with that obtained from pure FP and SX and must be due to particles composed of a mixture of both FP and SX.

It is possible to classify the particles by manually dividing the chart into sections as shown in Figure 4.16. Although AToFMS is not generally considered to be a quantitative technique, an estimate of the number of particles in each category, including a measure of the number of or co-associated particles, can be obtained by counting the number of points in each zone.
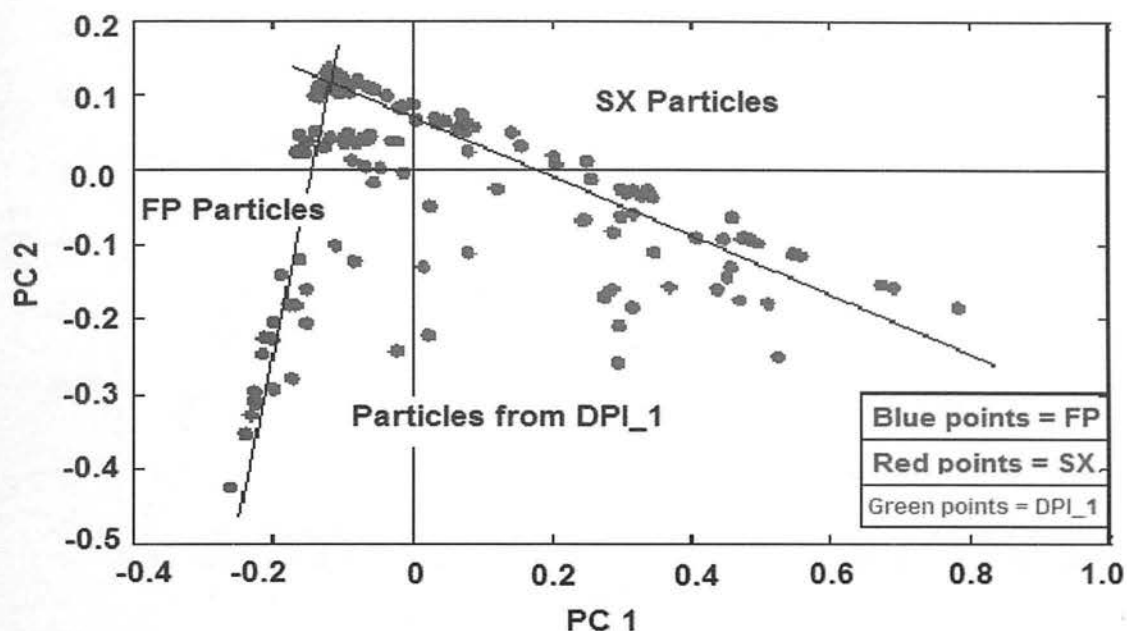
Figure 4.16. *PCA Chart for DPI_1 divided into zones for FP, SX and co-associated particles. The sample (DPI_1; FP/SX 250/50) was introduced via the aerodynamic lens. These data were collected at low laser energy (0.2 mJ).*

Defining ellipses around the clusters of points from samples of pure FP and SX, as shown in Figure 4.17, gave an improved method of identifying and classifying particles. These ellipses define an equal distance from the class centre using Mahalanobis[10] metrics, which take into account how particles distribute within the plot. For example, because FP particles distribute mainly along the vertical axis, this is assumed to be characteristic of this group and therefore the distance along this direction is underweighted, resulting in an equidistance ellipse that is tilted vertically.

The standard confidence ellipses have been overlaid onto the PCA plot for a DPI sample in Figure 4.18. In this chart the majority of the data points for the DPI sample appear towards the centre of the axis and are not overlaid by the standard ellipses. This shows that there is a difference in the mass spectral patterns for these particles compared to the reference standards of pure material.
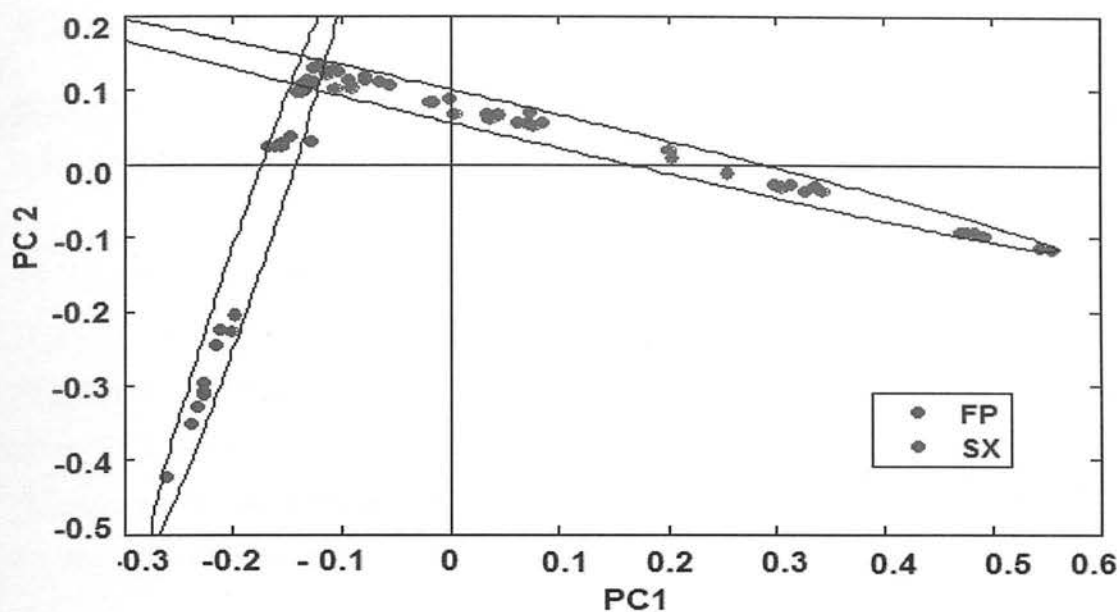
Figure 4.17. *Definition of ellipses using PCA for pure FP and SX. These data were collected at low laser energy (0.2 mJ).*

The ellipses defined in this way were overlaid onto the PCA chart of the co-ordinates taken from a DPI as shown in Figure 4.18. The co-ordinates were then classified according to the area in which they appeared on the chart and these were then counted to determine the number in each category. The results for this type of data analysis as applied to the investigation of co-association in particles from inhalation products are discussed in Chapter 5.
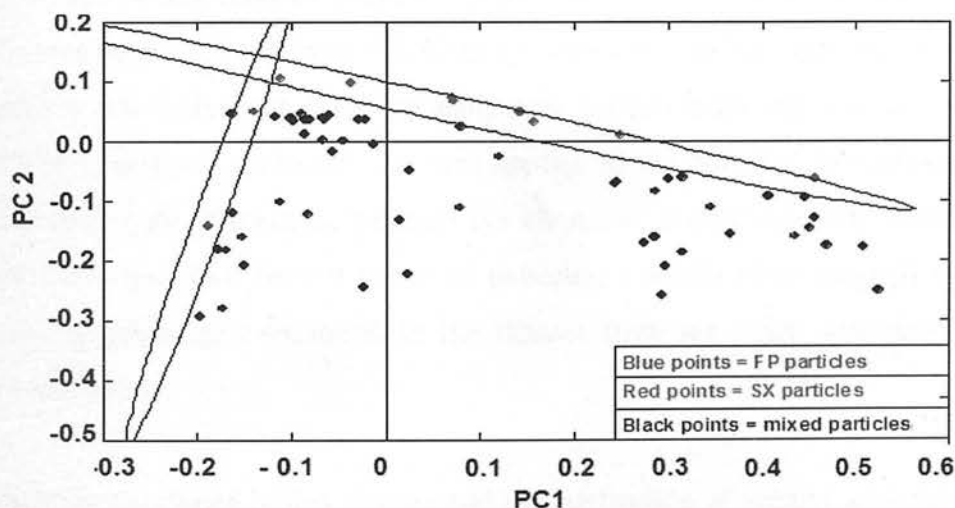
Figure 4.18. *Shows the ellipses defined (for samples of pure drug material) in Figure 4.17 overlaid onto data from DPI_1 (FP/SX 250/50). The sample was introduced via the aerodynamic lens and data were collected at low laser energy (0.2 mJ).*

4.5 Summary

Methods for analyzing AToFMS data were developed based on marker ion analysis and on multivariate statistical analysis.

The choice of marker ions from particles of pure drug material was based on the fragment ions observed in the average AToFMS spectra and these were previously interpreted in terms of the structure of the given molecule. The marker ions used were abundant in the average mass spectrum of each of the pure drug compounds, unique to the mass spectrum of the pure drug compounds and appeared in the mass spectra of the majority of the particles of each pure drug compound.

There are some risks associated with marker ion analysis especially when based on only one ion per compound, not least the fact that much of the data that is available is actually discarded. However, in this case samples were well defined blends of two or three compounds hence it was easy to attribute marker ions that were unique and representative of the individual drug compounds present. Thus the marker ion technique was found to be a useful screen of the data and gave a reasonable way of identifying and classifying particles.

It was found that the analysis of the AToFMS data using multivariate analysis based on principal component analysis (PCA) is a viable and efficient approach. Compared with marker ion analysis multivariate analysis is a much more sophisticated, rigorous and complete analysis technique that was applied to the whole of the dataset (rather than selected ions). Moreover, whereas the choice of marker ion was based on the average mass spectrum from a group of particles, a multivariate analysis approach was used to investigate variation in the dataset from the mass spectrum of each individual particle.

The methods developed in this chapter and the application of marker ion analysis and PCA are discussed in more detail in the next chapter and the methodology is extended to examine a range of inhalation products.

4.6 References

(1)   Microsoft Access™ software, (Microsoft Corporation, Seattle WA, USA) http://www.microsoft.com/en/us/default.aspx (Accessed 31 May 2008).

(2)   MS-Analyze™ TSI Shoreview, MN, USA. (http://www.tsi.com/). (Accessed 31 May 2008).

(3)   Matlab™   software,   (The   Mathworks,   Natick,   MA,   USA). http://www.mathworks.com/ (Accessed 31 May 2008).

(4)   Chemometrics: Data analysis for the laboratory and chemical plant. R. Brereton. First edition (2003), Wiley-Blackwell. ISBN 0-471-489 786.

(5)   Micronization of pharmaceutical powders for use in inhalation. J-M. Larran. Pharmaceutical Manufacturing and Packing Source. p1-4, Spring 2005.

(6)   Single particle detection efficiencies of aerosol time-of-flight mass spectrometry during the North Atlantic Marine Boundary layer experiment. M. Dall'Osto, R. Harrison, D. Bedows, E. Freney, M. Heal, and R. Donovan. *Environ. Sci. Technol.* 40, 5029-5035, (2006).

(7)   Particle morphology and density characterization by combined mobility and aerodynamic measurements. Part 1: Theory. P. DeCarlo, J. Slowick, D.R. Worsnop, P. Davidovits and J-L. Jimenez. *Aerosol Sci. and Tech.* 38, 1185-1205, (2004).

(8)   Private Communication from N. Mistry and J. Warrack (GSK Stevenage).

(9)   Principal component analysis. S. Wold, K. Esbensen and P. Geladi, *Chemometrics and Intelligent Laboratory Systems.* 2, 37-57 (1987).

(10) The Mahalanobis Distance. R. De-Maesschalck, D. Jouan-Rimbaud and D. Massart. *Chemometrics and Intelligent Laboratory Systems.* 50, 1-18, (2000).

Chapter 5

The Determination of Co-association Using Aerosol Time-of-Flight Mass Spectrometry (AToFMS)

5.1 Introduction

A major aim of the work presented in this thesis was to assess the amount of co-association in particles taken from a wide range of inhalation products. As discussed in Chapter 1 (see Section 1.5) there may be some advantage in terms of improved efficacy if the particles in an inhaled product are composed of a mixture of the active drugs (FP and SX). Hence, the data analysis was performed with an emphasis on this aspect based on either marker ion analysis or on multivariate analysis (*i.e.* principal component analysis).

In this chapter, the results from processing AToFMS data analysis using the techniques described in Chapter 4 are presented and discussed; the data obtained using the Aerodyne AMS instrument are described in Chapters 6 and 7. A comparison of AToFMS and AAMS data is given in Chapter 8.

AToFMS experiments were performed on a range of inhalation products using an aerodynamic lens (see Chapter 2) and low laser energy (0.2 mJ), (the effect of variation in the laser energy on the AToFMS spectrum is discussed in Chapter 3).

5.2 Assessment of Co-association using Marker Ion Analysis

In Chapter 4, the selection and use of marker ions to determine co-association was discussed. In the first part of this section, the AToFMS results for pMDIs and DPIs based on data analysis using marker ions are presented. The reproducibility of this type of data analysis is explored in later in Section 5.2.3.

5.2.1 Pressurized Metered Dose Inhalers (pMDIs)

A summary of data analysis for the pMDIs based on marker ions is shown in Figure 5.1. Particles were classified as (i) containing FP, (ii) containing SX (iii) mixed (co-associated) particles of FP and SX using the marker ion techniques described in Chapter 4.

The number of mixed particles was used to give an estimate of the degree of co-association in each sample. Figure 5.1 shows that for the FP/SX 250/25 formulation, ~45 to 55 % of the particles were classified as mixed; for the FP/SX 125/25 formulation ~40 to 50 % were classified as mixed; and for the FP/SX 50/25 formulation ~35 to 45 % % were classified as mixed. Typically less than 3.0 % of the particles remained unclassified (*i.e.* in this case the particles could not be identified or classified using this method).

Figure 5.1. Data analysis for pMDI aerosols using one marker ion for each component. Category FP – particles that contain FP; Category SX - particles that contain SX; Category- FPAND SX particles that contain FP and SX (i.e. mixed due to co-association). Samples are described in detail in Appendix A5.1 The data used to plot these bar-charts is shown in Appendix A5.3.

Thus it was shown that the degree of co-association was found to be between 35 to 55 % for the three formulations of pMDIs. The reproducibility of this measurement is discussed in Section 5.2.3.

5.2.2 Dry Powder Inhalers (DPIs)

The classification of particles taken from DPIs based on marker ion analysis is shown in Figure 5.2. The formulation for DPIs contained lactose which was not detected using the AToFMS (See Chapter 3). Hence, particles were classified similarly to the pMDIs as (i) containing FP, (ii) containing SX (iii) mixed particles of FP and SX using the marker ion techniques described in Chapter 4.

Similarly to the pMDI, the number of mixed particles was used to measure the degree of co-association in each sample. Based on the intra-batch measurements, in the FP/SX 250/50 formulation, ~79 to 92 % of the particles were found to be co-associated; for the FP/SX 500/50 formulation ~85 to 87 % of the particles were found to be co-associated. Typically less than 1.5 % of the particles remained unclassified using this method of classification.

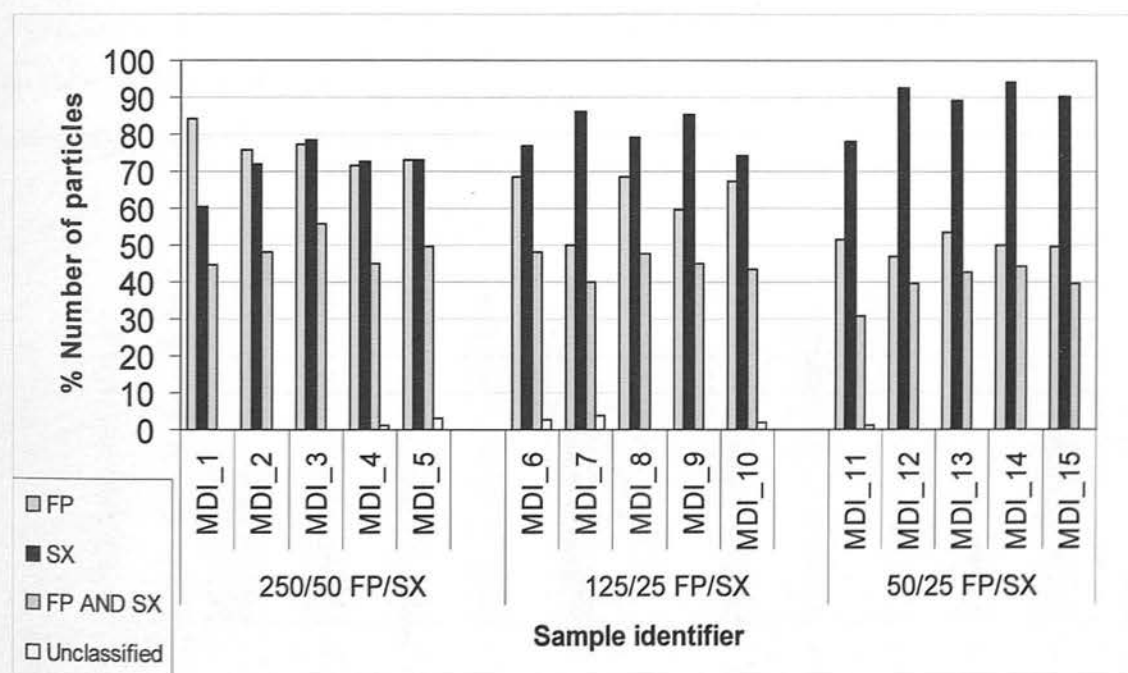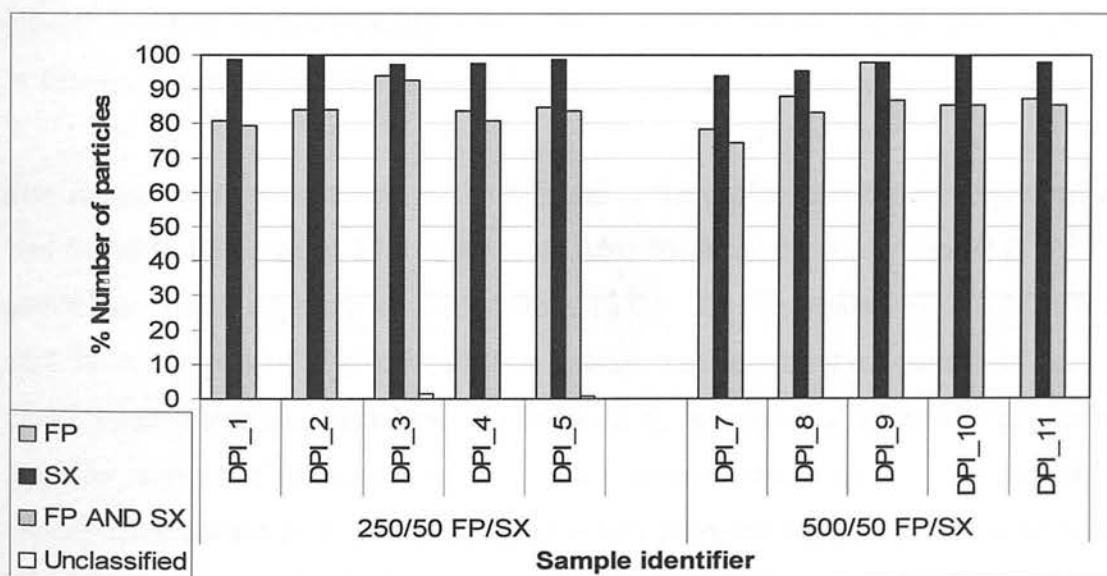*Figure 5.2. Data analysis for DPIs using one marker ion for each component. Category FP – particles that contain FP; Category SX - particles that contain SX; Category- FP AND SX particles that contain FP and SX i.e. mixed due to co-association. Samples are described in detail in Appendix A5.1 The data used to plot this bar-chart is shown in Appendix A5.3.*

Thus it was shown that the degree of co-association was found to be between 79 to 92 % for the DPIs with a similar range of measurements observed for the two formulations. The reproducibility of this measurement is discussed in Section 5.2.3.

5.2.3 Reproducibility of the Determination of Co-association using Marker Ion Analysis

To estimate the reproducibility of the experiment, the relative standard deviation (RSD) of the number of mixed particles in three runs of the same batch of each formulation was calculated (intra-batch). Also the RSD of runs of three different batches (of the same formulation) were used to estimate the inter-batch variation. The results for marker ion analysis are shown in Table 5.1.

Table 5.1 shows that the average number of co-associated particles found in the pMDI intra-batch measurements was found to be 42.2 to 50.2 %. Also the error shown by the relative standard deviation (RSD) for the pMDI intra-batch experiments varied from 5.4 % for samples of FP/SX 50/25 to 10.8 % for samples of FP/SX 250/25. The average number of co-associated particles found in the DPI intra-batch measurements was found to be similar (~85%) in both formulations. Also the error shown by the relative standard deviation (RSD) for the DPI intra-batch experiments varied from 1.1 % for samples of FP/SX 500/50 to 7.1 % for samples of FP/SX 250/50.

The average number of mixed particles found in the pMDI inter-batch measurements was found to be between 37.6 to 49.5 %. Also the error shown by the RSD for the pMDI intra-batch experiments varied from 10.0 % for samples of FP/SX 125/25 to 16.4 % for samples of FP/SX 50/25. The average number of mixed particles found in the DPI inter-batch measurements was found to be between 81.7 to 85.4 % indicating a similar amount of co-association in the two formulations. Also the error shown by the relative standard deviation (RSD) for the DPI intra-batch experiments varied from 7.8 % for samples of FP/SX 250/50 to 7.9 % for samples of FP/SX 500/50.

Type	Formulation	Batch type	Average	Std Dev	RSD %
pMDI	FP/SX 250/25	Inter	49.5	5.8	11.7
pMDI	FP/SX 250/25	Intra	50.2	5.4	10.8
pMDI	FP/SX 125/25	Inter	45.2	4.5	10.0
pMDI	FP/SX 125/25	Intra	45.4	2.0	4.3
pMDI	FP/SX 50/25	Inter	37.6	6.2	16.4
pMDI	FP/SX 50/25	Intra	47.2	2.3	5.4
DPI	FP/SX 250/50	Inter	85.4	6.7	7.8
DPI	FP/SX 250/50	Intra	85.8	6.1	7.1
DPI	FP/SX 500/50	Inter	81.7	6.4	7.9
DPI	FP/SX 500/50	Intra	85.9	1.0	1.1

Table 5.1. Determination of co-association (mixed particles) in pMDI and DPI aerosols based on marker ions. The table shows the average % number of particles found in inter- or intra- batch experiments. In each case and estimate of the error is given by the relative standard deviation % (RSD %) (i.e. the Standard Deviation/ Average (x 100 %)).

5.3 Assessment of Co-association Based on Principal Component Analysis

The results for the application of principal component analysis (PCA) to the AToFMS data to determine the degree of co-association are described in Section 5.3.1. The reproducibility of this measurement is discussed in Section 5.3.2.

The particles were classified using ellipses defined by the standards of FP and SX as described in Section 4.4.3. Using PCA, particles were classified as (i) FP, (ii) SX (iii) mixed particles of FP and SX. An example of a PCA chart used to classify the particles from a pMDI is shown in Figure 5.3 and from a DPI in Figure 5.4.
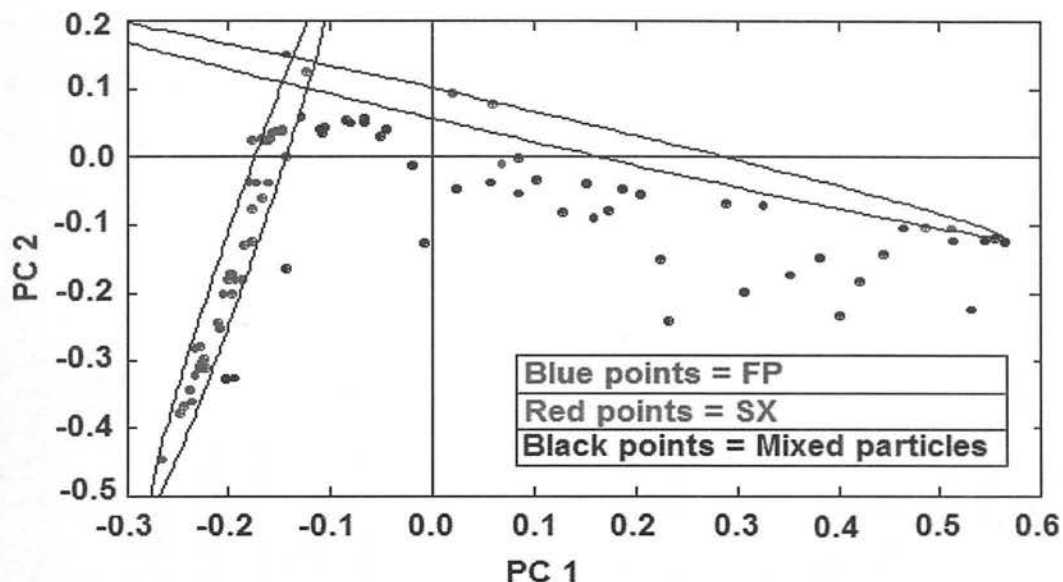
Figure 5.3. *Example of a PCA chart for a pMDI (FP/SX 250/25 (file MDI_1)). This chart shows data only from the pMDI but with the ellipses defined pure FP and SX overlaid on the chart used to classify the particles present.*
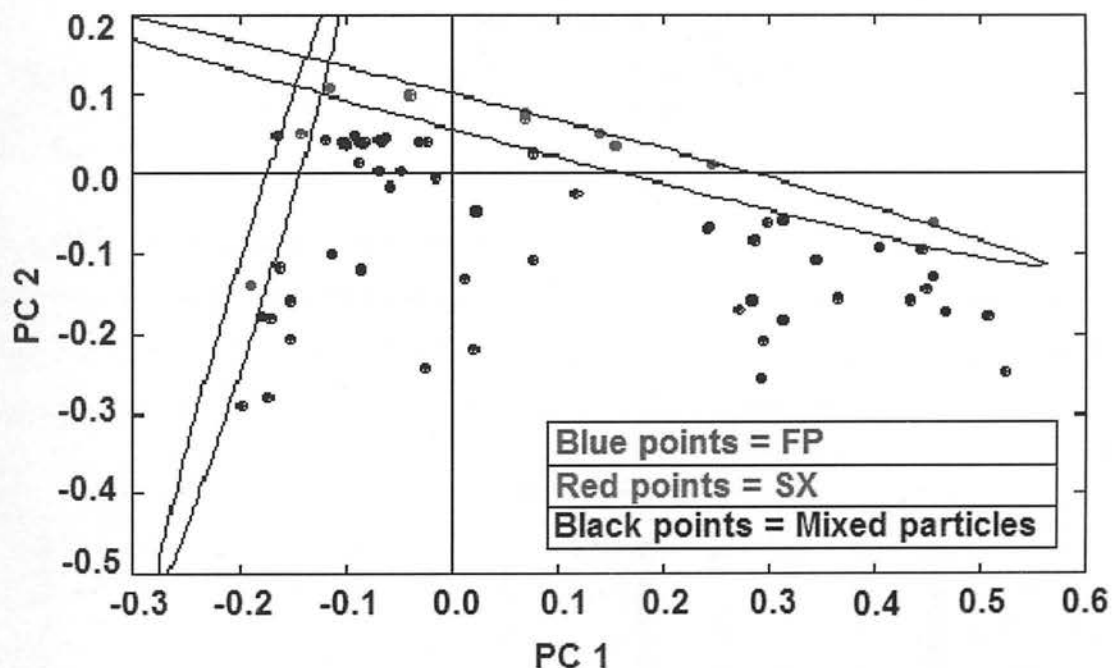
Figure 5.4. *Example PCA chart for DPI formulation FP/SX 250/50 (DPI_1). This chart shows data only from the DPI but with the ellipses defined by pure FP and SX overlaid on the chart used to classify the particles present.*

5.3.1 Particle Classification for Inhalation Products

A summary of data analysis for the pMDIs based on principal component analysis (PCA) is shown in Figure 5.5. As with the marker ion analysis, the number of mixed particles was used to give an estimate of the degree of co-association in each sample.

Based on the intra-batch measurements the results show that for the FP/SX 250/25 formulation 55.9 to 63.7 % of the particles were classified as mixed; for the FP/SX 125/25 formulation 62.4 to 68.6 % were classified as mixed; and for the FP/SX 50/25 formulation 58.3 to 71.7 % were classified as mixed.
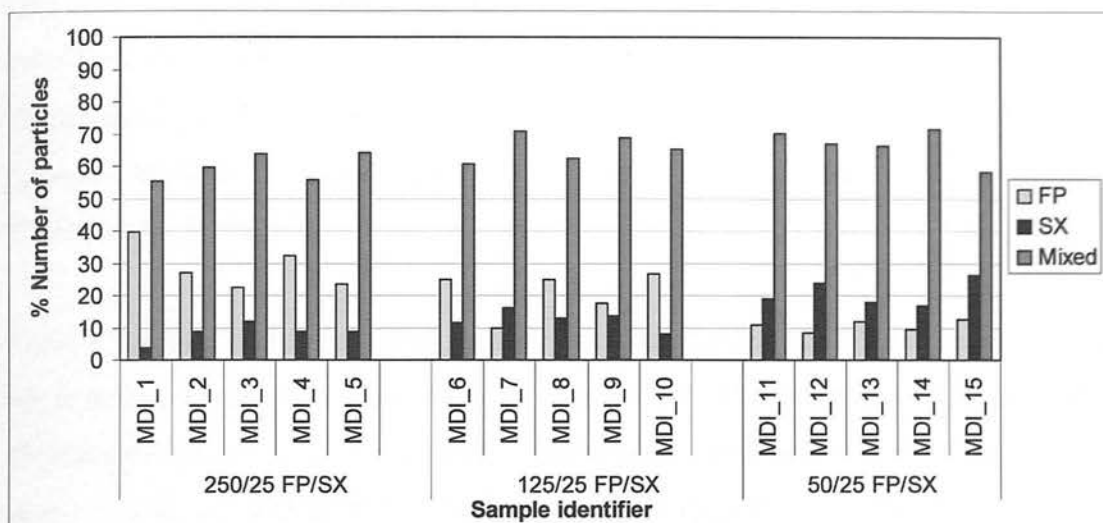
Figure 5.5. *Data analysis for samples from pMDIs using PCA ellipses. Samples are described in detail in Appendix A5. The data used to plot this bar-graph is also shown in Appendix A5.*

Figure 5.6 shows the data analysis for the set of samples from DPIs investigated and the particles were classified using ellipses defined by the standards of FP and SX. Approximately 83.1 to 92.6 % of the particles were classified as mixed particles for samples of FP/SX 250/50 and 85.3 to 93.0 % for FP/SX 500/50.
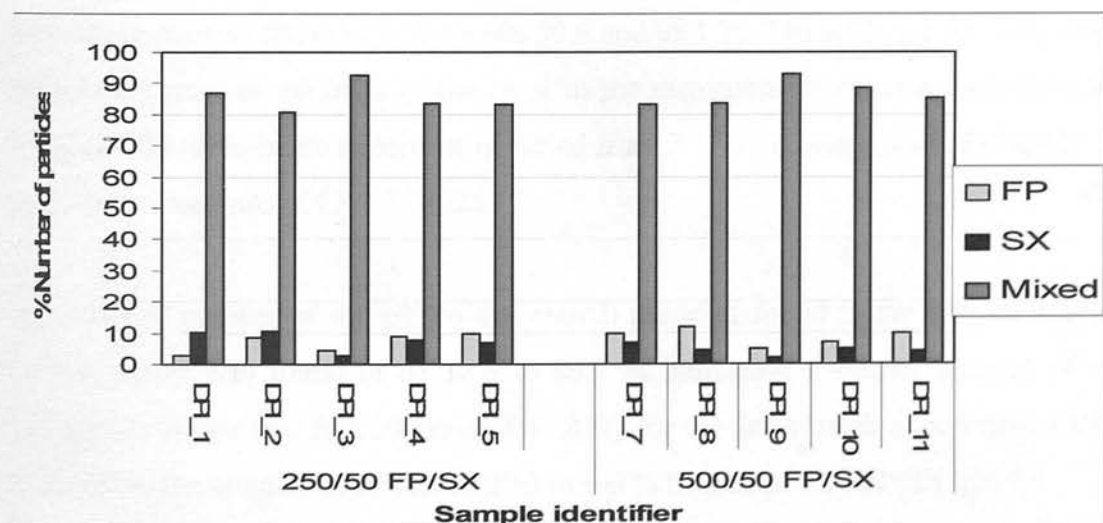
Figure 5.6. *Data analysis for samples from DPIs using PCA ellipses. Samples are described in detail in Appendix A5.1. The data used to plot this bar-graph is also shown in Appendix A5.3.*

5.3.2 Reproducibility of the Determination of Co-association Based on Principal Component Analysis.

Similarly to the marker ion analysis, the reproducibility of the experiment was estimated using the relative standard deviation (RSD) of the number of mixed particles determined using PCA from three runs of the same batch of each formulation (intra-batch). Also the RSD of runs of three different batches (but of the same formulation) were used to estimate the inter-batch variation. The results for the PCA are shown in Table 5.2.

Table 5.2 shows that the average number of mixed particles found in the pMDI intra-batch measurements was found to be 61.1 to 63.7 %. The error shown by the relative standard deviation (RSD) for the pMDI intra-batch experiments varied from 4.7 % for samples of FP/SX 125/25 to 10.3 % for samples of FP/SX 50/25. The average number of mixed particles found in the DPI intra-batch measurements was found to be between 86.4 and 88.9 % indicating a similar amount of co-association in both formulations. The error shown by the relative standard deviation (RSD) for the DPI intra-batch experiments varied from 4.4 % for samples of FP/SX 500/50 to 6.2 % for samples of FP/SX 250/50.

The average number of mixed (co-associated) particles found in the pMDI inter-batch measurements was found to be between 59.6 and 68.1 %. The RSD for the intra-batch experiment gave an estimate of the error in the measurement of co-association and for the pMDI intra-batch experiments varied from 3.1 % for samples of FP/SX 125/25 to 6.7 % for samples of FP/SX 50/25.

The average number of mixed (co-associated) particles found in the DPI inter-batch measurements was found to be 86.6 to 86.7 % indicating a similar amount of co-association in the two formulations. The RSD for the intra-batch experiment varied from 5.5 % for samples of FP/SX 250/50 to 6.0 % for samples of FP/SX 500/50.

Type	Formulation	Batch type	Average	Std Dev	RSD %
pMDI	FP/SX 250/25	Inter	59.6	4.2	7.0
pMDI	FP/SX 250/25	Intra	61.1	4.5	7.4
pMDI	FP/SX 125/25	Inter	64.7	5.6	8.6
pMDI	FP/SX 125/25	Intra	65.4	3.1	4.7
pMDI	FP/SX 50/25	Inter	68.1	2.0	3.0
pMDI	FP/SX 50/25	Intra	65.4	6.7	10.3
DPI	FP/SX 250/50	Inter	86.7	6.0	6.9
DPI	FP/SX 250/50	Intra	86.4	5.4	6.2
DPI	FP/SX 500/50	Inter	86.6	5.5	6.4
DPI	FP/SX 500/50	Intra	88.9	3.9	4.4

Table 5.2. Determination of co-association (mixed particles) in pMDI aerosols based on PCA. The table shows the average % number of particles found in inter- or intra-batch experiments. In each case and estimate of the error is given by the relative standard deviation (RSD) (i.e. the Standard Deviation/ Average (x 100 %)).

5.4 AToFMS Data Analysis Summary

The relavenace of the presence of co-association is discussed in Chapter 1. The synergistic effect of treatment for lung disease using the two active drugs simultaneously may be explained by the two drugs acting on the lung tissue simultaneously. Intuitively it might be that the easiest way for this to happen would be *via* particles that consist of a mixture of the two active materials. The data shown in

this chapter provides evidence of high levels of co-associated particles in the inhaler devices investigated.

It has been reported previously that quantitation using the AToFMS is difficult because of the shot-to-shot variation in the laser (See section 3.2). The data presented in this chapter, to investigate the composition of each particle is probably semi-quantitative at best. However the variation measured expressed as an RSD % (1 to 16 % for marker ions and 3 to 10 % for PCA) was good when the small amounts of sample per particle around the femtogram level or less (see Section 9.2.3) are considered.

In Figure 5.7, the average number of mixed (co-associated) particles found for DPIs is shown to be between 85 to 89 %. The spread of results was broader for the pMDI as the average number of mixed particles was between 42 and 50 % as given by the intra-batch data. The reproducibility of the measurement for both marker ions and PCA expressed as the RSD % was typically found to be between 1.1 and 10.8 % .

The results shown in this chapter are quoted to one decimal place, however the data is semi-quantitative at best. Further work would be required to (a) improve on the reproducibility of the experiment for example by improving the shot-to-shot reproducibility of the laser (see Section 3.2) and (b) increase the numbers of samples analyzed and particles measured to improve on the statistical significance of this data.

It might have been expected that PCA would provide a more reliable way to show the presence of co-association in these samples as it is a more sophisticated data analysis technique. However broad agreement between the marker ion analysis and the PCA was found as summarized in Figure 5.7. Also the errors estimated from the RSD were similar using both techniques.
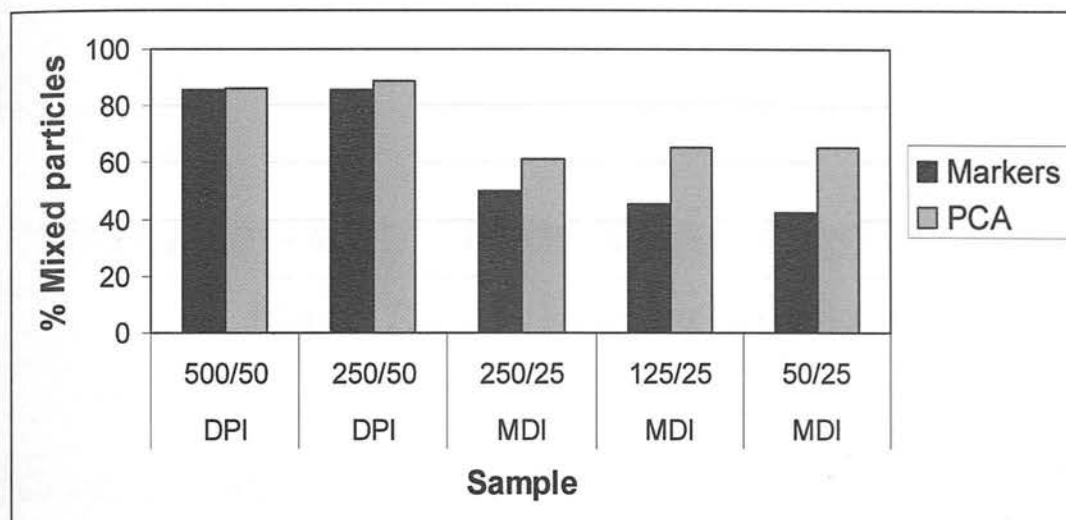
Figure 5.7. *Summary of data to measure co-association in DPI and pMDI aerosols based on marker ions and PCA. Data shown is based on three replicates of each batch for each formulation.*

The good agreement between the data analysis techniques may be because the samples analyzed consisted of well defined, simple mixtures of only two or three components. Even though the use of marker ions is a fairly crude technique, a good estimate of the degree of co-association was possible mainly because it was possible to choose marker ions that were unique and representative of the drug compounds.

PCA is an established technique that provides a rigorous approach to data analysis and uses all of the dataset so may avoid missing information (as for example in the marker ion technique where much of the data is discarded). If the inhalation products, were comprised of more complex mixtures then PCA analysis might give further advantage as it would become increasingly more difficult to choose marker ions that were unique and representative as the formulation became more complex.

For the data presented in this chapter however, it was possible to use either data technique to obtain a similar estimate of the degree of co-association.

The difference in co-association levels between DPIs and pMDIs is likely to result from the very different nature of the formulations and the mechanisms by which co-association may occur. The difference in co-associated for these devices and the level of co-association estimated using the AToFMS and the AAMS instruments are discussed further in Chapter 8.

Chapter 6

Data Analysis Methods for Aerodyne Aerosol Mass Spectrometry (AAMS)

6.1 Introduction

The potential of an Aerodyne Aerosol Mass Spectrometry (AAMS) for the analysis of inhalation products was explored. Initially a number of trial experiments were designed and performed using an AAMS instrument (described in Chapter 2). These were designed to show that the materials used in inhalation products would give data that could be used to determine the composition of the particles originating from the inhalation products. A second set of experiments were designed to further evaluate the instrumentation for the analysis of inhalation products and to assess the potential of the technology for the measurement of co-association. This chapter describes how the data processing methods were developed and the initial results produced are presented in Chapter 7. Note that this work was performed in the manufacturers' laboratories (Aerodyne, Boston, MA, USA) which meant that instrument time and access was limited.

The AAMS instruments have previously been used to produce quantitative data on the composition of environmental aerosol particles[1, 2] hence an estimation of the composition of individual particles for inhalation products is given along with an estimate of the errors encountered when making this type of measurement. The results for the efficiency of production of mass spectra and on the measurement of particle size are presented however the emphasis of this work was on the assessment of the degree of co-association.

During the AAMS experiment, the data for each particle size measurement is linked to the mass spectrum *via* a Microsoft Excel™ spreadsheet[3]. A spreadsheet was also

used to process the data using marker ions; the AAMS spectra of pure drug compounds showed some representative fragment ions which were used as markers to identify the particles in an analogous way to that described for the AToFMS data in Chapter 4. The data was also analyzed with multivariate statistical analysis software; this technique has previously been shown to give both a quantitative and qualitative assessment of particle composition[4].

6.2 Particle Size Analysis

Not all of the particles that are detected by light scattering in the particle sizing region of the instrument give a mass spectrum. The efficiency of mass spectrum production for the AAMS (E_{AAMS}) is given by Equation 6.1.

$$E_{AAMS} = P_{MS} / P_{Total} \times 100\% \qquad \textbf{Equation 6.1}$$

Where: P_{MS} = Number of particles that give a mass spectrum

            P_{Total} = Total number of particles detected by light scattering

The efficiency of mass spectrum production for the AAMS (E_{AAMS}) for material taken from pMDIs and DPIs is shown in Table 6.1. For pMDIs the efficiency was found to be between 23.7 to 38.5 % which is much higher than the efficiency of the AToFMS (see Section 4.2). For the DPIs the mass spectrum efficiency was determined on the samples shown as between 13.9 and 33.2 %.

Sample	Batch	Formulation	Number of particles (P_{Total})	Number of particles (P_{MS})	Mass spectrum efficiency (E_{AMSS})
MDI_1*	002/78	FP/SX 50/25	96	n/a	n/a
MDI_2	002/78	FP/SX 50/25	445	122	27.4
MDI_3	05/97F	FP/SX 50/25	422	102	24.2
MDI_4	AX7099/23	FP/SX 50/25	405	120	29.6
MDI_5	AX7099/23	FP/SX 50/25	378	103	27.2
MDI_6	AX7099/23	FP/SX 50/25	597	172	28.8
MDI_7	1/22	FP/SX 250/25	431	102	23.7
MDI_8	1/22	FP/SX 250/25	445	169	38.0
MDI_9	AX7102/82	FP/SX 250/25	435	121	27.8
MDI_10	DO40861	FP/SX 250/25	304	103	33.9
MDI_11	DO40861	FP/SX 250/25	403	155	38.5
DPI_1†	R15404-20	FP 100	183	50	27.3
DPI_2	R25237	250/50 FP/SX	346	48	13.9
DPI_3	R25240	500/50 FP/SX	385	128	33.2

Table 6.1. *The mass spectrum efficiency for pMDIs and DPIs. All samples were run under the same conditions except for MDI_11 where the spacer was removed from the sampling orifice. *No data are shown for file MDI_1 as this was a trial run. † DPI_1 was a Flovent® inhaler containing a blend of FP and lactose. DPI_2&3 were Seretide® containing a blend of FP, SX and lactose.*

As in the case of the AToFMS instrument, the shape of the particle has an influence on the particle size measurement determined with the AAMS instrument[5,6]. The influence of the particle shape on the measurement of aerodynamic size is discussed in Chapter 4 (Section 4.2).

The particle distribution for a series of pMDIs (FP/SX 50/25) is shown in Figure 6.1. In this case 78.3 % of the particles were found to be in the ranges between 200 and 500 nm.
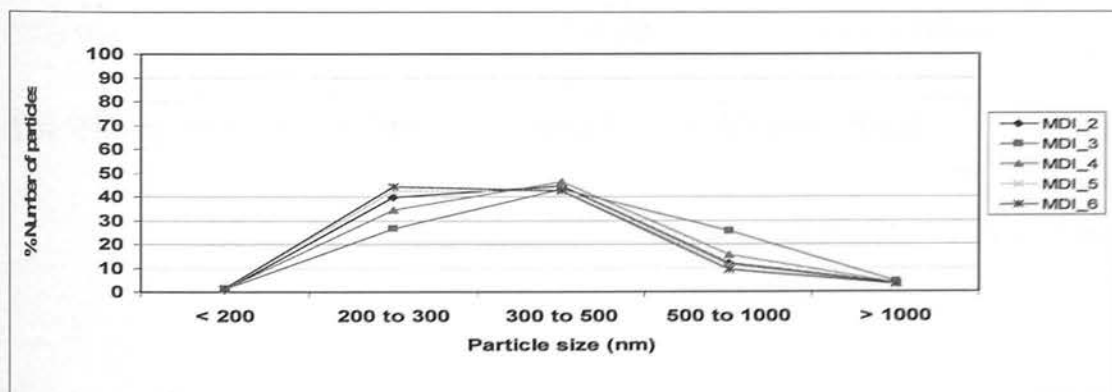
Figure 6.1. *Particle size distribution for a series of pMDIs (FP/SX 50/25). MDI_2 to 4 were repeats of the same batch; Samples MDI_4 to 6 were three runs, of different batches of the same formulation.*

Similarly an example particle distribution from a second series of pMDIs, (FP/SX 250/25) is shown in Figure 6.2 and in this case the particles are slightly larger as 73.8 % of the particles are between 300 and 1000 nm.
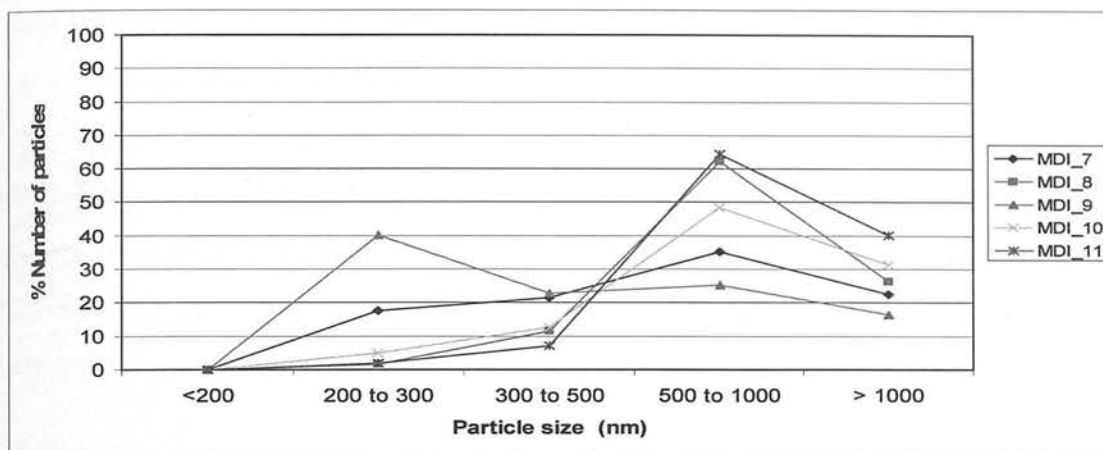
Figure 6.2. *Particle size distribution ranges for a series of pMDIs (FP/SX 250/25). Samples MDI_7 to 9 were repeats of the same batch; MDI_ 9 to 11 three runs, of different batches of the same formulation.*

The conclusion of the particle sizing experiments using the AAMS are that firstly the FP/SX 50/25 sample contained a high number of small particles; these were found later to be due from FP fines probably originating from the micronization process. The particle size distribution for the 5 runs appeared to be consistent both for inter – batch and intra-batch analysis. The particle size distribution for the FP/SX 250/25 samples appeared to show more variation for example the % number of particles in the 500 to 1000 μm category varied from 25 % to 60 % within the samples investigated. These samples were found to contain more SX either as pure particles or as a co-associated mixture (with FP).The increased variation in this data may have been due to the shape of the particles. Particle shape is discussed in Chapter 4.

6.3 Identification of Particles Based on Marker Ions

6.3.1 The Analysis of Marker Ions for Pure Drug Compounds

The aim of data analysis based on marker ions, was to be able to identify the particles from inhalation products in terms of composition and ultimately use this information

to make an assessment of the degree of co-association present. In this section the identification of marker ions based on the AAMS spectra of pure drug compounds is discussed.

The identification of particles from pure drug material using marker ions was based on the fragment ions observed in the average ToF-AAMS spectra for the pure drug compounds. To use an ion as a marker for a given compound, the ion must be abundant in the average mass spectrum of each of the compounds, be representative of the individual compound and appear in the mass spectra for the majority of the particles of each pure compound (*i.e.* similar criteria for AToFMS marker ion analysis).

The average ToF-AAMS mass spectrum take from 78 particles of pure FP is shown in Figure 6.3. This mass spectrum is similar to that acquired using the Q-AAMS instrument as described in Chapter 3 (Section 3.5.1).

An AAMS dataset was also acquired on pure particles of SX. The average mass spectrum taken from 92 particles of pure SX is shown in Figure 6.4. The SX mass spectrum is similar to that acquired using the Q-AAMS instrument as described in Chapter 3 (Section 3.5.1).
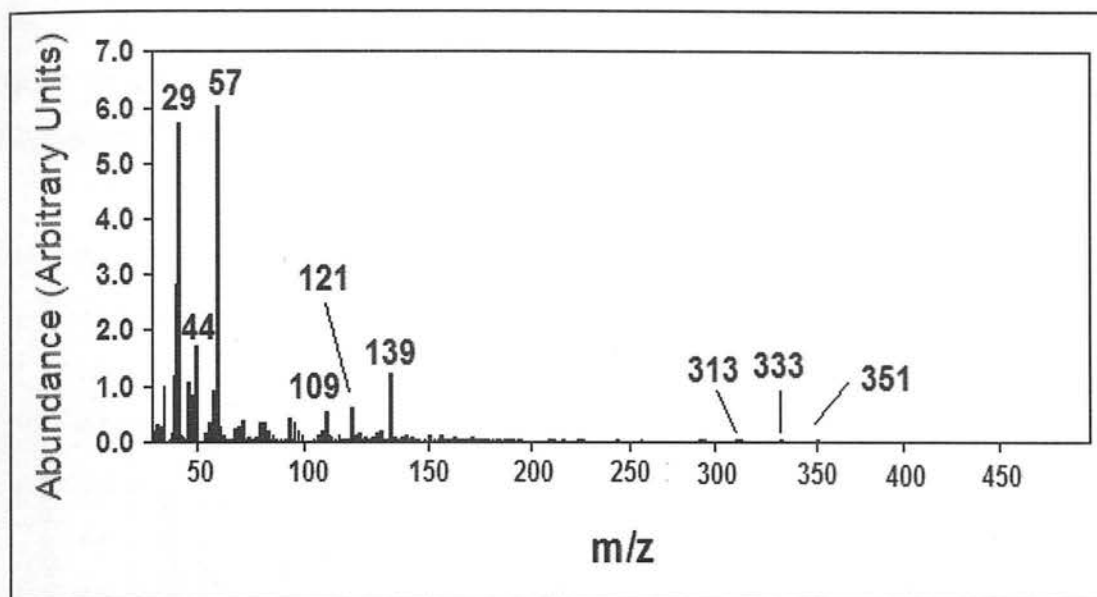
Figure 6.3. Average mass spectrum of FP taken from 78 particles of pure drug. The particle size range was from 249 to 1538 nm.
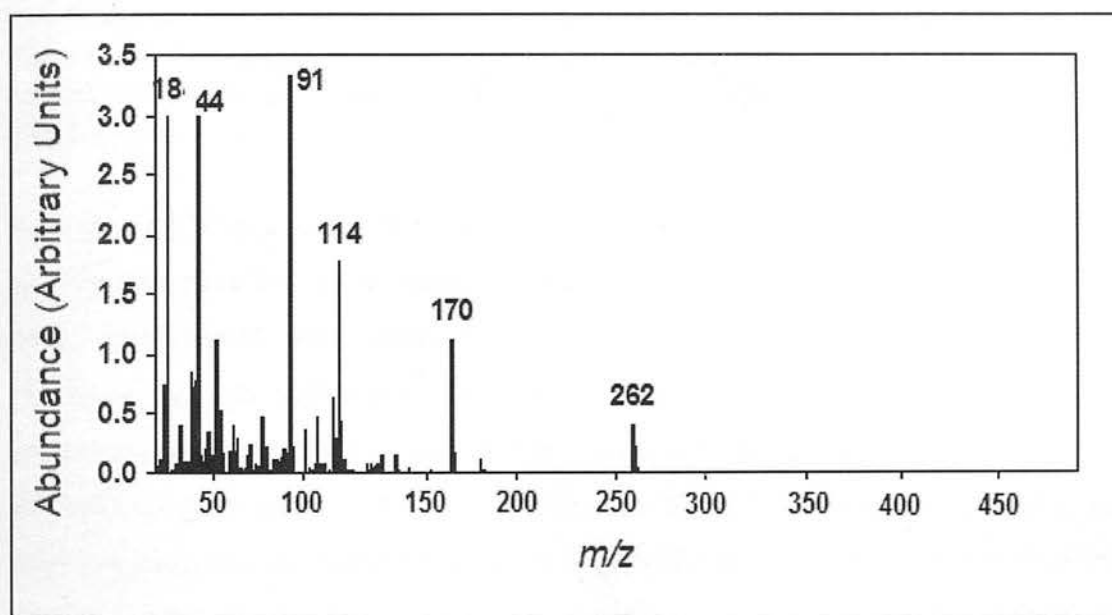
Figure 6.4. Average spectrum taken from 92 particles of pure SX drug material. The particle size range was from 207 to 1037 nm.

The major ions from the average mass spectrum of FP are compared with those from the average AAMS spectrum of SX in Figure 6.5. This bar-graph was used to determine the most relevant marker ions and to estimate the amount of overlap for the marker ions in the mass spectra of the two compounds.

Hence, the ion at *m/z* 57 was used as a marker ion for FP and *m/z* 91 used for SX based on the data shown in Figure 6.5. An interpretation of the fragmentation patterns is given in Chapter 3 (Section 3.5).
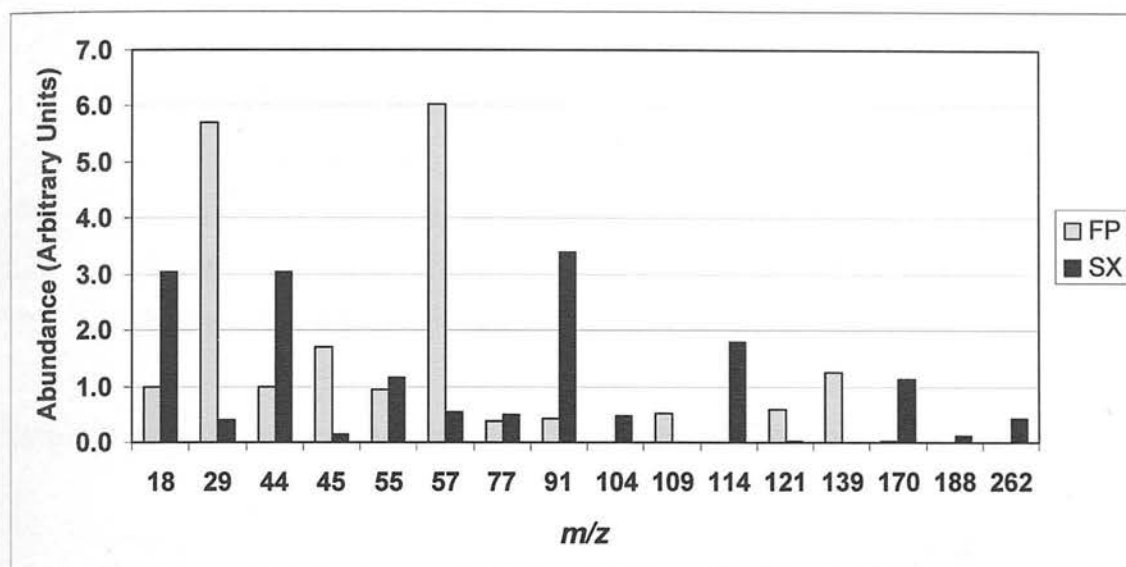
Figure 6.5. *Bar-graph to compare the major (the most abundant) ions in the mass spectra of FP and SX. This shows that m/z 57 is representative of FP and m/z 91 is representative of SX.*

Note that *m/z* 57 and *m/z* 91 could originate from other sources for example as generic hydrocarbon ions. The use of these ions as markers might be a problem if the samples under investigated were unknowns, for example from environmental samples. However, the data reported in this thesis was acquired on clinical grade material originating from inhalation products. This meant that the samples were already well defined. To give extra confidence that the ions chosen as markers were valid, data were acquired and analyzed for samples of pure FP and pure SX and this data was used as a reference for this work. The data acquired on the pure samples showed that although there was some commonality of the ions chosen as markers (for example there was an ion of low abundance for *m/z* 57 in the SX spectrum) it was shown that there was a high confidence (more than 70 %) of correctly identifying the particle using this method (see Section 6.3.2).

6.3.2 Determination of the Fractional Composition of Individual Particles Based on Marker Ion Analysis

The FP fraction based on marker ions was calculated using Equation 6.2.

$$FP_{fr} = [FP / (FP + SX)] \times 100\% \qquad \textbf{Equation 6.2}$$

FP_{fr} = Fraction of FP based on one marker ion for each compound

FP = Mass spectral signal for *m/z* 57

SX = Mass spectral signal for *m/z* 91

Similarly the SX fraction based on marker ions was calculated using Equation 6.3.

$$SX_{fr} = [SX / (FP+SX)] \times 100\% \qquad \textbf{Equation 6.3}$$

SX_{fr} = Fraction of SX based on one marker ion for each compound

FP = Mass spectral signal for *m/z* 57

SX = Mass spectral signal for *m/z* 91

Equation 6.2 was used to calculate the fraction of FP for each particle in a sample of the pure FP drug compound; this fraction is plotted against particle size to give the fractional composition chart shown in Figure 6.6. In this most (92 %) of the particles identified using the mass spectral signal for *m/z* 57 have an FP_{fr} fraction higher than 70 %.

If the marker ions used were completely unique then the fraction of SX in FP would be expected to be zero as in this case, the ion at *m/z* 91 would not appear in the FP spectrum. Hence, to investigate how representative the marker ions used were, the SX_{fr} was calculated for the pure FP drug compound. It can be seen from Figure 6.6 that this was low (below 20 %) but not zero. However Figure 6.5 shows that this ion is much more abundant in the SX spectrum compared with FP hence it was used as a marker ion for SX.
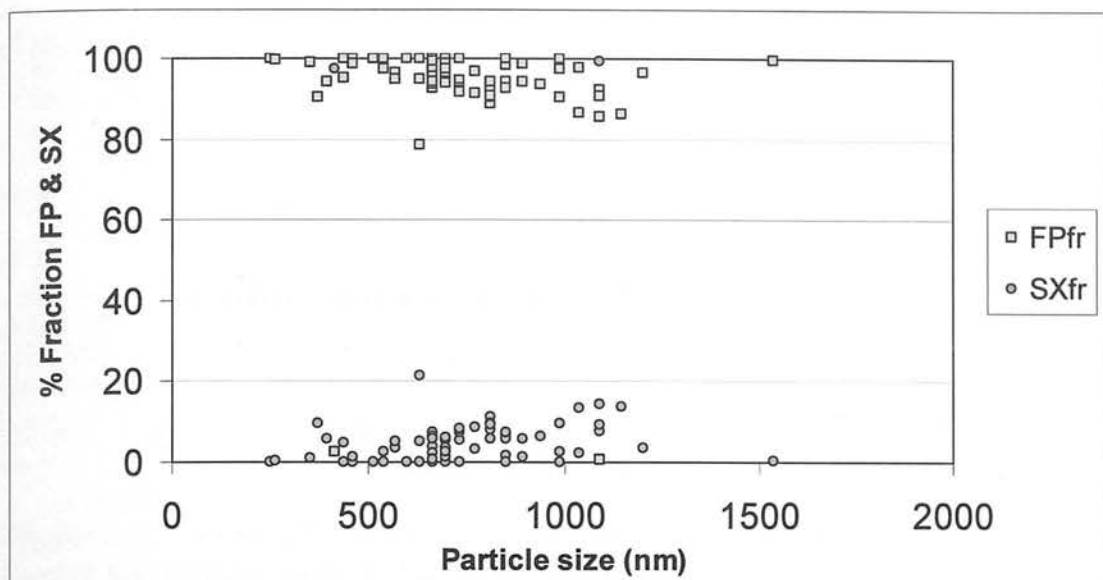
Figure 6.6. *Fractional composition chart for particles in pure FP, determined by marker ion analysis (using m/z 57 for FP and m/z 91 for SX).*

Figure 6.7 shows the fractional composition chart for pure SX drug compound, calculated using equation 6.3. In this case the majority of the particles (91 %) have an SX_{fr} fraction above 70 % and this is a good indication that the marker ion for SX (*m/z* 91) is representative of SX. The data points for the fraction of FP calculated using Equation 6.2 are also shown on this chart and give a fraction of below 30%.

There are a number of data points (6 % of the population shown in Figure 6.7) in the SX_{fr} range between 30 and 70 %. This area of the chart would be expected to represent co-associated particles in samples where both FP and SX are present. As the SX was known to be pure the data points in this region in Figure 6.6 were used as a baseline for the noise associated with the AAMS experiment.
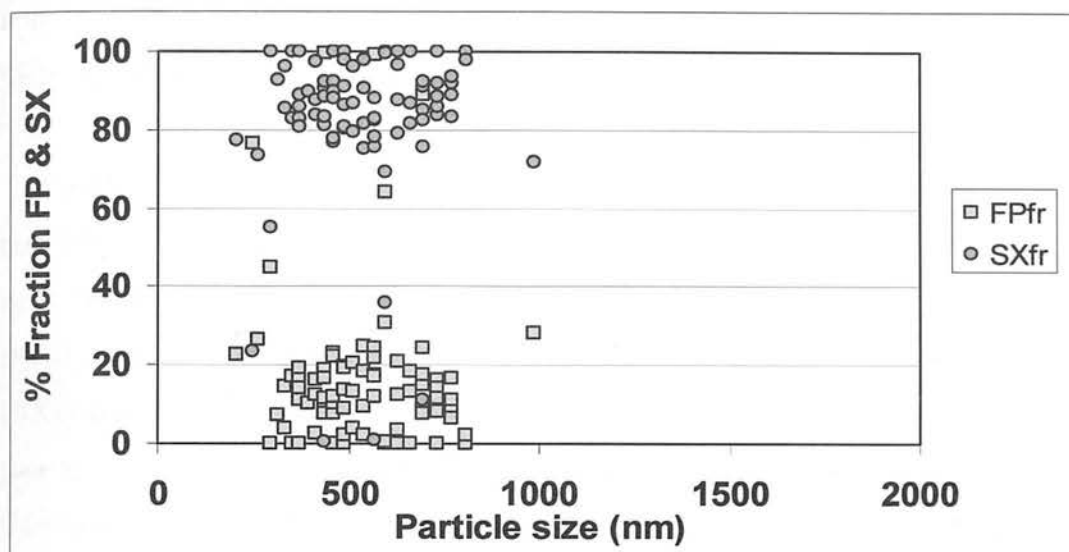
Figure 6.7. Fractional composition chart for particles in pure SX, determined by marker ion analysis (using m/z 57 for FP and m/z 91 for SX).

The particles were classified by using marker ion analysis in terms of a range for the fraction of each material, so as to account for the experimental error. Some variation in the vaporization efficiency of the particles taken from inhalation products was found and this is discussed in more detail in Section 6.5. Hence for identification and classification of particles based on fractional composition a threshold was used; *i.e.* if the SX_{fr} was above 70% the particle was identified as SX, (for consistency the same threshold was adopted for FP). The remaining particles (with a FP or SX fraction between 30 to 70 %) were identified as a co-associated mixture of both FP and SX.

Some example data for typical spectra taken from the various types of particles are discussed; for pMDIs three categories of particle are possible *i.e.* (i) pure FP, (ii) pure SX and (iii) mixed composition. Figure 6.8 shows example mass spectra of particles taken from a pMDI (Sample MDI_4; FP/SX 50/25).

The mass spectrum given in Figure 6.8 (a), acquired on a particle of diameter 314 nm, shows a number of fragment ions that are consistent with FP (for example, *m/z* 57, 121 and 139). The fraction of FP calculated for this particle using Equation 6.2 was 91.8 %, which showed that the particle composition was predominately FP. The mass spectrum given in Figure 6.8 (b), acquired on a particle of diameter 332 nm, shows a number of fragment ions that are consistent with SX (for example, *m/z* 91, 114, 170

and 262). The SX fraction (SX$_{fr}$) calculated for this particle using Equation 6.3 was 99.9 %, which showed that the particle composition was predominately SX.

The mass spectrum given in Figure 6.8 (c) was acquired on a particle of diameter 697 nm. This mass spectrum shows a number of fragment ions that are consistent with both FP (*m/z* 57, 121 and 139), and SX (*m/z* 91, 114, 170 and 262). The FP fraction (FP$_{fr}$) calculated for this particle using Equation 6.2 was 47.7 % and the SX fraction (SX$_{fr}$) calculated for this particle using Equation 6.3 was 52.3 % which showed that that the particle was composed of a mixture of FP and of SX. The application of the data analysis techniques based on marker ions to assess the degree of co-association in inhalation products is explored in further detail in Chapter 7.
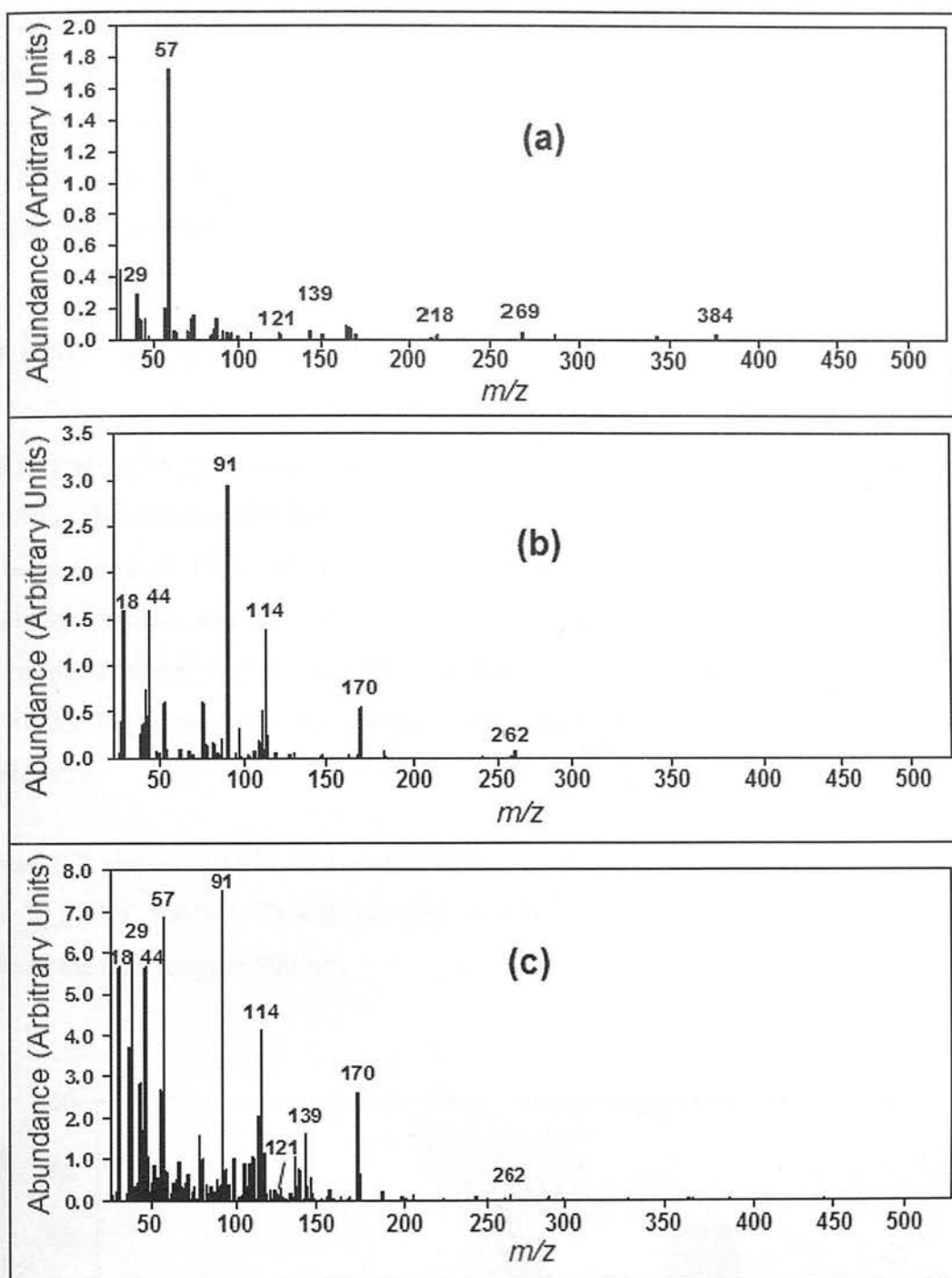
Figure 6.8. Single particle AAMS spectra (a) FP particle (314 nm) (b) SX particle (333 nm) (c) mixed (co-associated) particle (697 nm) taken from a pMDI (Sample MDI_4; FP/SX 50/25).

As for the AToFMS data there are some risks associated with marker ion analysis for AAMS data especially when it is based on only one ion per compound (all of the examples shown were based on one marker ion per compound), not least the fact that much of the data that is available is actually discarded. However, in this case samples were well defined blends of two or three compounds hence it was easy to attribute

marker ions that were unique and representative of the individual drug compounds present. Thus the marker ion technique was found to be a useful screen of the data and gave a reasonable way of identifying and classifying particles. Marker ion analysis was performed using multiple ions per compound, however this method was found to give no real advantage over the use of single marker ions and was not pursued.

6.4 Data Analysis for Dry Powder Inhalers (DPIs)

A practical difficulty was encountered during the experiments to acquire AAMS data on DPIs. The orifice at the inlet of the AAMS instrument was found to be susceptible to blockage with DPI particles so a study of quantitative data for this type of inhalation product was not possible and only qualitative data is presented. However, the results described below show that the data analysis methods could be applied if in the future the experiment were modified to make DPIs particles accessible to the experiment.

Figure 6.9 shows AAMS size distributions for the experiment on a DPI (Sample DPI_3; FP/SX 500/50). This shows that over 80 % of the particles in the population were in the size range > 500 nm.
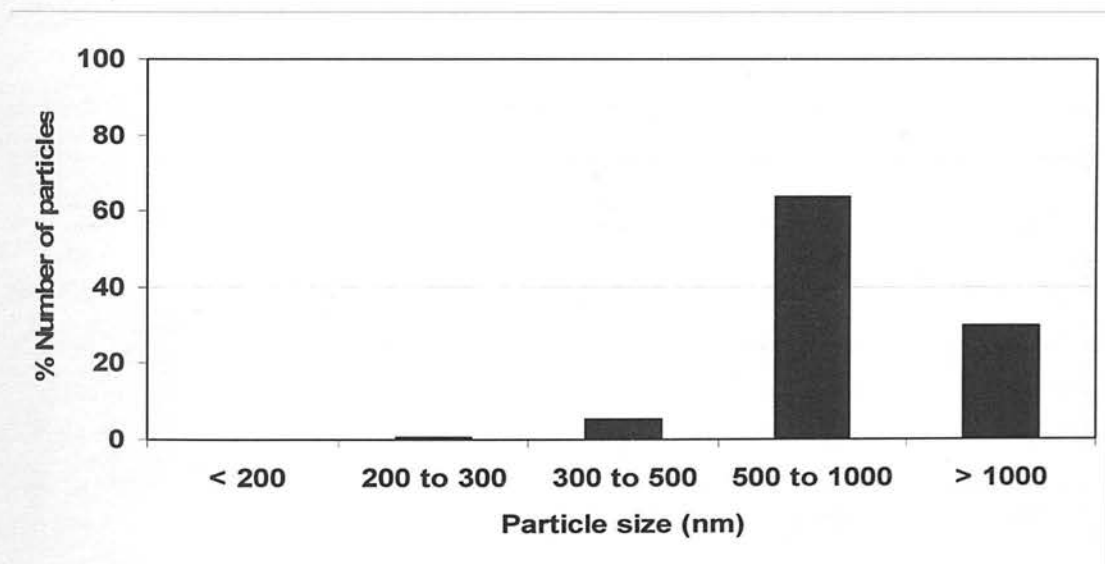
Figure 6.9. *Particle size distribution for 128 particles that gave mass spectra taken from a DPI (Sample DPI_3; FP/SX 500/50).*

Figure 6.10 shows the average mass spectrum taken from 51 particles of Flovent® (a blend of FP in excess lactose). The ions previously assigned to FP at *m/z* 29, 57, 121 and 139 are clearly visible as well as the ions at *m/z* 43, 73, 85 and 97 due to lactose.
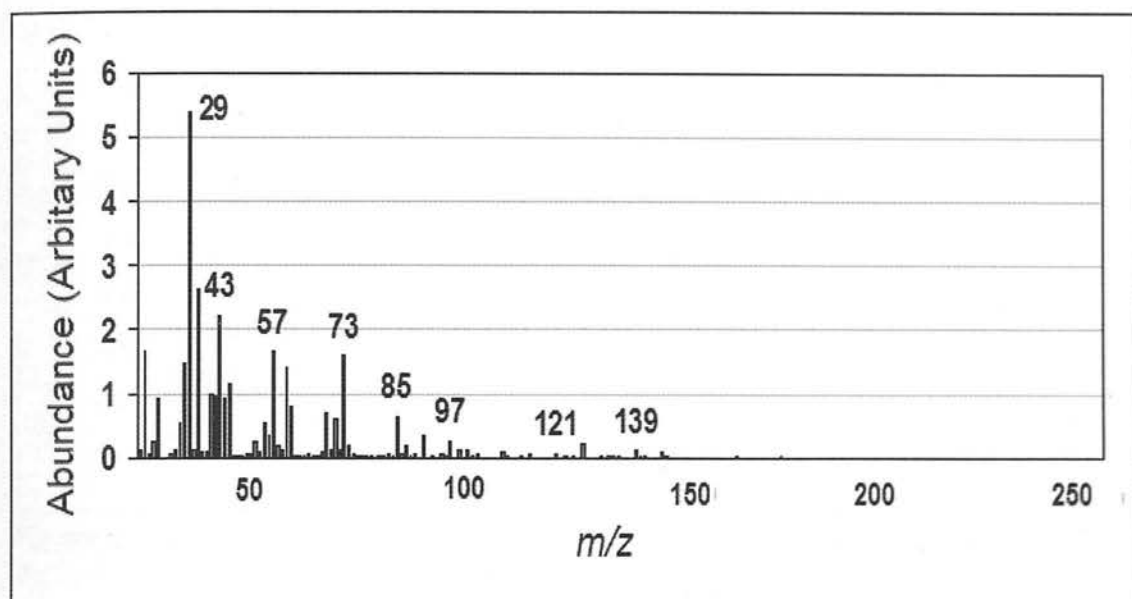
Figure 6.10. *Average ToF-AAMS spectrum taken from 50 particles (average particle size 942 nm) from a DPI (Sample DPI_1; Flovent® a blend of FP and lactose).*

Figure 6.11 shows a mass spectrum taken from a single particle of Flovent® (particle size of 894 nm). The mass spectrum consists of fragment ions from both FP and lactose (as discussed above for Figure 6.10) which indicates that the particle composition is a mixture of these two compounds.
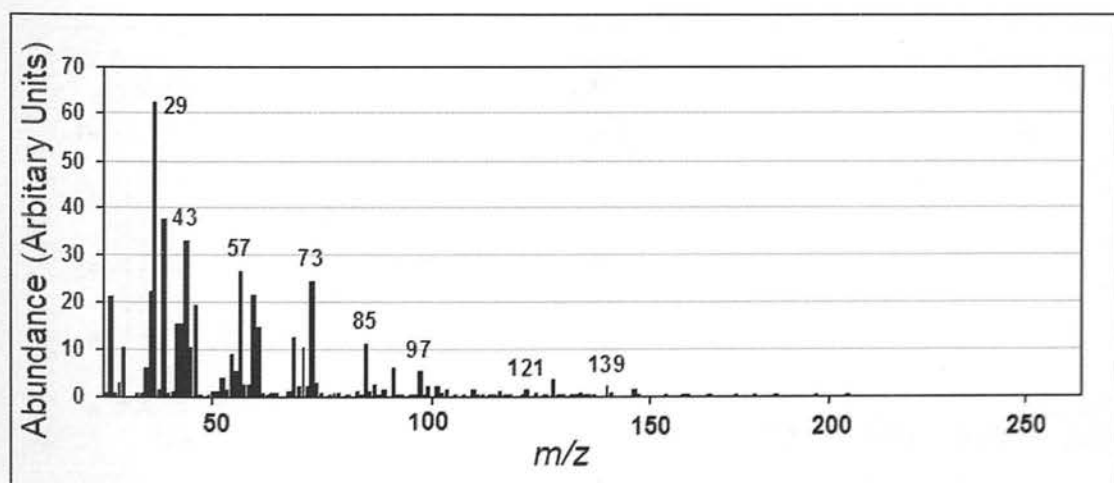
Figure 6.11. *ToF-AAMS spectrum of a single particle (894 nm) showing a mixture of FP and lactose (Sample DPI_1; Flovent® a blend of FP and lactose).*

The average ToF-AAMS spectrum for a DPI containing both FP and SX (Sample DPI_3; FP/SX 500/50) is shown in Figure 6.12. Major fragment ions can be observed for FP at m/z 57, 121 and 139, for SX at m/z 91, 114, 170 and 262 and for lactose at m/z 43, 73, 85 and 97. The ion at m/z 29 is common to both FP and lactose.
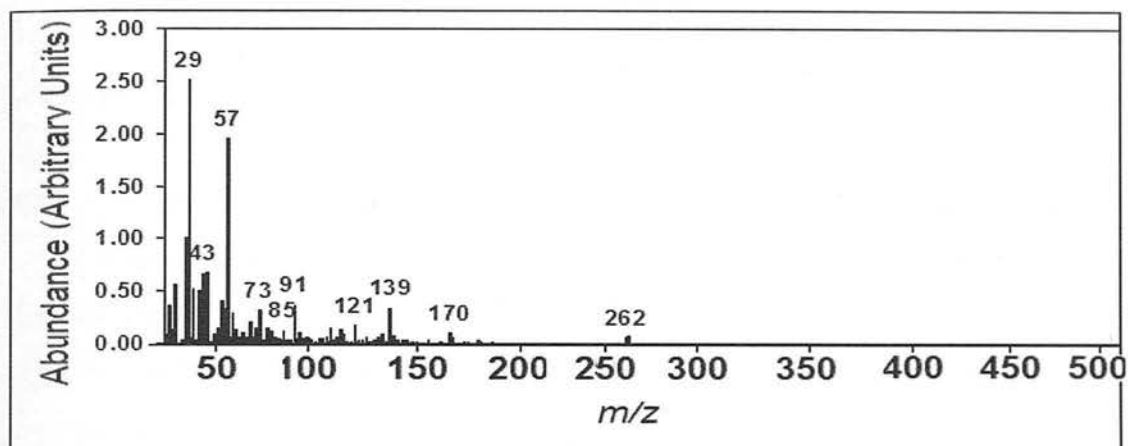
Figure 6.12. *Average ToF-AAMS spectrum from 126 particles taken from a DPI (Sample DPI_3; FP/SX 500/50).*

The ToF-AAMS spectrum acquired on a single particle taken from a DPI (Sample DPI_3; FP/SX 500/50) is shown in Figure 6.13. In this mass spectrum there are ions that are indicative of both FP and SX showing that this particle is of mixed composition and gives qualitative evidence for the presence of co-association. Also, the ion at m/z 85 is indicative of lactose showing that the particle is a mixture of three components.
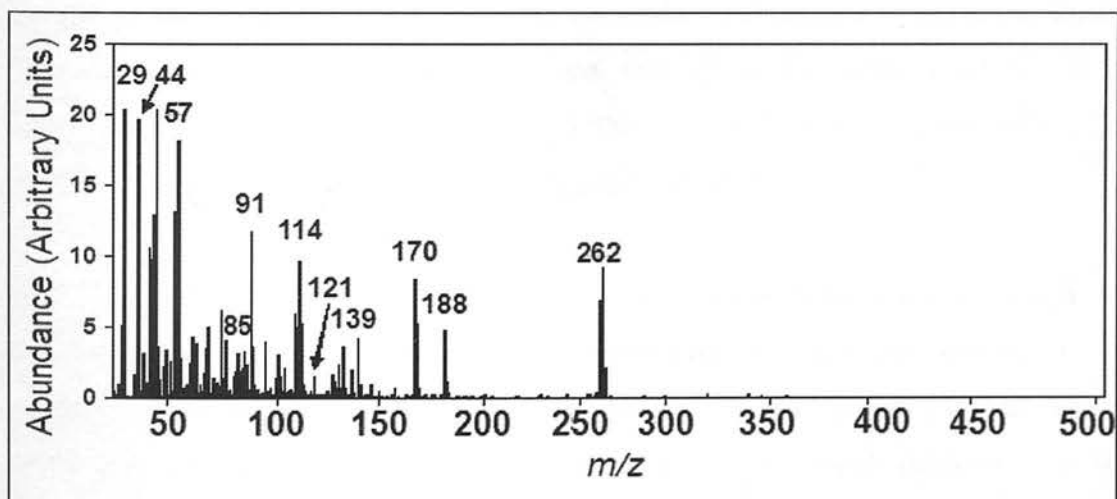
Figure 6.13. *ToF-AAMS spectrum taken from a single particle (of 1327 nm size) that consisted of a mixture of FP, SX and lactose (Sample DPI_3; FP/SX 500/50).*

6.5 Data Analysis Based on Multivariate Statistical Analysis

The mass spectra obtained from the AAMS experiment are typically complex and multivariate analysis has previously been used to process this type of data. Many of the multivariate methods applied to AAMS data are based on factor analysis for which the overall aim is to determine the dimensionality of the data and the relationships between the variables[7].

The most common form of factor analysis is principal component analysis (PCA) which was discussed in Chapter 4. More recently, multivariate statistical analysis has been developed to include methods such as positive matrix factorization (PMF) has been used successfully to de-convolute mass spectra acquired using the AAMS[8].

For all multivariate analysis the data is conditioned before it is analyzed to ensure that the data is in a suitable form for analysis. For example the data analysis for a variable that has a large numerical range, may be weighted towards the variance for the data at the higher end of the scale *i.e.* in this case the data analysis may be biased towards the larger values. Therefore in order to give all variables equal weight in the data analysis they are standardized and this is known as scaling[9].

The improvements in the scaling of the data using PMF (compared with PCA) mean that a more detailed analysis of the data can be made. For example in PCA analysis the data is scaled by columns or by rows, but in the PMF analysis there is the facility to scale each data point individually and this gives the opportunity for better modelling of the data. However although the end result may be better it is more complex to use PMF as a routine tool compared with PCA.

In the case of the application of PMF to the mass spectra of particles, so long as the spectral pattern of each component can be recognized, then the contributions of each component can be measured. For the work presented in this section the mass spectra of the pure drug compounds were compared with the components determined by de-convolution of the spectrum using PMF. However, it has been previously reported

that PMF can be applied to data taken from individual particles without prior knowledge of the compound identity or of the numbers of compounds present[10].

Although the inhalation products studied were well defined mixtures of two or three components the mass spectra still appeared as complex fingerprints of the material(s) present in each particle, hence PMF analysis was applied to the datasets on a particle-to-particle basis[4]. The aim of this was to detect the mass spectral pattern for each component and to identify and classify each particle in terms of composition.

Figure 6.14 shows the mass spectrum taken from a particle of mixed composition from a pMDI inhaler (Sample MDI_9; FP/SX 250/25) de-convoluted into the PMF components. In this case the PMF components, shown in Figures 6.14 (b) and (c), were comparable with mass spectra acquired on pure FP and pure SX respectively. In this case the fact that the mass spectrum from a particle was de-convoluted to give PMF components that appeared similar to the mass spectra of the pure drug materials, provided good evidence that the particle was composed of a co-associated mixture of FP and SX.
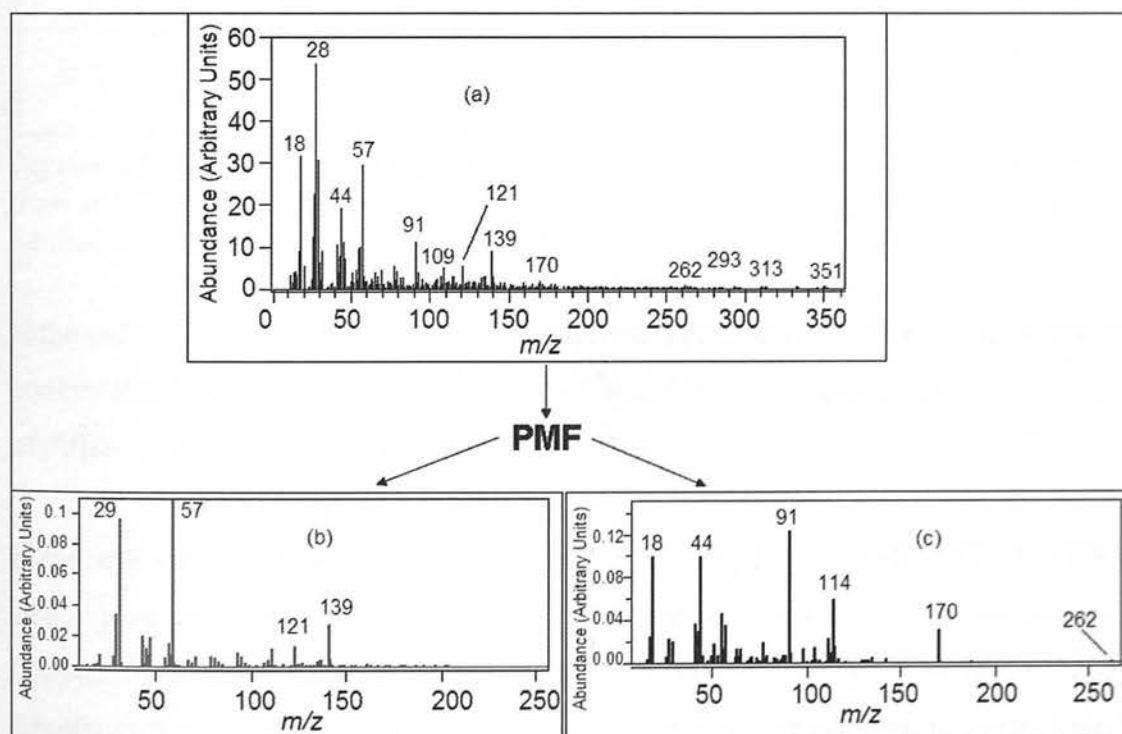
Figure 6.14. De-convolution of a mass spectrum to the PMF components. (a) Shows the mass spectrum taken from a particle composed of a mixture of FP and SX; (b) and (c) show the PMF components of FP and SX derived from the mixture. These mass spectra are comparable with the mass spectra of the pure compounds. (Example shown: Sample MDI_9, FP/SX 250/50).

Figure 6.15 shows the PMF de-convolution of a mass spectrum acquired on a particle of mixed composition taken from a DPI (Sample DPI_3; FP/SX 500/50). In this case the formulation consisted of three components *i.e.* FP, SX and lactose and the PMF components in the figure reflect this. The PMF components were found to be comparable with the mass spectra acquired on particles of pure FP, pure SX and pure lactose. An interpretation of the AAMS spectra of pure FP, pure SX and pure lactose is given in Chapter 3 (Section 3.5).
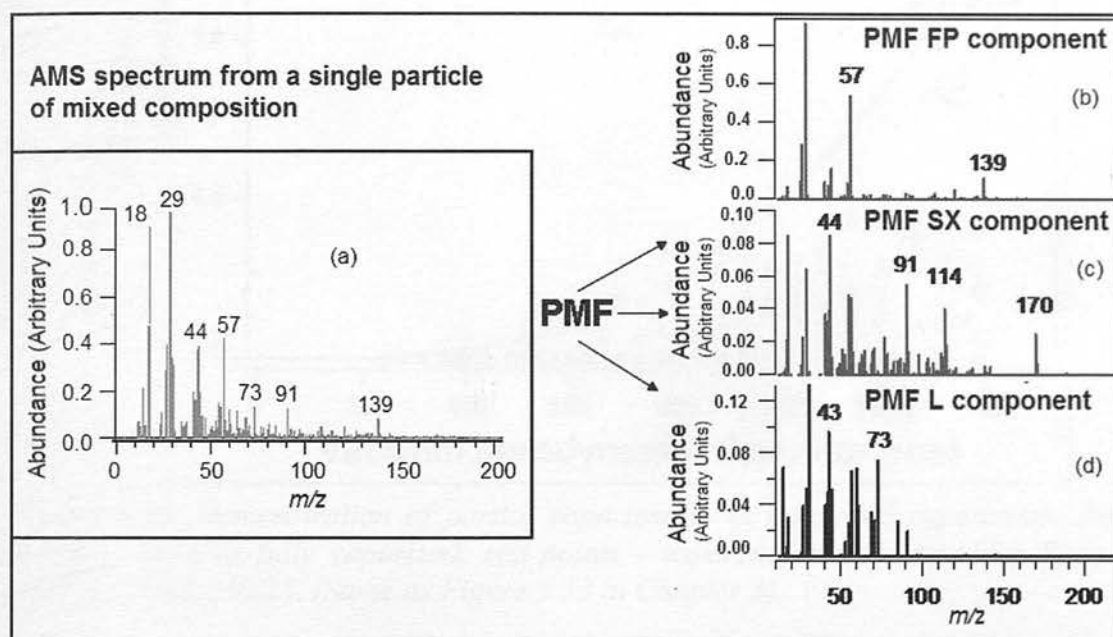
Figure 6.15. *PMF de-convolution of the mass spectrum of a three component particle from a DPI (Figure (a)) to show the PMF components for (b) FP (c) SX and (d) lactose (L). (Example data shown: Sample DPI_3; FP/SX 500/50).*

If the particle were only partially vaporized then quantitative measurements would be compromised because of non-representative sampling of the particle, *e.g.* in the case of different vaporization efficiencies of the material present.

If particle size is plotted against mass spectral signal for a pMDI (MDI_9 FP/SX 250/25) the graph shown in Figure 6.16 is obtained. As described previously (see Chapter 3) the points within 20% of the line represent fully vaporized particles (shown in blue), the remaining particles (shown in red) are only partially vaporized. Clearly many of the larger particles were not fully vaporized and hence were not used in the PMF analysis which limited the size of the data set used. For this sample 435 particles were detected by light scattering of which 169 gave a mass spectrum and 36

were found to be fully vaporized (see Table 6.1). In the future further work needs to be performed to improve the consistency of vaporization for this type of particle.
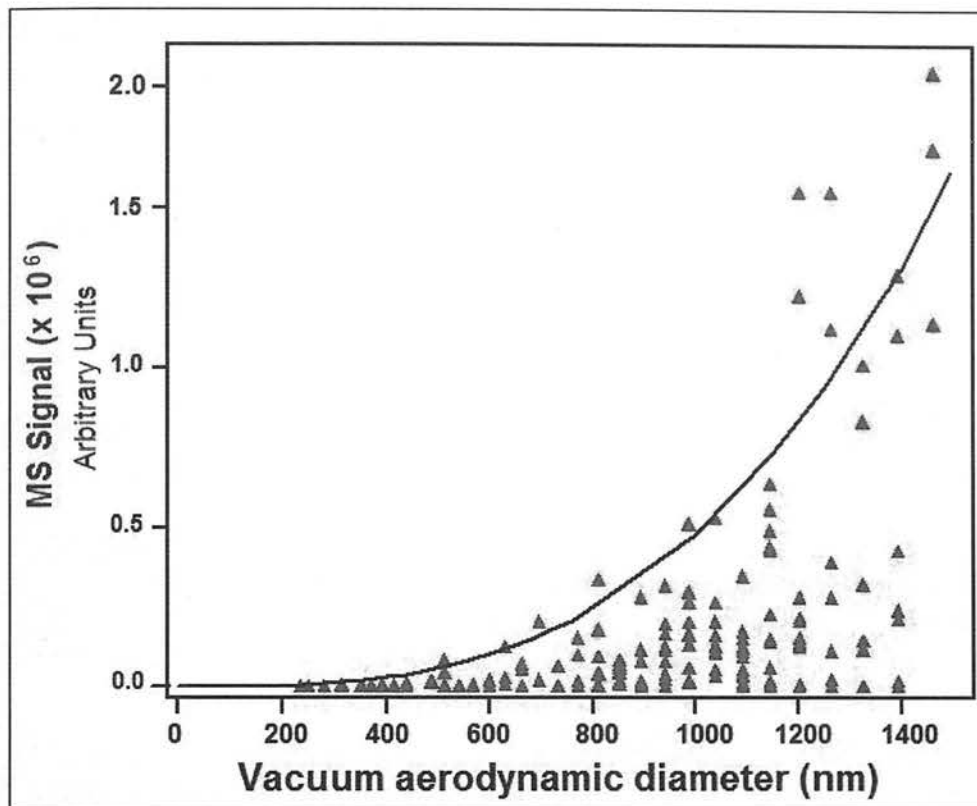
Figure 6.16. *Demonstration of partial vaporization in an AAMS experiment. Blue points - taken as fully vaporized; red points - vaporization is incomplete. Sample MDI_9 FP/SX 250/25. (Same as Figure 3.13 in Chapter 3).*

6.6 Summary of Data Analysis Methods for Aerodyne Aerosol Mass Spectrometry (AAMS)

Methods for analyzing AAMS data were developed based on marker ions and on multivariate statistical analysis.

As for the AToFMS data, the choice of marker ions from particles of pure drug material was based on the fragment ions observed in the average AAMS spectra (these were previously interpreted in terms of the structure of the given molecule). By choosing ions that were representative, the data sets for the inhalation products were then interrogated and a method for the assessment of the degree of co-association based on the number of mixed particles present was successfully developed.

A method for the analysis of the AAMS data using multivariate analysis, based on positive matrix factorization (PMF), was also developed. This type of multivariate analysis requires no prior knowledge of the compounds present as the mass spectra can be de-convoluted to give the PMF components which appear very similar to the mass spectra of the individual drug compounds.

Application of these data analysis methods to give an estimate of the degree of the level of co-association using the AAMS instrument is explored in Chapter 7.

6.7 References

(1)   Quantitative sampling using an Aerodyne aerosol mass spectrometer. Part 1: Techniques of data interpretation and error analysis, J.D. Allan, J-L. Jimenez H. Coe, K.N. Bower, L.R. Williams, J.T. Jayne and D.R. Worsnop. *J. Geophys. Res. 108 (D3), 4090, doi: 10.1029/2002JD002358, (2003).*

(2)   Quantitative sampling using an Aerodyne aerosol mass spectrometer. Part 2: Measurements of fine particulate chemical composition in two UK cities, J.D. Allan, H. Coe, K.N. Bower, L.R. Williams, M.W. Gallagher, M.R. Alfarra, J-L. Jimenez, E. Nemitz, A.G. McDonald, M.R. Canagaratna, J.T. Jayne and D.R. Worsnop. *J. Geophys. Res. 108 (D3), 4091, doi: 10.1029/2002JD002359, (2003).*

(3)   Microsoft Excel™ software, (Microsoft Corporation, Seattle WA, USA) http://www.microsoft.com/en/us/default.aspx (Accessed 23 June 2008).

(4)   The data processing using PMF was performed at Aerodyne (Boston, MA, USA) and received as a private communication from the Aerodyne Corporation.

(5)   Particle morphology and density characterization by combined mobility and aerodynamic diameter measurements. Part 1: Theory. P.F. DeCarlo, J.G. Slowik, D.R. Worsnop, P. Davidovits and J-L. Jimenez. *Aerosol Sci. and Tech. 38, 1185 -1205, (2004).*

(6)   Particle morphology and density characterization by combined mobility and aerodynamic diameter measurements. Part 2: Application to combustion-generated soot aerosols as a function of fuel equivalence ratio J.G. Slowik, K. Stainken, P. Davidovits, L.R. Williams, J.T. Jayne, C.E. Kolb, D.R. Worsnop, Y. Rudditch, P.F. DeCarlo and J-L. Jimenez. *Aerosol Sci. and Tech. 38, 1206-1222, (2004).*

(7)   Chemometrics: Data Analysis for the Laboratory and Chemical Plant. R. G. Brereton. John Wiley & Sons Ltd. (2003),ISBNs: 0-471-48977-8.

(8)   Deconvolution and quantification of hydrocarbon like and oxygenated organic aerosols based on aerosol mass spectrometry. Q. Zhang, M.R. Alfarra, D.R. Worsnop, J.D. Allan, H. Coe, M. Canagaratna and J.L. Jimenez. *Environ, Sci Technol. 39,4938-4952 (2005).*

(8(a)) Interpretation of Organic Components from Positive Matrix Factorization of Aerosol Mass Spectrometric Data. I. Ulbrich, M. Canagaratna, Q. Zhang, D. Worsnop, and J. Jimenez. *Atmospheric Chemistry and Physics, 9(9), 2891-2918, (2009).*

(9)   Multi- and Megavariate Data Analysis, Principles and Applications. L Eriksson, E. Johansson, N. Kettaneh-Wold and S. Wold. *Umetrics, Umea, Sweden, (2001). ISBN 91-973730-1-X.*

(10)   Positive matrix factorization: A non-negative factor model with optimal utilization of error estimates of data values. P. Pattero and U. Tapper *Environmetrics. 5, 111-126, (1994).*

Chapter 7

The Determination of Co-association using Aerodyne Aerosol Mass Spectrometry (AAMS)

7.1 Introduction

A major aim of the work presented in this thesis was to assess the amount of co-association in particles taken from a range of inhalation products. The data analysis was performed with emphasis on this aspect for both the AToFMS instrument (see Chapters 4 and 5) and the AAMS instrument. In this chapter, the results from a series of initial experiments designed to evaluate the potential of AAMS for assessing co-association in a range of inhalation products are presented and discussed. Note that these experiments were performed in the manufacturers' laboratories (Aerodyne, Boston, Ma, USA) which meant that instrument time and access was limited.

The data analysis was performed based on marker ion analysis or on multivariate analysis (*i.e.* positive matrix factorization (PMF)) as described in Chapter 6. Using these techniques, each particle was identified in terms composition as either fluticasone propionate (FP), salmeterol xinofoate (SX) or a co-associated mixture of both FP and SX. The reproducibility of the experiment and the major source of variation in the experiment are also discussed.

7.2 Assessment of Co-association Using Data from AAMS experiments

7.2.1 Assessment of Co-association Using Marker Ion Analysis

Figure 7.1 shows a fractional composition chart (see Chapter 6) determined from the marker ion analysis of each particle in a pMDI (MDI_2; FP/ SX 50/25). From this

chart it can be seen that the particles sizes were predominantly between 200 and 600 nm and that the majority of the particles measured were pure FP.

The results from for a number of repeat runs for the pMDI formulation FP/SX 50/25 is summarized in Table 7.1 and this indicates that between 10.8 and 14.0 % of the particles were of mixed composition. The error in this measurement is discussed in Section 7.2.2.
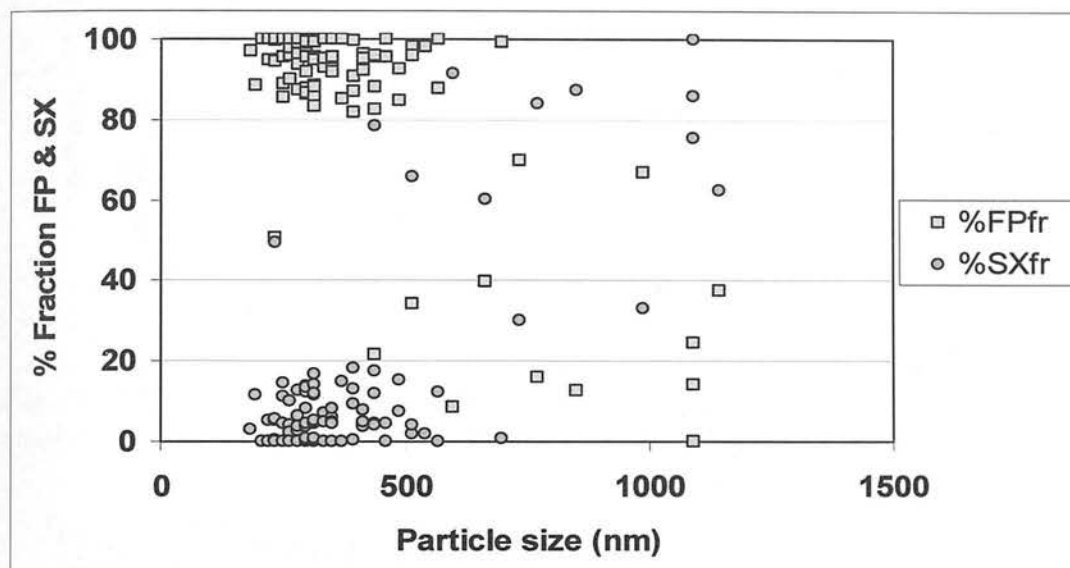
Figure 7.1. *Fractional composition chart for particles in a pMDI, determined by marker ion analysis (Sample MDI_2 ; FP/SX 50/25).*

File	Formulation	Batch/id	% FP	% SX	% Mixed
MDI_1	FP/SX 50/25.	002/78.	n/a	n/a	n/a
MDI_2	FP/SX 50/25.	002/78.	82.0	5.7	12.3
MDI_3	FP/SX 50/25.	05/97F	76.3	10.3	13.4
MDI_4	FP/SX 50/25.	AX7099/23	83.3	3.3	13.3
MDI_5	FP/SX 50/25.	AX7099/23	86.3	2.9	10.8
MDI_6	FP/SX 50/25.	AX7099/23	80.8	5.2	14.0

Table 7.1. *To show the % number of pure FP, pure SX and mixed (co-associated) particles as defined by the fractional composition determined from the marker ion analysis of pMDIs (Samples MDI_2 to MDI_6; FP/SX 50/25). *No data is shown for MDI_1 as this was used as a trial run.*

Figure 7.2 shows an example fractional composition chart (see Chapter 6) determined from marker ion analysis for each particle in a second pMDI (sample MDI_9; FP/ SX 250/25). From this chart it can be seen that the particles size is between 200 and 1500 nm. Also in this case more co-associated particles (compared with Figure 7.1) were

observed as depicted by the data points with a fractional composition of between 30 to 70% of either FP or SX. The results for a number of repeat runs for the pMDI formulation FP/SX 250/25 is summarized in Table 7.2 and this indicates that between 10.3 and 21.3 % of the particles were of mixed composition. The error in this measurement is discussed in Section 7.2.2.
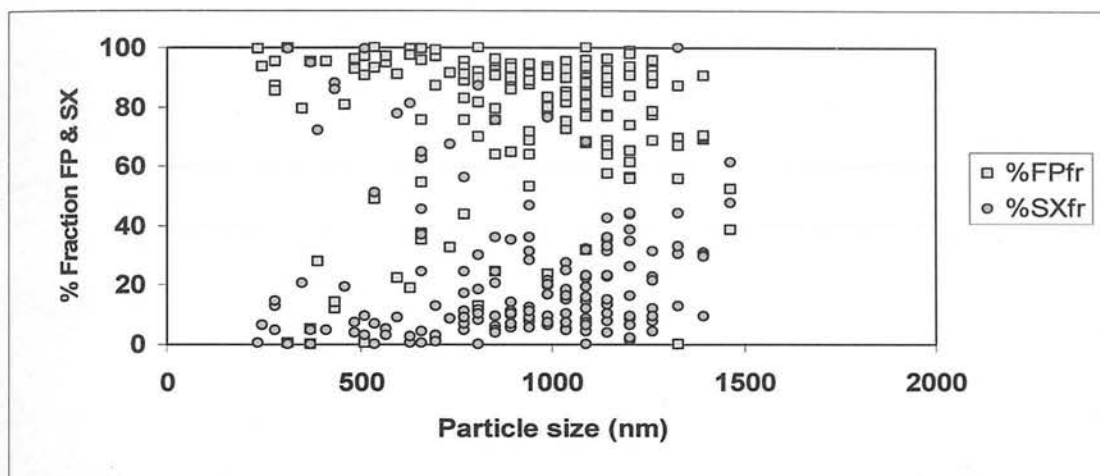
Figure 7.2. *Fractional composition chart for particles in a pMDI, determined by marker ion analysis. (Sample MDI_9; FP/SX 250/25).*

File	Formulation	Batch/id	FP	SX	Mixed
MDI_7	FP/SX 250/25.	1/22.	71.6	7.1	21.3
MDI_8	FP/SX 250/25.	1/22.	74.5	4.9	20.6
MDI_9	FP/SX 250/25.	1/22.	84.9	4.8	10.3
MDI_10	FP/SX 250/25.	AX7102/82.	77.7	4.9	17.5
MDI_11	FP/SX 250/25.	DO40861.	76.1	5.2	18.7

Table 7.2. *To show the % number of pure FP, pure SX and mixed (co-associated) particles as defined by the fractional composition determined from the marker ion analysis of pMDIs (Samples MDI_7 to MDI_12; FP/SX 250/25).*

7.2.2 Reproducibility of the Measurement for Assessment of Co-association Using Marker Ion Analysis

The relative standard deviation (RSD) of the number of mixed particles in three runs of the same batch of each formulation was calculated to give an estimate of the variation in the intra-batch measurement. The RSD % was also calculated for runs of three different batches of the same formulation to estimate variation in the inter-batch measurement. The variation in the results for marker ion analysis determined in this way is shown in Table 7.3.

The average number of mixed particles found in the pMDI inter-batch measurements FP/SX 250/25 was found to be 15.5 %. Also the error shown by the RSD for the pMDI inter-batch experiments was found to be 29.2 %. The average number of mixed particles found in the pMDI intra-batch measurements FP/SX 250/25 was found to be 17.4 %. Also the error shown by the RSD for the pMDI inter-batch experiments was found to be 35.3 %. The average number of mixed particles found in the pMDI inter-batch measurements FP/SX 50/25 was found to be 13.0 %. Also the error shown by the RSD for the pMDI inter-batch experiments was found to be 4.8 %. The average number of mixed particles found in the pMDI intra-batch measurements FP/SX 50/25 was found to be 12.7 %. Also the error shown by the RSD % for the pMDI inter-batch experiments was found to be 13.2 %.

The RSD % shown in Table 7.3 is much higher for the FP/SX 250/25 formulation compared with the FP/SX 50/25 formulation. This is because, for the FP/SX 50/25 formulation, the majority of the particles were shown to be mainly small particles of FP (*i.e.* FP fines) (see Section 6.2). Previously, small FP particles from a sample of pure FP were easily identified; however there was an amount of noise associated with larger particles especially those from a sample of pure SX (see Section 6.3.2). This was probably due to a difference in the vaporization efficiency of each compound. Hence, the larger error for the FP/SX 250/25 formulation was attributed to the presence of larger SX containing particles in the formulation which were difficult to vaporize efficiently.

Type	Formulation	Batch type	Average	RSD %
pMDI	FP/SX 250/25	Inter-batch	15.5	29.2
pMDI	FP/SX 250/25	Intra-batch	17.4	35.3
pMDI	FP/SX 50/25	Inter-batch	13.0	4.8
pMDI	FP/SX 50/25	Intra-batch	12.7	13.2

Table 7.3. Determination of co-association (mixed particles) in pMDI aerosols based on marker ion analysis. The table shows the average % number of particles found in inter- or intra- batch experiments. In each case an estimate of the error is given by the relative standard deviation % (RSD %) (i.e. the Standard Deviation/ Average (x 100 %)).

7.2.3 Assessment of Co-association in Inhalation Products Based on Multivariate Statistical Analysis

The data analysis using PMF was based on fully vaporized particles determined as described in Chapter 6. The results obtained from the PMF analysis of the pMDI data set of AAMS data are give in Table 7.4 and this shows the fraction of FP, SX or mixed particles in each sample. A comparison of the data from each formulation was performed and the results shown are broadly comparable with the marker ion analysis. However, the PMF data analysis was found to be extremely sensitive to background noise probably originating from inconsistent vaporization of larger particles containing SX. This was especially so for MDI_7, MDI_10 and MDI_11 (samples of the FP/SX 250/25 formulation which comprised of relatively large particles containing significant amounts of SX according to the marker ion analysis discussed earlier in this chapter). These datasets were found to be too noisy to provide any meaningful results and were excluded from Table 7.4.

Sample	Formulation	FP	SX	Mix
MDI_1*	FP/SX 50/25.	n/a	n/a	n/a
MDI_2	FP/SX 50/25.	89.8	4.1	6.5
MDI_3	FP/SX 50/25.	26.0	15.9	59.6
MDI_4	FP/SX 50/25.	79.3	4.1	16.4
MDI_5	FP/SX 50/25.	87.9	3.9	8.7
MDI_6	FP/SX 50/25.	86.2	2.9	10.5
MDI_7	FP/SX 250/25.	n/a	n/a	n/a
MDI_8	FP/SX 250/25.	64.3	9.6	26.1
MDI_9	FP/SX 250/25.	85.8	2.3	11.6
MDI_10	FP/SX 250/25.	n/a	n/a	n/a
MDI_11	FP/SX 250/25.	n/a	n/a	n/a

*Table 7.4. PMF results for AAMS data. *MDI_1 was a trial run. n/a = data not available due to high level of background noise.*

Comparison of the PMF results for the two formulations is shown in Figure 7.3 for FP/SX 50/25 and Figure 7.4 for FP/SX 250/25. The PMF analysis determined that most of the particles in these samples contained a high amount of FP which is consistent with the results from the marker ion analysis. The figures also show that the samples of the FP/SX 250/25 formulation comprised a slightly higher number of

mixed (co-associated) particles (~19% compared with ~11% for the FP/SX 50/25 formulation), although the bulk of the particles were found to consist mainly of FP.
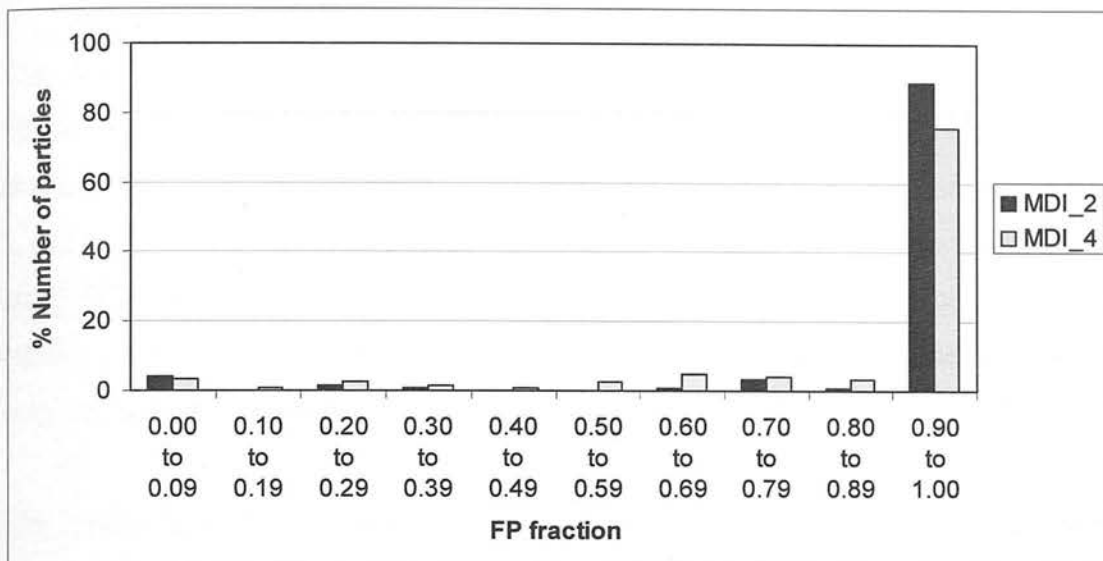
Figure 7.3. *Comparison of FP fractions from PMF analysis of pMDIs (MDI_2 and MDI_4; FP/SX 50/25)*
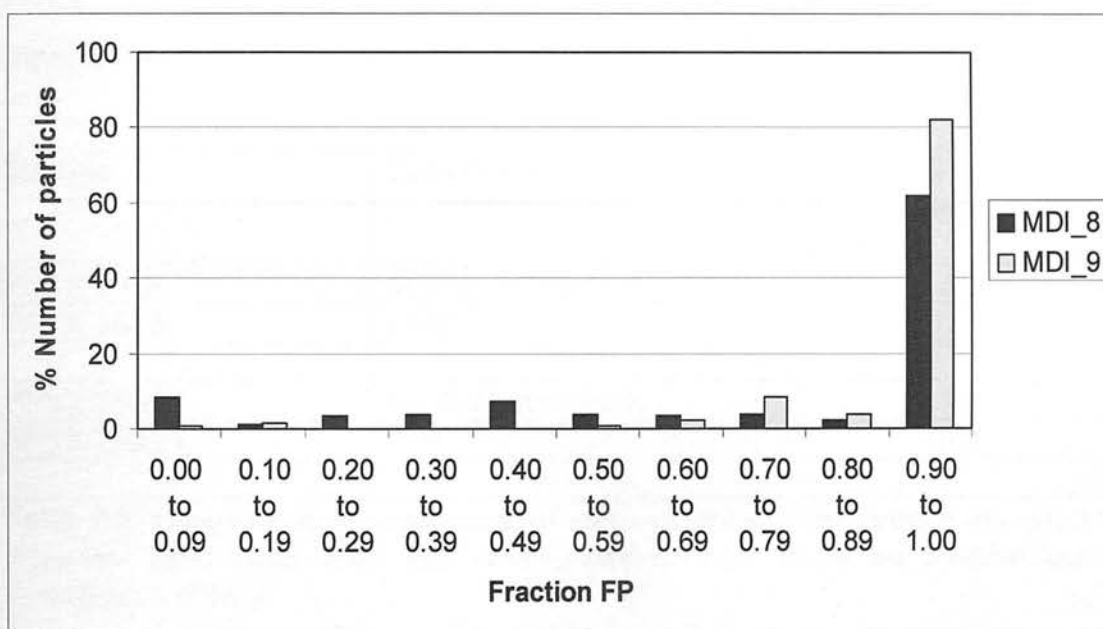
Figure 7.4. *Comparison of FP fractions from PMF analysis of pMDIs (MDI_8 and MDI_9; FP/SX 250/25).*

7.3 Summary of Data Analysis for AAMS

The results for the measurement of co-association were described for a number of pMDIs. The results showed that the presence of co-association can be determined using this instrument although further work would be required to improve the

consistency of the data produced especially in terms of quantification. (This was not possible in the current work as access to the instrument was limited).

The AAMS data acquired on the pMDIs was analyzed using both marker ions and positive matrix factorization (PMF) and it was shown that the particles present could be identified using either method. It would be expected that PMF analysis would give a more consistent result (compared with marker ion analysis) as it is based on the analysis of the complete data set rather than a single ion to represent each component. However the PMF analysis was hampered by the noise in the data, probably originating from inconsistent vaporization of the sample particles.

The results from the intra-batch analyses (repeat analysis of the same material) were averaged and are summarised in Table 7.5 which shows that co-associated particles were observed in both formulations. Lower levels of co-association were found in the FP/SX 50/25 formulation because this material was dominated by smaller particles (fines) of FP.

Sample	Technique	Average % number of coassociated particle present
FP/SX 50/25	Marker ion analysis	12.7
FP/SX 50/25	PMF	7.1
FP/SX 250/25	Marker ion analysis	17.4
FP/SX 250/25	PMF	10.9

Table 7.5. Comparison of assessment of co-association using marker ion analysis (from the intra-batch data) and multivariate analysis based on positive matrix factorization (PMF).

A comparison of the AAMS results with the AToFMS results is given in Chapter 8 and this shows that there is broad agreement between data acquired using the two techniques in the determination of the level of co-association found.

There is potential for the AAMS experiment to be the preferred instrument for this type of analysis as it can detect both pure FP and pure SX particles, co-associated particles and the excipient (in this case lactose) and has previously been shown to

produce quantitative data. However, the initial results presented in this chapter highlighted some limitations of the AAMS experiment in the current configuration (*i.e.* primarily noise associated with the vaporization of larger SX containing particles) and some areas for focus in future work are discussed in Chapter 9.

Chapter 8

Conclusions

8.1 Introduction

Two commercial single particle mass spectrometers were used in this work and although the general layout of these instruments was similar, there were some differences in their design. For example, the ionization source of the Aerosol Time-of-Flight Mass Spectrometer used a single step process involving laser ablation and ionization while the Aerodyne Aerosol Mass Spectrometer used a two step process involving thermal desorption from a hot plate followed by electron ionization. These instruments were compared and evaluated in terms of their design and the characteristics of the data acquired on aerosols of pharmaceutical materials.

Data analysis methods for single particle mass spectrometry were developed based on the mass spectrometric fragmentation patterns indicative of either pure or co-associated particles. Data analysis was performed by either using representative ions from the mass spectrum taken from each particle or by using multivariate statistical analysis as a pattern recognition tool applied to the complete mass spectrum for each particle.

High levels (above 50%) of co-association were found in the emitted doses from both pMDI and DPI products. Although the design of each instrument was different, reasonable agreement in the levels of co-association was found as long as the size of particle that was analyzed by the mass spectrometer in each case was taken into account.

8.2 Measurement of Co-associated Particles

For both the AToFMS and AAMS instruments, the mass spectra that were acquired from particles of pure drugs showed unique fragment ions that could be reasonably interpreted in terms of the structures of the drug compounds (see Chapter 3).

The measurement of co-association was based on the appearance of the mass spectra for each of the single particles analyzed. This enabled the identification and classification of the individual particles as a pure material or as a co-associated mixture of drug compounds.

The inhalation products analyzed were well defined samples containing the two active drugs present (FP and SX) and this was reflected in the mass spectra. For example Figure 8.1 shows the mass spectra taken from two single particles of similar size, from a pMDI (Sample FP/SX 250/25) using the AToFMS instrument (Figure 8.1a) and the AAMS instrument (8.1b). The ions present in the two spectra are different because of (i) the different ionization techniques used (see Chapter 3) and (ii) the different detector polarity used (negative ions for AToFMS and positive ions for AAMS). However, both mass spectra show a combination of ions originating from FP or SX which indicates a co-associated mixture of the two compounds.
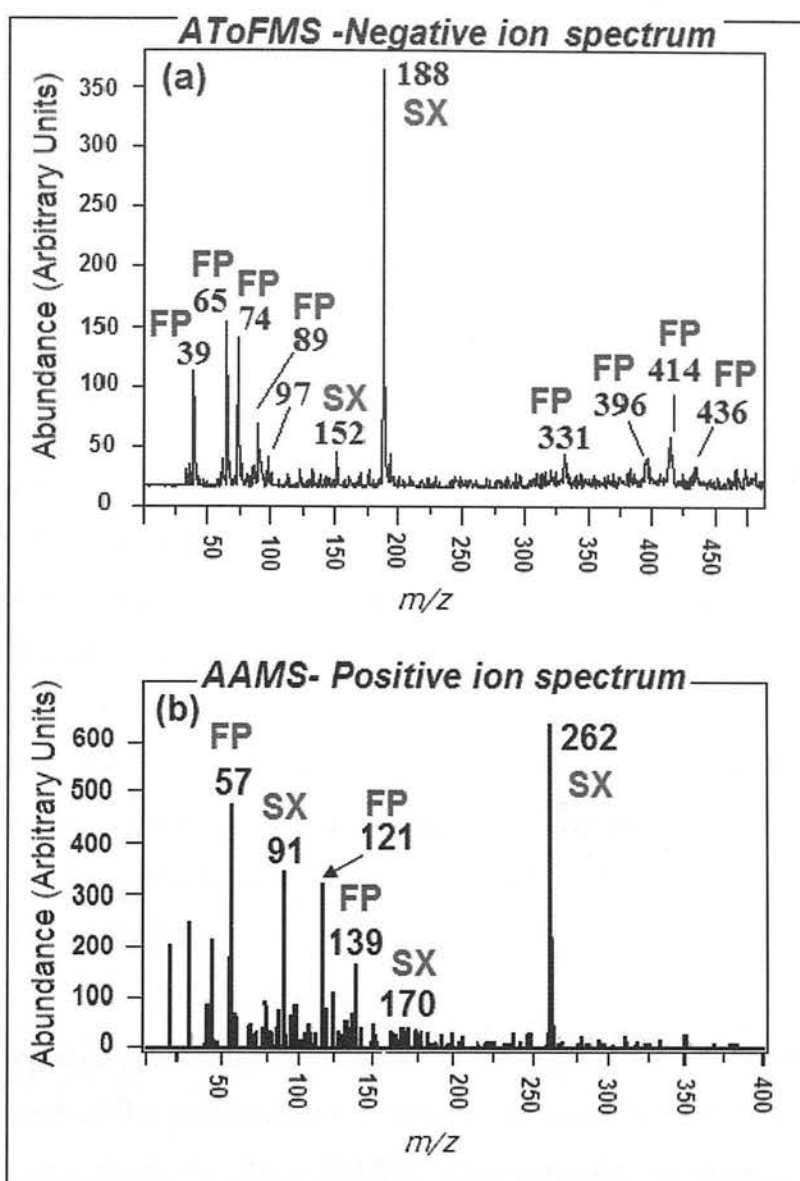
Figure 8.1. *Mass spectra of particles of similar size taken from a pMDI aerosol (Sample FP/SX 250/25) using (a) the AToFMS instrument (negative ion mass spectrum) for a particle of size = 1.2 μm and (b) the AAMS instrument (positive ion spectrum) for a particle of size = 1.0 μm. Both spectra show a number of ions previously found to be unique to FP and SX, indicating that each of these particles is of mixed composition.*

For the DPIs, co-association was observed and measured using the AToFMS instrument, however, the AToFMS experiment is limited in that lactose is not detected (See Chapter 3); *i.e.* a particle containing only FP could not be distinguished from a particle containing a mixture of FP and lactose. A mass spectrum of pure lactose was acquired using the AAMS instrument and lactose ions were also identified in particles comprised of a mixture of FP, SX and lactose which indicated a potential advantage of the AAMS instrument. However some experimental difficulties were encountered with the analysis of DPI particles using the AAMS and further work would be

required to develop the accessibility of the experiment to this type of particle. This work was not performed at the time because of the limited access to the instrument.

8.3 Estimation of the Level of Co-association

The synergistic effect of treatment for lung disease using the two active drugs simultaneously may be explained by the two drugs (FP and SX) acting on the lung tissue simultaneously. Probably the easiest and most consistent way for this to happen would be *via* particles that consist of a mixture of the two active materials. The data presented in this thesis provides strong evidence of high levels of co-associated particles in the inhaler devices investigated and goes some way to explaining the synergistic effect discussed in Chapter 1 (Section 1.5).

Further work in this area could show an advantage of GSK inhalation products in which co-associated particles exist compared with competitor products that contain a mixture of pure particles. A further series of experiments would need to be designed and executed to confirm this.

It has been reported previously that quantitation using the AToFMS is difficult or not possible because of the shot-to-shot variation in the laser (See Section 3.2). The data presented in this thesis for the AToFMS, to investigate the composition of each particle is probably semi-quantitative at best. However the variation measured expressed as an RSD % (1 to 16 % for marker ions and 3 to 10 % for PCA) was good when the small amounts of sample per particle (~ femtograms or less) (see Section 9.2.3) are considered. This level of variation is broadly comparable with the level of error expected when mass spectrometery is applied quantitatively to measure at the femtogram level in other application such as drug metabolism[1] or environmental analysis[2].

The use of multivaraiate analysis was a good method for handling large amounts of data. For some samples over 100 particle were analyzed and each was associated with a mass spectrum typically containing many ions. PCA charts were used identify and classify groups of particles based on the mass spectral pattern. Further analysis of the

PCA charts was performed by defining each particle category mathematically with an ellipse for each particle type. This worked well and the ellipses were able to take into account some of the variation in the AToFMS experiment. Although this was still a semi-quantitative measurement of the composition of each particle it is probably the best estimate of the composition of this type of particle to date.

Groups of particles with similar mass spectra could be used to identify and classify individual single particles. This is an advantage compared with techniques previously associated with inhalation product analysis that provide an an average analysis of a group of particles such as the Anderssen Cascade Impactor (see Section 1.6). The single particle mass spectrometry technique also provides an advantage compared with techniques previously used to analyze single particles such as Raman spectroscopy which is slower and relies on analyzing samples of the material off-line (i.e. particles from an inhaler are deposited on a plate and each particle is imaged). The SPMS technique provides some advantage in being able to analyze the particles from ana inhaler aerosol in near real-time and avoid possible artefacts that may be associated with off-line analysis.

Although the experimental difficulties associated with the experiments on the AAMS instrument meant a limited data set, some good qualitative evidence for the presence of co-association was obtained from the positive matrix factorization analysis (PMF). It was shown that mass spectra from single particle of mixed composition could be deconvoluted to give spectra very similar to those obtained from pure samples of FP and SX. It is envisaged that this might be developed into a more reproducible and quantitative technique as applied to pharmaceutical aerosols in the future as it is currently regularly used quantitatively in other fields (see Section 6.5).

The AAMS instrument also shows some advantage in that is able to detect excipients that may be in the formulation. Compounds such as magnesium stearate, cellulose octaacetate and lactose are all potentially useful excipients for drug formulations and these can all be detected by the AAMS but not the AToFMS. This is because the electron ionization source of the AAMS is able to ionize these materials, whereas they do not absorb laser energy at the given wavelength of the AToFMS laser (see Section 3.2.1).

In general the larger particles in the formulation of inhalation products would be more likely to be of mixed composition as a result of co-association between smaller particles. As the upper limit of the particle size range of the AToFMS instrument is larger than that of the AAMS instrument (see Chapters 5 and 7), then it would be expected that more co-associated particles would be detected using the AToFMS instrument and this was found to be the case.

Figure 8.2 shows a comparison of typical particle sizing data for a pMDI (FP/SX, 50/25) using the AAMS and the AToFMS instruments. Both instruments measured particles at the lower end of the respirable range (which is 0.6 to 6.0 μm) and this figure shows that more of the larger particles (> 1000 μm) were detected using the AToFMS instrument compared with the AAMS instrument. The particle size range measured for the pMDI using the AToFMS instrument was typically 0.5 to 1.5 μm with an average particle size of 0.9 μm. Alternatively, using the AAMS instrument the typical particle size range found was 0.2 to 1.0 μm with an average of 0.3 μm. The difference in particle size range detected was attributed to the different designs of the aerodynamic lens in each of the instruments used.
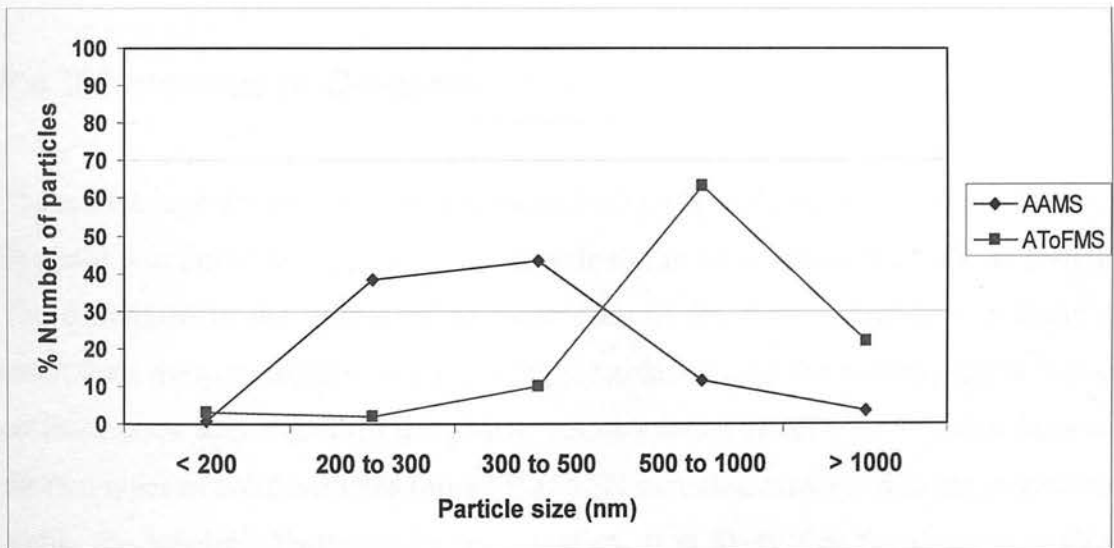
Figure 8.2. Comparison of particle sizing distributions (PSD) as measured using the AAMS and AToFMS instruments for sample FP/SX 50/25.

Table 8.1 shows a comparison of the average level of co-association found in pMDI samples using the results from the marker ion analysis. The AToFMS gives a

measurement of co-association higher than that given by the AAMS which is explained by the larger average particle size accessible to AToFMS experiment.

	AToFMS		AAMS	
Sample/ Formulation	Average particle size (µm)	Number of mixed particles (%)	Average particle size (µm)	Number of mixed particles (%)
FP/SX 250/25	1.0	50.2 (±10.8 %)	0.4	17.4 (±-35.3%)
FP/SX 50/25	0.8	45.4 (±4.3%)	0.4	13.7 (± 13.2%)

Table 8.1. The level of co-association in a series of pMDI determined using (a) the AToFMS instrument and (b) the AAMS instrument. In this case the data taken from the AToFMS experiment was processed using marker ions and is from three repeat runs of the same sample in each case (see Chapter 5).The data for the AAMS experiment was based on marker ions from three repeat runs of the same sample (see Chapter 7).

8.4 Differences in Co-association in DPIs and MDI's

There were high levels of co-association in both DPIs and pMDIs (see Chapters 5 and 7) and it was noted that higher levels were found in DPIs compared with the pMDIs. The difference in the degree of co-association in the different devices is likely to result from the very different nature of the formulations and the mechanisms by which co-association may occur. In the pMDI, co-association is believed to occur between the two types of solid particles (pure FP and SX particles) while still in the suspension within the inhaler[3]. Furthermore, on actuation, it is likely that the droplets emitted from the device contain multiple particles of FP and of SX. When a droplet collapses through propellant evaporation these particles can remain associated[4]. Alternatively, coalescence of droplets within the plume could also lead to co-association.

In DPIs co-association would arise from drug-drug interactions as a result of high shear forces during the blending process. However, lactose added to the blend as an excipient will both reduce the level of co-association by acting as a diluent and potentially increase the level of co-association by acting as a 'carrier' of both drug types. The dominant mechanisms contributing to the levels of co-association observed in such combination products require further study.

8.5 Summary

The SPMS experiments presented in this thesis were successful in that particles composed of the individual drug compounds could be recognised and distinguished from particles that were composed of a co-associated mixture of the drug materials. Furthermore, an estimate of the degree of co-association was made for a range of inhalation products there was broad agreement between the results obtained from two commercially available SPMS instruments.

Single particle mass spectrometry (SPMS) techniques were applied to the analysis of the aerosols originating from inhalation products. This was specifically to investigate the levels of co-association between FP and SX in individual particles. High levels of co-association were observed for both pMDIs and DPIs. The results presented, gave a unique particle analysis in terms of measurement of size and composition for inhalation products which previously proved difficult using other techniques.

The instruments used for this work were originally designed for environmental studies and would benefit from some further development to modify the experiment for pharmaceutical analysis. For example to allow accessibility to the larger particles in the respirable range and more consistent mass spectra for the larger, more fragile organic molecules found in inhalation products.

Application of this technique in the future may give some benefit to the patient from a better understanding of the manufacturing process and as a tool to monitor the optimization of the amount of co-association in terms of clinical efficacy.

8.6 References

(1) Microdosing assessment to evaluate pharmacokinetics and drug metabolism in rats using liquid chromatography-tandem mass spectrometry. J. Ni, H. Ouyang, M. Aiello, C. Seto, L. Borbridge, T. Sakuma, R. Ellis, D. Welty and A. Acheampong. *Pharma. Research.* 25, 1572-1582, (7), (2008).

(2) Femtogram detection and quantitation of residues using laser ionization orthogonal time-of-flight mass spectrometry. Q. Yu[t], Z. Cao[t], L. Li[t], B. Yan[t], W. Hang, J. He and B. Huang. *Anal. Chem.* 81, (20), 8623–8626, (2009).

(3) Characterisation of the aggregation behaviour in a salmeterol and fluticasone propionate inhalation aerosol system. Y. Micheal, M. Snowden, B.Z. Chowdhry, I.C. Ashurst, C. Davies-Cutting and T. Riley. *Int. J. Pharmaceutics.* 221, 165-174 (2001).

(4) Development of a systematic theory of suspension inhalation aerosols. I. A framework to study the effects of aggregation on the aerodynamic behaviour of drug particles. I. Gonda. *Int. J. Pharmaceutics.* 27, 99 -116 (1985).

Chapter 9

Suggested Further Work

9.1 Scope for Future Developments

The blending process used in the manufacture of inhalation products is currently not well understood; for example a link between the blending process and the degree of co-association present has not been established. This is mainly because in the past it has not been easy to detect or quantify co-association in individual particles using existing analytical techniques. In the current manufacturing process for inhalation products the materials are blended for a given amount of time (typically a few minutes) and give an unknown and uncontrolled amount of co-association. However, from the work presented in this thesis it appears likely that a better understanding of the blending and co-association processes can be obtained from SPMS.

The current US Food and Drug Administration (FDA) process analytical technologies (PAT) initiative[1] has an objective of giving a benefit to the patient through a better understanding of the manufacturing process. There would be some benefit in applying single particle mass spectrometry (SPMS) techniques to investigate the relationship between the blending process to co-association and hence to the efficacy of the inhalation product.

In the future inhalation products in development could be clinically tested to relate the amount of co-association (measured with SPMS) to the clinical efficacy. While this might appear to be an expensive exercise in the short term, there could be longer term benefits to the manufacturer (in this case GSK) in terms of a possible extension of the product lifetime (*via* a new patent) and to the patient in terms of improved characterization of the inhalation product.

9.2 Future Developments in Instrument Design

9.2.1 Particle Sizing

The experiments described in this thesis show the detection and estimation of the level of co-association in a range of inhalation products. As mentioned in Chapter 8, it is likely that there would be more co-association in the larger particles. However, the sizes of the particles detected with both the AAMS (~ 0.2 to 1.0 μm) and the AToFMS instruments (~ 0.5 to 1.5 μm) were at the lower end of the respirable range (0.6 to 6 μm). This was at least partially due to the poor transmission of the larger particles through the aerodynamic lens. Hence, for further study of co-association, the particle sizing range would need to be extended so that the experiment is accessible to larger particles. The most likely way to do this would be through further development of the aerodynamic lens to enable transmission of the larger particles, a possible starting point for this would be with the use of modelling programs such as FLUENT[2].

The measure of aerodynamic diameter is very dependent on the shape of the particle as well as its size. Currently the calibration of the particle size measurement is typically performed using spherical latex beads. However, it is known that the particle shape is irregular for FP, SX and lactose from scanning electron microscope images shown in Section 4.2. It is likely that the calibration would be improved using materials that are closer in character and morphology to the drug compounds used in the inhalation products (for example *via* a series of FP particles micronized to a range of different sizes which had previously been checked with scanning electron microscopy).

The future of calibration for the SPMS experiment may follow the example of a recently reported method of calibration where the particle sizing and mass spectrometer were calibrated simultaneously using the same sample[3]. This was performed by producing polyethylene glycol (PEG) containing micro-particles, that gave a reproducible sample set used for calibration of particle size and an easily recognized mass spectrum that was used in calibration of the *m/z* axis.

9.2.2 Vaporization/Ionization

For both of the commercial instruments, the consistency of vaporization of particles was found to be limited. For the AAMS instrument this originated from particle bounce and for the AToFMS instrument from shot-to-shot variability of the laser beam.

For the AAMS instrument the ionization source design is such that the particle should vaporize as it hits the hotplate. However, it has been shown that a source of poor vaporization is particle bounce, *i.e.* rather than being vaporized, the particle instead bounces on the hotplate (even at high temperature >500 °C) in which case it may remain non-vaporized or only partially vaporized[4]. Further development of the hotplate in terms of the shape and texture may improve the consistency of vaporization especially of the larger particles[4].

For the AToFMS instrument a major source of inconsistent particle ablation/ionization is in the shot-to-shot variation in the laser beam. The Gaussian profile of the laser beam means that there is scope for each particle that crosses the laser beam to be exposed to a different amount of energy if it crosses the profile at a different point. To ensure that all particles are subjected to the same amount of laser energy, the laser energy profile can be flat topped[5,6]. This makes it more likely that each particle would be exposed to the same amount of laser energy hence the mass spectra would be more representative of the sample.

An additional problem of using laser desorption ionization is that if the analyte molecule does not absorb radiation at the laser wavelength then ionization will not occur. There are two possible solutions to this : (a) Treat the particles so that they can absorb radiation at the given wavelength of the laser or (b) Separate the ablation and ionization into two steps

It was shown previously that it is possible to coat the analyte particles with a material that is more able to absorb at the given wavelength[7]. For example this technique was employed to enhance the detection of small (10 to 20 nm) ammonium sulfate particles (which are difficult to ionize due to poor UV absorption at 266 nm) with laser ablation

aerosol mass spectrometry by coating them with naphthyl acetate which absorbs the energy from the laser and facilitates ionization. This would however be a complex solution and the consistency in application to inhalation products would need to be investigated.

Perhaps a more practical solution is to separate the ablation and ionization. This has been demonstrated successfully for AToFMS type instruments using a low power (typically infra-red) laser pulse for evaporation followed by a more intense pulse for ionization that use laser desorption as the ionization technique[8] although such instruments are not currently commercially available. The ablation and ionization techniques are separated in the AAMS instruments and these typically use a hotplate for vaporization and electron ionization, although once the particle is vaporized the use of a range of ionization techniques is possible[4, 9].

For successful application of single particle mass spectrometry (SPMS) to inhalation products the instrument should be capable of detecting the range of compound classes used as drugs and excipients. An important aspect of this is the method of ionization, which would ideally be compatible a wide a range of compounds. For example the active drugs in pMDI formulations are two structurally and chemically very different classes of compound *i.e.* FP and SX are a steroid and a beta-agonist respectively. The DPI formulations also contain lactose; a third structurally different compound.

There are a number of alternative ionization techniques, most of which are not currently commercially available; these include soft ionization techniques such as lithium attachment[10], chemical ionization[11] or synchrotron radiation[12, 13]. The mass spectra obtained using these techniques are typically dominated by the protonated $(M+H)^+$ or the lithiated molecule $(M + Li)^+$ and show little fragmentation. This would be an advantage in compound identification so long as all the compounds of interest had different molecular weights.

9.2.3 Mass Spectrometer

Although the amount of material in each particle is very small, the sensitivity of the mass spectrometers used were compatible with the detection and quantitation at this

level. For example, a homogeneous, spherical, 1 μm diameter particle of FP would have a mass of approximately 0.7 fg (approximately one million molecules) and both instruments were able to detect particles of 1 μm aerodynamic size that consisted of either pure FP, pure SX or a co-associated mixture of both.

In the future drug compounds will probably become more potent and lower levels of drug may thus be incorporated in the formulated product, hence improved sensitivity would be required. Also the formulated products of the future may be comprised of more complex mixtures, of three, four, or more, active drugs. Thus the mass spectrometer should still retain sensitivity to the drug compounds even if they are diluted in this type of complex mixture.

If the softer ionization techniques mentioned above were used, then it is likely that the mass spectra would show few fragments. In this case mass spectrometry techniques such as accurate mass measurement and tandem mass spectrometry (MS/MS) would be useful in maximising the amount of information available from the SPMS experiment. Currently accurate mass measurement are available using the Aerodyne AAMS instruments[14], however the signal-to-noise ratio in the mass spectrum is only good enough to give an average mass spectrum taken from several particles. Hence there is scope to develop this to be compatible with single particles with the aim of increasing the confidence of assignment of ions in the mass spectra obtained.

9.2.4 Quantitative Analysis

AToFMS is not generally considered a quantitative technique mainly because of the shot-to-shot variation in the laser as discussed in Chapter 3. However by identifying and counting the number of mixed particles identified a semi-quantitative estimate of the composition of single particles was made. An improvement in the quantitation would originate from better consistency in the ablation/ionization step.

The AAMS has been reported as a quantitative technique[9,10] and this is possible because the vaporization and ionization steps are separated. In this case the identification and classification of particles present are based on the fractional composition of each particle. For the work on inhalation products, an improvement in

the quantitation would originate from better consistency in the vaporization step and further development of positive matrix factorization (PMF) as a data analysis technique.

The quantitative measurement of the composition of each particle gives an additional piece of information when measuring co-association. Further development of the AAMS technique to be able to produce quantitative results with improved consistency, would give a real advantage over the AToFMS instrument for this application.

9.2.5 Automation

The automation of an analytical technique (and sample preparation) can give advantages in terms of the speed of the analysis and also in terms of consistency of the data produced. It is envisaged that ultimately SPMS would be used as a technique where high numbers of samples would need to be analyzed (for example in for quality control analysis in a pharmaceutical manufacturing environment), hence automation of the SPMS technique would be advantageous.

Many of the individual operations involved in inhalation product analysis have already been automated; for example it has been shown previously that automated actuation of inhaler devices can be performed[15]. Also, sampling of particles from the settling chamber for a given time is relatively easy to do. Hence most of the effort in automating the SPMS experiment for inhalation products would be centred on the sample conditioning apparatus and the automation of the flow of air to sweep particles from the inhalation product into the settling chamber.

9.3 References

(1)   FDA PAT initiative (2004).
        http://www.fda.gov/cder/OPS/PAT.htm, (Accessed 1 Sept 2008).

(2)   Transmission efficiency of an aerodynamic focussing lens system: comparison
        of model calculations and laboratory measurement for the aerodyne aerosol
        mass spectrometer. P.S. Liu, R. Deng, K. A. Smith, L. R. Williams, J. T. Jayne,

M. Canagaratna, K. Moore, T.B. Onasch, D.R. Worsnop and T. Deshler. *Aerosol Sci. and Tech.* <u>41</u>, 721-733 (2007).

(3)   Online aerosol mass spectrometry of single micrometer-sized particles containing poly(ethylene glycol). M.J. Bogan, E. Patton, A. Srivastave, S. Martin, D.P. Fergenson, P.T. Steele, H.J. Tobias, E.E. Gard and M. Frank. *Rapid Commun. Mass Spectrom.* <u>21</u>, (7), 1214-1220 (2007).

(4)   Chemical and Physical Characterization of Aerosols with the Aerodyne Aerosol Mass Spectrometer: Laboratory and Field Applications. D.R. Worsnop, J.T. Jayne, M. Canagaratna, T. Onasch, L.R. Williams, M. Northway A. Trimborn, J. Slowik, P. Davidovits, P. DeCarlo, J-L. Jimenez and Q. Zhang. *Lecture at 54th ASMS conference Seattle, US June 2006.*

(5)   Improvements in ion signal reproducibility obtained using a homogeneous laser beam for on-line laser desorption/ionization of single particles. R. Wenzel and K. Prather. *Rapid Commun. Mass Spectrom.* <u>18</u>, 1525-1533, (2004).

(6)   Desorption/ionization fluence thresholds and improved mass spectral consistency measured using flattop laser profile in the bioaerosol mass spectrometry of single bacillus endospores. P.T. Steele, A. Srinvastava, M. Pitesky, D. Fergenson, H. Tobais, E.E. Gard and M. Frank. *Anal. Chem.* <u>77</u>, 7448-7454, (2005).

(7)   Enhancing the detection of sulphate particles for laser ablation aerosol mass spectrometry. D.B. Kane and M.V. Johnson. *Anal. Chem.* <u>73</u>, 5365-5369, (2001).

(8)   Coupling two-step laser desorption/ionization with aerosol time-of-flight mass spectrometry for the analysis of individual organic particles. B.D. Morrical, D.P. Fergenson and K.A. Prather. *J Am. Soc. Mass Spectrom.* <u>9</u>, 1068-1073, (1998).

(9)   Development of an aerosol mass spectrometer for size and composition analysis of submicron particles. J.T. Jayne, D.C. Leard, X. Zhang, P. Davidovitis, K. Smith, C.E. Kolb and D. Worsnop. *Aerosol Sci. and Technol.* <u>33</u>, 49-70, (2000).

(10)   Chemical and microphysical characterization of ambient aerosols with the Aerodyne aerosol mass spectrometer. M.R. Canagaratna, J.T. Jayne, J-L. Jimenez, M.R. Afarra, Q. Zhang, F. Drenwick, H. Coe, A. Middlebrook, A. Delia, L.R. Williams, A.M. Trimbourne, M.J. Northway, P.F. DeCarlo, C.E. Kolb, P. Davidovits and D.R. Worsnop. *Mass Spectrom. Rev.* <u>26</u>, 185-222, (2007).

(11)   Transportable real-time single particle ion trap mass spectrometer. W. Harris, P.T. Reilly, W. Whitten and J. Ramsey. *Rev. Sci. Instruments.* <u>76</u>, 064102, (2005).

(12)   Synchrotron radiation based time-of-flight mass spectrometer for organic constituents. E.R. Mysak, K.R. Wilson, M. Jimmenez-Cruz, M. Ahmed and T. Baer. *Anal. Chem.* <u>77</u>, *5953-5960, (2005).*

(13)   Coupling a versatile aerosol apparatus to a synchrotron: Vacuum ultraviolet light scattering, photoelectric imaging and fragment free mass spectrometry. J. Shu, K.R. Wilson, M. Ahmed and S.R. Leone. *Rev. Sci. Instruments.* <u>77</u>, *043106, (2006).*

(14)   A field-deployable high-resolution time-of-flight aerosol mass spectrometer. P.F. DeCarlo, J.R. Kimmel, A. Trimbourn, M. Northway, J.T. Jayne, A.C. Aiken, M. Gonin, K. Fuhrer, T. Hovarth, K.S. Docerty, D.R. Worsnop and J-L.Jimenez. *Anal. Chem.* <u>74</u>, *8281-8289, (2006).*

(15)   Advances in analytical sample preparation. R. Cripwell. Joint Pharmaceutical Analysis Group meeting (Faster and Smarter Analysis), School of Pharmacy London 3 & 4 April 2008.

Appendices

Appendices are linked to individual Chapters *e.g.* Appendix A3 refers to Chapter 3 *etc*.

Section 1 – Supplementary Data

A3 Appendices to Chapter 3

A3.1 LC/MS of FP and SX Including Accurate Mass Measurement

The electrospray ionization (ESI)[1] mass spectra of FP and SX were acquired to aid interpretation of the SPMS data. These data were acquired using a time-of-flight (ToF) instrument (Agilent, San Jose, CA, US). Many of the ions found in the mass spectra for FP and SX were found to be common to their ESI, EI and laser desorption mass spectra. The advantage of acquiring mass spectra using the Agilent time-of-flight instrument was that accurate mass measurements could be made and used as an aid to structural elucidation. The LC/MS conditions given in Tables A3.1 and A3.2 were used for acquiring ESI spectra and UV spectra of FP and SX.

Parameter	Value
Flow rate	1.4 mL min^{-1}
Column	Zorbax C18, 2.1 x 30 mm (3 µm particle size)
Injection volume	10 µL
Oven temperature	50 °C
Mobile Phase A	Water/ 0.1% v/v formic acid
Mobile phase B	Methanol/ 0.1 % v/v formic acid
Gradient	40 to 95% B in 2 minutes, hold at 95% for 2 min then re-equilibrate at 40% B for 1 minute.
Detector wavelength	190 to 400 nm (UV spectra collected *via* Diode array detector on HPLC)

Table A3.1. HPLC conditions for LC/MS experiment to analyze FP and SX.

Parameter	Value
Ion polarity	Positive
Capillary voltage	4000 v
Fragmentor voltage	300 v
Drying gas flow	7 L min^{-1}
Drying gas temp	300 °C
Nebuliser gas pressure	15 psig
m/z range	100 to 1000

Table A3.2. Electrospray mass spectrometry conditions for LC/MS experiment to analyze FP and SX.

A3.1.1 LC/MS analysis of fluticasone propionate (FP)

The ESI mass spectrum of FP is shown in Figure A3.1. The instrument was calibrated for accurate mass measurements which are shown on the mass spectrum. A list of accurately mass measured ions from this mass spectrum is given in Table 3.3.

Figure A3.1. The ESI mass spectrum of FP acquired using LC/MS using a ToF mass spectrometer. The ions are annotated with the accurate mass measurements which are summarized in Table A3.3 together with an explanation based on the suggested empirical formulae. Note that fragmentation was induced by in-source collision induced dissociation.

Calculated mass based on empirical formula	Found	Mass Accuracy (mDa)	Empirical formula	Explanation
523.17432	523.17373	0.08	$C_{25} H_{31} F_3 O_5 S$ Na	$(M+Na)^+$
501.19238	501.19190	0.2	$C_{25} H_{32} F_3 O_5 S$	$(M+H)^+$
481.18615	481.18587	0.4	$C_{25} H_{31} F_2 O_5 S$	Ion (a)
333.16671	333.16610	0.04	$C_{20} H_{23} F_2 O_2$	Ion (b)
313.16048	313.16040	0.6	$C_{20} H_{22} F O_2$	Ion (c)
295.14991	295.15156	2.3	$C_{20} H_{20} F O$	Ion (d)
293.15425	293.15460	0.9	$C_{20} H_{21} O_2$	Ion (e)
265.15934	265.15946	0.8	$C_{19} H_{21} O$	Ion (f)
275.14368	275.14379	0.7	$C_{20} H_{19} O$	Ion (g)
179.08841	179.08767	0.1	$C_8 H_{13} F_2 O_2$	Ion (h)
121.06652	121.06626	0.3	$C_5 H_{10} F O_2$	Ion (i)

Table A3.3 ESI accurate mass data for FP (taken from mass spectrum shown in Figure A3.1). Structures for the ions (a) to (i) are shown in Figure A3.2.

The suggested fragmentation pattern based on accurate mass determinations for the ions shown in the ESI mass spectrum of FP is shown in Figure A3.2. This shows that the protonated molecule at *m/z* 501 loses of HF probably by trans-elimination of the fluoride (F⁻) at position 6 on the steroid B ring. The remainder of the ESI mass spectrum shows fragmentation consisting mainly of losses of water or HF.

Figure A3.2. *Suggested fragmentation pattern for FP based on accurate mass measurements based on electrospray ionization. This is based on accurate mass measurements for ions (a) to (i) listed in Table A3.3.*

A3.1.2 LC/MS mass spectrometry analysis of salmeterol xinofoate (SX)

The ESI mass spectrum of SX is shown in Figure A3.3. Prior to the acquisition of this data, the instrument (Agilent ToF) was calibrated for accurate mass measurements which are shown on the mass spectrum and summarized in Table A3.4.
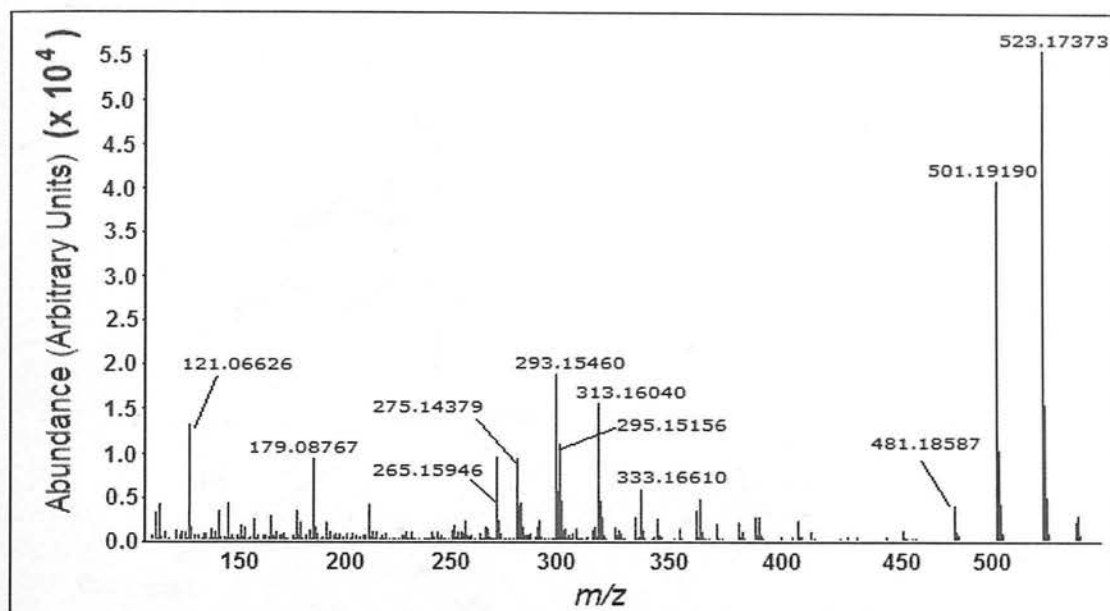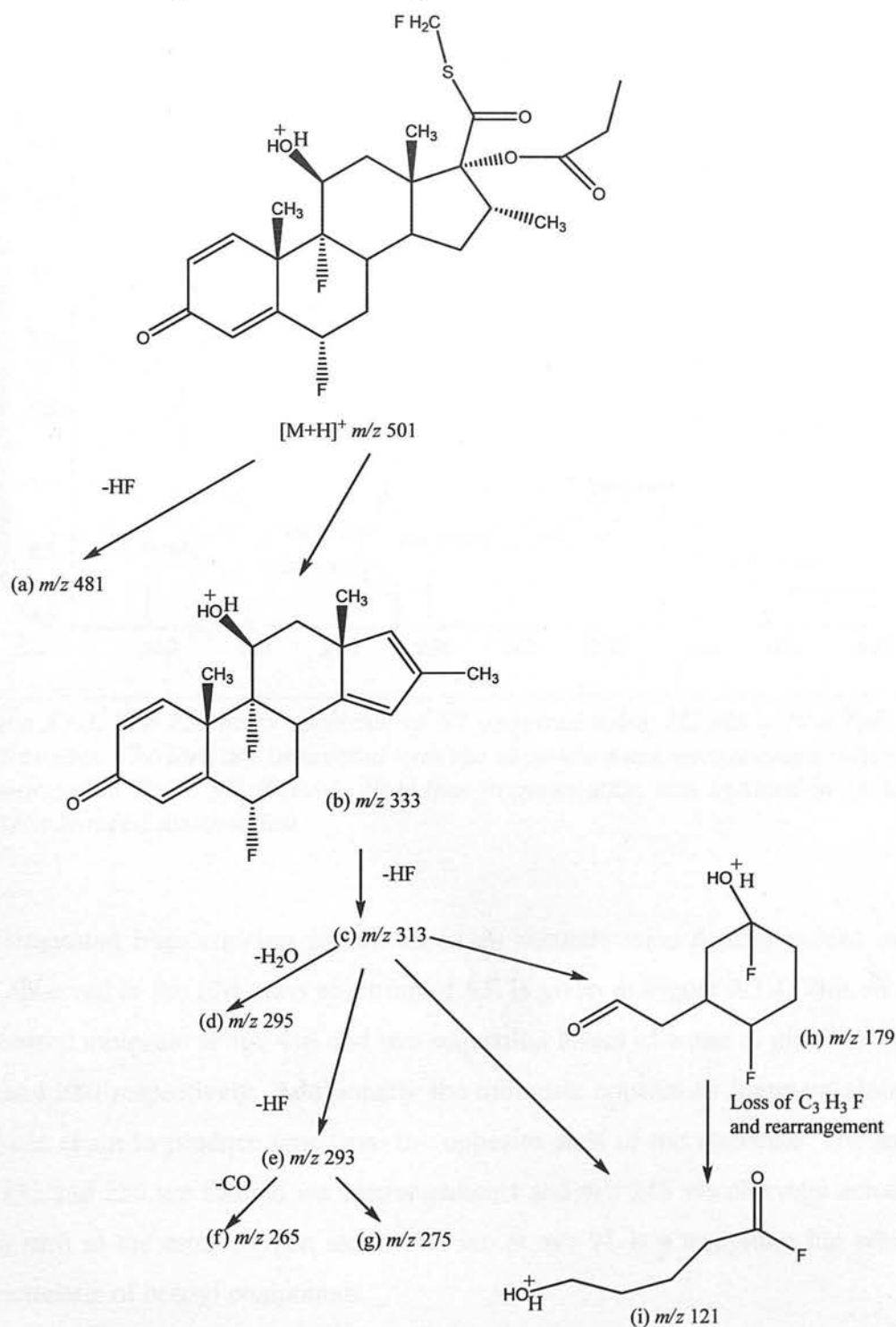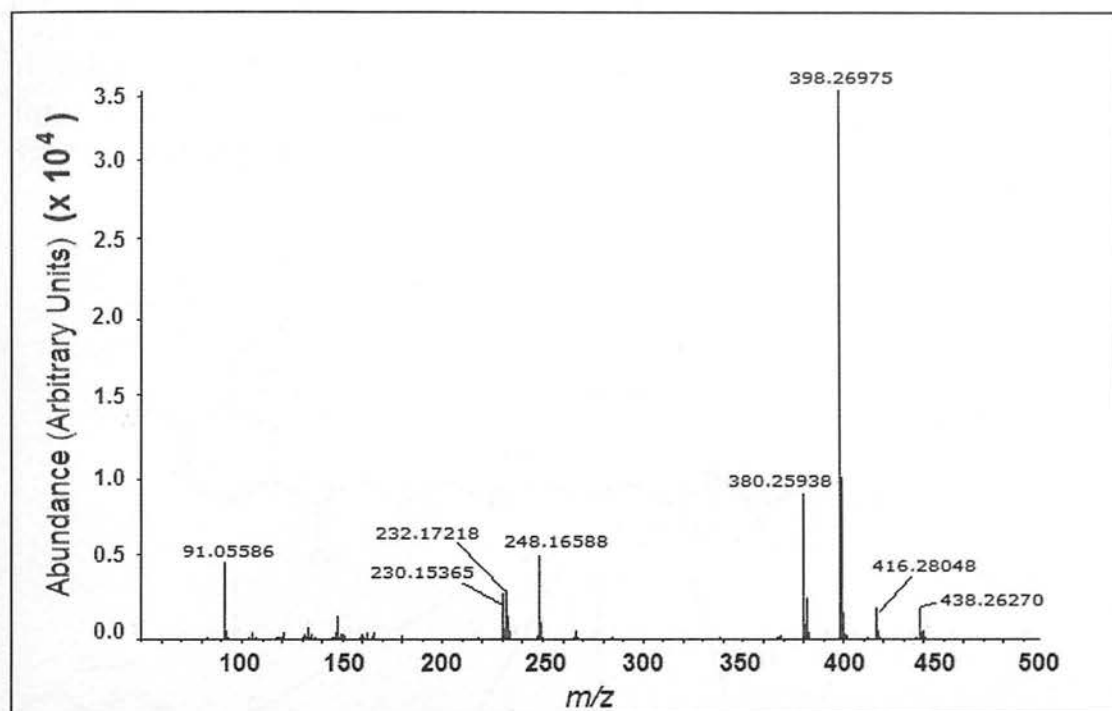

Figure A3.3. *The ESI mass spectrum of SX acquired using LC/MS with a ToF-mass spectrometer. The ions are annotated with the accurate mass measurements which are summarized in Table 3.7 (below). Note that fragmentation was induced by in-source collision induced dissociation.*

The suggested fragmentation pattern based on accurate mass determinations for the ions observed in the ESI mass spectrum of SX is given in Figure A3.4. This shows a protonated molecule at *m/z* 416 and two sequential losses of water to give ions at *m/z* 398 and 380 respectively. Additionally the molecule appears to fragment along the aliphatic chain to produce ions from the opposite ends of the molecule. The ions at *m/z* 232 and 230 are formed *via* rearrangements and *m/z* 248 *via* cleavage across the chain next to the ester oxygen atom. The ion at *m/z* 91 is a tropylium ion which is characteristic of benzyl compounds.

166

Calculated	Found	Difference (mDa)	Formula from mass measurement	Explanation (Shown in Fig. A3.4)
438.26219	438.26270	0.5	$C_{25} H_{37} N O_4 Na$	$(M+Na)^+$
416.28025	416.28048	0.2	$C_{25} H_{38} N O_4$	(a)
398.26968	398.26975	0.07	$C_{25} H_{36} N O_3$	(d)
380.25911	380.25938	0.3	$C_{25} H_{34} N O_2$	(e)
248.16515	248.16588	0.7	$C_{15} H_{22} N O_2$	(f)
232.17024	232.17218	1.9	$C_{15} H_{22} N O$	(b)
230.15458	230.15365	0.9	$C_{15} H_{20} N O$	(c)
91.05481	91.05586	1.0	$C_7 H_7$	(g)

Table A3.4. *ESI accurate mass data for SX. Structures for the ions (a) to (g) are shown in Figure A3.4.*
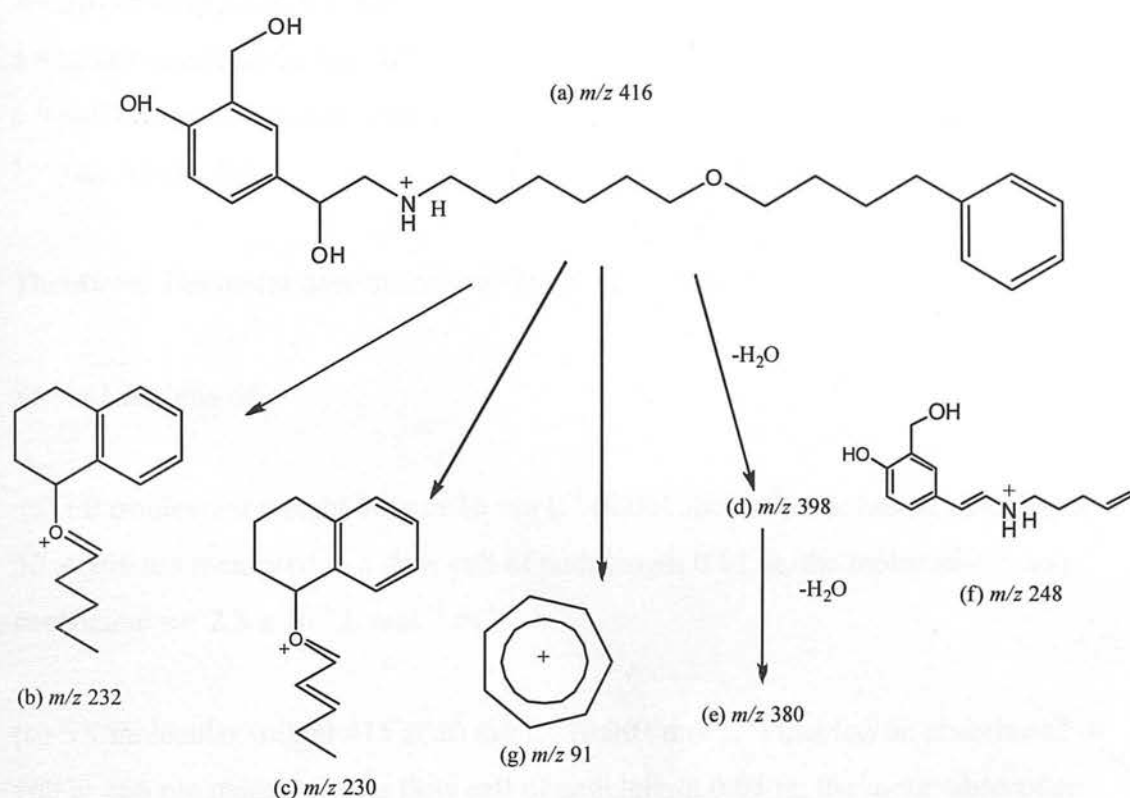

Figure A3.4. *Suggested fragmentation pattern for salmeterol xinofoate based on accurate mass measurements taken from the electrospray ionization mass spectrum shown in Figure A3.3.*

Appendix A3.2 Molar Absorption of FP and SX

The molar absorptions[2] of the solutions of FP and SX were calculated from an HPLC
experiment (Conditions given in Appendix A3.1) using Equation A3.1. The UV
spectra were acquired for FP and SX solutions (10 mg L^{-1}). The absorbance for each
compound was compared at 266 nm (the wavelength of the ablation laser in the
AToFMS instrument). The path length of the UV cell in the Agilent 1100 UV diode
array detector was 0.1 cm.

$$A = \varepsilon cl \qquad \textbf{(Equation A3.1)}$$

A = absorbance (arbitrary units) taken at 266 nm.
ε = molar absorption coefficient (L mol^{-1} m^{-1})
c = solution concentration (mol L^{-1})
l = path length (m)

Therefore; The molar absorption coefficient ε = A/cl

So for solutions of:

(a) FP (molecular weight 500) at 10 mg L^{-1} (0.002 mol L^{-1}) that has an absorbance of
50 at 266 nm measured in a flow cell of path length 0.01 m, the molar absorption
coefficient $\varepsilon = 2.5 \times 10^6$ L mol^{-1} m^{-1}.

(b) SX molecular weight 415 at 10 mg L^{-1} (0.003 mol L^{-1}) that has an absorbance of
160 at 266 nm measured in a flow cell of path length 0.01 m, the molar absorption
coefficient $\varepsilon = 5.3 \times 10^6$ L mol^{-1} m^{-1}.

Therefore at 266 nm the absorptivity of SX is approximately double that of FP.

Appendix A3.3 Principal component analysis

Principal component analysis is a way of identifying patterns in such a way to highlight similarities and differences between data sets[3]. The principle of using principal component analysis is illustrated with an arbitrary dataset of weight against height shown in Table A3.5.

Sample identifier	Height (m)	Weight (kg)
1	1.3	49
2	1.25	46
3	1.6	53
4	1.7	52
5	1.8	54
6	1.26	47
7	1.4	50
8	1.5	51
9	1.3	48
10	1.1	45
11	1.1	46
12	1.7	52
13	1.8	54
14	1.4	49
15	1.5	51
16	1.6	51
17	1.7	55
18	1.8	54
19	1.4	50
20	1.3	48

Table.3.5. An arbitrary data set (weight v height) used to illustrate principal component analysis.

The data set is plotted in a graph of weight against height as shown in Figure A3.6. Before principal component analysis is performed the data is conditioned so that it becomes more meaningful. For example variables may have substantially different numerical ranges. In the graph shown in Figure A3.6 all of the components appear in one corner of the graph and it is apparent that the scale in which the data is viewed needs to be adjusted.
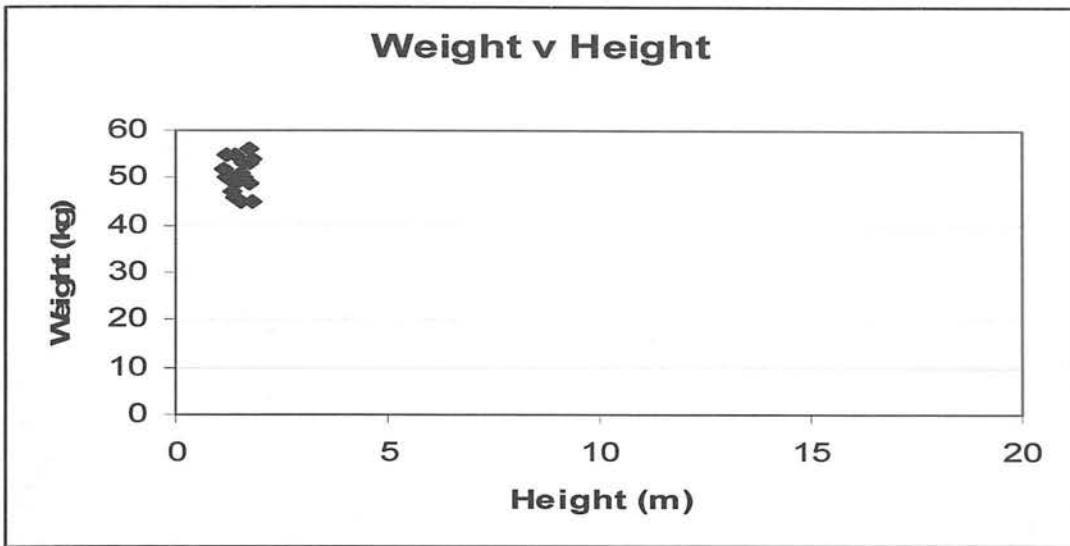
Figure A3.6. Graph using arbitrary dataset of weight and height (See Table 3.5).

In order to give both variables equal rating in the data analysis they are standardized or 'scaled' and this means that the length of each co-ordinate axis in the variable space is regulated according to pre-determined criteria.. Figure A3.7 shows the same graph after scaling both the x and y axis. This is much easier to read visually and if there were an untypical observation it would be much easier to see.
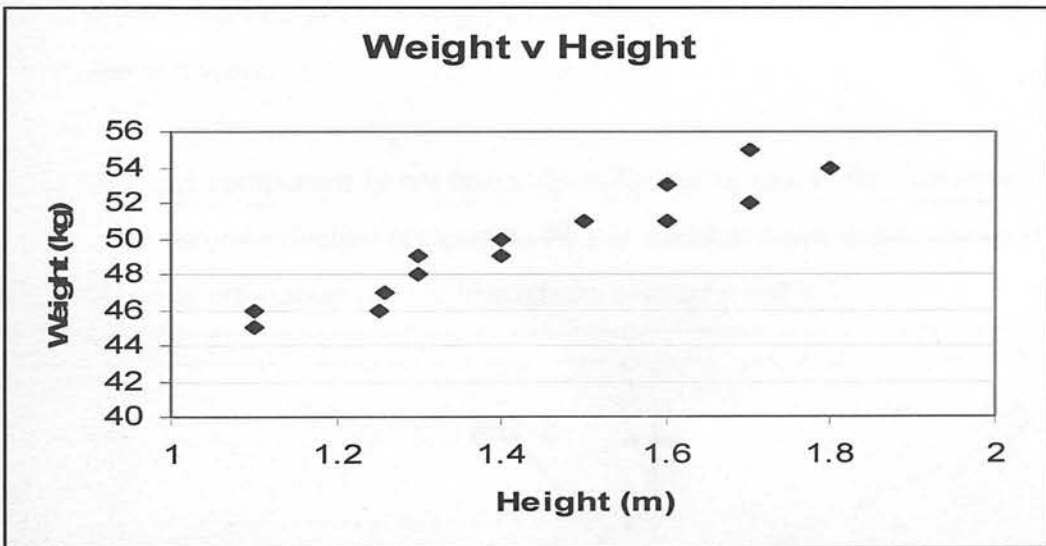
Figure A3.7. Graph using arbitrary dataset of weight and height (See Table 3.5)) with adjusted scale.

Further conditioning or pre-processing of the data is performed by mean centring. This is done by subtracting the mean value from each of the data points to give a data set centred on 0 as shown in Figure A3.8.
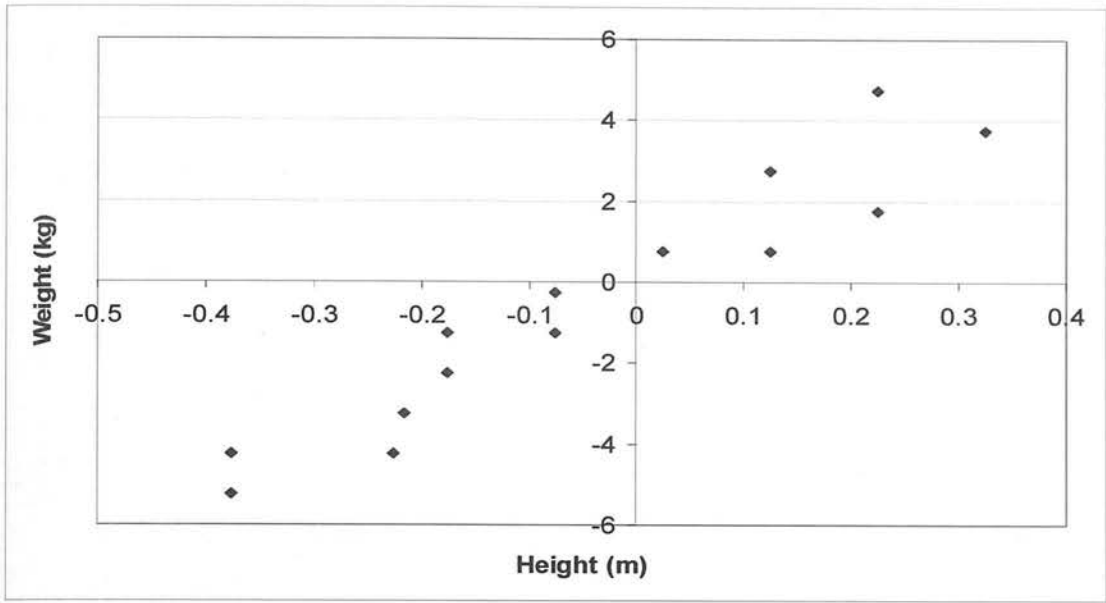
Figure A3.8. Mean centred data (See Table 3.5).

After the data has been scaled and mean centred, the first principal component is calculated. This component is the line that best approximates the data by a least squares fit. This line goes through the average point (0) as shown in Figure A3.9 and shows the maximum variance in the data set (PC1). Each observation is now projected on this line in order to get a coordinate value. which. This new co-ordinate is known as a score.

One principal component is not normally sufficient to model the variation of a data set. So the second principal component PC2 is calculated and this is shown in Figure A3.9 by a line orthogonal to PC1 through the average point.
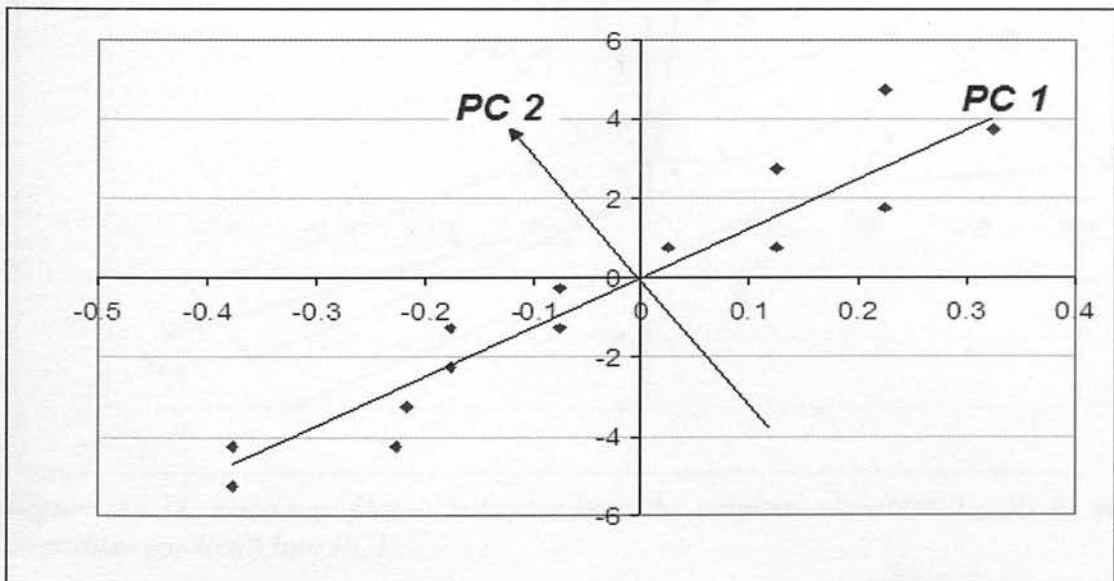
Figure A3.9. The first two principal components (See Table 3.5).

The first two principal components define a plane from which the data set can be visualized as shown in Figure A3.10. The co-ordinate values of the observations on this plane are called scores and the plotting of this type of projection is a scores plot.
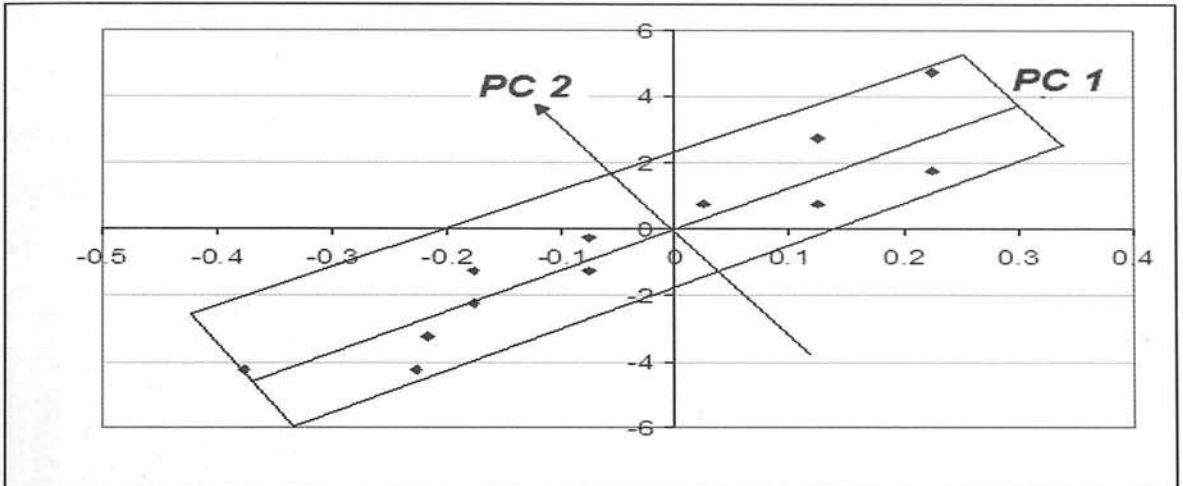
Figure A3.10. *First two principal components define a plane from which the data set (See Table 3.5) can be visualized.*

Geometrically the principle component loadings express the orientation of the model plane. The direction of PC1 in relation to the original variables is given by the cosine of the angles $\alpha 1$, $\alpha 2$ and $\alpha 3$. These values indicate how the original variables x1, x2 and x3 load (*i.e* contribute) to PC1 – hence they are called the loadings. A second set of loading coefficients expresses the direction of PC2.
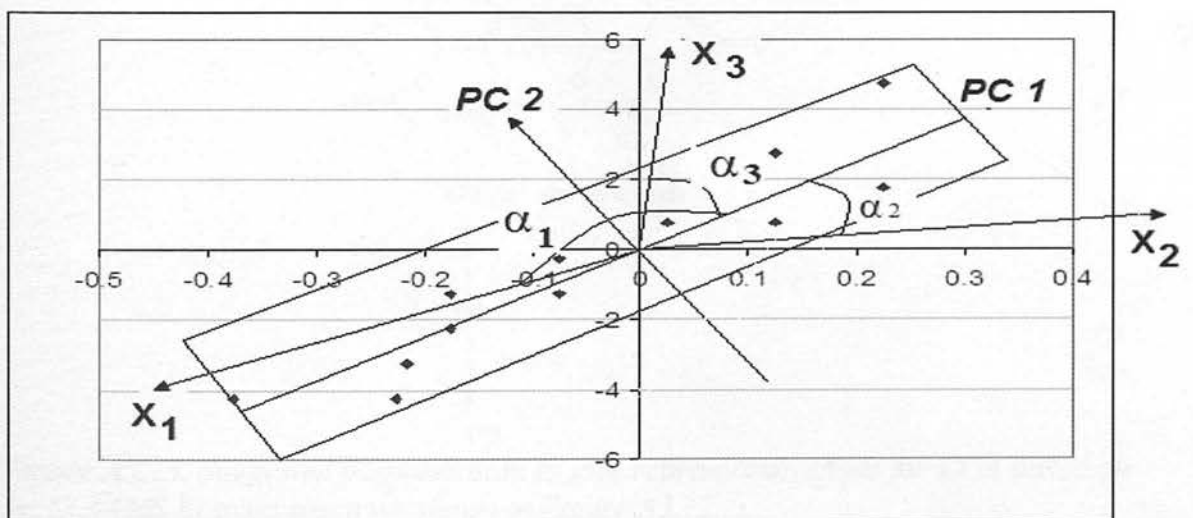
Figure A3.11. *Loadings plot – indicates how the original variables X_1, X_2 X_3 etc contribute (or load) into PC1.*

Appendix A3.4 Q-AAMS Spectra for Excipients

The average Q-AAMS EI mass spectrum for COA is shown in Figure A3.12. Unique ions for COA are shown at *m/z* 169 and at *m/z* 109; The ion at m/z 169 corresponds to the loss of seven moieties of acetic acid. The final loss of acetic acid is shown in Figure A3.13. The major fragmentation products are summarized in Figure A3.13. Although a major ion is observed in the mass spectrum of COA at *m/z* 43, this is not unique as it is also observed in the mass spectra of both SX and lactose. For COA and lactose *m/z* 43 is likely to be due to acetate, for SX it may be due to an alternative ion with the formula C_2H_5N.
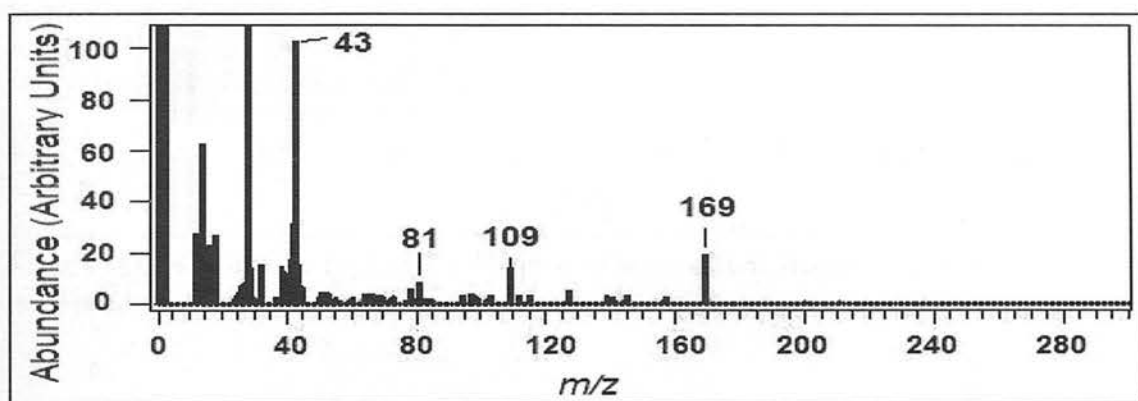
Figure A3.12. Average Q-AAMS spectrum of cellobiose octaacetate (COA), showing potential marker ions.
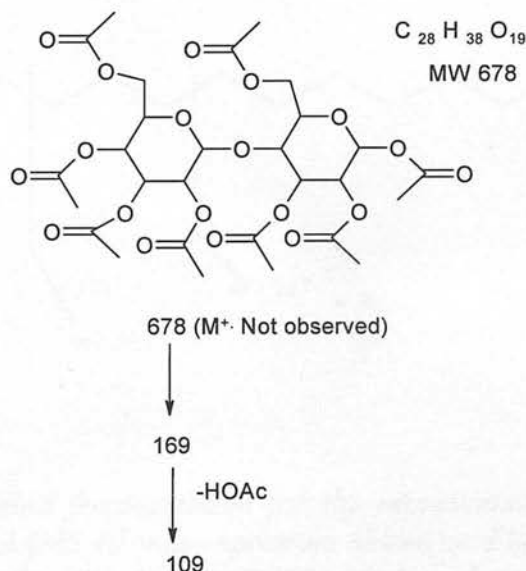
Figure A3.13. Suggested fragmentation to give representative ions for COA based on the Q-AAMS EI mass spectrum shown in Figure A3.12.

The average Q-AAMS EI mass spectrum for magnesium stearate is shown in Figure A3.7. No intact molecular ion is observed, but the unique fragmentation pattern for

this molecule is clearly visible and the major ions are shown in Figure A3.8. Also shown in the mass spectrum is an elemental ion at *m/z* 24 due to the magnesium ion (Mg^+).
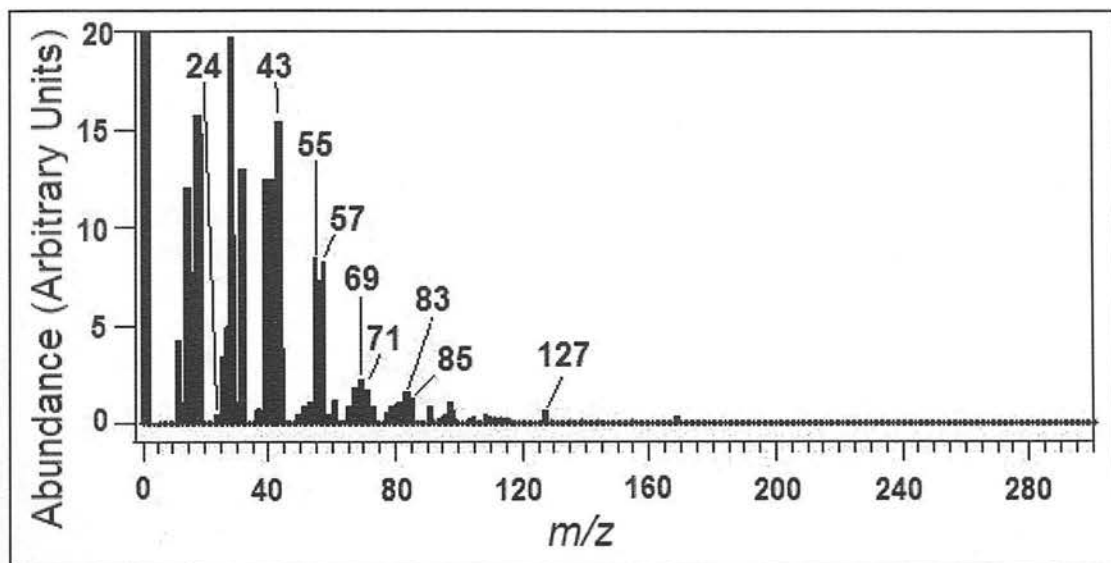
Figure A3.14. *Average Q-AAMS spectrum of magnesium stearate, showing potential marker ions.*
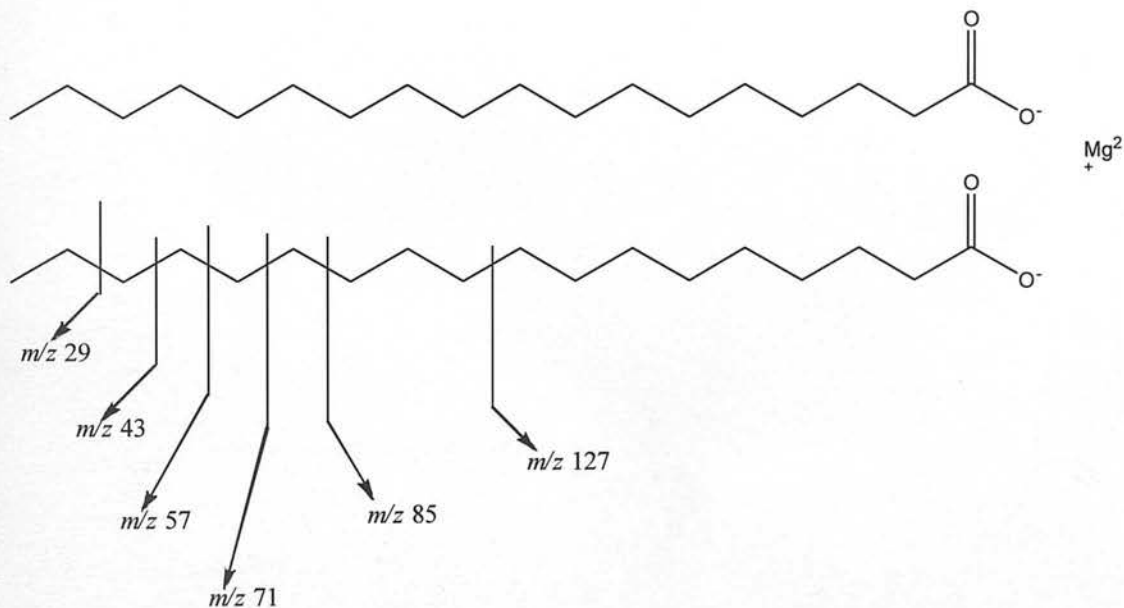
Figure A3.15. *Suggested fragmentation for the representative ions of magnesium stearate based on Q-AAMS EI mass spectrum shown in Figure A3.14. Magnesium stearate has the formula $[CH_3 [CH_2]_{16} COO]_2^- Mg^{2+}$ and most of the fragmentation observed involves stearic acid; the ion at m/z 24 is consistent with magnesium (Mg^+).*

A3.5 References

(1)   A global view of LC/MS. R. Willoughby, E. Sheenan and S. Mitrovich. First edition (1998). Global View Publishing. ISBN 0966081307.

(2)   The elements of physical chemistry. P. Atkins. Third Edition (2004). Oxford University Press. ISBN 019879290.

(3)   Multi- and Megavariate Data Analysis, Principles and Applications. L Eriksson, E. Johansson, N. Kettaneh-Wold and S. Wold. Umetrics, Umea, Sweden, (2001). ISBN 91-973730-1-X.

A4 Appendices to Chapter 4

A4.1 Samples Used as Examples in Chapter 4

FP   Pure drug material

SX   Pure drug material

MDI_1   pMDI formulation: FP/SX 250/25

DPI_3   DPI formulation: FP/SX 250/50

A full list of samples is given in Appendix A5.1.

A4.2 Average AToFMS Spectra of Pure Drug Compounds
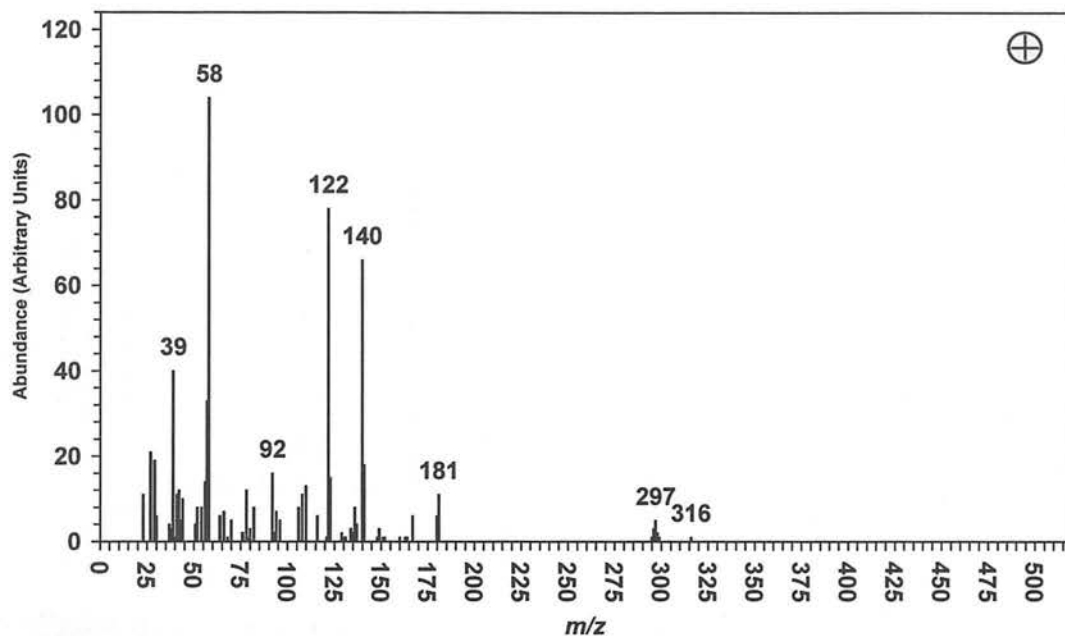
Figure A4.1. *Average positive ion mass spectrum for pure FP particles at fixed laser energy (0.2 mJ). Particles were introduced via an aerodynamic lens for the acquisition of this data.*
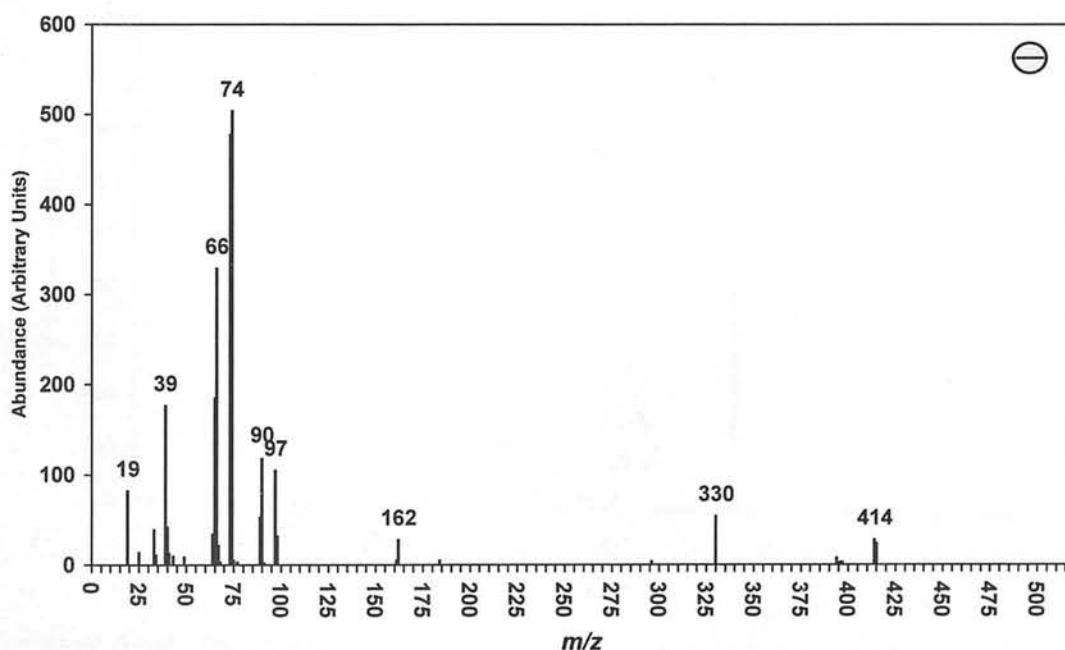
Figure A4.2. *Average negative ion mass spectrum for pure FP particles at fixed laser energy (0.2 mJ). Particles were introduced via an aerodynamic lens for the acquisition of this data.*
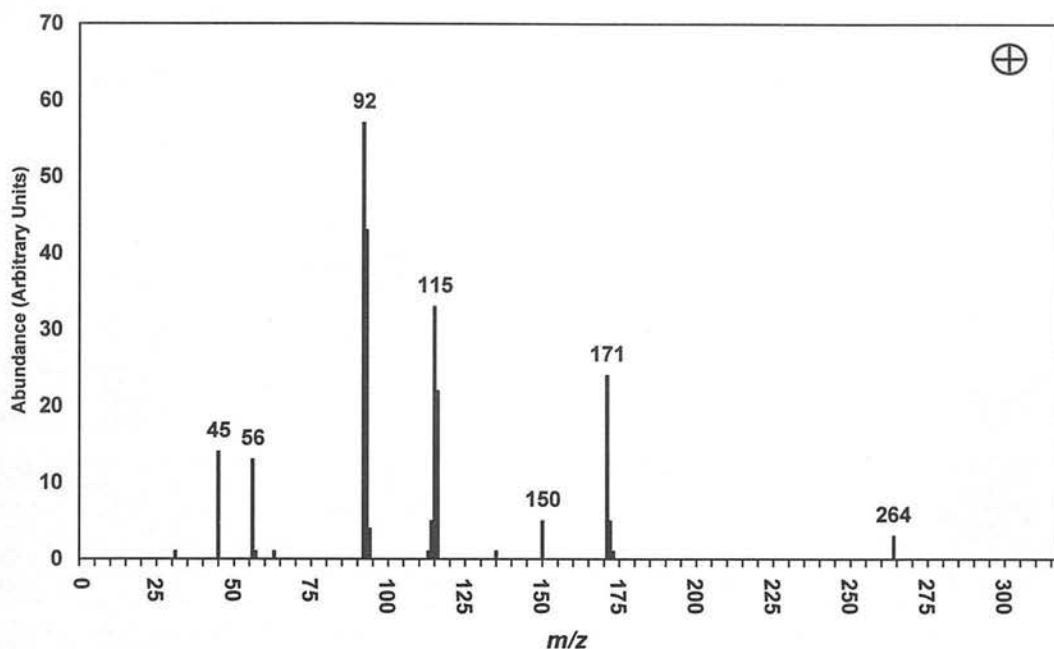
Figure A4.3. *Average positive ion mass spectrum for pure SX particles at fixed laser energy (0.2 mJ). Particles were introduced via an aerodynamic lens for the acquisition of this data.*
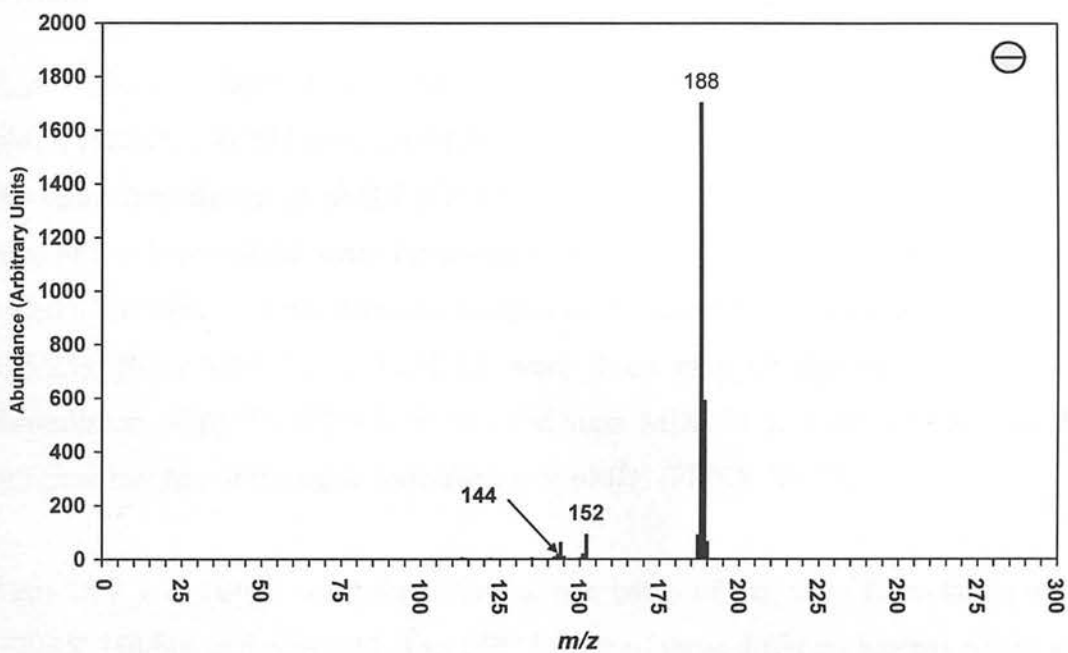
Figure A4.4. *Average negative ion mass spectrum for pure SX particles at fixed laser energy (0.2 mJ). Particles were introduced via an aerodynamic lens for the acquisition of this data.*

A5 Appendices to Chapter 5

A5.1 List of Samples for AToFMS Experiments

| MDI AToFMS Identifier	FP/SX formulation	Batch/id		DPI AToFMS Identifier	FP/SX formulation	Batch/id
MDI_1	250/25	Lot031012991		DPI_1	250/50.	R252654
MDI_2	250/25	SE004/97F		DPI_2	250/50.	R252237
MDI_3	250/25	AX7102/82.		DPI_3	250/50.	R252265.
MDI_4	250/25.	AX7102/82.		DPI_4	250/50.	R252265.
MDI_5	250/25.	AX7102/82.		DPI_5	250/50.	R252265.
MDI_6	125/25.	002/78		DPI_6	500/50.	R252400
MDI_7	125/25	AX7100/60		DPI_7	500/50.	R252323
MDI_8	125/25.	1/18, 04/97F.		DPI_8	500/50.	R252238
MDI_9	125/25.	1/18, 04/97F.		DPI_9	500/50	R252238
MDI_10	125/25.	1/18, 04/97F.		DPI_10	500/50	R252238
				DPI_11	500/50	R252400
MDI_11	50/25	002/78				
MDI_12	50/25	AX7099/32		SERE_1		LOT R262956
MDI_13	50/25	05/97F		Flovent_1		F100
MDI_14	50/25.	05/97F		FP_2	FP	
MDI_15	50/25.	05/97F		SX_4	SX	

Table A5.1. Samples used in AToFMS experiments, showing formulation and batch identifier.

Runs MDI_1 to MDI_3 were three runs of one batch of the same formulation of pMDI (FP/SX 250/25) and runs MDI_3 to MDI_5 were of three different batches of the same formulation of pMDI (FP/SX 250/25). Runs MDI_6 to MDI_8 were three runs of one batch of the same formulation of pMDI (FP/SX 125/25) and runs MDI_8 to MDI_10 were of three different batches of the same formulation of pMDI (FP/SX 125/25). Runs MDI_11 to MDI_13 were three runs of one batch of the same formulation of pMDI (FP/SX 50/25) and runs MDI_13 to MDI_15 were of three different batches of the same formulation of pMDI (FP/SX 50/25).

Runs DPI_1 to DPI_3 were three runs of one batch of the same formulation of DPI (FP/SX 250/50) and runs DPI_3 to DPI_5 were of three different batches of the same formulation of DPI (FP/SX 250/50). Runs DPI_6 to DPI 9 were three runs of one batch of the same formulation of DPI (FP/SX 500/50) and runs DPI_9 to DPI_11) were of three different batches of the same formulation of DPI (FP/SX 500/50).

A5.2 The Classification of Particles by Size

The particles were classified by particle size range; the ranges used for this were (a) > 1600 nm, (b) 1200 to 1600 nm (c) 1200 to 800 nm (d) 400 to 800 nm and (e) < 400 nm. The numbers of particles in each category were counted and the results for the pMDIs are shown in Table A5.2 and for the DPIs in Table A5.3.

Type	Formulation	File	Particle size range				
			> 1600 nm	1200 to 1600 nm	800 to 1200 nm	400 to 800 nm	< 400 nm
pMDI	FP/SX, 250/25	MDI_1	2.0	6.9	44.6	36.6	9.9
	FP/SX, 250/25	MDI_2	1.0	21.2	36.5	31.7	9.6
	FP/SX, 250/25	MDI_3	5.0	15.0	43.0	33.0	4.0
	FP/SX, 250/25	MDI_4	1.0	13.7	49.0	25.5	10.8
	FP/SX, 250/25	MDI_5	2.0	13.9	47.5	28.7	7.9
pMDI	FP/SX, 125/25	MDI_6	2.9	15.4	41.3	29.8	10.6
	FP/SX, 125/25	MDI_7	3.0	6.0	47.0	32.0	12.0
	FP/SX, 125/25	MDI_8	3.0	9.0	40.0	36.0	12.0
	FP/SX, 125/25	MDI_9	2.0	12.7	37.3	26.5	21.6
	FP/SX, 125/25	MDI_10	2.0	5.9	39.6	38.6	13.9
pMDI	FP/SX, 50/25	MDI_11	0.0	7.9	30.7	52.5	8.9
	FP/SX, 50/25	MDI_12	1.8	16.5	33.0	37.6	11.0
	FP/SX, 50/25	MDI_13	2.0	7.0	26.0	52.0	13.0
	FP/SX, 50/25	MDI_14	1.9	7.5	28.3	46.2	16.0
	FP/SX, 50/25	MDI_15	2.9	4.9	27.2	45.6	19.4

Table A5.2. *Particle size distribution for pMDIs. The % number of particles in each size range is shown.*

Type	Formulation	File	Particle size range				
			> 1600 nm	1200 to 1600 nm	800 to 1200 nm	400 to 800 nm	< 400 nm
DPI	FP/SX 250/50	DPI_1	16.2	32.4	47.1	4.4	0.0
	FP/SX 250/50	DPI_2	14.0	42.1	31.6	10.5	1.8
	FP/SX 250/50	DPI_3	13.4	43.4	37.3	3.0	3.0
	FP/SX 250/50	DPI_4	20.3	31.6	34.2	10.1	3.8
	FP/SX 250/50	DPI_5	19.2	27.7	43.8	9.2	0.0
DPI	FP/SX 500/50	DPI_7	9.8	30.4	47.1	10.8	2.0
	FP/SX 500/50	DPI_8	12.8	35.8	38.5	11.0	1.8
	FP/SX 500/50	DPI_9	16.0	32.0	39.0	10.0	3.0
	FP/SX 500/50	DPI_10	15.5	31.1	39.8	11.7	1.9
	FP/SX 500/50	DPI_11	15.7	28.4	43.1	10.8	2.0

Table A5.3. *Particle size distribution for DPIs. The % number of particles in each size range is shown.*

The average particle size distributions are shown in Figure A5.1 for the pMDIs and in Figure A5.2 for the DPIs. Figure A5.1 shows that most of the particles (approximately 80 %) from the pMDI samples were in the 400 to 1200 nm range.

Figure A5.2 shows that most of the particles (approximately 80 %) for the DPI samples were in the range between 800 and 1600 nm.
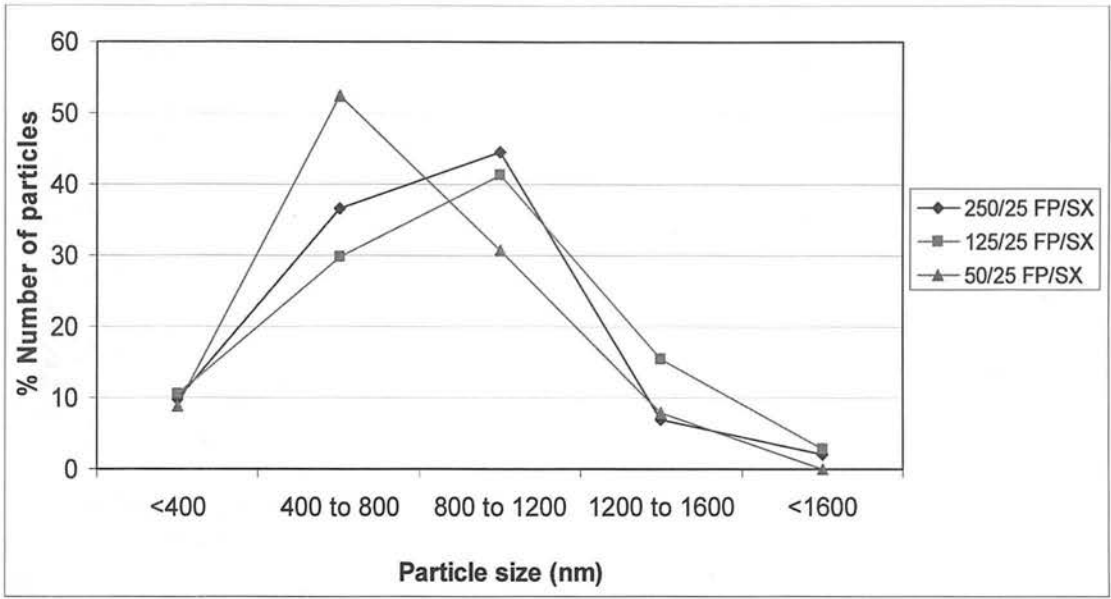
Figure A5.1. *Particle size distributions for pMDI aerosols. Example data shown for samples of FP/SX 250/25 (file MDI_1), FP/SX 125/25 (file MDI_6) and FP/SX 50/25 (file MDI_11).*
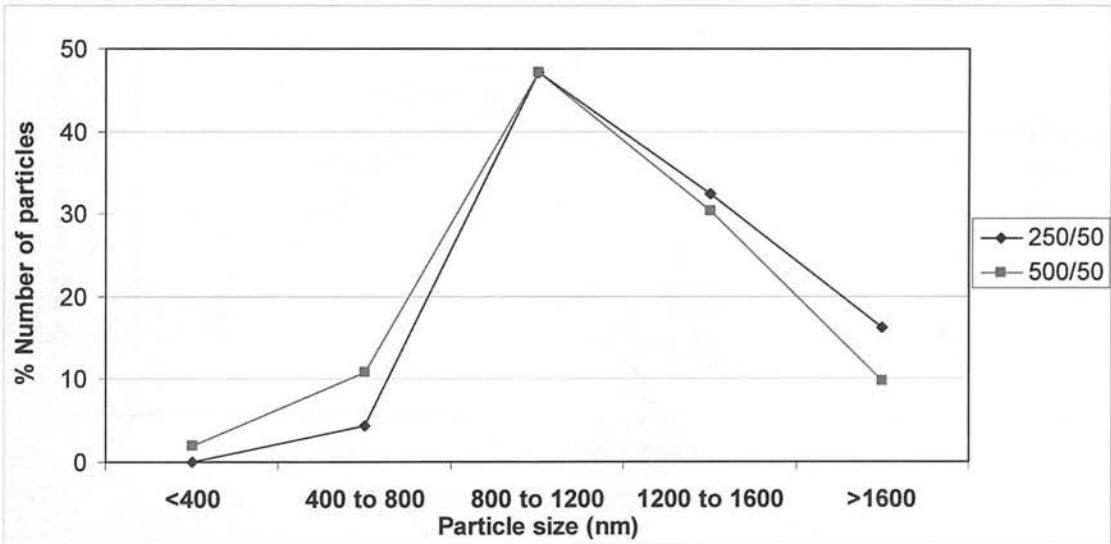
Figure A5.2. *Size distributions for DPI particles. Example data shown for FP/SX 250/50 (file DPI_1), and FP/SX 500/50 (file DPI_7).*

A5.3 Particle Size Distribution Graphs for Individual Samples
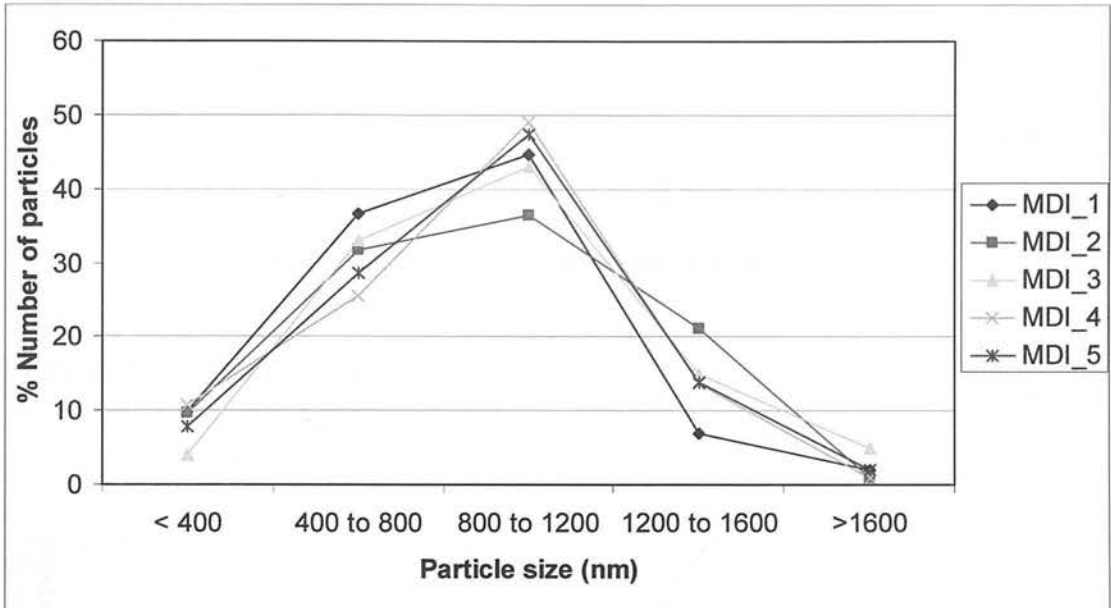
Figure A5.3. *Particle size distribution for pMDIs (formulation FP/SX 250/25).*
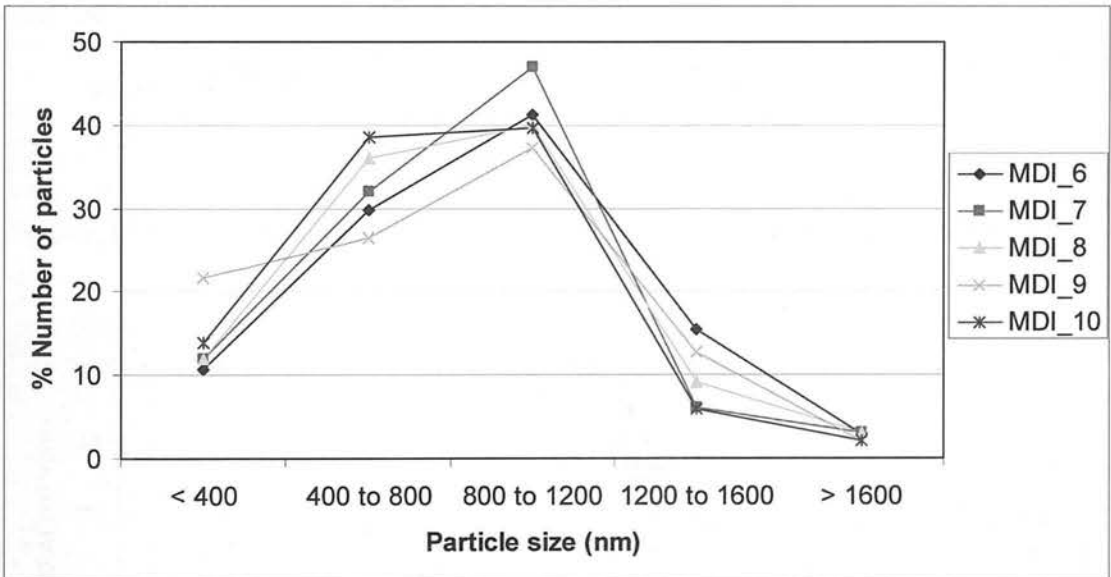
Figure A5.4. *Particle size distribution for pMDI(s) (formulation FP/SX 125/25).*
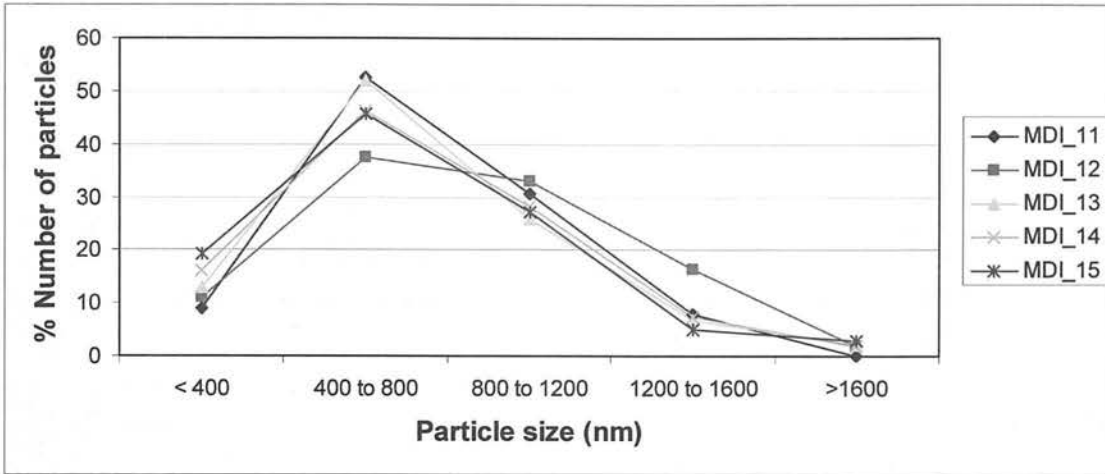
Figure A5.5. Particle size distribution for pMDIs (formulation FP/SX 50/25).
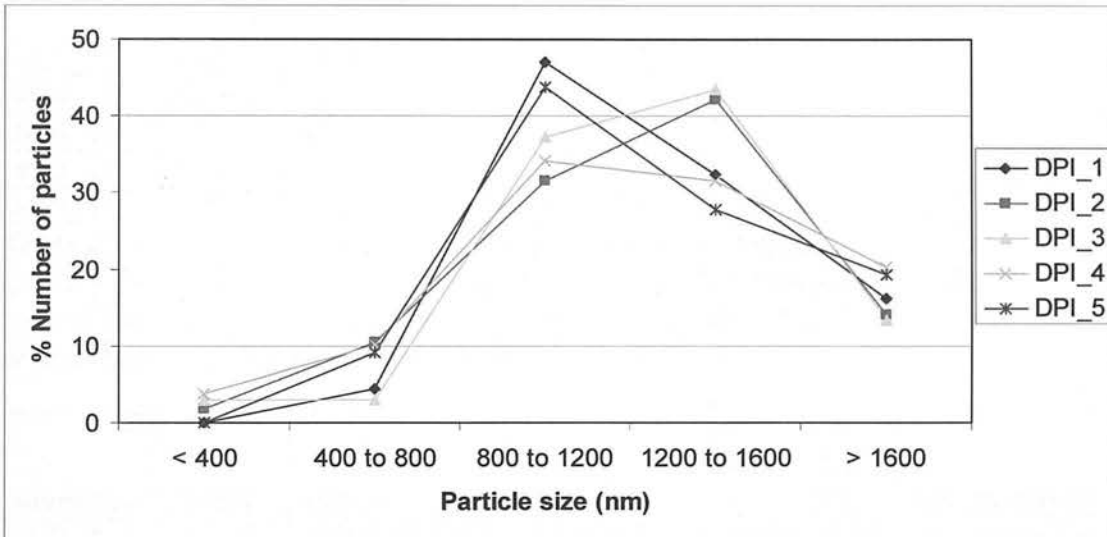
Figure A5.6. Particle size distribution for DPIs (formulation FP/SX 250/50).
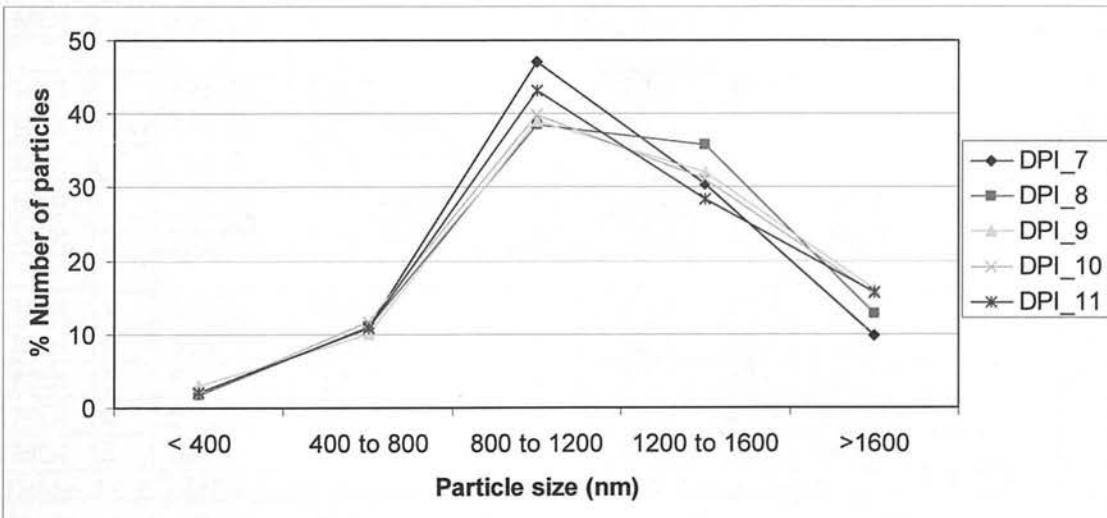
Figure A5.7. Particle size distribution for DPIs (formulation FP/SX 500/25).

A5.4 Data Tables

Identifier	FP/SX	Batch	Total	FP	SX	FP AND SX	FP OR SX	Unclass.
MDI_1	250/25.	Lot031012991	101	85	61	45	101	0
MDI_2	250/25.	SE004/97F	104	79	75	50	104	0
MDI_3	250/25.	AX7102/82.	102	79	80	57	102	0
MDI_4	250/25.	AX7102/82.	102	73	74	46	101	1
MDI_5	250/25.	AX7102/82.	101	74	74	50	98	3
MDI_6	125/25.	002/78	104	71	80	50	101	3
MDI_7	125/25.	AX7100/60	100	50	86	40	96	4
MDI_8	125/25.	1/18, 04/97F.	101	69	80	48	101	0
MDI_9	125/25.	1/18, 04/97F.	102	61	87	46	102	0
MDI_10	125/25.	1/18, 04/97F.	101	68	75	44	99	2
MDI_11	50/25.	002/78	101	52	79	31	100	1
MDI_12	50/25.	AX7099/32	109	51	101	43	109	0
MDI_13	50/25.	05/97F	101	54	90	43	101	0
MDI_14	50/25.	05/97F	106	53	100	47	106	0
MDI_15	50/25.	05/97F	103	51	93	41	103	0

Table A5.4. *pMDI Data analysis based on marker ion analysis. (For FP, m/z-74 and for SX -188). Category FP – particles that contain FP, Category SX - particles that contain SX, Category FPANDSX- particles that contain FP and SX i.e. mixed due to co-association. Table shows number of particles in each category.*

Identifier	FP/SX	Batch	FP	SX	FP AND SX	FP OR SX	Unclassified
MDI_1	250/25.	Lot031012991	84.2	60.4	44.6	100.0	0.0
MDI_2	250/25.	SE004/97F	76.0	72.1	48.1	100.0	0.0
MDI_3	250/25.	AX7102/82.	77.5	78.4	55.9	100.0	0.0
MDI_4	250/25.	AX7102/82.	71.6	72.5	45.1	99.0	1.0
MDI_5	250/25.	AX7102/82.	73.3	73.3	49.5	97.0	3.0
MDI_6	125/25.	002/78	68.3	76.9	48.1	97.1	2.9
MDI_7	125/25.	AX7100/60	50.0	86.0	40.0	96.0	4.0
MDI_8	125/25.	1/18, 04/97F.	68.3	79.2	47.5	100.0	0.0
MDI_9	125/25.	1/18, 04/97F.	59.8	85.3	45.1	100.0	0.0
MDI_10	125/25.	1/18, 04/97F.	67.3	74.3	43.6	98.0	2.0
MDI_11	50/25.	002/78	51.5	78.2	30.7	99.0	1.0
MDI_12	50/25.	AX7099/32	46.8	92.7	39.4	100.0	0.0
MDI_13	50/25.	05/97F	53.5	89.1	42.6	100.0	0.0
MDI_14	50/25.	05/97F	50.0	94.3	44.3	100.0	0.0
MDI_15	50/25.	05/97F	49.5	90.3	39.8	100.0	0.0

Table A5.5. *pMDI Data analysis based on marker ion analysis. (For FP, m/z-74 and for SX -188). Category FP – particles that contain FP, Category SX - particles that contain SX, Category FPANDSX- particles that contain FP and SX i.e. mixed due to co-association. Table shows % number of particles in each category.*

Identifier	FP/SX	Batch	Total	FP	SX	FP AND SX	FP OR SX	Unclass
DPI_1	250/50.	R252654	68	55	67	54	68	0
DPI_2	250/50.	R252237	57	48	57	48	57	0
DPI_3	250/50.	R252265.	68	64	66	63	67	1
DPI_4	250/50.	R252265.	79	66	77	64	79	0
DPI_5	250/50.	R252265.	130	110	128	109	129	1
DPI_7	500/50.	R252323	102	80	96	76	100	0
DPI_8	500/50.	R252238	109	96	104	91	109	0
DPI_9	500/50	R252238	100	98	98	87	100	0
DPI_10	500/50	R252238	103	88	103	88	103	0
DPI_11	500/50	R252400	102	89	100	87	102	0

Table A5.6. *DPI data analysis based on marker ion analysis. (For FP, m/z-74 and For SX -188). Category FP – particles that contain FP, Category SX - particles that contain SX, Category FPANDSX -particles that contain FP and SX i.e. mixed due to co-association. Table shows number of particles in each category.*

Identifier	FP/SX	Batch	FP	SX	FP AND SX	FP OR SX	Unclassified
DPI_1	250/50.	R252654	80.9	98.5	79.4	100.0	0.0
DPI_2	250/50.	R252237	84.2	100.0	84.2	100.0	0.0
DPI_3	250/50.	R252265.	94.1	97.1	92.6	98.5	1.5
DPI_4	250/50.	R252265.	83.5	97.5	81.0	100.0	0.0
DPI_5	250/50.	R252265.	84.6	98.5	83.8	99.2	0.8
DPI_7	500/50.	R252323	78.4	94.1	74.5	98.0	0.0
DPI_8	500/50.	R252238	88.1	95.4	83.5	100.0	0.0
DPI_9	500/50	R252238	98.0	98.0	87.0	100.0	0.0
DPI_10	500/50	R252238	85.4	100.0	85.4	100.0	0.0
DPI_11	500/50	R252400	87.3	98.0	85.3	100.0	0.0

Table A5.7. *DPI data analysis based on marker ion analysis. (For FP, m/z-74 and For SX -188). Category FP – particles that contain FP, Category SX - particles that contain SX, Category FPANDSX - particles that contain FP and SX i.e. mixed due to co-association. Table shows % number of particles in each category.*

A7 Appendices to Chapter 7

A7.1   Sample list for AAMS Experiments

Sample	Batch	Formulation
MDI_1*	002/78	FP/SX 50/25
MDI_2	002/78	FP/SX 50/25
MDI_3	05/97F	FP/SX 50/25
MDI_4	AX7099/23	FP/SX 50/25
MDI_5	AX7099/23	FP/SX 50/25
MDI_6	AX7099/23	FP/SX 50/25
MDI_7	1/22	FP/SX 250/25
MDI_8	1/22	FP/SX 250/25
MDI_9	AX7102/82	FP/SX 250/25
MDI_10	DO40861	FP/SX 250/25
MDI_11	DO40861	FP/SX 250/25
DPI_1	R15404-20	FP/L
DPI_2	R25237	FP/SX 250/50
DPI_3	R25240	FP/SX 500/50

Table A7.1. List of samples used in the experiments described in Chapter 7. Sample MDI_1 was a trial run and no data from this run was used. Sample MDI_11 was run with no inlet orifice in place.

A7.2 Data Tables

A7.2.1 Particle size data

File	Dose	>1000 nm	500 to 1000 nm	Number of particles 300 to 500 nm	200 to 300 nm	< 200 nm	Total particles
MDI_1	FP/SX 50/25.	n/a	n/a	n/a	n/a	n/a	n/a
MDI_2	FP/SX 50/25.	4	14	53	47	1	122
MDI_3	FP/SX 50/25.	4	26	44	27	1	102
MDI_4	FP/SX 50/25.	4	18	54	40	1	120
MDI_5	FP/SX 50/25.	3	11	42	42	1	102
MDI_6	FP/SX 50/25.	5	16	73	76	2	122
MDI_7	FP/SX 250/25.	1	15	9	17	1	46
MDI_8	FP/SX 250/25.	23	36	22	18	0	102
MDI_9	FP/SX 250/25.	27	76	14	2	0	122
MDI_10	FP/SX 250/25.	17	31	28	49	0	122
MDI_11	FP/SX 250/25.	32	50	13	5	0	103
MDI_12	FP/SX 250/25.	41	100	11	3	0	155

Table A7.2. *The number of particles in each classification category.*

File	Dose	>1000 nm	500 to 1000 nm	% Number of particles 300 to 500 nm	200 to 300 nm	< 200 nm	Total particles
MDI_1	FP/SX 50/25.	n/a	n/a	n/a	n/a	n/a	n/a
MDI_2	FP/SX 50/25.	3.3	11.5	43.4	38.5	0.8	122
MDI_3	FP/SX 50/25.	3.9	25.5	43.1	26.5	1.0	102
MDI_4	FP/SX 50/25.	3.3	15.0	45.0	33.3	0.8	120
MDI_5	FP/SX 50/25.	2.9	10.8	41.2	41.2	1.0	102
MDI_6	FP/SX 50/25.	4.1	13.1	59.8	62.3	1.6	122
MDI_7	FP/SX 250/25.	2.2	32.6	19.6	37.0	2.2	46
MDI_8	FP/SX 250/25.	22.5	35.3	21.6	17.6	0.0	102
MDI_9	FP/SX 250/25.	22.1	62.3	11.5	1.6	0.0	122
MDI_10	FP/SX 250/25.	13.9	25.4	23.0	40.2	0.0	122
MDI_11	FP/SX 250/25.	31.1	48.5	12.6	4.9	0.0	103
MDI_12	FP/SX 250/25.	26.5	64.5	7.1	1.9	0.0	155

Table A7.3. *The % number of particles in each classification category.*

A7.2.2 Analysis of Particle Composition

A7.2.2.1 Data analysis for pMDI using marker ion analysis

File	Formulation	Batch/id	Total	FP	SX	Mixed
MDI_1	FP/SX 50/25.	002/78.	n/a	n/a	n/a	n/a
MDI_2	FP/SX 50/25.	002/78.	122	100	7	15
MDI_3	FP/SX 50/25.	05/97F	97	74	10	13
MDI_4	FP/SX 50/25.	AX7099/23	120	100	4	16
MDI_5	FP/SX 50/25.	AX7099/23	102	88	3	11
MDI_6	FP/SX 50/25.	AX7099/23	172	139	9	24
MDI_7	FP/SX 250/25.	1/22.	102	76	5	21
MDI_8	FP/SX 250/25.	1/22.	169	121	12	36
MDI_9	FP/SX 250/25.	AX7102/82.	126	107	6	13
MDI_10	FP/SX 250/25.	DO40861.	103	80	5	18
MDI_11	FP/SX 250/25.	DO40861.	155	118	8	29

Table A7.4. Particle classification to show the fractional composition for the series of pMDI. The table shows the number of particles in each category.

File	Formulation	Batch/id	Total %	FP	SX	Mixed
MDI_1	FP/SX 50/25.	002/78.	n/a	n/a	n/a	n/a
MDI_2	FP/SX 50/25.	002/78.	100.0	82.0	5.7	12.3
MDI_3	FP/SX 50/25.	05/97F	100.0	76.3	10.3	13.4
MDI_4	FP/SX 50/25.	AX7099/23	100.0	83.3	3.3	13.3
MDI_5	FP/SX 50/25.	AX7099/23	100.0	86.3	2.9	10.8
MDI_6	FP/SX 50/25.	AX7099/23	100.0	80.8	5.2	14.0
MDI_7	FP/SX 250/25.	1/22.	100.0	74.5	4.9	20.6
MDI_8	FP/SX 250/25.	1/22.	100.0	71.6	7.1	21.3
MDI_9	FP/SX 250/25.	AX7102/82.	100.0	84.9	4.8	10.3
MDI_10	FP/SX 250/25.	DO40861.	100.0	77.7	4.9	17.5
MDI_11	FP/SX 250/25.	DO40861.	100.0	76.1	5.2	18.7

Table A7.5. Particle classification to show the fractional composition for the series of pMDI. The table shows the % number of particles in each category.

Appendix Section 2

Publications – Anthony New

Recent posters/presentations

1. ***(Oral presentation)-*** *Desorption Electrospray Ionization* (DESI) and Direct Analysis in Real Time (DART) mass spectrometry. A.P. New. *Pharmaceutical Analytical Sciences Group (PASG) meeting -New directions: Science and Technology. Sept 2007 (Northampton, UK).*

2. ***(Poster)-*** Atmospheric Desorption Analysis of Pharmaceutical Solid Dosage Forms: Progress over the Past Year. A. Marcus and A.P. New. *Proceedings of the 55th conference on mass spectrometry and allied topics. June 2007 (Denver, CO, USA).*

3. ***(Poster)-*** An initial assessment of the use of conductivity profiles in process manufacturing. A.P. New, D. Elder, D. Rudd, G. Bone and D. Taylor. *British Pharmaceutical Conference, Sept 2006, (Manchester, UK).*

4. ***(Poster)-*** Evaluation of the use of desorption ionization techniques for the analysis of formulated products. A. Marcus and A.P. New. *Proceedings of the 54th conference on mass spectrometry and allied topics. June 2006 (Seattle, WA, USA).*

Patent

1. Temperature controlled membrane interface device. A.P. New, D.G. Lamarca, C.S. Creaser. *UK Patent Application GB 2392114A, 25 Feb 2004.*

Research Papers (Chronological order 1988 -present)

1. Experiments on cyanoguanadino compounds using discharge assisted thermospray ionization. N.J. Haskins and A.P. New. *Biomed. and Environ. Mass Spectrom.* <u>17</u>,*169 -171, (1988).*

2. A comparison of positive and negative ion FAB-MS data for some sulphonyl hydrazones and derivatives. A.P. New, N.J. Haskins and M.J. Frearson. *Biomed. and Environ. Mass Spectrom.* <u>18</u>,*620-623,(1989).*

3. Cluster ion formation between solvent and matrix using fast atom bombardment mass spectrometry. N.J. Haskins and A.P. New. *Rapid Commun. Mass Spectrom.* <u>3</u>, *335-337, (1989).*

4. A coordinated approach towards the molecular weight determination of peptides by gel electrophoresis and fast atom bombardment mass spectrometry. P. Camilleri, N.J. Haskins, A.J. Hill and A.P. New. *Rapid Commun. Mass Spectrom.* <u>3</u>, *440-443, (1989).*

5. Fast atom bombardment mass spectrometry (FAB-MS) and fast atom bombardment tandem mass spectrometry (FAB MS/MS) of some monosaccharide oximes. A.P. New, N.J. Haskins and B. Lee. *Rapid Commun. Mass Spectrom.* <u>4</u>, *432-435, (1990).*

6. The use of tandem mass spectrometry for the differentiation of bile acid isomers and for the identification of bile acids in biological extracts. C. Eckers, A.P. New, P. East and N.J. Haskins. *Rapid Commun. Mass Spectrom.* <u>4</u>, *449-453, (1990).*

7. Deuterated Solvents in High Performance Liquid Chromatography- Fast Atom Bombardment Mass Spectrometry. T. McLean, A.P. New, N.J. Haskins and P. Camilleri. *J.Chem. Soc. Chem. Comm.* <u>24</u>, *1773-1775, (1992).*

8. An investigation into the stereochemistry of the borate di-esters of some monosaccharides using tandem mass spectrometry. A.P. New, N.J. Haskins and D.E. Games. *Rapid Commun. Mass Spectrom. 7, 1099-1107, (1993).*

9. Analyzing the complexation of amino acids and peptides with cyclodextrin using electrospray ionization mass spectrometry. P. Camilleri, N.J. Haskins, A.P. New and M.R. Saunders. *Rapid Commun. Mass Spectrom. 7, 949-952, (1993).*

10. Structures of polysporins A-D, four new peptaibols Isolated from Trichoderma polysporum. A.P. New, C. Eckers, N.J. Haskins, W.A. Neville, S. Elson, J.A. Hueso and A. Rivera. *Tetrahedron Letters. 37(17), 3039-3042 (1996).*

11. Biodegradation of bromobenzene, chlorobenzene, iodobenzene and fluorobenzene: batch and continuous experiments. L.M. Freitas dos Santos, A.P. New, M. Gilges and D.G. Lamarca. *Trans. IChemE. 77 Part B 43-46 (1999).*

12. Biodegradation of 2, 3 and 4-iodobenzoic acids and ethyl-4-iodobenzoate. L.M. Freitas dos Santos, A.P. New and M. Kingswood. *J.Chem Technol. Biotechnol. 74, 815-820 (1999).*

13. Analytical techniques used for monitoring the biodegradation of fluorinated compounds in waste streams from pharmaceutical production. A.P. New, L.M. Freitas dos Santos and A. Spicq. *Journal of Chromatography A. 889, 177-184, (2000).*

14. Preliminary investigation of the application of on-line membrane extraction of trifluoro acetic acid as an aid to improvement of negative ion electrospray mass spectrometry data. A.P. New, J-C. Wolff, S. Crabtree, G. Okafo, J. Lee, K. Divan and L.M. Freitas dos Santos. *Journal of Chromatography A. 913, 205-208, (2001).*

15. Aerobic biotransformation of 4-fluorocinnamic acid to 4-fluorobenzoic acid. L.M. Freitas dos Santos, A. Spicq, A.P.New, G. LoBiundo, J-C. Wolff and A. Edwards. *Biodegradation, 12, 23-29, (2001).*

16. Analysis of semi-volatile organic compounds by membrane inlet mass spectrometry. C.S. Creaser, D.G. Lamarca, L.M. Freitas dos Santos and A.P. New. *Advances in Mass Spectrom. 15, 817-818, (2001).*

17. Reversed-phase membrane inlet mass spectrometry applied to the real-time monitoring of low molecular weight alcohols in chloroform. C.S. Creaser, D.G. Lamarca, J. Brum, C. Werner, A.P. New and L. Freitas dos Santos. *Anal. Chem. 74, 300-304, (2002).*

18. Biodegradation studies of 4-fluorobenzoic acid and 4-fluorocinnamic acid: an evaluation of membrane inlet mass spectrometry as an alternative to high performance liquid chromatography and ion chromatography. C.S. Creaser, D.G. Lamarca, A.P. New, J-C. Wolff and L.M. Freitas dos Santos. *Analytica Chimica Acta. 454, 137-145, (2002).*

19. On-line biodegradation monitoring of nitrogen containing compounds by membrane inlet mass spectrometry. C.S. Creaser, D.G. Lamarca, L.M. Freitas dos Santos, G. LoBiondo and A.P. New. *Journal of Chemical Technology and Biology. 78, 1193-1200, (2003).*

20. A universal temperature controlled membrane interface for the analysis of volatile and semi-volatile organic compounds. C.S. Creaser, D.G. Lamarca, L.M Freitas dos Santos, A.P. New and P.A. James. *The Analyst. 128, 1150-1156, (2003).*

21. Detection and assessment of co-association in inhalable drug particles using aerosol time-of-flight mass spectrometry. A.P. New, D. Prime, S. Zomer, D. Elder, R. Donovan and E. Freney. *Rapid Commun. Mass Spectrom. 22, 3873-3882 (2008). (Attached inside back cover).*

RCM

Detection and assessment of co-association in inhalable drug particles using aerosol time-of-flight mass spectrometry

Anthony New[1]*, Dave Prime[2], Simeone Zomer[3], David Elder[4], Robert Donovan[5] and Evelyn Freney[5]

[1]Novel Analytical Technologies, GlaxoSmithKline, Park Road, Ware SG12 0DP, UK
[2]Inhaled Product Development, GlaxoSmithKline, Park Road, Ware SG12 0DP, UK
[3]Process Technologies, GlaxoSmithKline, NFSP(S), Harlow SM19 5AW, UK
[4]Product Development, GlaxoSmithKline Park Road, Ware SG12 0DP, UK
[5]School of Chemistry, University of Edinburgh, West Mains Road, Edinburgh, EH9 3JJ, UK

Aerosol Time-of-Flight Mass Spectrometry (AToFMS) was used to examine co-association between two inhaled drugs, fluticasone propionate (FP) and salmeterol xinofoate (SX), in fine aerosolised particles emitted from Seretide®/Advair® inhaled combination products. Principal Component Analysis (PCA) was used to identify fragmentation patterns indicative of either pure or co-associated particles (particles containing both drugs). A third component of the particles emitted from dry powder inhalers (DPIs), lactose, gave only a very weak mass spectral signal and no interpretable data was acquired for this compound; however, it was not found to interfere with the detection of the two drug substances. High levels of co-association were found in the emitted doses from both pressurised metered dose inhaler (pMDI) and dry powder inhaler (DPI) products. Copyright © 2008 John Wiley & Sons, Ltd.

The two most common chronic respiratory diseases are asthma and chronic obstructive pulmonary disease (COPD). According to the World Health Organisation (WHO) estimates in 2007, 300 million people currently suffer from asthma and 210 million suffer from COPD.[1] Two classes of drugs widely used in the treatment of these diseases are β2-agonists and corticosteroids; both being preferably delivered directly to the lungs by inhalation. Typically, patients use either pressurised metered dose inhaler (pMDI) or dry powder inhaler (DPI) devices to administer the drugs.

In recent years, inhaled products have become available which deliver both types of drug within a single dose: e.g. Seretide®/Advair® which include fluticasone propionate (FP), an inhaled corticosteroid (ICS), and salmeterol xinofoate (SX), a long-acting β2-agonist (LABA). Some studies have shown that in Seretide®/Advair® inhalers the two drugs provide an enhanced clinical effect beyond that achieved when the two drugs are administered concurrently from two separate inhalers.[2] It has been suggested that this increased effect is due to higher levels of co-deposition of the two drugs in the lungs when delivered from a single inhaler, possibly because the drugs are co-associated when emitted from the device. Although it has been shown that there is some affinity between FP and SX in solution,[3] in the past the composition of single particles has been difficult to ascertain. Some work using Raman

imaging[4] presented statistical evidence of significant co-association of FP and SX particles emitted from a Seretide® inhaler when deposited onto a surface within a cascade impactor.

Conventional analysis of a formulated inhaled product can involve highly resource-intensive sample preparation. For example, experiments to determine particle size and composition using the Andersen Cascade Impactor (ACI)[5] involve washing the plates taken from the impactor followed by high-performance liquid chromatography (HPLC) analysis.

The ability of single particle mass spectrometry (SPMS) to make near real-time measurements of particle size and chemical composition[6,7] is an attractive alternative in the field of pharmaceutical aerosol analysis.

In the work presented here we have employed a commercially available single particle mass spectrometer, a TSI 3800 aerosol time-of-flight mass spectrometer, to analyse particles originating from both pressurised metered dose inhalers (pMDI) and dry powder inhalers (DPI). A sample introduction apparatus was used in these experiments to disperse particles appropriately but no manual sample preparation was required and the experiments were performed directly on the commercial products.

Although the aerosol time-of-flight mass spectrometry (AToFMS) technique was developed mainly for the study of environmental aerosols,[8,9] it has also been used in a number of studies encompassing the analysis of inhaled pharmaceutical products[10-12] and tablets.[13]

Correspondence to: A. New, Novel Analytical Technologies, GlaxoSmithKline, Park Road, Ware SG12 0DP, UK.
E-mail: apn33849@googlemail.com

EXPERIMENTAL

Sample introduction apparatus

A schematic diagram of the apparatus used for the introduction and dispersion of particles taken from samples is shown in Fig. 1. The apparatus is designed for the introduction of standard aerosolised powders of active pharmaceutical ingredients. It was constructed from glass and allowed aerosolised particles to be suspended in Brownian motion in the 5 L settling chamber and sampled through the inlet of the AToFMS instrument.

The liquid impinger stage was the upper stage (stage 1) from a twin impinger[14] which is designed to separate the fine, potentially respirable, fraction of the dose from an inhaled delivery device from the coarse, non-respirable material. The upper stage is designed to remove the majority of particles with an aerodynamic diameter greater than approximately 6 μm when the air flow rate is 60 L min⁻¹.

Hence, this stage would be expected to remove the large, non-respirable material, such as the coarse lactose carrier particles in the dose from a DPI or the larger droplets emitted from a pMDI. It would be expected to remove only a small percentage of the individual particles of micronised drug or small agglomerates of drug particles.

Sample types

Three different types of sample were examined in these experiments, *viz.* micronised powders of the pure active pharmaceutical ingredients (APIs), and the emitted doses from DPIs and pMDIs. Micronised API powders were introduced into a flow of air from a large air syringe using a Penn-Century™ device (Penn-Century, Philadelphia, PA, USA) as a powder syringe, as shown in Fig. 1. A flow of air at approximately 60 L min⁻¹ was generated using a 3 L air syringe and the powder injected into the flow.

For DPIs a similar apparatus was used except that the DPI was actuated and then placed in a box designed to allow a flow of air through the device such that the dose was emitted from the mouthpiece into the twin impinger. The flow of air was again provided using an air syringe at approximately 60 L min⁻¹. The apparatus for the introduction of pMDIs was similar except that the pMDI was actuated directly into the impinger stage (a flow of air was not required as the expansion of the propellant is sufficient to carry the emitted particles into the settling chamber).

Materials

Data sets were acquired using the AToFMS instrument on clinical grade samples of the pure active pharmaceutical ingredients fluticasone propionate (FP) and salmeterol xinofoate (SX) and of lactose (the carrier used in the DPI samples). The structures of FP and SX are shown in Table 1. Data sets from both pure active pharmaceutical ingredients (FP and SX) were used as reference standards for comparison with the samples from pMDIs and DPIs. Lactose gave only a very weak mass spectral signal and no interpretable data was acquired for this compound.

Data sets were then acquired using the AToFMS instrument to analyse aerosolised powders from Advair Diskus® dry powder inhalers of strengths 500 μg FP/50 μg SX and 250 μg FP/50 μg SX and from Seretide® pressurised metered dose inhalers of strengths 250 μg FP/25 μg SX, 125 μg FP/25 μg SX and 50 μg FP/25 μg SX. Samples from Flovent® (100 μg FP per dose) and Serevent® (50 μg SX per dose), which contain only *one* active pharmaceutical ingredient, were also analysed to assess the effect of the matrix. [Samples of Advair Diskus®, Seretide®, Flovent® and Serevent® were supplied by GSK, Greenford, UK.]

Sample analysis using the AToFMS instrument

All experiments were performed using a TSI 3800 AToFMS instrument (TSI, Shoreview MN USA). This instrument is described in detail elsewhere,[7,15] and hence only a brief description of the operation is provided below.

The initial configuration of the inlet used a nozzle-skimmer design; however, during the course of this work the inlet was upgraded to an aerodynamic lens which has the capability to give improved transmission efficiencies[16] especially for smaller particles.

The measurement of particle size by the AToFMS instrument is derived from a measurement of the time taken for a particle to pass between two laser beams in the sizing region; this yields the aerodynamic diameter of the particle. Particle size measurements were calibrated with a range of polystyrene beads of known size (Duke Scientific, Palo Alto, CA, USA).

After sizing, the particles are directed into the mass spectrometer where they are ablated and ionised using a quadrupled Nd:YAG laser (266 nm, 5 ns pulses) which is synchronised and triggered by the particle sizing lasers. The
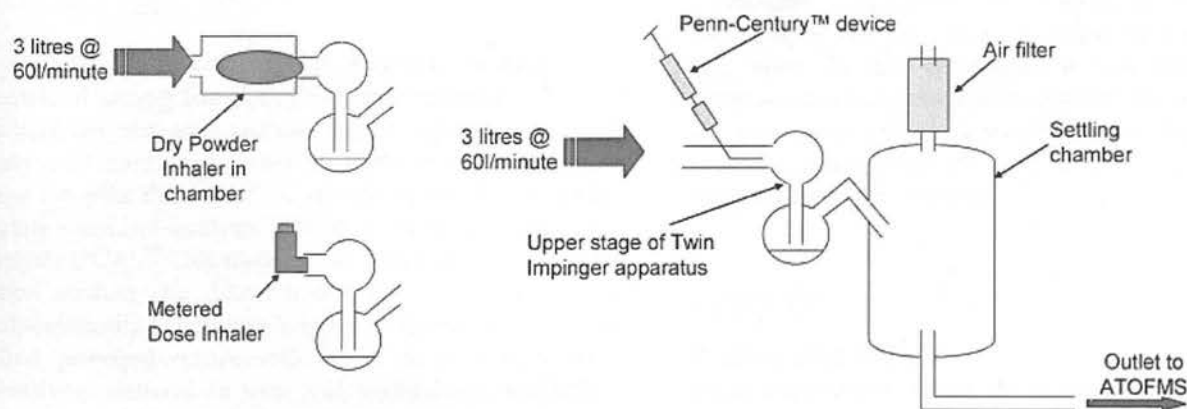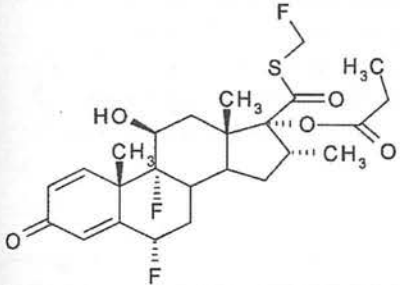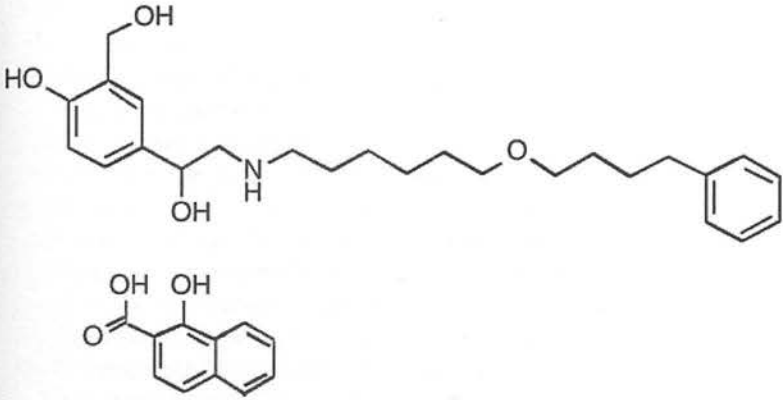

Figure 1. Left panel: inlets for the dry powder inhalation chamber and metered dose inhaler. Right panel: the inlet for the Penn-Century ™ device, attached to AToFMS inlet apparatus (settling chamber).

Table 1. The structures of fluticasone propionate (FP) and salmeterol xinofoate (SX)

Fluticasone propionate (FP)
$C_{25} H_{31} F_3 O_5 S$
MW 500

Salmeterol xinofoate (SX)

Salmeterol (free base)
$C_{25} H_{37} N O_4$
MW 415

Xinofoate
$C_{11} H_8 O_3$
MW 188

AToFMS instrument utilises two separate time-of-flight mass spectrometers, of opposite polarity, which allows the simultaneous detection of both positive and negative ions from the same particle. The vacuum was 6.5×10^{-6} Torr in the sizing region and 3.0×10^{-7} Torr in the mass spectrometer.

Initial experiments (using the nozzle-skimmer inlet) were performed to investigate the effect of the laser energy on fragmentation and the general quality of mass spectral data within the range 0.1 to 1.0 mJ (the power density[15] for a 1.0 mJ, 5 ns pulse, focused on an area of $400\,\mu m^2$, is $\sim 1 \times 10^8$ W/cm^2; see Figs. 5 and 6). Experiments using the aerodynamic lens as the inlet were all performed at the low laser energy settings (<0.2 mJ) in an attempt to obtain data showing the greatest differentiation between the individual FP and SX mass spectra. Data were processed using MS Analyze™ (TSI), collated in MS Access™ databases, and then analysed with multivariate statistical analysis software based on Matlab™ (The Mathworks, Natick, MA, USA).

Application of multivariate analysis to data acquired using the AToFMS instrument

Multivariate statistical analysis can be applied to chemical analysis data and can be used as a tool to extract trends from large complex data sets.[17] A specific application of multivariate chemical analysis (MCA) is principal component analysis (PCA).[18] This multivariate statistical pattern recognition method can detect trends in large data sets, by mathematically generating a series of fewer new variables called principal components (PCs). It is a method of identifying patterns in data and highlighting similarities and differences between data sets. Once the patterns have been identified, the data sets can be compressed to the PCs with minimal loss of information.

PCA identifies the axis of maximum variance along which to project the data sets. The data matrix that was used here in the PCA corresponds to the normalised spectra of FP and SX standards stacked along rows. As an additional pre-processing step, variables along the matrix columns were auto-scaled. From the PCA assessment, two sets of vectors were extracted, the scores and the loadings, that can be projected into two-dimensional diagrams to inspect the major trends that are responsible for most of the variation in the data matrix.

The scores plots shown in the Results section indicate the groups of particles that show similar spectra, i.e. those falling within the same cluster (or confidence ellipse), and this can be used to compare datasets. The loadings plots (not shown) were used to ascertain the weights ascribed to the original variables (m/z values) in projecting the spectra derived from each particle onto the scores plot. The most influential m/z values are those that cluster furthest away from the origin of the loadings plot.

Principal components are ordered in terms of size, indicated by the percentage variation in the dataset that they span. In this application it was found that two components were sufficient to describe the main trends in the data; hence a single scatter plot of the first and second principle components (PC1 vs. PC2) could be used to interpret the main patterns.

RESULTS

Particle size effects

Initial experiments using the instrument fitted with the nozzle-skimmer inlet were carried out to examine the variation in spectral data as a function of laser energy. From these experiments the effect of particle size, in the 0.5 to

4.5 μm range, could be determined. Additional experiments were performed, at low laser energy settings (0.2 mJ), in an attempt to maximise the difference between the mass spectra of the individual active pharmaceutical ingredients (FP and SX). For these experiments, using the aerodynamic lens, smaller particles, i.e. those in the range 0.5 to 1.5 μm, were detected.

Mass spectra

There were some potential difficulties when applying AToFMS to drug compounds such as FP and SX. The amount of material in each particle is very small – e.g. a homogeneous, spherical, 1 μm diameter particle of FP would have a mass of approximately 0.7 fg. Also, it is known that ablation of particles (especially the larger particles) is incomplete with the laser desorption ionization energies employed with the AToFMS instrument.[19] However, the material that is ablated is generally representative of the materials present in the particles, so long as the materials are homogeneously distributed within the particles.[20]

The appearance of the mass spectra acquired using the AToFMS instrument depends fundamentally on the ability of the analyte molecules, or the matrix, to absorb the laser energy at 266 nm and on the laser energy utilised. However, it has been reported that both FP and SX absorb energy only weakly at 266 nm in solution;[3] lactose absorbs weakly as it gave only a very weak mass spectral signal.

Despite these limitations, it was possible to acquire mass spectra on single particles of both active pharmaceutical ingredients (FP and SX) that showed unique fragment ions that may be reasonably interpreted as being deriving from the parent active pharmaceutical ingredients.

For the AToFMS instrument the laser wavelength is fixed but the laser energy may be varied and typical positive ion spectra for particles taken from standards of pure FP and SX, acquired at high and low energy are shown in Fig. 2. At higher laser energy (~0.8 mJ) the mass spectra show many ions at lower m/z values. In this case, the ions with lower m/z values are difficult to interpret in terms of the FP structure, probably because they are formed by secondary, tertiary or further fragmentation as the molecule is reduced to hydrocarbon cations of the type: C_n^+, C_nH^+, $C_nH_2^+$, $C_nH_3^+n$, etc.[21] Moreover, it was found that spectra acquired at higher laser energy showed ions common to both FP and SX.

At low laser energy (~0.2 mJ) the positive ion spectra show relatively few ions, many of which are unique to either FP or SX. The FP molecule fragments to the ion at m/z 333 by the concerted loss of the 17α and 17β side chains from the D ring of the steroid. The ion at m/z 58 probably originates from the propionyl group in the 17β side chain.

We suggest that the ion at m/z 333 then loses HF and water to give the ions at m/z 294 and 276, respectively. It is likely that these are losses involving *trans*-elimination of water or HF from the 6 and 11 positions on the steroid ring, respectively.
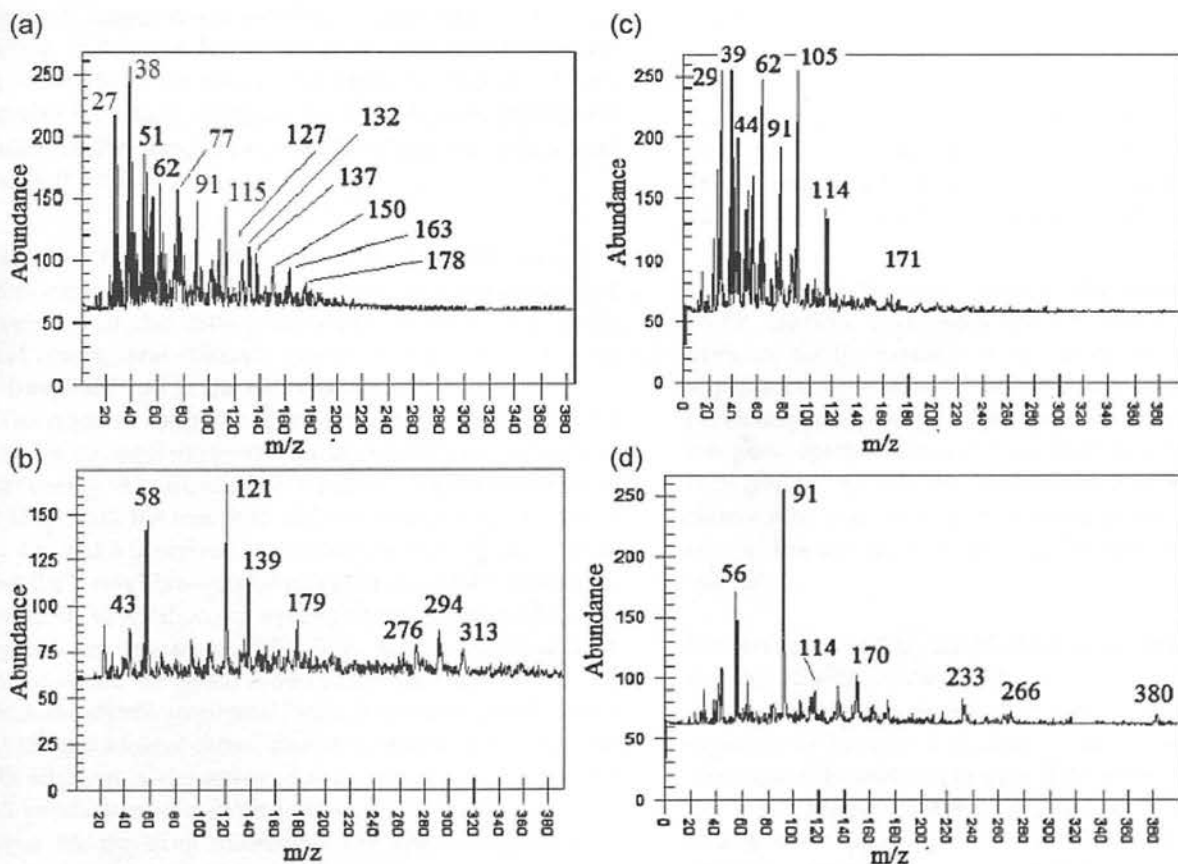

Figure 2. Mass spectra acquired using the AToFMS instrument with positive ion detection for (a) a particle of FP aerodynamic size 2.09 μm at high laser energy (0.92 mJ); (b) a particle of FP aerodynamic size 2.03 μm at low laser energy (0.11 mJ); (c) a particle of SX aerodynamic size 1.80 μm at high laser energy (0.87 mJ); and (d) a particle of SX aerodynamic size 0.73 μm at low laser energy (0.11 mJ) (using nozzle-skimmer inlet).
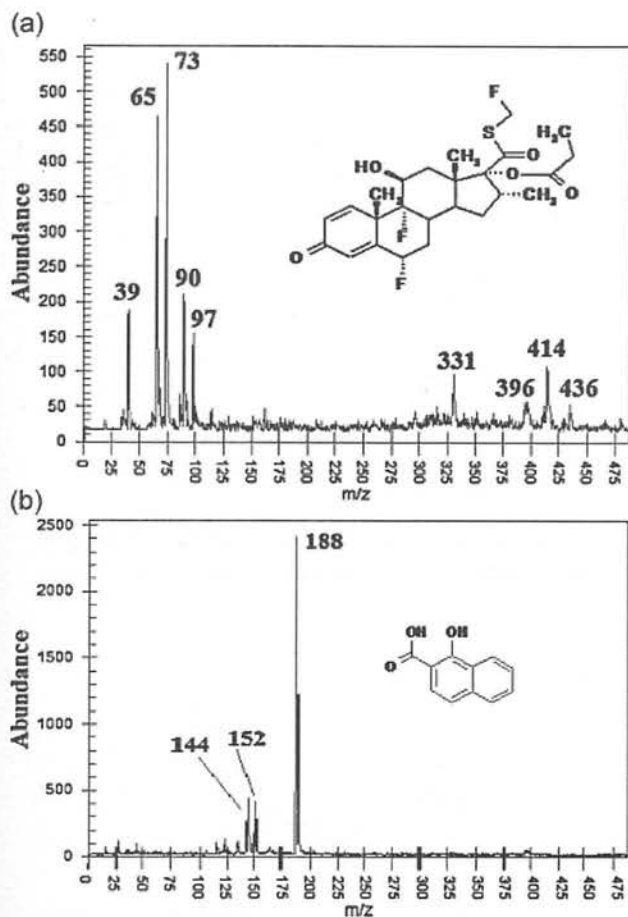
(a)

(b)

Figure 3. Negative ion AToFMS spectra taken from (a) a particle of FP with an aerodynamic size of 1.11 μm and (b) a particle of SX with an aerodynamic size of 0.47 μm, showing the mass spectrum for the xinofoate counter-ion (data collected using an aerodynamic lens inlet and a laser energy 0.2 mJ).

(a)

(b)

Figure 4. Typical negative ion spectra of single particles taken from (a) particle of mixed composition of aerodynamic diameter 1.2 μm taken from a DPI (dose of FP/SX 250 μg/50 μg) and (b) particle of mixed composition of aerodynamic diameter 1.2 μm taken from a pMDI (dose of FP/SX 250 μg/25 μg) aerodynamic lens inlet, laser energy 0.2 mJ. Both spectra show fragment ions consistent with FP and SX.

The spectrum for SX acquired at low laser energy is dominated by the ion at m/z 91 due to a tropylium-type structure, but also shows fragment ions attributable to the alkyl chain and benzyl group at m/z 232 and the hydroxylated end of the molecule at m/z 248.

The negative ion mass spectra obtained from FP and SX particles of approximately 1.2 μm particle size, using low laser energy (0.2 mJ), are shown in Fig. 3. For the spectrum of FP (Fig. 3(a)), the loss of the SCH₂F group gives the ion at m/z 436 and a concerted loss of the 17α and 17β side chains from the D ring of the steroid givea the ion at m/z 331 which is analogous to what occurs in the positive ion spectrum. The negative ion spectrum of SX (Fig. 3(b)) is dominated by the ion at m/z 188 which is due to the xinofoate counter-ion which shows two sequential losses of water to give the ion at m/z 152 and a loss of carbon dioxide to give the ion at m/z 144.

In addition to the active pharmaceutical ingredients, the DPI products also contain lactose, an excipient used as a carrier for the drug molecules. The spectra acquired for lactose using the AToFMS instrument were extremely weak in both positive and negative ion mode (presumably due to the lack of a strong chromophore in the lactose molecule capable of absorbing radiation at 266 nm), and did not interfere with the API mass spectra.
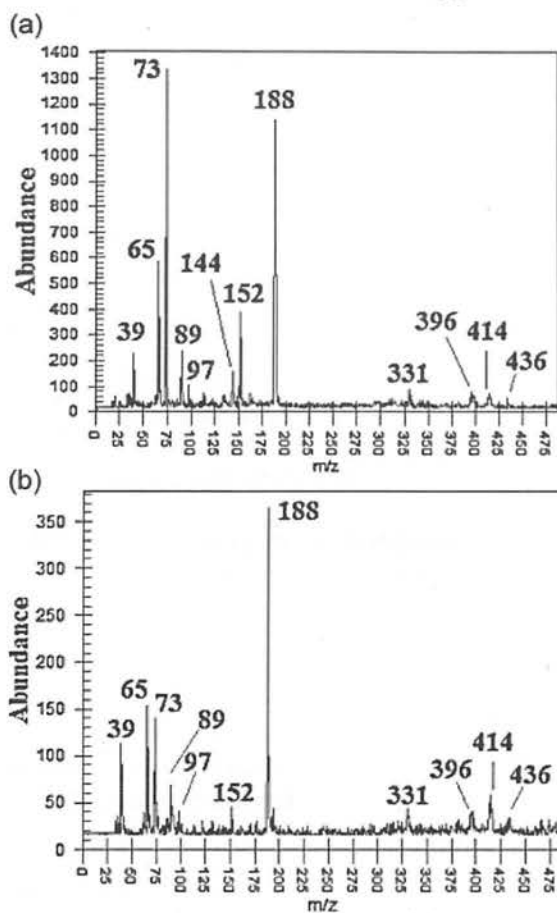
The particles taken from aerosols originating from DPI and pMDI inhalers gave mass spectra which showed good evidence for the presence of co-association because of the appearance of both sets of fragment ions which were previously assigned to either FP or SX. Typical negative ion mass spectra obtained from individual particles from both DPI and pMDI inhalers are shown in Fig. 4. It can be clearly seen that both spectra show ions similar to those seen in the spectra taken from pure standards of both FP and SX.

Multivariate analysis of data acquired using the AToFMS instrument

The mass spectral pattern is an important parameter in these experiments because it is used to categorise the chemical composition (speciation) of each of the particles. Thus ions in the mass spectral pattern, originating from the unique fragmentation pathways for each of the active pharmaceutical ingredients, were used to identify and categorise the chemical composition of any given particle.

For a typical data set acquired using the AToFMS instrument, there are a large number of individual particles (from our work typically in the order of approximately 100
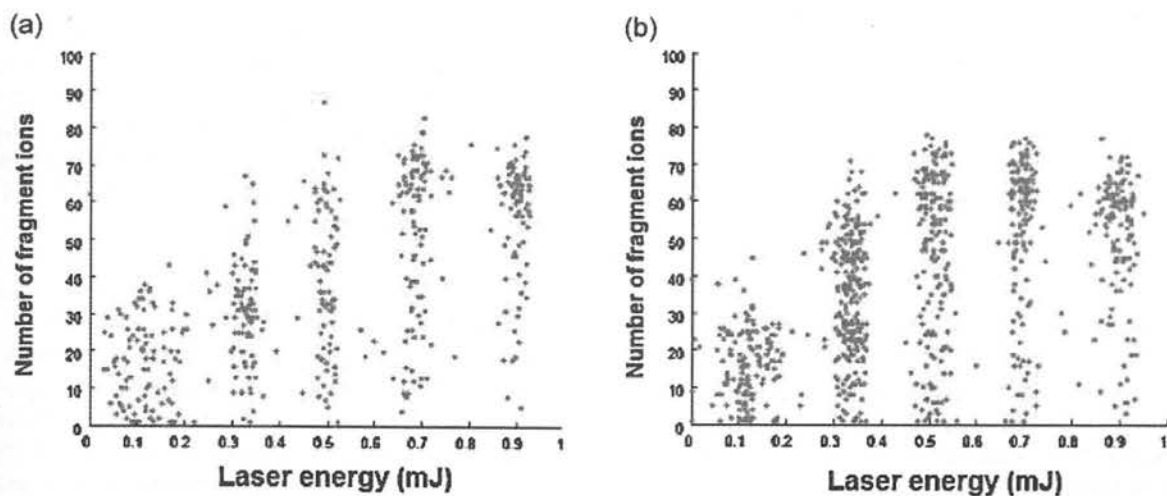
Figure 5. Variation in the number of fragment ions per particle for (a) FP and (b) SX (using the nozzle-skimmer inlet). This figure is available in colour online at www.interscience.wiley.com/journal/rcm.
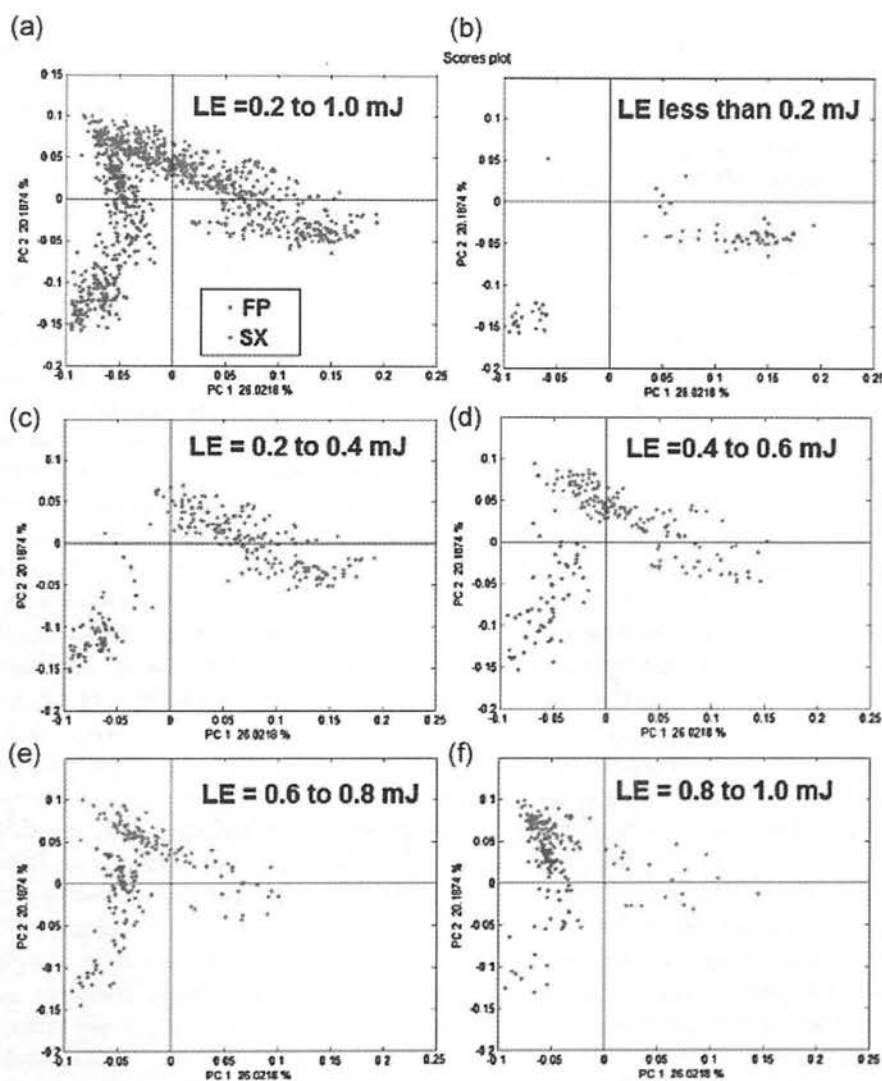

Figure 6. PCA charts for FP and SX to show the effect of varying the laser energy (LE): (a) PCA chart for the complete data set and (b–f) the PCA charts for the data acquired at the given laser energy ranges. This figure is available in colour online at www.interscience.wiley.com/journal/rcm.

particles per sample) and each is associated with a mass spectrum containing many fragment ions. For ease of comparison of these large, complex, datasets, multivariate statistical analysis in the form of principal component analysis (PCA) was utilised.

The PCA model was based on the pure active pharmaceutical ingredients (FP and SX), taken as reference standards and these were compared with samples from the inhaled products (pMDI and DPI). During method development the PCA model was assessed for robustness caused by changes in instrument parameters that could potentially lead to a change in the mass spectral fragmentation patterns. Further tests were performed to investigate the effect of the matrix for DPIs but this was found to be minimal as the lactose carrier gives a poor response to laser ablation and ionisation. Particles were categorised and counted via PCA scatter plots to obtain a semi-quantitative estimate of the amount of co-association present.

The number of fragment ions in each mass spectrum (both positive and negative ion), at varying laser energy for each of the reference standards (FP and SX), is shown in Fig. 5. As expected, at lower laser energies lower numbers of fragment ions were observed.

The individual data sets for each of the active pharmaceutical ingredients which were acquired with the AToFMS instrument using the nozzle-skimmer inlet are plotted on the same PCA chart (Fig. 6). Each data point represents an individual particle and its associated mass spectrum. Figure 6(a) shows the entire data set generated to investigate the effect of varying the laser energy. The laser energy was increased from 0.1 mJ to 0.8 mJ and the PCA plots are shown in Figs 6(b)–6(e). The PCA plots show that the clusters attributable to either FP or SX converge with increasing laser energy. At high laser energy the relatively fragile API molecules are mainly fragmented to produce significantly greater numbers of lower mass ions that are common to both FP and SX. Hence the mass spectral patterns become more complex and lose their definition as the spectra have many more ions in common. Conversely, at lower laser energy there are many more unique fragment ions for each API and hence the PCA clusters, based on the mass spectral patterns, show greater separation. This demonstrates that the PCA model is sensitive to changes in the mass spectra.

The laser energy setting of 0.2 mJ gave the most unique ions in the mass spectra of the standards of drug compounds. Hence, further data sets were acquired at this laser energy, using the AToFMS instrument now equipped with an aerodynamic lens to determine the extent of co-association in the pMDI and DPI samples.

Figure 7(a) shows a PCA chart for the standards of FP and SX with the standard clusters defined by ellipses. These ellipses define an equal distance from the class centre using Mahalanobis[22] metrics, which take into account how particles distribute within the plot. For example, because FP particles distribute mainly along the vertical axis, this is assumed to be characteristic of this group and therefore the distance along this direction is under-weighted, resulting in an equidistance ellipse that is tilted vertically.

The standard confidence ellipses have been overlaid onto the PCA plot for a DPI sample in Fig. 7(b). This plot shows that the majority of the data points for the DPI sample appear in the centre of the plot and are not overlaid by the standard ellipses, thus showing that there is a difference in the mass spectral patterns for these particles compared with the reference standards.

To confirm that the matrix effect of the lactose carrier was minimal, additional experiments were performed on Flovent® and Serevent® DPIs. The formulated product for Flovent® is a blend of FP and lactose and that of Serevent® is a blend of SX with lactose, i.e. each device contains only *one* active pharmaceutical ingredient. Approximately 80–85% of the PCA components for these DPI products containing a single API (either FP or SX) are overlaid by the corresponding ellipse for FP or SX, as in Fig. 8(a). This confirms that both FP and SX can be detected in the presence of lactose and that the matrix effect from the carrier is minimal. This is also good confirmatory evidence that this PCA approach is valid for identifying particles containing either FP or SX alone, and it will differentiate these particles from those containing a mixture of both FP and SX, i.e. that PCA identifies particles where co-association of these active pharmaceutical ingredients has occurred.

The presence of co-association is thought to be derived from blending during the formulation process and from the mixing process that occurs in the aerosol plume following actuation.

There are a number of limitations in using the AToFMS instrument for quantitation, mainly originating from shot-to-shot intensity differences within the laser beam,[23] which can lead to variations in vaporisation and ionisation and thus to differences in the mass spectral signal intensities.

The variations in the mass spectral fragmentation patterns are shown by the broad clusters on the PCA plots. Therefore, if the variation within each experiment is assumed to be addressed by the spread of these clusters, an estimate of the number of co-associated particles can then be obtained by counting the data points that are not overlaid by the reference standard confidence ellipses.

The data in Fig. 8 for Flovent® and Serevent®, which contain only a single active pharmaceutical ingredient, shows that this is a reasonable model for detecting single particles of FP or SX within a lactose blend and, by inference, those PCA data points that do not fall within the standard confidence ellipses can be assumed to be from particles containing both active pharmaceutical ingredients due to co-association.

The PCA model shows some sensitivity to the minimal amount of fragmentation used as an input parameter. However, whatever value is used for this parameter, the amount of mixed particles is always found to be greater than the number of particles containing a single API. The data are shown in Figs. 9 and 10 and use the PCA model based on a minimum of 20 input fragment ions, i.e. only combined positive and negative spectra that showed at least 20 fragment ions were included.

Figure 9 shows the particle counts taken from the PCA charts from a set of experiments performed on two strengths of DPI (samples 1 to 5, FP/SX 250 µg/50 µg and samples 7 to
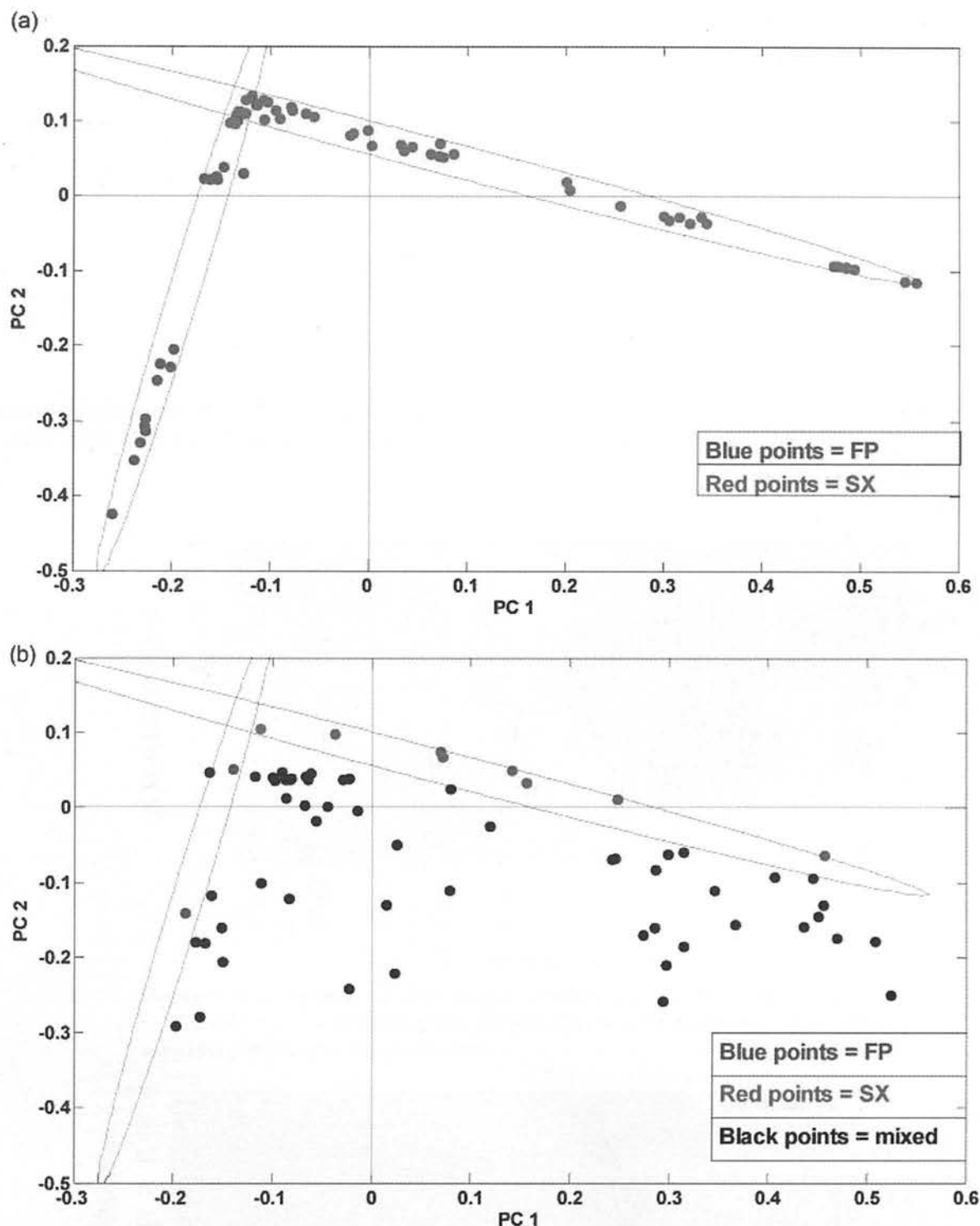
(a)

(b)

Figure 7. (a) Definition of ellipses using PCA for standards of FP and SX overlaid on the same chart. (b) The standard ellipses defined in (a) overlaid onto data from a sample and used to categorize the particles in the sample, (i.e. (b) shows data points from the sample only). Example sample shown is FP/SX 250 μg/50 μg. (file DPI _1). This figure is available in colour online at www.interscience.wiley.com/journal/rcm.

1, FP/SX 500 μg/50 μg). For each batch the first three runs were the same sample and the last three runs were three different batches of the same strength. Taking the above assumptions into account, these data consistently show that at least 80% of the PCA co-ordinates in each sample originate from co-associated particles.

Similarly, Fig. 10 shows the particle counts taken from the PCA charts from a set of experiments performed on three strengths of a pMDI product (samples 1 to 5, FP/SX 50 μg/25 μg; samples 6 to 11, FP/SX 125 μg/25 μg; and

samples 11 to 15, FP/SX 50 μg/25 μg). For each batch the first three runs were the same sample and the last three runs were three different batches of the same strength of this product. Taking the above assumptions into account, these data consistently show at least 50% of the PCA co-ordinates in each sample originate from co-associated particles.

The difference in co-association levels between DPIs and pMDIs is likely to result from the very different nature of the formulations and the mechanisms by which co-association may occur. In the pMDI, co-association is believed to occur between
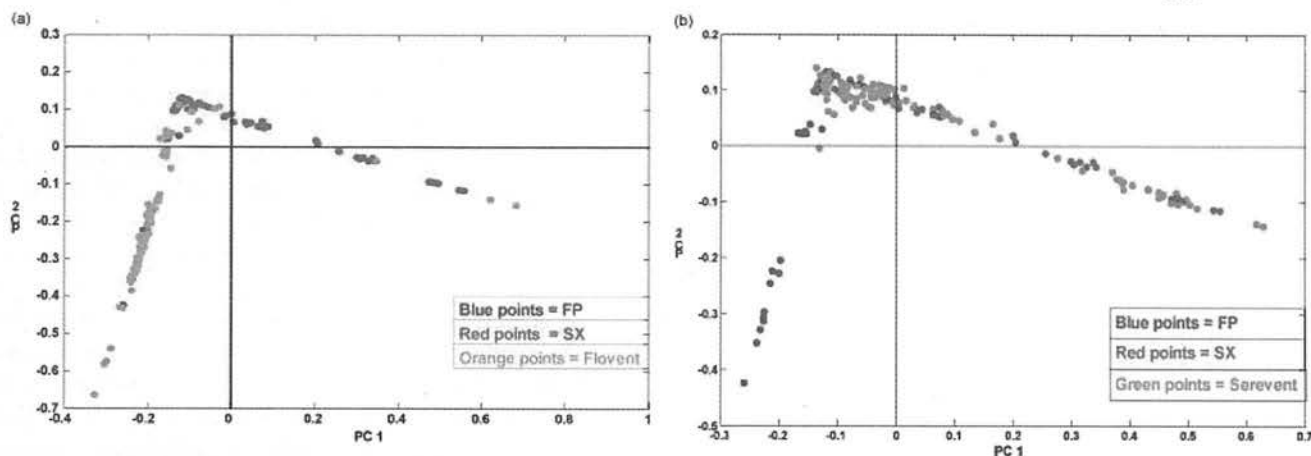
Figure 8. Comparison of (a) Flovent® and (b) Serevent® data sets with standards of FP and SX, by principal component analysis (PCA). This figure is available in colour online at www.interscience.wiley.com/journal/rcm.
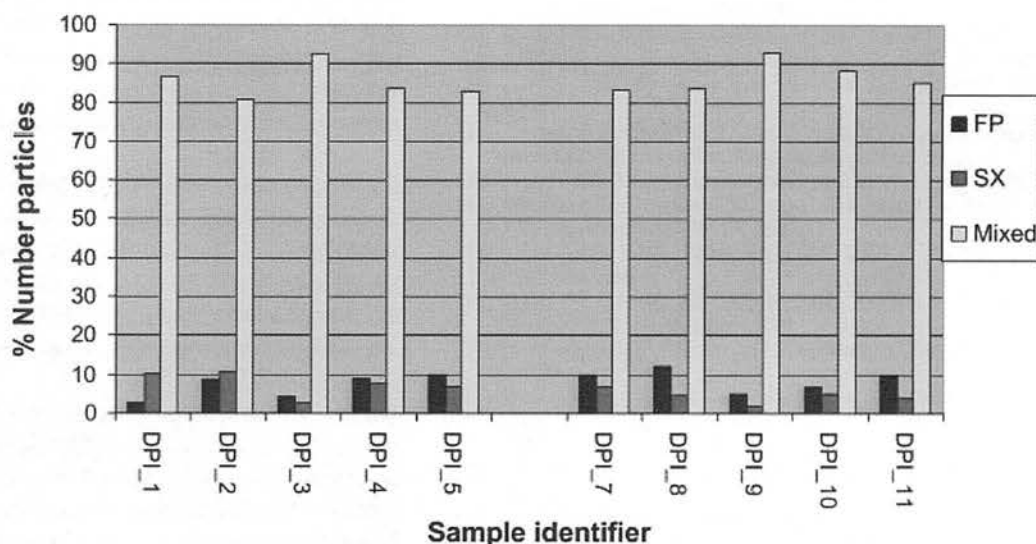

Figure 9. Data analysis for DPIs using PCA ellipses. DPI_1 to 5 were 250 µg/50 µg FP/SX, DPI_7 to 12 were 500 µg/50 µg FP/SX. This figure is available in colour online at www.interscience.wiley.com/journal/rcm.
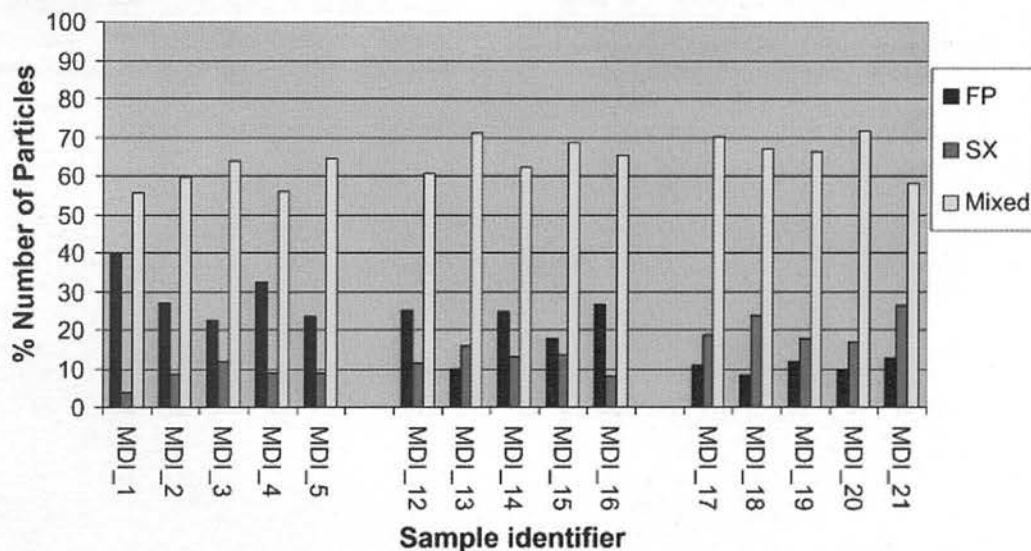

Figure 10. Data analysis for pMDIs using PCA ellipses. MDI_1 to 5 were 250 µg/25 µg FP/SX, MDI_12 to 16 were 125 µg/25 µg FP/SX and MDI_17 to 21 were 50 µg/25 µg FP/SX. This figure is available in colour online at www.interscience. wiley.com/journal/rcm.

the two types of solid particles (pure FP and SX particles) while still in the suspension within the inhaler.[24] Furthermore, on actuation, it is likely that the droplets emitted from the device contain multiple particles of FP and of SX. When a droplet collapses through propellant evaporation, these particles can remain associated.[25] Alternatively, coalescence of droplets within the plume could also lead to co-association.

In DPIs co-association would arise from drug–drug interactions as a result of high shear forces during the blending process. However, lactose added to the blend as an excipient will both reduce the level of co-association by acting as a diluent and potentially increase the level of co-association by acting as a 'carrier' of both drug types. The dominant mechanisms contributing to the levels of co-association observed in such combination products require further study.

CONCLUSIONS

We have shown that it is possible to detect the active pharmaceutical ingredients fluticasone propionate (FP) and salmeterol xinofoate (SX) from inhaled drug products using an AToFMS instrument. The spectral fragmentation patterns are unique and can be recognised using principal component analysis (PCA).

The combination of AToFMS and PCA is a useful approach for detecting co-association of different active pharmaceutical ingredients. An estimate of the number of co-associated particles was derived by counting the PCA co-ordinates in those specific areas of the PCA plots which were not overlaid by the reference standard active pharmaceutical ingredients confidence ellipses.

Using this process it was shown that at least 80% of the respirable particles in a DPI product and at least 50% of the respirable particles in the pMDI product were comprised of co-associated active pharmaceutical ingredients (FP and SX). The data suggest that high levels of these co-associated particles are emitted from both DPI and pMDI products examined after actuation of the devices.

A mass spectrum could not be obtained for the lactose carrier used in DPI products but the carrier lactose appears to have minimal interference with these measurements. There is potential for association of FP or SX (or both) with lactose and

future work would involve development of techniques that could further differentiate and speciate the particles generated.

Acknowledgements

REFERENCES

1. World Health Organisation. 2007. Available: http://www.who.int/respiratory/en/ (accessed 5 November 2007).
2. Nelson HS, Chapman KR, Pyke SD, Johnson M, Pritchard JN. *J. Allergy Clin. Immunol.* 2003; **112**: 29.
3. Micheal Y, Chowdhry B, Ashurst I, Snowden M, Davies-Cutting C, Gray C. *Int. J. Pharmaceutics* 2000; **200**: 279.
4. Theophillus A, Moore A, Prime D, Rossomanno S, Whitcher B, Chrystyn H. *Int. J. Pharmaceutics* 2006; **313**: 14.
5. May KR. *J. Sci. Instrum.* 1945; **22**: 187.
6. Nash DG, Baer T, Johnson MV. *Int. J. Mass Spectrom.* 2006; **258**: 2.
7. Noble CA, Nordemeyer T, Salt K, Morrical B, Prather KA. *Trends Anal. Chem.* 1994; **13**: 5.
8. Noble CA, Prather KA. *Mass Spectrom. Rev.* 2000; **19**: 248.
9. Sullivan RC, Prather KA. *Anal. Chem.* 2005; **77**: 3861.
10. Noble CA, Prather KA. *Aerosol Sci. Technol.* 1998; **29**: 294.
11. Karisson R, Gailli M, Etzler F. *Proc. XIII Symp. 'Drug Delivery to the Lungs',* London, December, 2002.
12. Fields TB. *Polymeric Materials Sci. Eng.* 2002; **87**: 337.
13. Martin AN, Farquart GR, Jones AD, Frank M. *Rapid Commun. Mass Spectrom.* 2007; **21**: 3561.
14. Hallworth GW, Westmoreland DG. *J. Pharm. Pharmacol.* 1987; **39**: 966.
15. Gard EE, Mayer JE, Morrical BD, Dienes T, Fergenson DP, Prather KA. *Anal. Chem.* 1997; **69**: 4083.
16. Su Y, Sipin MF, Furutani H, Prather KA. *Anal. Chem.* 2004; **76**: 712.
17. Brereton R. *Chemometrics: Data Analysis for the Laboratory and Chemical Plant* (1st edn). Wiley-Blackwell: Chichester, 2003. ISBN 0471489786.
18. Wold S. *Chemometrics Intelligent Laboratory Systems* 1987; **2**: 37.
19. Murphy D. *Mass Spectrom. Rev.* 2007; **26**: 150.
20. Hinz K-P, Spengler B. *J. Mass Spectrom.* 2007; **42**: 843.
21. Silva PJ, Prather KA. *Anal. Chem.* 2000; **72**: 3553.
22. De-Maesschalck R, Jouan-Rimbaud D, Massart DL. *Chemometrics Intelligent Laboratory Systems* 2000; **50**: 1.
23. Steele PT, Srivasava A, Pitesky ME, Fergenson D, Tobias H, Gard EE, Frank M. *Anal. Chem.* 2005; **77**: 7448.
24. Micheal Y, Snowden M, Chowdhry BZ, Ashurst IC, Davies-Cutting C, Riley T. *Int. J. Pharmaceutics* 2001; **221**: 165.
25. Gonda I. *Int. J. Pharmaceutics* 1985; **27**: 99.